# ESTIMATION OF BLOOD FLOW USING DOPPLER ULTRASOUND WITH A NARROW BEAM

Robin Daniel Willink

A thesis submitted to the University of Leicester
for the degree of Doctor of Philosophy

Division of Medical Physics,
Faculty of Medicine,
University of Leicester

1994





ProQuest LLC
789 East Eisenhower Parkway
P.O. Box 1346
Ann Arbor, MI 48106-1346

"For my thoughts are not your thoughts, neither are your ways my ways," says the LORD. "For as the heavens are higher than the earth, so are my ways higher than your ways and my thoughts than your thoughts."

Isaiah 55:8,9

To my mother

and remembering David Tunley and Kerrin Smith

## CONTENTS

## ABSTRACT

Estimation of mean spatial blood velocity, and hence volumetric flow, using Doppler ultrasound is typically performed under the assumption that the beam samples each part of the cross section of the blood vessel equally. This allows the mean velocity to be regarded as being proportional to the conventional mean Doppler shift frequency. In this work a new frequency estimator of mean velocity is presented for the case where the beam is assumed to be of negligible width compared to the vessel diameter and directed through the vessel axis. This estimator is proportional to the mean velocity if it can be further assumed that the velocity profile is axi-symmetric and is monotonic, or has an idealised bidirectional form. In practice neither the assumption of a uniformly insonating beam nor the assumption of an infinitely narrow beam are valid. Also the Doppler spectrum, as a representation of the velocity distribution of blood cells, is corrupted by spectral broadening, noise, filtering and the stochastic nature of the signal. In addition difficulty exists in the measurement of the representative Doppler angle. The effects on both estimators of these potential sources of error are discussed and compared. The question of volumetric flow measurement at various arterial sites is addressed by modelling the velocity profiles in the vessel throughout the cardiac cycle. Some sources of error affect only the new estimator, so one conclusion drawn is that mean velocity estimation and volumetric flow measurement are better performed using the conventional frequency with a uniformly insonating beam. Nevertheless if the beam is more accurately described as being very narrow and centrally positioned the new estimator performs better than the conventional frequency estimator. This description may well be appropriate if the blood vessels are large and the Doppler beam is transmitted and received using a linear array transducer such as in modern duplex systems.

## ACKNOWLEDGEMENTS

It is important, but not always easy, to bear in mind those people on whom I have relied and from whom I have received during these years. "No man is an Island, entire of itself; every man is a piece of the Continent, a part of the main", and so I thank those who encouraged John Donne while he composed this. Thanks are also due to the staff of the Medical Physics department of the Leicester Royal Infirmary, some of whom are mentioned here. I am grateful to Glen Bush and Troy Johnson for the design and construction of the video frame store, and to Mike Smith for the initial programs. Fernando Schlindwein was a unique example to follow and, with those who assisted him, provided the digital signal processor and the analysis program which I doctored. John Brooks, Mike Squires and Tim Lyon offered constructive support in the mechanical workshop. Troy Johnson, Vaughan Acton and Dave Heaton were well regulated in the electronics workshop, and John Pelmore provided a lab which was raided many times for bits of kit. Many thanks go to Professor David Evans for supervising this work, and for originally suggesting the existence of the new estimator. Thanks also to Ronney Panerai for statistical discussions and diversions, to Tina Craig and Lea Bickerdike who typed, posted and administered, to Harry Hall, and his box of tools, for providing technical assistance, and to Steve Bentley for heaps, but basically for just being Steve Bentley. I am very grateful to Abigail Thrush and Tim Hartshorne who probed beneath the surface on many and various occasions, and also to Hayley Handford and Yvonne Sensier. The Medical Physics network managers Glen Bush and Mike Smith ensured a working environment for the Microsoft Equation Editor without whom this would not have been possible, and Nizamettin Aydin, Lingke Fan, Colin Tysoe, Raimes Moraes and Julia Smith provided academic parallelism. Thankyou also to Dave Bonnett for his concern and encouragement, and to Mike Barnes for all sorts of things, including an office with an outlook. The University of Leicester paid me, the staff of the fracture clinic and the cafetaria were there when I needed them, and Radio 5 and especially the England cricket team entertained me on Steve's radio of a evening. Sundries may have been missed above, but add to the total anyway, and have been gratefully received.

## STATEMENT OF ORIGINALITY

The material in this thesis presented without reference to the work of others is original. The work has been undertaken and the thesis written solely by myself. Some of the material in this thesis is contained in the publication "A mean blood velocity statistic for the Doppler signal from a narrow ultrasound beam" by R.Willink and D.H.Evans, which is in press with I.E.E.E. Transactions on Biomedical Engineering. Further material is contained in other manuscripts submitted for publication.

R.D.Willink

## PREFACE - NOTATION AND NUMBERING

The extensive use of equations, derivations and diagrams in this thesis means that many symbols have been needed. The vast majority of these symbols are used without ambiguity throughout the thesis. Most of this consistent notation is listed on the following page. In other cases a symbol may signify different quantities in different chapters. Such symbols include $a$, $b$, $x$, $y$, $\alpha$ and $\beta$. Efforts have been made to minimise such ambiguity, and indeed **within each individual chapter no ambiguity exists**. Notation which is specific to a chapter, or is not used often enough, is not included in the list below. If these symbols are important they are listed at the end of the chapter(s) in which they appear. Both the following list and the lists at the end of the individual chapters are merely to assist the recollection of the meanings of each symbol. In every case the meaning is described in the text itself.

Some general rules apply in the use of symbols. The bar notation, e.g. $\bar{v}$, signifies averaging over space, or another related domain, usually at any one point in time. In agreement with this, when applied to frequencies and frequency bin index numbers, the bar notation, e.g. $\bar{f}$, implies the conventional notion of the mean frequency of a spectrum after the frequency components are weighted by their intensity. The hat notation, e.g. $\hat{f}$, implies the frequency calculated according to the new method. Temporal averaging is indicated by the subscript 'ave', e.g. $Q_{\text{ave}}$. Capitalised subscripts are generally used to denote variables under certain conditions, e.g. $p_N(f)$ for the power density of a noise spectrum. Lower case subscripts are used to denote a particular value of a general variable within a range, e.g. $v_m$ is the maximum blood velocity present in the artery. Variable quantities are italicised, and fixed quantities are not.

Equations, figures (i.e. charts and diagrams) and tables are numbered within each chapter independently, so that the first equation in chapter 12 is referred to as 'equation (12.1)' or simply '(12.1)'. The first figure in that chapter is 'fig.12.1' and the first table is 'table 12.1'. For simplicity, equations introduced earlier are sometimes duplicated in later chapters, and are renumbered for use in those chapters. Where appropriate derivations of equations are given in appendices E and F.

### Important abbreviations

| | |
|---|---|
| IWMB | intensity weighted mean bin number |
| PIWMB | position and intensity weighted mean bin number |
| IWMF | intensity weighted mean frequency |
| PIWMF | position and intensity weighted mean frequency |

## Common notation used unambiguously throughout

| | |
|---|---|
| $\overline{B}_D$ | IWMB if the spectrum was deterministic |
| $\overline{B}$ | the observed IWMB |
| $\hat{B}_D$ | PIWMB if the spectrum was deterministic |
| $\hat{B}$ | the observed PIWMB |
| $c$ | speed of sound in blood |
| $E_{\text{IWMF}}$ | percentage error in the mean velocity calculated from IWMF |
| $E_{\text{PIWMF}}$ | percentage error in the mean velocity calculated from PIWMF |
| $f$ | general frequency variable |
| $\overline{f}$ | IWMF of observed (deterministic) spectrum |
| $\overline{f}_S$ | IWMF of theoretical (deterministic) signal spectrum |
| $\hat{f}$ | PIWMF of observed (deterministic) spectrum |
| $\hat{f}_S$ | PIWMF of theoretical (deterministic) signal spectrum |
| $f_m$ | maximum frequency in theoretical Doppler signal |
| $f_{\max}$ | maximum frequency in Doppler signal |
| $F$ | transmit frequency |
| $i$ | generalised index number of a frequency bin |
| IMAX | the index of the highest frequency bin, i.e. for a single-sided spectrum this is one less than the number of available frequency bins |
| $n$ | 'bluntness' parameter defining the shape of a simple velocity profile |
| $p_i$ | power recorded in the $i$'th frequency bin |
| $\tilde{p}_i$ | mean power in the $i$'th frequency bin |
| $p(f)$ | power spectral density function of Doppler signal |
| $p_S(f)$ | power spectral density function of theoretical Doppler signal |
| $P$ | total spectral power in spectrum |
| $\tilde{P}$ | total spectral power in deterministic spectrum |
| $R$ | internal radius of vessel |
| $r$ | radial distance from the vessel axis |
| $t$ | parameter defining the form of the theoretical Doppler spectrum |
| $v$ | velocity of a blood particle |
| $v_m$ | maximum blood particle velocity present |
| $\overline{v}$ | actual mean velocity |
| $\overline{v}'$ | estimate of mean velocity |
| $\theta$ | the angle between the ultrasound beam and the direction of motion of the blood particle(s) (In chapters 4 and 7 which deal with the finite angular dimensions of the beam this is defined in terms of the line from the centre of the transducer to the centre of the sample volume.) |
| $\tau$ | time variable |

# CHAPTER 1 - AN INTRODUCTION TO VOLUMETRIC FLOW MEASUREMENT USING ULTRASOUND

In the latter half of the twentieth century major advances in the clinical study of blood flow have been afforded by the availability of ultrasonography, and chiefly by the technique known as Doppler ultrasound. In this technique inferences are made about the flow of blood by studying the Doppler shifted signal of ultrasonic radiation transmitted and received outside the body, but scattered from blood particles within the body. As such, examinations made using Doppler ultrasound are regarded as being 'non-invasive' and safe, and are cost-effective and easy to perform. In addition blood vessels in situ can be visualised by the ultrasonic technique known as 'B-mode' imaging, where an image of tissue structure is built up from the pattern of reflections received by the transducer resting on the skin surface. The techniques of Doppler ultrasound and B-mode imaging have many clinical applications and are widely in use.

Doppler ultrasound primarily provides information about blood velocity and not volume, and much research has been undertaken to advance velocity measurement. However quantification of the volumetric flow rate ultrasonically is problematic, and remains an unfinished area of study. In many clinical cases the quantification of a *change* in flow over time, perhaps as a result of the administration of a drug, may be an acceptable result, so that determination of the absolute flow is not necessary. However absolute flow remains a more fundamental quantity. Generally of more limited value than an estimate of flow made over many cardiac cycles would be an estimate made over one cycle, and of less value still a single estimate of instantaneous volumetric flow rate. However an estimate over many cycles ultimately can be formed from a continuous estimate of the instantaneous rate, so that instantaneous flow estimates can be the building blocks of general flow quantification.

The instantaneous volumetric rate of flow of a fluid through any cross section of a tube is equal to the area of the cross section multiplied by the velocity averaged spatially throughout the cross section. Therefore one way of determining the flow rate is to obtain independent estimates of area and mean velocity that are appropriate to the same point in time. Error in the continuous estimation of instantaneous flow may therefore arise from error in the measurement of the changing area, error in the measurement of the fluctuating mean velocity, or error in the referencing in time of these quantities. The work in this thesis focuses strongly on the estimation of instantaneous mean velocity, and the consequent reduction of the error in volumetric flow measurements. The measurement of cross-sectional area is a separate problem, and is only discussed in this introductory chapter and in appendix A. Accurate referencing in time is essentially an engineering problem. In one context it is described briefly in appendix A.

## General flow equation

This thesis is heavily reliant on the use of mathematical symbolism to express the physical ideas relating to the measurement of flow and velocity. It is fitting therefore that the first equation introduced is fundamental to the problem, and describes what has already been mentioned. If the area of the cross section perpendicular to the vessel axis changes with time $\tau$ and has an area given by $A(\tau)$ as in fig.1.1, and if the component of the spatial mean velocity parallel to this axis through this cross section is $\bar{v}(\tau)$, then the instantaneous flow rate, $Q(\tau)$, is given by

$$Q(\tau) = A(\tau).\bar{v}(\tau) \tag{1.1a}$$

and the average flow rate, $Q_{ave}$ , throughout a cardiac cycle of duration $T$ is

$$Q_{ave} = \frac{1}{T}\int_{\tau}^{\tau+T} A(\tau).\bar{v}(\tau)\,d\tau \tag{1.1b}$$

The goal therefore is the evaluation of these flows, whether explicitly in terms of the factors $A(\tau)$ and $\bar{v}(\tau)$ as in these equations, or in another way. There follows a description of how ultrasound can be used to achieve this. Subsequently this chapter introduces the main subject of this thesis, namely the estimation of the instantaneous mean velocity, $\bar{v}(\tau)$, in a way which differs from conventional methods.

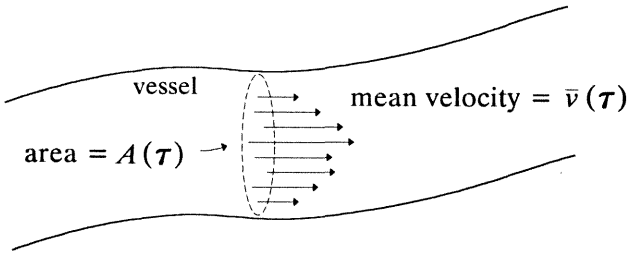


**Fig.1.1 - flow rate = area × mean velocity**

## The Doppler equation

The basis of quantitative blood velocity study using ultrasound is the equation which describes the observed shift in frequency of the radiation scattered from a particle moving with a given velocity. If $f$ is the shift in frequency and $v$ is the speed of the particle then

$$f \approx \frac{2Fv\cos\theta}{c} \tag{1.2}$$

where $F$ is the transmit frequency, $c$ is the speed of sound in the medium and $\theta$ is the angle at the particle between the direction to the transducer and the direction of motion. This is the basic Doppler equation, in which the Doppler shift frequency $f$ is seen to be proportional to the velocity $v$. The approximation is based on the inequality $c >> v$, which is true as $c \approx 1580\ \mathrm{m\,s^{-1}}$ and $v \sim 1\ \mathrm{m\,s^{-1}}$.

The transmit frequency is well known, and the speed of sound in blood is known to an accuracy of ~0.5%, the uncertainty being due to dependence on the blood haematocrit. So if the angle $\theta$ is known the velocity of the particle can be recovered from the measured frequency, i.e.

$$v \approx \frac{cf}{2F\cos\theta} \tag{1.3}$$

In practice $\theta$ is measured relative to the axis of the blood vessel. It follows that the velocity $v$ in (1.3) is the component of the velocity along this axis, as seen in fig.1.2.

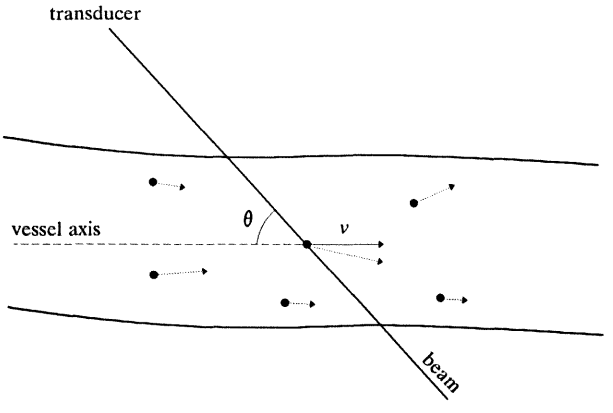


**Fig.1.2 - geometry for the Doppler equation**

## The Doppler spectrum and the velocity distribution

The particles, or scatterers, of significance are the red blood cells, their contribution to the scattering of the ultrasound beam being much greater than that of other blood components. More specifically the individual scatterers can be thought of as fluctuations in the local concentrations of the red blood cells, as modelled by Angelsen (1980). With such a model it is still appropriate to regard the velocity of the scatterers as being the velocity of the red blood cells. If on average all these scatterers present the same cross section to the beam then, for a fixed intensity of insonation, the mean received power in the Doppler signal is proportional to the number of red blood cells in the insonated region, called the 'sample volume'. Ideally therefore the Doppler shift spectrum has the same form as the distribution of velocities of cells in the sample volume, enabling blood flow to be studied with accuracy by considering the spectrum. An example of this is shown in fig.1.3 where the spectral density function, denoted by $p(f)$ has the same form as the number density of scatterers $\rho(v)$ with velocity, $v$. The maximum frequency $f_m$ is related to the maximum velocity $v_m$ by the Doppler equation, (1.2).

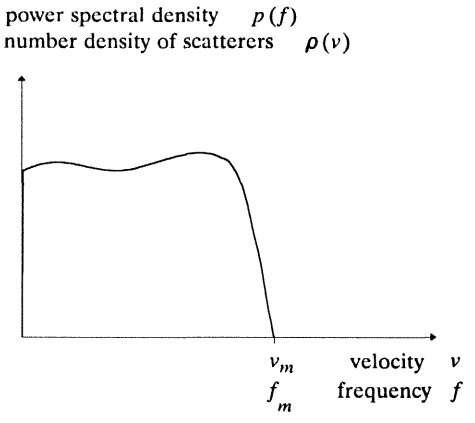


**Fig.1.3 - equivalence of the ideal Doppler shift spectrum and the velocity distribution**

## Methods of flow estimation using ultrasound

Various ultrasonic techniques exist for the continuous evaluation of the product given in (1.1a) and so for the measurement of volumetric flow. Generally speaking the product evaluated is not that given in (1.1a) but is

$$Q'(\tau) = A'(\tau).\overline{v}'(\tau) \tag{1.4}$$

where the prime notation reflects the fact that the factors $A'(\tau)$ and $\overline{v}'(\tau)$, which may be evaluated explicitly or implicitly, and the product are estimates of the true values. The technique of greatest relevance to the work of this thesis is the duplex method which is described in the following paragraphs. The main subject of this thesis, that is the calculation of $\overline{v}'(\tau)$ from the form of a single spectrum, is also relevant to the attenuation compensation method, which is the first of the other methods briefly mentioned

*The duplex method*

In duplex ultrasound dynamic B-mode images of an artery are obtained, so that the vessel is oriented longitudinally on the screen, generally at an angle to the image horizontal. Overlaid on these images is the cursor defining the direction of the beam used to generate the Doppler signal giving blood velocity information. This beam lies in the image plane so that the user can intelligently manipulate the Doppler beam to insonate along a known path beneath the skin. The returning Doppler signal is electronically gated so that the echoes returning from a section of this path, the sample volume, are retained and others originating from scatterers at different depths are discarded. The length and depth of this sample volume are adjustable, and are indicated by cursors on the image also. Machine time is shared between the generation of the images and the generation of the Doppler signal, until the sample volume is deemed to be positioned across the appropriate cross section of the vessel. This is determined from the position of the cursors on the dynamic images and the quality of the preliminary Doppler signal. By visually aligning a variable angle cursor with the orientation of the artery on the image, the Doppler angle, $\theta$, necessary for velocity calculation is estimated. The image is then frozen to allow all the machine time to be devoted to instantaneous velocity measurement. An example of such an image, with overlaid cursors defining the sample volume and the measured Doppler angle, is given in fig.1.4.

In duplex ultrasound the estimate of mean velocity often obtained is that which would be appropriate if the Doppler beam insonated the cross section uniformly. The estimate of mean velocity in this case is found from (1.3) and the estimated angle by replacing $f$ by the

observed mean Doppler shift frequency, which is denoted by $\bar{f}(\tau)$ and defined more fully in chapter 2. So in this case

$$\bar{v}'(\tau) = \frac{c\,\bar{f}(\tau)}{2F\cos\theta} \tag{1.5}$$

One reason why this velocity estimate tends to be too high is that the low frequencies in the spectrum are filtered to remove the Doppler signal received from the slowly moving and massive vessel walls, and hence $\bar{f}(\tau)$ is too high.

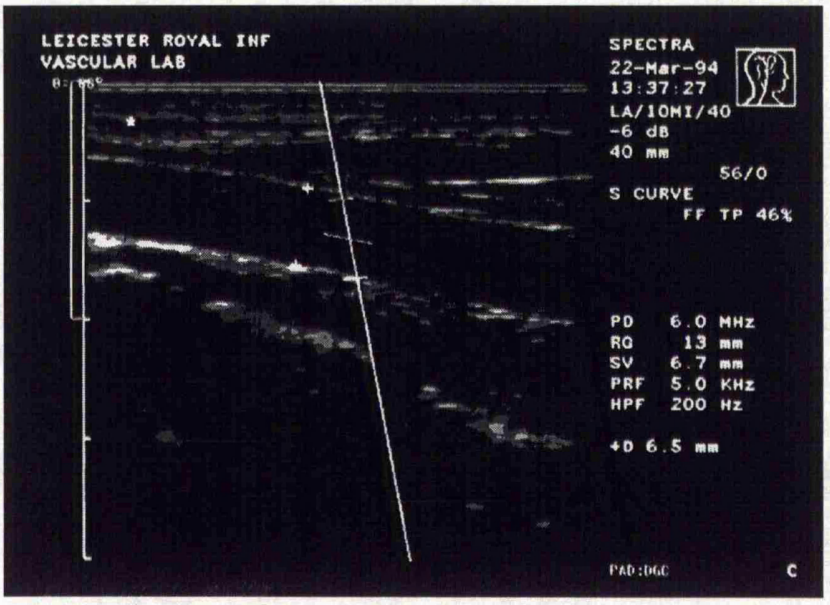


**Fig.1.4 - A frozen B-mode image of a carotid artery in a duplex system. The beam direction is defined by the long oblique line. Perpendicular to this are short cursors defining the extent of the sample volume. The cursor for angle estimation is oriented to be parallel to the axis of the artery. The diameter is measured from the cross-shaped cursors.**

Typically a single estimate of vessel diameter is obtained by visual measurement on one or several frozen B-mode images. With the help of on-screen calipers the diameter from any one image can be read from the screen. On fig.1.4 these calipers are crosses, the lower one not being particularly visible. So using an assumption of circularity a single estimate of cross-sectional area, say $A''$, is available. Therefore in estimating the instantaneous flow given in (1.1a) the duplex method usually evaluates the quantity

$$Q'(\tau) = \frac{c}{2F} \cdot \frac{A''\bar{f}(\tau)}{\cos\theta}$$

Errors in the measurement of flow throughout a cycle therefore chiefly result from the use of a constant cross-sectional area, uncertainty in the determination of the appropriate angle, possible failure of the Doppler beam to insonate the cross section uniformly and the need to apply a high-pass filter before spectral analysis.

*The attenuation compensation method*

The attenuation compensation method of flow estimation involves the formation of two concentric pulsed beams. One beam insonates the cross-section uniformly, and the other has a sample volume, of the same length and at the same depth, entirely within the lumen. This is illustrated in fig.1.5. The total power in the Doppler signal of the wide beam (bound by the dashed lines) is theoretically proportional to the cross sectional-area $A(\tau)$ and inversely proportional to $\cos\theta$ . It follows that this method does not require explicit estimates of the area $A(\tau)$ and angle $\theta$ which are sources of error in the duplex method. The constant of proportionality between power and blood volume can be found by comparing the relative powers of the two received Doppler signals. In practice a single broad beam is transmitted with an annular array transducer and the two received beams are formed electronically and are collected simultaneously.

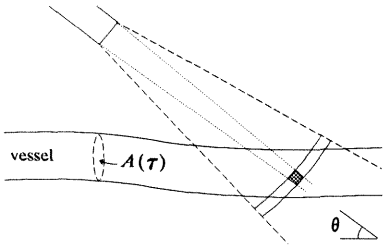


**Fig.1.5 - insonation in the attenuation compensation method**

*Flow measurement using a multigate system*

In a multigate system the beam is narrow and positioned through the vessel axis. The flow is examined by electronically gating the received Doppler signal to provide separate spectra for many points across the vessel diameter. This can provide an estimate of instantaneous flow if the velocity profile can be assumed to be axi-symmetric. Error is introduced if the beam does not pass through the centre of the vessel.

*Flow measurement by assuming the form of the velocity profile*

If it is assumed that the velocity profile has a particular form, then the mean velocity $\bar{v}(\tau)$ can be found from the maximum observed frequency, $f_{max}$ , provided (some of) the fastest particles are insonated. This method of mean velocity estimation is not affected by the need to filter the low frequencies of the Doppler signal.

## Simplification by the estimation of diameter

If the blood vessel can be assumed to have a circular cross section with internal radius $R(\tau)$, which is estimated by $R'(\tau)$, then (1.4) becomes

$$Q'(\tau) = \pi R'^2(\tau)\, \bar{v}'(\tau) \tag{1.6a}$$

and the flow throughout the cycle is estimated by

$$Q'_{ave} = \frac{\pi}{T} \int_{\tau}^{\tau+T} R'^2(\tau)\, \bar{v}'(\tau)\, d\tau \tag{1.6b}$$

Often however, as in the duplex method described above, only a single estimate of the arterial radius, say $R''$, is used. So estimates of the instantaneous flow and the flow throughout the cycle are

$$Q'(\tau) = \pi R''^2\, \bar{v}'(\tau) \tag{1.7a}$$

and

$$Q'_{ave} = \frac{\pi R''^2}{T} \int_{\tau}^{\tau+T} \bar{v}'(\tau) d\tau \tag{1.7b}$$

If $\bar{v}'(\tau)$ is accurate then this estimate of average flow is in error to the extent that $R''^2$ is not representative of the instanteous true value $R(\tau)^2$ throughout the cycle.

Eriksen (1992) obtained representations of diameter and mean velocity waveforms in the common carotid and femoral arteries of a limited number of volunteers, thus enabling the estimation of representative volumetric flow waveforms. He found that if the time-averaged diameter was used with the mean velocity waveform to estimate volumetric flow throughout the cycle the result was underestimation to the order of $1-4\%$. That is, calculation of volumetric flow using (1.7b) where $R'' = D_{ave}/2$, and $D_{ave}$ is the time-averaged diameter, gave results $1-4\%$ smaller than the 'true' flow analogous to (1.6b). If a single estimate of diameter taken at diastole was used it appeared that the estimate of cross-sectional area could be too low by 6% in the common carotid artery, or by 2% in the femoral artery. Similarly if the single estimate of diameter was made at systole the area could be overestimated by 7% in the carotid artery and 4% in the femoral artery. If these errors in area are in relation to the effective area leading to the correct measurement of volume flow then these are the errors in the resulting flow estimates.

Eriksen obtained each diameter waveform by combining the waveforms of several cycles, referenced using the ECG signal, and with durations normalised. The mean velocity waveform was found similarly, at the same site but from another set of cardiac cycles. The beam used to generate the velocity information did not insonate the vessel cross section uniformly. However the use of the resulting velocity waveforms was justified by noting the close similarity reported in earlier literature of velocity waveforms derived with restricted sample volumes to those derived from electromagnetic flowmetry.

## Evolution of the project

The feasibility of the measurement of changing vessel diameter from analysis of B-mode image data led to the goal of this project being the measurement of volumetric flow by the evaluation of (1.6a) and (1.6b) instead of the more commonly used (1.7a) and (1.7b). However it was apparent that errors in a flow estimate involving a single estimate of diameter, according to the usual equations (1.7a) and (1.7b), may primarily be due to errors in the measured mean velocity, $\overline{v}'(\tau)$, and not to the nature of $R''$ as a single estimate of the changing radius $R(\tau)$. The study of Eriksen described above supports the view that if a sensible estimate of $R''$ is available and $\overline{v}'(\tau)$ is systematically in error by more than a few per cent then effort spent on the evaluation of (1.6a) and (1.6b) in preference to (1.7a) and (1.7b) may not be justified. Concern about the large systematic error possible in $\overline{v}'(\tau)$ in the case where the ultrasound beam is not as broad as the blood vessel, yet is assumed to be, then led to the development of an estimator of $\overline{v}(\tau)$ for the opposite limiting case, i.e. where the beam can be regarded as being of negligible width and directed through the centre of the vessel, as is assumed in the multigate method. The definition and justification of this estimator, valid when the instantaneous velocity profile is unidirectional and also satisfies other certain assumptions, is the basic result presented in this thesis. The properties of this estimator are also examined, and compared with those of the estimator that is valid when the beam does insonate each part of the cross section equally. Such comparison might tend to promote the view that these estimators are alternatives, to be chosen between. However it is important to realise that the different estimators, which can both be evaluated from the same spectrum, are valid under different assumptions about the beam. So choice exists primarily in the selection of the beam used for insonation, and not in the way that the resulting Doppler spectrum is processed for velocity information.

## Thesis structure

Both estimators are defined in chapter 2, where particular attention is given to the justification of the new result. Chapter 3 summarises many of the reasons why these estimators of mean velocity may be in error, and proposes a simple well-known model of a velocity profile for the quantification of these errors. The sources of error are addressed in no particular order in chapters 4 to 10. In chapter 11 the definition of the new estimator is generalised to be valid when there is a certain form of mixed flow, i.e. where flow in both the forward and reverse directions occur simutaneously. Chapter 12 returns the focus to the basic problem of volumetric flow measurement. The more general form of the estimator is applied to this problem at various sites of the body, i.e. with flows with differing degrees of pulsatility. In chapter 13, as a conclusion to the main work, the errors in the use of the two estimators for volumetric flow are summarised and compared by considering an example case. Appendix A gives a brief description of a system designed for the original task of flow estimation taking into account fluctuations in vessel diameter. Associated problems are raised and relevant conclusions are stated. Appendices B and C focus on the effect on the new estimator of idealised departures from the assumed nature of the velocity profile, and appendix D discusses measurement of mean velocity when the velocity distribution changes within the period of recording of the Doppler signal. Finally appendices E and F give proofs of the results which are stated without the necessary justification in the main text.

## Notation for this chapter

| | |
|---|---|
| $A(\tau), A'(\tau)$ | instantaneous cross-sectional area of blood vessel, and its estimate |
| $A''$ | single estimate of cross-sectional area |
| $D_{ave}$ | time-averaged internal diameter of blood vessel |
| $\bar{f}(\tau)$ | 'instantaneous' mean Doppler shift frequency |
| $Q(\tau), Q'(\tau)$ | instantaneous volumetric flow rate, and its estimate |
| $Q_{ave}$ , $Q'_{ave}$ | average volumetric flow rate in one cardiac cycle, and its estimate |
| $R(\tau), R'(\tau)$ | instantaneous internal radius of blood vessel, and its estimate |
| $R''$ | single estimate of internal radius |
| $T$ | period of cardiac cycle |
| $\overline{v}(\tau), \overline{v}'(\tau)$ | instantaneous spatial mean velocity, and its estimate |

# CHAPTER 2 - A NEW ESTIMATOR OF MEAN BLOOD VELOCITY

It has already been seen that the Doppler principle allows the determination of the velocities present in a sample of flowing blood from the received shifts in frequency of the scattered beam. The velocity of each scatterer in question is the component of its velocity in a direction a known angle, $\theta$, from the insonating beam. In particular, if the intensity of the received signal in a given frequency range is assumed to be proportional to the amount of blood travelling in the corresponding velocity range, the spatial mean velocity can be estimated by evaluating the intensity weighted mean frequency (IWMF) of the returning Doppler signal. The evaluation of this frequency, denoted by $\bar{f}$ in chapter 1, is the basis for the estimation of mean blood velocity with many types of commercial ultrasound scanners. A major factor in the accuracy of this estimate is the degree to which the whole cross section of the vessel can be regarded as being insonated uniformly by the ultrasound beam (Evans 1982a)(Gill 1982). The sample volume is defined laterally by the Doppler beam dimensions and axially by electronic gating of the received signal. For accurate measurement of the spatial mean velocity this volume should extend across the entire oblique cross section of the vessel. More specifically the calculated IWMF statistic is only valid if the Doppler beam transmission and reception profile is uniform throughout this cross section. In practice this is often not the case, and scatterers at the lateral periphery are given less weighting than the scatterers in the centre of the vessel. For flow where the blood particles move more quickly nearer the centre of the vessel the resulting estimate of mean velocity is higher than the true value. This problem is particularly relevant in the case of duplex scanning if the transducer uses the same crystals to transmit the beams for both imaging and Doppler operations. The optimum image of the vessel is obtained with a narrow beam, yet the optimum Doppler beam is broad.

Some work has been performed to derive the errors associated with the IWMF statistic for various ultrasound beam shapes and positions. Using parabolic flow and beams with a rectangular or Bessel function shape, Gill (1982) considered the errors for short and long sample volumes and various beamwidths and angles of incidence. Among his conclusions were that of the possible causes of non-uniform insonation "the most significant potential source of error remains the variation of the weighting factor ... across the ultrasound beam", where this factor is a function of the beam intensity profile and the sensitivity pattern of the receiver. Cobbold et al. (1983), using computer simulation, investigated the effect of a rectangular or Gaussian shaped Doppler beam being displaced from the centre of the vessel, and suggested that "when the beam width is roughly equal to the vessel diameter the estimated mean velocity is not a sensitive function of beam profile and position". Evans (1982a, 1985) calculated the amount of error for centrally placed beams with rectangular profiles of various widths and with plug (i.e. uniform across the vessel) and parabolic

velocity profiles. For a parabolic velocity profile the maximum overestimate could be 33% of the true value, occurring when the beam is of infinitesimal width, and was in the range of 30-33 % for beamwidths less than a quarter of the diameter.

The errors involved if IWMF is used when the beam does not provide uniform insonation are therefore considerable. In this chapter an alternative statistic is derived for the estimation of instantantaneous spatial mean velocity when it can be assumed that the sample volume is infinitely thin, i.e. of negligible width compared to the vessel diameter. In this case knowledge of the velocity profile can, under other assumptions, be inferred from the Doppler signal power spectrum, enabling the true mean velocity to be calculated. It is suggested that in practice, with the larger blood vessels, such an assumption of negligible beamwidth may be more appropriate than the assumption of uniform insonation.

## Discrete spectral analysis

The derivation of the mean velocity from the spectrum makes use of the principles that the mean intensity of a reflected wave is theoretically proportional to the number of scatterers and the Doppler shift frequency is proportional to the scatterer velocity. So, as mentioned in chapter 1, the continuous Doppler signal spectrum is equivalent, apart from constant scale factors, to the velocity distribution of scatterers in the sample volume. In the typical case spectral analysis yields a discrete frequency spectrum. Consider a frequency range comprising IMAX+1 frequency bins of equal width, with each bin containing the intensity of the appropriate fraction of the Doppler signal. The bins are numbered 0-IMAX and represent a range of positive frequencies (velocities). The bin numbered by the generalised index $i$ is referred to as the $i$'th bin, and the zero frequency point corresponds to the centre of the zero'th bin. This configuration is shown in fig.2.1a.

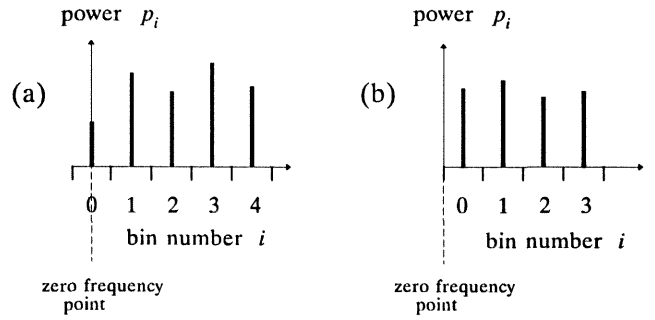


**Fig.2.1 - possible configurations of frequency bins in spectral analysis**

The description of the available frequencies after spectral analysis as 'bins' can be misleading. For example, analysis by Discrete (or Fast) Fourier Transform represents the signal as the sum of component 'spikes' at well defined and equally spaced single frequencies, as suggested in fig.2.1. It is not true to say that all the power at any one frequency in the continuous spectrum contributes to the power of the nearest spike. Rather each signal frequency is leaked into a number of adjacent spikes. This leakage can be regarded as small if there are a large number of spikes. The terminology 'bin' for a spike is used to convey the idea that the power in any spike is primarily due to signal frequencies nearest that spike frequency. Hence the powers recorded are thought of as being the powers in the signal frequencies in well-defined and non-overlapping bands.

The random nature of the Doppler signal, and the finite length of the data segment used to produce these spectral estimates, dictate that the observed powers in the bins after spectral analysis, denoted by $p_i$ and shown in fig.2.1, are random estimates of their expected values. These expected values would be the powers observed if the signal remained stationary and could be sampled for an infinite duration. They are denoted by $\tilde{p}_i \equiv E[p_i]$, where $E[\ ]$ is the expectation operator. For brevity the tilde notation is used throughout to denote such an expected value.

So if the signal was deterministic, i.e. if there was no random element, then the *i*'th bin would contain the power, $\tilde{p}_i$ , present in the Doppler signal in the frequencies corresponding to that bin. Such a $\tilde{p}_i$ value is therefore proportional to the volume of blood moving with velocities corresponding to the *i*'th frequency bin.

## Mean velocity estimation with a uniformly insonating beam

In this section a conventional statistic for mean blood velocity estimation is presented. This statistic is that appropriate for the case where the sample volume is assumed to be representative of the whole cross section, for example when the intensity of the insonating beam is uniform throughout the cross section. It is helpful to refer throughout this thesis to such a uniformly insonating beam as being 'wide'. The relevant quantity is the deterministic value of the intensity weighted mean bin number (IWMB). This is the discrete form of the IWMF, $\bar{f}$, already mentioned. It is calculated by weighting each bin only by its intensity (or power, i.e. the contents of the bin), and is defined by

$$\overline{B}_D = \frac{\sum_{i=0}^{\mathrm{IMAX}} i\,\tilde{p}_i}{\sum_{i=0}^{\mathrm{IMAX}} \tilde{p}_i} \qquad (2.1a)$$

where the subscript $D$ denotes that the contributing powers are the deterministic, i.e. expected, quantities $\tilde{p}_i$ . This is proportional to the mean velocity because the $i$ values are proportional to frequency and hence to velocity, and, under the 'wide' beam assumption, the corresponding $\tilde{p}_i$ values are proportional to the number of red blood cells travelling with these velocities. As mentioned earlier this statistic generally gives an overestimate of the true mean frequency if insonation is not uniform. A simple known linear relationship exists between frequency and bin number, so that the IWMF can be found from the IWMB.

In practice these $\tilde{p}_i$ values are not available, and are replaced by the observed values $p_i$. The observed IWMB statistic, denoted by $\overline{B}$, is then defined by

$$\overline{B} = \frac{\sum_{i=0}^{\mathrm{IMAX}} i\, p_i}{\sum_{i=0}^{\mathrm{IMAX}} p_i} \qquad (2.1b)$$

This statistic is presented for comparison with the new statistic described in the following paragraphs. This new statistic is the main subject of this thesis.

## Mean velocity estimation with a narrow beam

An alternative estimate of mean frequency is a 'position and intensity weighted mean frequency' (PIWMF). Under some assumptions about the velocity profile, this estimate is appropriate if the beam can be assumed to be of constant negligible width compared to the diameter of the vessel, and is positioned through the vessel axis. The estimate effectively takes into account the different proportions of scatterers at different radial positions insonated by such a beam. The calculation is made by weighting each frequency bin according to its intensity and calculated position from the vessel axis.

*Model geometry and assumptions*

Relevant geometry for the derivation of the new statistic is shown in figs.2.2a and 2.2b. Fig.2.2a shows the longitudinal view of the vessel with the narrow sample volume extending across the vessel at the Doppler angle, $\theta$. The central dashed line lies on a plane which is perpendicular to the vessel axis and contains the point where the sample volume intersects the vessel axis. Fig.2.2b gives the projection of the sample volume onto that plane, showing the sample volume of constant negligible beamwidth across the centre of the vessel cross section, which is assumed to be circular with internal radius $R$. The quantity $x$ is a measure of the projection onto this plane of the distance along the sample volume from its centre.

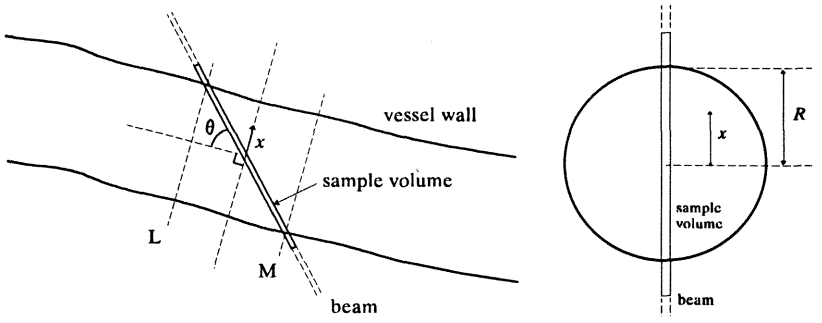


**Fig.2.2a,b - geometry of the insonation of a blood vessel by a thin Doppler beam**

If the velocity profile can be regarded as being axi-symmetric, and is known along a diameter, then the true mean flow can be found. This velocity profile can be found from the spectral analysis of the Doppler signal if it is further assumed that -

(i) each half of the velocity profile is a monotonic increasing function of distance from the vessel wall. An example of a profile satisfying this condition is shown in fig.2.3. The velocity $v$ increases monotonically from zero at the vessel walls (at $x = R$ and $x = -R$) to a maximum value $v_m$ at the vessel axis. It is not necessary for the profile to be strictly monotonic increasing, i.e. points in the profile of zero gradient are permissible.

(ii) the Doppler beam dimensions are constant along the sample volume,

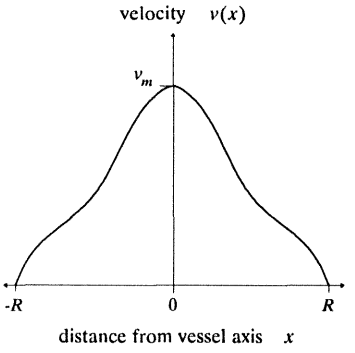


**Fig.2.3 - an axi-symmetric monotonic velocity profile**

(iii) the sample volume can be thought of as being infinitely thin so that all scatterers a given distance **along** the sample volume have the same velocity,

(iv) the length, and position in depth, of the sample volume are sufficient for its projection to extend over a diameter of the cross section,

(v) the beam is directed through the centre of the vessel,

(vi) the velocity profile can be regarded as being constant with axial position throughout the angled sample volume, i.e. constant between lines L and M on fig.2.2a,

(vii) the concentration of scatterers throughout the sample volume is constant, and

(viii) the 'cross section' of the scatterers presented to the beam is independent of their velocity. These last two assumptions mean that the mean power in the Doppler signal received from scatterers in any given volume, within the sample volume, can be regarded as being proportional to that volume, and is independent of the velocities in that volume.

The validity of these assumptions are discussed in chapter 3. The errors caused by the failure of such assumptions are the subjects of following chapters. A by-product of assumption (vi) is that in the development of the results in this thesis the sample volume can be treated as lying in the plane in which $x$ is defined, as suggested in fig.2.2b.

It is helpful to refer throughout this thesis to a beam which is infinitely thin *and directed through the vessel axis* as being 'thin'.

It should be noted that assumptions (iv), (vi) and (viii) are necessary for an estimate of mean velocity to be made if alternatively a 'wide' beam is assumed. Assumption (vii) is also necessary if 'mean red cell velocity' is to be interpreted as 'mean blood velocity'. Also a weakened form of assumption (ii) is necessary, namely that the beam dimensions in the direction parallel to the vessel axis remain constant throughout the sample volume. The absence of variation in this direction, together with assumption (vi), allows the dimension *into* the page of fig.2.2b to be ignored, and so with either a 'thin' beam or a 'wide' beam the situation can be treated as two dimensional.

*Estimation of the velocity profile*

The index of the bin 'containing' the maximum velocity, $v_m$, is denoted by $H$, where clearly $H \leq \mathrm{IMAX}$. This is the highest frequency bin with non-zero contents (power), so that $\tilde{p}_i = 0$ for $i > H$. So $\tilde{p}_H$ is a proportional measure of the fraction of the sample volume occupied by scatterers in the highest velocity group. Given that the velocity profile along

the diameter is symmetric and monotonic this group of $\tilde{p}_H$ scatterers must occupy the central section in the sample volume. As a negligible beamwidth is assumed this section is 'rectangular'. The limits of this central section are denoted by $x = s_H$ and $x = -s_H$ as shown in fig.2.4. Similarly the group of $\tilde{p}_{H-1}$ scatterers with the next highest velocity can be thought of as occupying the space in the sample volume from $s_H$ to $s_{H-1}$ and $-s_H$ to $-s_{H-1}$. The profile is symmetric by assumption so it is sufficient to consider only the positive $x$ values, i.e. $s_H$, $s_{H-1}$ etc.

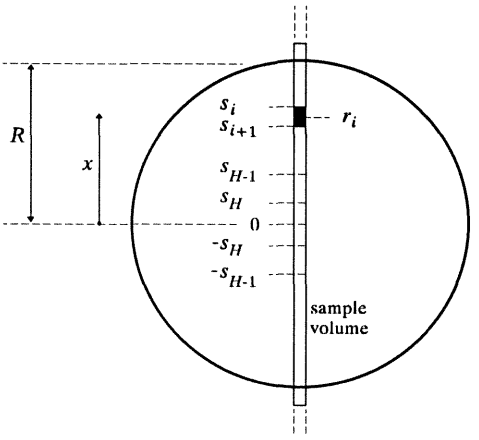


**Fig.2.4 - the regions of the sample volume occupied by scatterers of different bins**

A constant beam shape along the sample volume is assumed so that a constant of proportonality $k$ can be introduced such that

$$
\begin{aligned}
s_H &= k\,\tilde{p}_H \\
s_{H\text{-}1} &= k\left(\tilde{p}_H + \tilde{p}_{H\text{-}1}\right) \\
s_{H\text{-}2} &= k\left(\tilde{p}_H + \tilde{p}_{H\text{-}1} + \tilde{p}_{H\text{-}2}\right) \\
&\vdots
\end{aligned}
$$

or

$$s_i = k \sum_{j=i}^{H} \tilde{p}_j \qquad 0 \le i \le H$$

As the bins above $H$ are empty of power this can more generally be written as

$$s_i = k \sum_{j=i}^{\mathrm{IMAX}} \tilde{p}_j \qquad 0 \le i \le \mathrm{IMAX}$$

which defines $s_i = 0$ for all bins above $H$.

The total mean power in the Doppler signal is denoted by $\tilde{P}$, and so for this single-sided spectrum is

$$\tilde{P} = \sum_{i=0}^{\text{IMAX}} \tilde{p}_i \tag{2.2}$$

The quantity $s_0$ must be equal to the radius $R$, so that the constant $k$ can be identified, and

$$s_i = \frac{R}{\tilde{P}} \sum_{j=i}^{\text{IMAX}} \tilde{p}_j \qquad 0 \le i \le \text{IMAX} \tag{2.3}$$

It is appropriate also to define $s_{\text{IMAX}+1} = 0$ as this represents the inner extent of the area occupied by scatterers of the IMAX'th bin, if they exist, which must be the very centre of the vessel. The relationship between these $s_i$ values, the velocity (i.e. frequency) profile and the frequency bins can be seen in fig.2.5.

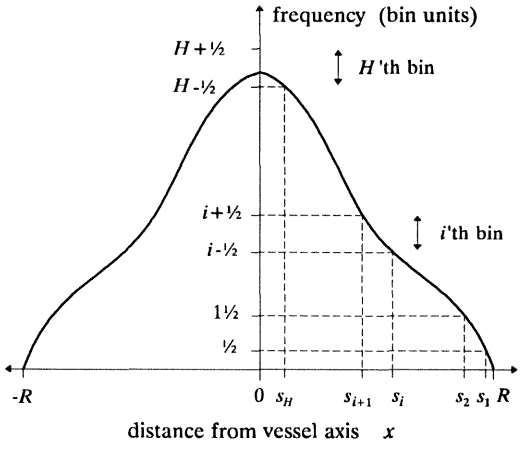


**Fig.2.5 - division of the velocity (frequency) profile into bins**

The velocity corresponding to the $i$'th bin is deemed to be the average velocity of the scatterers bounded by the positions $s_i$ and $s_{i+1}$. An appropriate position for this velocity is the centre of this region. If this midpoint is called $r_i$ then

$$r_i = \frac{s_i + s_{i+1}}{2} \qquad 0 \le i \le \text{IMAX} \tag{2.4}$$

which in combination with (2.3) leads simply to

$$r_i = \frac{R}{\tilde{P}} \left( \sum_{j=i+1}^{\text{IMAX}} \tilde{p}_j + \frac{\tilde{p}_i}{2} \right) \qquad 0 \le i \le \text{IMAX} \tag{2.5}$$

This equation gives a radial distance from the centre of the vessel for the blood cells travelling with the velocity corresponding to the *i*'th bin, and therefore represents the inverse of the velocity profile. If the number of bins is increased without limit, and their widths similarly reduced, then (2.5) becomes the equation for the inverse of the velocity profile, $v(x)$, in the case of a continuous spectrum, i.e.

$$x(v) = \frac{R}{\tilde{P}} \int_{f(v)}^{f_m} p(u)du$$

where $f$ is related to $v$, and $f_m$ to $v_m$, by the Doppler equation (1.2), $u$ is a dummy variable and $\tilde{P}$ can be thought of now as the total power in the continuous spectrum.

*Calculation of the mean velocity estimator*

The correct representative frequency in bin units can be expressed in a form similar to that of (2.1a), i.e. as a normalised sum of terms from each bin. With reference to fig.2.4, the scatterers with velocities in the range corresponding to the *i*'th bin will occupy a ring bounded by the radial distances $x = s_i$ and $x = s_{i+1}$ with an area equal to $\pi\left(s_i^2 - s_{i+1}^2\right)$. As a constant density of scatterers is assumed throughout the cross section the weight given to the *i*'th velocity bin should be the area of this ring. With the factor $\pi$ cancelling from both numerator and normalizing denominator this weight is $\left(s_i^2 - s_{i+1}^2\right)$. The mean frequency in bin units over the whole cross section, is then given by

$$\text{mean frequency in bin units} = \frac{\sum_{i=0}^{H} i'(s_i^2 - s_{i+1}^2)}{\sum_{i=0}^{H}(s_i^2 - s_{i+1}^2)} = \frac{\sum_{i=0}^{\text{IMAX}} i'(s_i^2 - s_{i+1}^2)}{\sum_{i=0}^{\text{IMAX}}(s_i^2 - s_{i+1}^2)} \qquad (2.6)$$

where nothing is added to either numerator or denominator in extending the summations to the index IMAX. The quantity $i'$ is the frequency, expressed in bin units, corresponding to the mean velocity of the scatterers in the ring bounded by $s_i$ and $s_{i+1}$, whereas the quantity $i$ has been assumed to correspond to the mean velocity in the *section* of the ring intersecting the sample volume. If all the scatterers in the *i*'th ring actually had the minimum possible velocity, i.e. giving a Doppler frequency of $i$-½, then $i'$ would be equal to $i$-½. Alternatively the maximum possible value of $i'$ is $i$+½. These obviously represent extreme cases, corresponding to profiles with an unrealistic steplike nature. For normal spectra, when the contributions from all the bins are considered, the error in a mean frequency measurement due to this frequency quantization will be considerably less than ±½ a bin

width, and will approach zero as the number of bins increases, i.e. as the frequency resolution is improved.

In general $i'$ will be slightly less than $i$. This is because, under the monotonic profile assumption, the lower velocity scatterers in the ring bounded by $s_i$ and $s_{i+1}$ are those which are further from the centre and occupying laminae with larger circumferences. These therefore are under-represented in the section of the sample volume between $s_i$ and $s_{i+1}$.

It is helpful to clarify terminology. The 'bin number' of the $i$'th bin is $i$, and is of course an integer. The 'mean bin number' will in general be fractional. The 'mean frequency in bin units' for the scatterers in the $i$'th ring, $i'$, is fractional and hence is not equal to $i$ as shown above, and consequently the 'mean frequency in bin units' over all or a subset of the cross section is also fractional.

The quantity $i'$ is approximately equal to $i$ so that the weighted mean frequency in bin units given by (2.6) is approximated by the deterministic form of the 'position and intensity weighted mean bin number' (PIWMB), denoted by $\hat{B}_D$. Substituting $i$ for $i'$ and recognising that the denominator of (2.6) is the square of the radius gives

$$\hat{B}_D = \frac{\sum_{i=0}^{IMAX} i\,(s_i^2 - s_{i+1}^2)}{R^2} \tag{2.7}$$

From (2.3) it can be seen that

$$s_i - s_{i+1} = \frac{R}{\tilde{P}} \cdot \tilde{P}_i$$

and from the definition of $r_i$ in (2.4)

$$s_i + s_{i+1} = 2r_i$$

Therefore factorising the difference of squares in (2.7) gives

$$\hat{B}_D = \frac{2\sum_{i=0}^{IMAX} i\,\tilde{P}_i\left(r_i/R\right)}{\tilde{P}} \tag{2.8}$$

The $i$'th bin is seen to be weighted according to both its intensity and position, as suggested in the title PIWMB. Remembering that $\tilde{P}$ is defined by (2.2), it can be seen that equation (2.8) for PIWMB is therefore the same as (2.1a) for IWMB except that each term

in the summation is additionally weighted by a dimensionless factor which is, from (2.5)

$$\frac{2r_i}{R} = \frac{2\sum_{j=i+1}^{IMAX} \tilde{p}_j + \tilde{p}_i}{\tilde{P}}$$

The velocity profile information discussed earlier is present implicitly in this term. It is seen that no estimate of the vessel radius is required. Making use of the definition of the total power, $\tilde{P}$, in (2.2) gives the definition of the deterministic PIWMB

$$\hat{B}_D = \frac{\sum_{i=0}^{IMAX} i\,\tilde{p}_i \left( 2\sum_{j=i+1}^{IMAX} \tilde{p}_j + \tilde{p}_i \right)}{\left( \sum_{i=0}^{IMAX} \tilde{p}_i \right)^2} \qquad \text{(2.9a)}$$

The PIWMB observed in practice is denoted by $\hat{B}$ and is therefore

$$\hat{B} = \frac{\sum_{i=0}^{IMAX} i\,p_i \left( 2\sum_{j=i+1}^{IMAX} p_j + p_i \right)}{\left( \sum_{i=0}^{IMAX} p_i \right)^2} \qquad \text{(2.9b)}$$

This equation therefore allows the estimation of the weighted mean bin number, and hence the mean velocity, correct for the 'thin' beam insonation, from the IMAX+1 length array of bin contents given by $p_i$. It is valid no matter how the spectral estimation is performed, as long as the spectral power estimates are an array of numbers from equally spaced frequency bins. Note that if the $p_i$ values are whole numbers then both the numerator and denominator of (2.9b) can be found using integer arithmetic.

If the bracketed term in the numerator is called $q_i$, that is

$$q_i = \left( 2\sum_{j=i+1}^{IMAX} p_j + p_i \right)$$

then a useful form for computation is

$$\hat{B} = \frac{\sum_{i=0}^{IMAX} i\, p_i\, q_i}{\left(\sum_{i=0}^{IMAX} p_i\right)^2}$$

where

$$q_{IMAX} = p_{IMAX} \qquad \text{and recursively} \qquad q_{i-1} = q_i + p_{i-1} + p_i$$

so that $\hat{B}$ is most easily computed by summing from the IMAX'th bin to the zero'th bin.

## Continuous forms

It is possible to define integral forms of the 'discrete' statistics $\overline{B}_D$ and $\hat{B}_D$. These are their limiting forms as the number of frequency bins increases indefinitely, expressed in terms of frequency. The 'wide' beam estimator is the IWMF, $\bar{f}$, discussed above. This is familiar (Arts and Roevros 1972)(Gerzberg and Meindl 1977) (Gill 1979) and for this single-sided spectrum is defined by

$$\bar{f} = \frac{\int_0^\infty f.p(f)df}{\int_0^\infty p(f)df} \tag{2.10}$$

The 'thin' beam estimator is the position and intensity weighted mean frequency, PIWMF, mentioned earlier, which is denoted by $\hat{f}$ and defined by

$$\hat{f} = \frac{2\int_0^\infty f.p(f)\left(\int_f^\infty p(u)du\right)df}{\left(\int_0^\infty p(f)df\right)^2} \tag{2.11}$$

where $u$ is a dummy variable. This equation follows from (2.9a) by noting that as the number of bins increases the '$+\tilde{p}_i$' in each of the terms of the numerator becomes negligible,

unless a finite proportion of the total power is contained in the corresponding single frequency component, i.e. unless the spectrum contains a delta function at the frequency corresponding to the *i*'th bin.

Equation (2.11) is therefore readily acceptable in the practical case where the spectrum does not contain any delta functions, but might be thought ambiguous and problematic in the mathematical case where a delta function is present. That is, the meaning of the term in the numerator

$$\int_f^\infty p(u)\,du$$

when the spectrum contains a delta function at $f$ might appear to be ambiguous. The problem can be addressed by considering the related question - "What is the value of the quantity

$$\int_{x_0}^\infty g(x)\,dx$$

when the function $g(x)$ is a delta function with value 1 at the limit of integration $x_0$ ? " The answer by convention is ½ , which is a sensible answer as by symmetry

$$\int_{-\infty}^{x_0} g(x)\,dx$$

should also be equal to ½ . When the integral form (2.11) is related to the discrete form (2.9a) this value of ½ expresses the fact that the '$+\tilde{p}_i$' terms in the numerator of (2.9a) are not multiplied by the factor of 2 applicable to the $\overline{p}_j$ terms. The result is that (2.11) is a valid formula for PIWMF even in the case where delta functions are present.

The same considerations apply to the integral equations (11.8) and (E.10) introduced in chapter 11 and appendix E respectively, although this is not discussed in those chapters.

Equations (2.10) and (2.11) for IWMF and PIWMF make use of the power spectrum $p(f)$, which corresponds to the deterministic $\tilde{p}_i$ values. These expressions are widely used in some of the following chapters where the random nature of the finite-length segment of the Doppler signal is not considered.

## Bounds on PIWMB

The work of chapter 10 shows that an expected power of zero implies an observed power of zero, and a finite expected power implies a finite observed power. The converses of these statements can also be regarded as true if the dynamic range of recording is adequate. So $H$ can be redefined without inconsistency as the index of the highest bin with non-zero *observed* power, i.e. $p_H \neq 0$ and $p_i = 0$ for $i > H$. It is shown in appendix E that, in relation to IWMB and this bin number $H$, PIWMB is bound by

$$\frac{\overline{B}^2}{H} \leq \hat{B} \leq \overline{B} \tag{2.12}$$

where the deterministic quantities $\overline{B}_D$ and $\hat{B}_D$ can be inserted instead. That the value of IWMB is an upper bound for PIWMB is evident from the fact that PIWMB, in assuming that the profile is monotonic, weights the low frequency components more, i.e. those from the scatterers in laminae of large circumference near the vessel walls. In addition, the ratio $\hat{B}/\overline{B}$ can be made as close to zero as required by defining an idealised signal with a very large power in the zero'th bin, a small power in the $H$'th bin, and all other bins empty. So the ratio of the estimators might be as high as 1 or, in extreme cases, as low as zero.

Analogously, as the Doppler shift frequencies from this flow are defined to be positive, the PIWMF is bound in relation to IWMF and the highest signal frequency, $f_{\max}$ , by

$$\frac{\bar{f}^2}{f_{\max}} \leq \hat{f} \leq \bar{f} \tag{2.13}$$

and the ratio $\hat{f}/\bar{f}$ might be as high as 1 or as low as zero.

## The correction for the continuous monotonic profile

The derivation of the definition of PIWMB was made by substituting $i$ for the correct value $i'$ in (2.6). Because in general $i' \leq i$, PIWMB as defined by (2.9a) is too high. If the profile can be approximated as a continuous series of line segments where the vertices are at the edges of the bins, and where the frequency is $i - \frac{1}{2}$ when the radial distance is $s_i$ , as shown in fig.2.6, then a close approximation to the correct estimator is

$$\text{PIWMB} = \hat{B}_D - \frac{1}{6} \sum_{i=0}^{\text{IMAX}} \frac{\tilde{p}_i^2}{\tilde{P}^2} \tag{2.14}$$

where $\hat{B}_D$ is given by (2.9a). The derivation of this result is given in appendix E. As expected the correction term is negative and approaches zero as the number of bins is increased. This can be seen by noting that, as there are $H+1$ non empty bins, $\tilde{p}_i^2/\tilde{P}^2$ is of the order of $1/H^2$ so that the summation is of the order of $1/H$. The expression of choice for the statistic PIWMB therefore remains (2.9b).

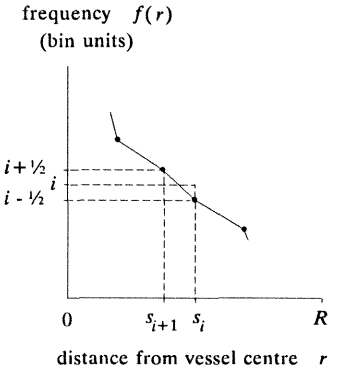


**Fig.2.6 - a piecewise linear model of a velocity (frequency) profile**

## An alternative frequency bin configuration

The expressions derived have been formulated for the case where the zero-frequency point is at the centre of the zero'th bin, as in fig.2.1a. For the case where the zero'th frequency bin is interpreted as corresponding entirely to positive frequencies, with its lower edge at zero, as shown in fig.2.1b, the result is that the estimator of mean velocity, say $\hat{\hat{B}}$, is

$$\hat{\hat{B}} = \frac{\sum_{i=0}^{IMAX} i\, p_i\, q_i}{\left(\sum_{i=0}^{IMAX} p_i\right)^2} + \frac{1}{2} \qquad (2.15)$$

A derivation of this result is given in appendix E. So PIWMB is shifted by the same magnitude as the origin of the frequency scale, which is not surprising because (2.9b) is linear in the frequency variable $i$.

## Summary

The estimator PIWMB defined by (2.9a) is proportional to spatial mean blood velocity if the Doppler beam is assumed to be of negligible thickness compared to the vessel diameter, and directed through the centre of the vessel, and the velocity profile is axi-symmetric and monotonic. This is an alternative statistic to IWMB which is the statistic valid where uniform insonation can be assumed, an assumption thought to be poorer in many real cases. The random nature of the Doppler signal means that the statistics observed in practice are found from spectral estimates which are stochastic. The observed form of PIWMB is thus defined by (2.9b). For a Doppler signal corresponding to only positive blood velocity components PIWMB is bound between zero and IWMB. PIWMF and IWMF are continuous frequency forms of these statistics derived from the underlying power spectrum.

When applied to bin numbers, $B$, and frequencies, $f$, the bar notation, e.g. $\overline{B}$, denotes an 'intensity weighted' quantity. The 'position and intensity weighted' quantities are denoted by the hat notation, e.g. $\hat{B}$.

The corresponding mean velocity estimates, $\overline{v}'$, are found using the inverted Doppler equation (1.3). If $\Delta f$ is the width in frequency of each bin, then for IWMB and PIWMB these are

$$\overline{v}' = \frac{c\,\Delta f}{2F\cos\theta}\cdot\overline{B} \qquad \text{and} \qquad \overline{v}' = \frac{c\,\Delta f}{2F\cos\theta}\cdot\hat{B}$$

and for IWMF and PIWMF these are

$$\overline{v}' = \frac{c}{2F\cos\theta}\cdot\bar{f} \qquad \text{and} \qquad \overline{v}' = \frac{c}{2F\cos\theta}\cdot\hat{f}$$

## Notation for this chapter

| | |
|---|---|
| $E[\ ]$ | expectation operator |
| $H$ | the index of the highest observed frequency bin with non-zero power |
| $i'$ | frequency equivalent to the mean velocity of scatterers in the ring corresponding to the $i$'th bin |
| $q_i$ | a convenient intermediate form of a partial sum of the spectral powers |
| $r_i$ | appropriate radial distance for the centre of the region of scatterers of the $i$'th bin with a 'thin' beam |
| $s_i$ | calculated extent of radial position of scatterers with velocities in the $i$'th bin and above with a 'thin' beam |
| $u$ | a dummy variable |
| $x$ | distance along the sample volume from the centre of the vessel |

# CHAPTER 3 - AN INTRODUCTION TO POSSIBLE ERRORS

This chapter presents a brief discussion of the assumptions made in chapter 2 in the derivations of IWMB and PIWMB as proportional estimators of mean blood velocity, and identifies associated and other possible sources of error. A standard family of velocity profiles is described for the quantitative error analysis performed in later chapters. The theoretical Doppler spectra corresponding to these velocity profiles are derived for both 'wide' and 'thin' beams, and the associated mean frequencies IWMF and PIWMF are established.

## Validity of assumptions

The failure of assumptions made in chapter 2 would generally lead to errors in IWMB and/or PIWMB. Assumptions made which are not the subjects of following chapters are briefly discussed here.

*Assumption (ii) - needed for PIWMB to be valid:*
*The Doppler beam dimensions are constant along the sample volume.*

The assumption of constant beam dimensions along the sample volume is most valid if the sample volume is small and positioned near the centre of the focal zone of the transducer. However this is compromised by the need for assumption (iv) to be satisfied, that the sample volume is longer than the vessel diameter, and can accomodate motion of the whole vessel in that dimension during the cardiac cycle. The necessity of this assumption is questionable given the fact that divergence of the beam away from a single focal point at the centre of the vessel would mean that more scatterers further from the centre would be insonated but each seemingly with proportionately less power. Thus the resulting spectrum would be the same as for a 'thin' beam. This raises the interesting possibility that PIWMB is valid for any shaped beam which is focused to a point at the centre of the vessel and is without sidelobes in the vessel cross section. This could be the subject of further study.

*Assumption (vi) - needed for either IWMB or PIWMB to be valid:*
*The velocity profile is constant over the relevant extent of the angled sample volume.*

This assumption treats the intersecting volume of the beam and vessel as being representative of a cross section perpendicular to the vessel axis if the beam is 'wide', and as being representative of a diameter if the beam is 'thin'. The mean velocity through this cross section is then recoverable from the signal. This may not be justified near a stenosis owing to turbulence both upstream and downstream from the narrowing. The need for the sample volume to be at an angle to the cross section means that the mean spatial velocity is more properly being measured in a cylinder in the vessel and not through a cross section.

On fig.2.2a the ends of this cyclinder are the cross sections at the points L and M. The output is then equivalent to the velocity waveform smoothed over the time required for the pressure wave to travel the distance between points L and M. This distance is of the order of millimetres, say 5 mm, and the velocity of the pressure wave might be 10 m/s. So the time difference between the phases of the cardiac cycle at the two points is of the order of 0.5 milliseconds. As spectral analysis by Fourier transform requires that the mean velocity is calculated over a period of time anyway, which is often of the order of 10 milliseconds duration, the effect of the separation of L and M is small.

*Assumption (vii) - needed for PIWMB to be valid:*
*The concentration of scatterers throughout the sample volume is constant.*

The validity of this assumption leads to the idea that the (mean) intensity of the reflected Doppler signal in a given frequency range is proportional to the **volume** of blood (red cells) travelling with a velocity in the corresponding range, as proposed by Shung et al. (1992). This is a modification of the more commonly stated idea that the (mean) intensity is proportional to the **number** of red cells with velocities in that range. For a given haematocrit these are equivalent. However the assumption of proportionality with number is less robust because it is known not to be valid where the haematocrit is not fixed. If the derivation of PIWMB in chapter 2 was made using the assumption of proportionality with number rather than with volume then this assumption of a constant concentration of scattering centres would still be needed, as the derivation of (2.3) would show.

*Assumption (viii) - needed for both IWMB and PIWMB to be valid:*
*The scattering cross section is constant throughout the sample volume.*

If low and high velocity blood components are to be weighted correctly then neither must be preferentially favoured by a larger scattering cross section. It has been suggested that red blood cells, which are not spherical but are disk like, may be aligned differently at different flow rates, so presenting different surfaces to the beam. However it would seem that if the scatterers are local fluctuations in red cell concentration, as in Angelsen's model (1980), this effect might not be relevant.

## Summary of sources of error

The usefulness of both IWMB and PIWMB is of course dependent on the accuracy of the spectral power estimates, $p_i$, as a description of the velocity distribution of scatterers in the supposed sample volume. Of course the same can be said about the spectrum from which these estimates are found, $p(f)$, and the validity of IWMF and PIWMF. Of fundamental importance is the accurate knowledge of the (representative) angle between

the ultrasound beam and the direction of the vessel axis enabling an accurate conversion from frequency to velocity. Even for a spectrum with the correct form, an error in the calculation of this angle will lead to an error in measured mean velocity for both IWMB and PIWMB. Angle measurement and the associated error are briefly discussed in chapter 4.

For the purposes of error analysis in the rest of the thesis, it is useful to denote by $p_s(f)$ the spectrum that does mirror exactly the form of the velocity distribution in the sample volume. (The subscript $S$ is introduced here to signify the theoretical, i.e. ideal, **signal**.) An example of such a spectrum has already been given in fig.1.3, where this notation $p_s(f)$ should now properly replace $p(f)$ in the labelling of the y-axis. In addition to angle measurement as a source of error, there are a number of reasons why the array of spectral estimates, $p_i$, might not be those that would be found from this theoretical signal $p_s(f)$, and so why IWMB and PIWMB might not lead to the correct measure of mean velocity.

(a) A source of error is the possible failure of assumptions made about the nature of the sample volume, i.e. the shape of the ultrasound beam. In particular IWMB will be in error if the beam does not uniformly insonate the vessel cross section, and PIWMB will be in error if the beam is not of negligible width compared to the vessel diameter (failure of assumption (iii)), or if the beam does not pass through the centre of the cross section (failure of assumption (v)). These effects are studied in chapters 5 and 6. Furthermore the finite dimensions of the transducer and target in practice mean that there is no unique Doppler angle operating in the generation of the spectrum, i.e. in the conversion from particle velocity to Doppler shift frequency. The result is that the observed spectrum is a broadened version of that which would be seen with the desired single Doppler angle. The results of this broadening are considered in chapter 7.

(b) Other errors may result from a corruption of the Doppler signal due to an external source. The presence of noise in the signal will alter both mean velocity estimates, and the use of a high-pass filter to remove the unwanted large amplitude signal from the pulsating vessel walls also has an effect. These sources of error are studied in chapters 8 and 9 respectively.

(c) Under the important assumptions (vii) and (viii) above, the *mean* spectral power in a frequency range is proportional to the amount of scatterers with velocities in the corresponding range. However both IWMB and PIWMB are calculated from powers which are random estimates, $p_i$ , of these mean values, $\tilde{p}_i$. Therefore both IWMB and PIWMB are liable to error due to statistical fluctuations. This is an important

consideration in assessing the accuracy of any velocity estimate, and is addressed in chapter 10.

(d) The 'thin' beam estimator PIWMB has been derived for the case of an axi-symmetric velocity profile which is monotonically increasing from the vessel wall to the vessel centre. The failure of one or both of these profile assumptions will introduce error in the resulting velocity estimate. Presupposed in assuming the axi-symmetric nature of the profile is the assumption that the cross section is circular. This is a common assumption in work of this type where the blood vessel is arterial. Symmetry of the profile about the vessel axis is most likely to exist if the site of investigation is far away from sites of curvature in the vessel and from vessel junctions. The effects of one form of asymmetry in the profile are discussed in appendix B. The assumption of monotonicity in assumption (i) is the most restrictive assumption, but will best be satisfied in the case of vessels feeding a low impedance vascular bed, e.g. the carotid or renal arteries. Effects of non-monotonicity are studied in appendix C, and in the context of volumetric flow and with real Doppler signals in chapter 12.

## Standard velocity profiles

In each of the cases (a)-(d) above the resulting error in mean velocity would seem to depend on the actual form and scale of the velocity profile. Therefore to quantify the error it is necessary to assume a profile with a well-defined form. A commonly used family (Gill 1979)(Roevros 1974)(Angelsen 1980)(Aldis and Thompson 1992) of axi-symmetric velocity profiles is given by

$$v = v_m\left(1-\left(\frac{r}{R}\right)^n\right) \tag{3.1}$$

Here the velocity $v$ at a distance $r$ from the centre of the vessel of radius $R$ decreases from the maximum velocity $v_m$ at the vessel centre to zero at the vessel wall. The shape of the profile is determined by the bluntness parameter $n$, as seen in fig.3.1, which shows the velocity profile for various values of $n$. When $n=2$ equation (3.1) describes a parabola corresponding to the theoretical steady profile of a Newtonian fluid observed in a rigid tube a long way from the entrance. A Newtonian fluid is one whose viscosity is independent of the velocity gradient. This 'parabolic' flow, which has already been mentioned in chapter 1, is sometimes called Poiseuille flow. When $n=\infty$ the velocity is $v_m$ at all points in the cross section. This 'plug' form, which has also been mentioned in chapter 1, represents the theoretical profile at the entrance to a tube which is narrow compared to the feeding reservoir.

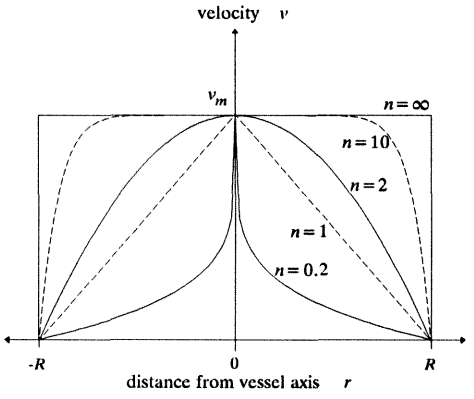


**Fig.3.1 - velocity profiles following equation (3.1)**

So if this equation is used to describe steady flow profiles in a vessel then values of $n \geq 2$ should be considered. Values of $0 < n < 2$ lead to profiles which are more peaked, as seen in fig.3.1, and lack physiological meaning in the context of steady flow.

The mean velocity throughout the cross section, $\bar{v}$, can by found by integrating the contributions of the lamina of circumference $2\pi r$ from 0 to $R$, and dividing by the total area. So

$$\bar{v} = \frac{\int_0^R 2\pi r\, v\, dr}{\pi R^2}$$

$$= \frac{v_m}{R^2}\int_0^R 2r\left(1-\frac{r^n}{R^n}\right)dr$$

$$= \frac{v_m}{R^2}\left[r^2 - \frac{2r^{n+2}}{(n+2)R^n}\right]_0^R$$

$$= \frac{v_m}{R^2}\left(R^2 - \frac{2}{(n+2)}R^2\right)$$

$$= \frac{n}{(n+2)}\cdot v_m \qquad (3.2)$$

which is a known result. So for parabolic flow, for example, the mean velocity is half the maximum, central velocity.

*Derivation of theoretical signal spectrum*

If the velocity profile and the shape and location of the insonating beam are known the associated theoretical Doppler power spectrum, $p_s(f)$, can be found. For any axi-symmetric profile $v(r)$ this ideal spectrum must be

$$p_s(f) \equiv \left| \frac{d\Phi_s(f)}{df} \right| = \left| \frac{d\Phi_s(f)}{dr} \cdot \frac{dr}{dv} \cdot \frac{dv}{df} \right| \tag{3.3}$$

where $\Phi_s(f)$ is the cumulative power. For a profile given by (3.1) rearranging for $r$ gives

$$r = R\left(1 - \frac{v}{v_m}\right)^{\frac{1}{n}}$$

so that

$$\left|\frac{dr}{dv}\right| = \frac{R}{n\, v_m}\left(1 - \frac{v}{v_m}\right)^{\frac{1}{n}-1} \qquad 0 \le v \le v_m$$

Furthermore the Doppler frequency $f$ is proportional to the scatterer velocity $v$ so that the quantity $|dv/df|$ is constant. The ratio $v/v_m$ can be replaced by $f/f_m$ where $f_m$ is the maximum frequency in the theoretical signal, i.e. the frequency corresponding to $v_m$.

The quantity $|d\Phi_s(f)/dr|$ depends on the shape of the insonating beam. For uniform insonation throughout the whole vessel each elemental ring of thickness $dr$ is fully insonated so that, because the density of scatterers is assumed to be constant, the incremental power $d\Phi_s(f)$ returning from such a ring a distance $r$ from the centre is such that $\left|d\Phi_s(f)/dr\right| \propto 2\pi r$. So from (3.3) the spectrum for a 'wide' beam is

$$\begin{aligned} p_s(f) &\propto 2\pi r \cdot \left|\frac{dr}{dv}\right| \\ &= 2\pi R\left(1 - \frac{v}{v_m}\right)^{\frac{1}{n}} \cdot \frac{R}{n v_m}\left(1 - \frac{v}{v_m}\right)^{\frac{1}{n}-1} \\ &\propto \frac{1}{n v_m}\left(1 - \frac{v}{v_m}\right)^{\frac{2}{n}-1} \qquad 0 \le v \le v_m \\ &\propto \frac{t}{f_m}\left(1 - \frac{f}{f_m}\right)^{t-1} \qquad 0 \le f \le f_m \end{aligned}$$

where $t \equiv 2/n$. However for a 'thin' beam the width of the sample volume at each point is uniform but negligible. Therefore $\left| d\Phi_S(f)/dr \right|$ is constant as scatterers are assumed to be equally spread in the sample volume. So for a 'thin' beam

$$\begin{aligned} p_S(f) &\propto \left|\frac{dr}{dv}\right| \\ &= \frac{R}{nv_m}\left(1-\frac{v}{v_m}\right)^{\frac{1}{n}-1} && 0 \le v \le v_m \\ &\propto \frac{t}{f_m}\left(1-\frac{f}{f_m}\right)^{t-1} && 0 \le f \le f_m \end{aligned}$$

where now $t \equiv 1/n$. This is the same equation as for the spectrum with a 'wide' beam but with a different definition of $t$. Obviously in both cases the spectrum is zero above $f_m$.

Letting the constant of proportionality be 1, putting $x = \left(1-\frac{f}{f_m}\right)$ so that $\frac{df}{dx} = -f_m$, and integrating between zero and the maximum frequency $f_m$ gives

$$\begin{aligned} \int_0^{f_m} p_S(f)df &= \int_0^{f_m} \frac{t}{f_m}\left(1-\frac{f}{f_m}\right)^{t-1} df \\ &= -t\int_1^0 x^{t-1}dx \\ &= t\left[\frac{x^t}{t}\right]_0^1 \\ &= 1 \end{aligned}$$

So the spectrum given by

$$p_S(f) = \frac{t}{f_m}\left(1-\frac{f}{f_m}\right)^{t-1} \qquad 0 \le f \le f_m \qquad (3.4)$$

is the theoretically observed spectrum if the velocity profile follows (3.1) and if the beam is 'wide' or 'thin', normalised to have a total power of 1. The form of the spectrum is defined by the parameter $t$. Note that for $t < 1$ the spectrum is undefined at $f = f_m$. For the 'wide' beam, i.e. where IWMF is appropriate, $t \equiv 2/n$ and the equation is well known (Gill 1979)(Roevros 1974)(Angelsen 1980)(Aldis and Thompson 1992). For the 'thin'

beam, i.e. where PIWMF is appropriate, $t \equiv 1/n$ . It is obviously helpful that the spectra derived for the 'wide' and 'thin' beams are defined by equations of the same family. As useful examples, the spectra for $t = 1$ (uniform spectrum, parabolic velocity profile with a 'wide' beam), $t = 0.5$ (parabolic profile with a 'thin' beam) and $t = 0$ (spike spectrum, plug profile for either beam) are given by the solid lines in fig.3.2.

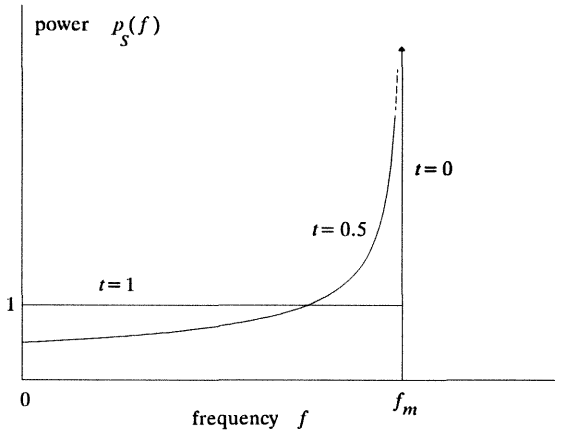


**Fig.3.2 - examples of spectra following equation (3.4)**

*Derivation of the corresponding mean frequencies*

The corresponding IWMF, $\bar{f}_S$ , can be found by substituting (3.4) into (2.10) and again using the substitution $x = 1 - f/f_m$ so that $f = f_m(1-x)$ and $df/dx = -f_m$ .

$$\begin{aligned}
\bar{f}_S &= \int_0^{f_m} f \frac{t}{f_m}\left(1 - f/f_m\right)^{t-1} df \\
&= -\int_1^0 f_m(1-x)\, t\, x^{t-1}\, dx \\
&= f_m\left[x^t - t \cdot \frac{x^{t+1}}{t+1}\right]_0^1 \\
&= f_m\left(1 - \frac{t}{t+1}\right) \\
&= \frac{f_m}{t+1}
\end{aligned}$$

(3.5)

Also the PIWMF, $\hat{f}_S$ , can be found by substituting (3.4) into (2.11), using the same substitution and also the substitution $y = 1 - u/f_m$ so that $du/dy = -f_m$

$$\begin{aligned}
\hat{f}_S &= 2\int_0^{f_m} f \frac{t}{f_m}\left(1 - f/f_m\right)^{t-1}\left[\int_f^{f_m} \frac{t}{f_m}\left(1 - f/f_m\right)^{t-1} du\right] df \\
&= -2\int_1^0 f_m(1-x)\, t\, x^{t-1}\left[-\int_x^0 t\, y^{t-1} dy\right] dx \\
&= 2\int_0^1 f_m(1-x)\, t\, x^{t-1}.x^t\, dx \\
&= 2f_m\left[\frac{x^{2t}}{2} - t\frac{x^{2t+1}}{2t+1}\right]_0^1 \\
&= f_m\left(1 - \frac{2t}{2t+1}\right) \\
&= \frac{f_m}{2t+1}
\end{aligned} \qquad (3.6)$$

Comparison of (3.5) and (3.6) for the same spectrum shows that $\hat{f}_S \le \bar{f}_S$ in agreement with (2.13), and that the difference between these frequencies is greater the higher the value of $t$, i.e. the more uniform the spectrum if we choose $t \le 1$. Substituting the definitions of $t$ for 'wide' and 'thin' beams into (3.5) and (3.6) leads to

$\bar{f}_S = \frac{n}{n+2} \cdot f_m$ with a 'wide' beam and $\hat{f}_S = \frac{n}{n+2} \cdot f_m$ with a 'thin' beam

which when compared with (3.2) confirm that if used with their appropriate beams IWMF and PIWMF estimate mean velocity accurately.

## Discussion and summary

These profiles, spectra and mean frequency results are used in the following chapters, which as outlined above describe the errors in the velocity estimates IWMB (IWMF) and PIWMB (PIWMF) from various sources. Generally only profiles with $n \ge 2$ are considered. However the case of the triangular profile given by $n = 1$ is also sometimes used with a 'thin' beam as then $t = 1$ and the spectrum has the mathematically attractive uniform nature. For simplicity each source of error is treated alone. It is not suggested that when two or more sources of error are present together the errors merely add. The

somewhat idealised nature of the velocity profiles described by (3.1) suggest that the individual results only approximate those that occur in practice anyway.

Some errors are systematic, and predictable if the form of the velocity profile is known, so that they might be corrected for. This is so for the error in IWMF if the beam is not 'wide' or the error in PIWMF if the beam is not 'thin' provided the beam profile and position, and the vessel radius, are known. This is also true for the error due to high-pass filtering in the reasonable case that the filter transfer function is known. Again, knowledge of the beam geometry and vessel orientation enables both the extent and location of the spectral broadening function to be known and so the error to be predicted. Other errors may also be systematic and repeatable so that they also do not cause problems in comparative studies, yet not be quantifiable. This is the case for the effect of noise in the Doppler signal, where though it may not be accurately known it is reasonable to assume that the noise level remains constant from one investigation to the next. A third type are random errors. These are unpredictable and show no consistency from investigation to investigation so, for a given level of accuracy, these errors are the most serious. Examples of these are the error caused by the random nature of the Doppler signal, the error due to misalignment of the beam, and the error due to failure to accurately measure the representative Doppler angle.

It may be helpful to recap the use of notation at this point, notation which is used consistently in the following chapters. The spectrum with a form that follows exactly the velocity distribution of scatterers in the sample volume is given by $p_s(f)$. It has a maximum frequency of $f_m$, which corresponds to the greatest velocity, $v_m$, of particles in the sample volume. Therefore using the IWMF or PIWMF of this spectrum, together with its appropriate beam, leads to the correct calculation of spatial mean blood velocity through the cross section. This IWMF and PIWMF are denoted by $\bar{f}_s$ and $\hat{f}_s$ respectively. If the profile has the form of (3.1) then $p_s(f)$ is given by (3.4) , $\bar{f}_s$ by (3.5) and $\hat{f}_s$ by (3.6). The observed spectrum however is denoted by $p(f)$, and has a maximum frequency of $f_{\max}$ . This is also a deterministic spectrum as the finite duration of the practical data segment (leading to random spectral estimates) is ignored. The observed IWMF is denoted by $\bar{f}$ and is defined by (2.10). The observed PIWMF is denoted by $\hat{f}$ and is defined by (2.11). Many of the following chapters are therefore concerned with the relationships between the observed frequencies, $\bar{f}$ and $\hat{f}$, and the desired frequencies $\bar{f}_s$ and $\hat{f}_s$ . First however is a short treatment of the important question of angle measurement.

## Notation for this chapter

$\Phi_s(f)$ cumulative power in the theoretical Doppler signal

# CHAPTER 4 - MEASUREMENT OF THE DOPPLER ANGLE

Although in this thesis it is discussed relatively briefly, angle measurement is considered before other potential sources of error because it is needed for the conversion of frequency to velocity, and so is fundamental to velocity measurement by ultrasound. The principles of this short chapter are therefore applicable to both IWMB and PIWMB, and indeed to any form of velocity estimator derived from the Doppler spectrum. A given error in angle will produce the same fractional error in IWMB and PIWMB, so that in placing these estimators alongside each other, which is a major theme of this thesis, little is gained by too detailed a study of angle measurement.

The need to measure the Doppler angle, $\theta$, is clear when a velocity $v$ is to be recovered from a frequency $f$ via the equation

$$v \approx \frac{c f}{2F \cos\theta} \tag{4.1}$$

Again $c$ is the speed of sound, and $F$ the transmit frequency. This is the inverted form of the basic Doppler equation, and has already been presented as equation (1.3).

## Sensitivity to error

It is desirable that the Doppler angle should be low, because a given error in the measurement of an angle affects the cosine less when the angle itself is smaller. This follows from noting that the derivative of $\cos\theta$ is $-\sin\theta$, so that

$$\cos(\theta+\xi) \approx \cos\theta - \xi \sin\theta$$

where $\xi$ is a small unknown error in angle, measured in radians. The resulting error in the cosine is proportional to $\sin\theta$ and so is small when $\theta$ is small. This principle is demonstrated graphically in fig.4.1, which is based on a diagram given by Evans et al. (1989) and shows errors in measured velocity if the Doppler angle is overestimated by a small amount. Very similar but opposite errors are appropriate if the error in the angle is negative.

For Doppler angles between the typical values of $\pi/6$ and $\pi/3$, i.e. 30° and 60°, the percentage error is approximately proportional to $\xi$ and can be found from

$$E \approx \xi \times \left(1.15 + 2.4\left(\theta - \tfrac{\pi}{4}\right)\right) \times 100\% \qquad \text{or equivalently} \qquad E \approx \xi_d \times \left(2 + 0.073(\theta_d - 45)\right)\%$$

where $\theta$ is also measured in radians, and $\xi_d$ and $\theta_d$ are the angles measured in degrees. The dashed lines show these linear approximations to the curves.

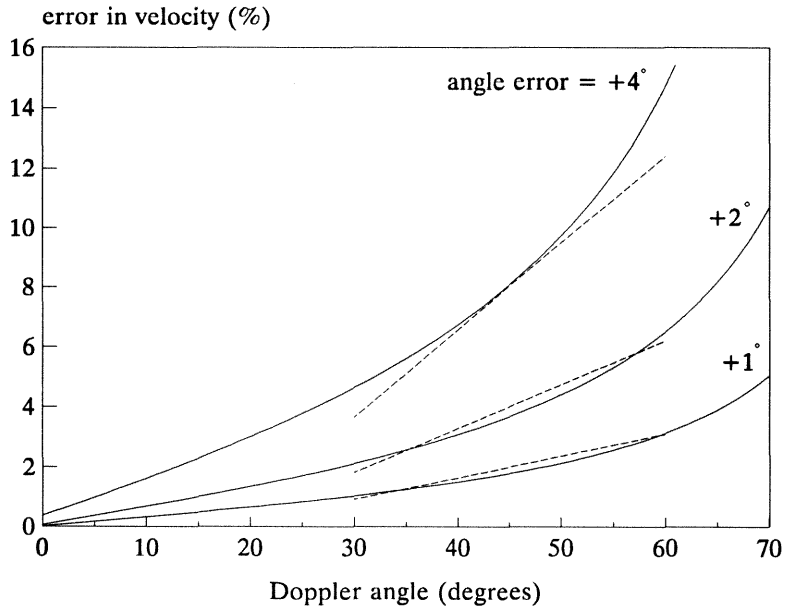


**Fig.4.1 - errors in the measured velocity if the true angle is overestimated by a small amount (solid lines), and linear approximations to the errors over a typical range of angles (dashed lines)**

In duplex ultrasound such an error arises if the direction cursor, which is visually aligned with the estimated axis of the blood vessel, is set at the wrong angle. This might occur for example if there is local curvature of the vessel. More commonly, this will occur if the discrete range of angles available does not allow the vessel axis to be well represented. For example on the Diasonics Spectra scanner with the 7.5 MHz linear array probe the possible angle readouts when the cursor is aligned with the vessel axis are spaced in steps of 3 degrees. Assuming that the vessel axis is correctly identified, and that the cursor is adjusted to be most closely aligned with it, then the error in the angle measured between the beam and the vessel axis may be ±1.5°. If the correct angle is near 30° this corresponds to possible errors in the calculated cosine of ±1.5%, and if the correct angle is near 60° the error in the cosine may be ±4.5%. The error magnitudes in the calculated velocity are therefore very similar, and can be read approximately from fig.4.1.

## Definition of the beam direction

In addition to the problem of aligning such a cursor with the vessel axis visually, the cursor may not provide the best representation of the beam direction. For example when the transducer and the sample volume both have finite extent as is true in the practical case, what is 'direction' of the beam? It is suggested below that for a transducer with finite extent such as a linear array, and a sample volume which is a point target, the cursor is not representative if it is drawn from the centre of the transducer to the target. The geometry of such a situation is shown in fig.4.2, in which the uncertainty about how to define the Doppler angle, $\theta$, is made more obvious. The angular extent of the transducer at the target is $2\varepsilon$, and the position of the target beneath the transducer is in part defined by a deviation of the angle bisector from the perpendicular, denoted by $\phi$.

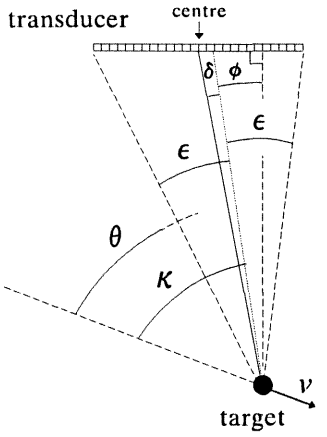


**Fig.4.2 -the geometry of a finite aperture transducer and a moving point target**

The representative beam direction might be defined by the line which is drawn from the target to bisect the *length* of the transducer, i.e. the solid line. Alternatively it might be defined by the line bisecting the range of *angles* of insonation, so that the beam 'direction' is considered to be along the dotted line. It is not known how manufacturers define the beam direction in commercial duplex scanners. However it is thought likely than the solid *length* bisector is favoured. One reason for suggesting this is that the point where the *angle* bisector intersects the transducer generally alters if the beam is steered to insonate another target. So if the dotted line was chosen the point from which the beam is deemed to originate would not be fixed, which would seem undesirable.

The range of angles of insonation means that a scatterer with a unique velocity, $v$, gives rise to a Doppler spectrum which has a range of frequencies. If $\theta$ is defined to be *the angle to the solid length bisector*, as is thought likely, then two mechanisms exist whereby it is suggested that subsequent estimation of the velocity leads to an underestimate.

(i)

The difference between the two directions is the angle $\delta$, which can be shown to be approximately equal to $\varepsilon^2\phi$ and so in general is very small. Nevertheless it is intuitive that for a non-zero value of $\phi$ the dotted angle bisector lies closer to the perpendicular than the solid length bisector. It follows that, if each point on the transducer surface is equally active, the majority of the spectrum is obtained from angles greater than $\theta$. In this way using $\theta$ as the representative angle will result in an underestimate of the correct velocity, $v$.

(ii)

If, for example, the IWMF of the spectrum is obtained to estimate the velocity then, from (4.1), the mean cosine of the range of angles is more relevant than the cosine of the mean angle. If the mean angle is denoted by $\kappa$ (which is equal to $\theta+\delta$ and is shown in fig.4.2) then the mean cosine is given by

$$\begin{aligned}\text{mean cosine} &= \frac{1}{2\varepsilon}\int_{-\varepsilon}^{\varepsilon}\cos(\kappa+\psi)\,d\psi \\ &= \frac{1}{2\varepsilon}\int_{-\varepsilon}^{\varepsilon}\cos\kappa\cos\psi\,d\psi - \frac{1}{2\varepsilon}\int_{-\varepsilon}^{\varepsilon}\sin\kappa\sin\psi\,d\psi \\ &= \frac{1}{2\varepsilon}\cos\kappa\left[\sin\psi\right]_{-\varepsilon}^{\varepsilon} - \frac{1}{2\varepsilon}\sin\kappa\left[-\cos\psi\right]_{-\varepsilon}^{\varepsilon} \\ &= \cos\kappa\ \frac{\sin\varepsilon}{\varepsilon}\end{aligned}$$

Because $\sin\varepsilon/\varepsilon < 1$ the 'mean cosine' is less than the 'cosine of the mean'. The result is that the 'correct' representative angle is greater than $\kappa$, and so the velocity, $v$, is underestimated further. Similar analysis for the PIWMF of the spectrum has not been carried out.

These qualitative results are extendable to the situation where many velocities are present in the sample volume. A quantitative analysis of the effects of these mechanisms on mean velocity estimation, using either IWMB or PIWMB, requires a greater knowledge of the characteristics of a 'multidirectional' beam.

As shall be seen in later chapters, there are other reasons why the Doppler angle should be kept low. The spectral broadening, which in chapter 7 is shown to affect PIWMF, is less influential at small Doppler angles. Similarly a low angle reduces the error caused by the filtering described in chapter 9.

## Summary

The question of the estimation of the relevant Doppler angle has been discussed briefly. As the frequency and the angle appear independently in the Doppler equation, a given error in estimation of the single angle affects IWMB and PIWMB equally. It is desirable to keep the Doppler angle low for several reasons. A guide to the accuracy of the resulting velocity measurement is given by noting from fig.4.1 that if a 2° error is made when the Doppler angle is 50° the velocity is in error by approximately 4½%.

## Notation for this chapter

| | |
|---|---|
| $\delta$ | the difference in angle between lines drawn from the target bisecting the length of the transducer and bisecting the angle subtended by the transducer |
| $\varepsilon$ | half of the angular extent of the transducer at the target |
| $\kappa$ | the angle at the target between the direction of motion and the angle bisector of the transducer |
| $\xi$ | error in the measured representative angle |
| $\psi$ | dummy angle variable |

# CHAPTER 5 - BEAMS OF A FINITE WIDTH

Other factors notwithstanding IWMB and PIWMB give proportional measures of the true spatial mean velocity when the beam is 'wide' and 'thin' respectively. When the beam is not 'wide' but insonates more intensely the centre of the cross section the resulting estimate of mean velocity found from the deterministic form of IWMB, $\overline{B_D}$ , is generally too high, as is well known. This is due to the fact that the central portion of the cross section generally contains the faster moving blood cells. As indicated in chapter 2 this effect has previously been studied. By contrast if the beam is not 'thin' but the beamwidth is finite then the deterministic form of PIWMB, $\hat{B}_D$ , in assuming the sample volume to be 'thin', weights the central, higher velocity, regions too lightly. The result is that using PIWMB underestimates the mean velocity.

This chapter discusses and compares the accuracy of both these estimators when the beam falls between the extremes of providing uniform insonation, and of being of negligible width. To achieve quantifiable results the beam is modelled as having either a Gaussian or more simply a rectangular (i.e. uniform) intensity profile, in each case with the centre of the beam passing through the centre of the vessel. Attention is given to the nature of PIWMB as providing an underestimate of mean velocity. For the commonly used velocity profiles described by (3.1) numerical simulation with a computer is used to find the amounts of error incurred with IWMB and PIWMB. The results allow conclusions to be drawn about the superiority of one or other estimator for different ratios of beamwidth to vessel diameter, and the usefulness of a weighted mean of the two estimators.

## Computer simulation

Numerical simulation using a computer was performed to find the errors in the deterministic values of both IWMB and PIWMB for beams with Gaussian or rectangular intensity profiles of various dimensions, and with various velocity profiles defined by (3.1). For both Gaussian beams, as shown shortly, and for rectangular beams it is sufficient to consider the projection of a single 'slice' of the beam onto the circular cross section. In the simulation the square enclosing this cross section was divided into a square 'checker board' array of 1001 x 1001 elements, and each element was assigned a velocity according to (3.1). The velocity scale was such that the spectrum occupied approximately 90% of the frequency range of 128 bins. For a given beam the elements in the array corresponding to the path of the beam were then considered. Each element was weighted by the beam intensity response at that point and placed in the bin to which its velocity corresponded. This provided the appropriate equivalent Doppler power spectrum. The weighted mean 'frequency' estimates IWMB and PIWMB and their equivalent velocities were then

calculated. The degree of departure of these estimates from the true mean velocity was found, for various beam and velocity profiles.

## Gaussian beam

To justify the use of a single cross section in the simulation the three dimensional nature of the practical beam is considered and directions $y'$, $z'$ and $z''$ are defined in relation to the beam axis as in fig.5.1. The dimension into the page, i.e. perpendicular to both beam and vessel, is defined by $y'$. In the plane of the page, the direction perpendicular to the beam is given by $z'$ and the direction of the vessel axis by $z''$.

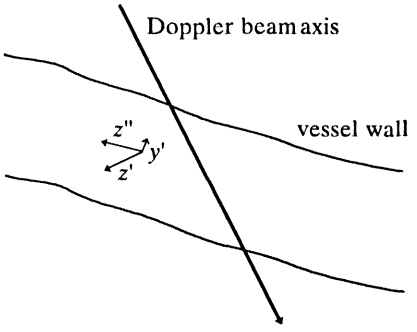


**Fig.5.1 - definition of directions**

The Gaussian curve used is that of the beam intensity response, i.e. curve of intensity received at the transducer after reflection from the target. This curve is the square of the received amplitude at the transducer, and consequently is less broad, with a standard deviation lower by a factor of $\sqrt{2}$. The curve of received amplitude at the transducer is in turn less broad than the curve of received amplitude at a target, e.g. a hydrophone used for the measurement of beam dimensions, because of imperfect focusing of the received beam.

The intensity response, $I$, of a circular Gaussian beam, scaled to have a maximum response of unity, is given by

$$I = e^{\frac{-\left(y'^2+z'^2\right)}{2\sigma^2}}$$

where $\sigma$ is the standard deviation, the quantities $y'$ and $z'$ are distances in the directions defined above in fig.5.1, and the origin in the $y', z'$ plane is at the centre of the beam. This is illustrated in fig.5.2 where separate 'slices' of the intensity response are shown.

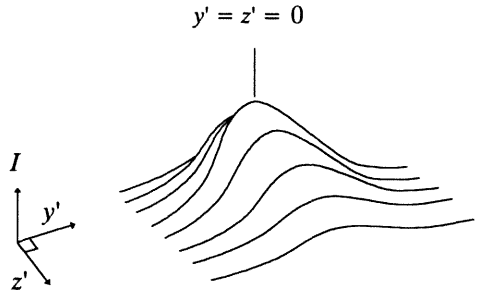


**Fig.5.2 - slices of a Gaussian shaped intensity profile**

By rearranging to give

$$I = e^{\frac{-z'^2}{2\sigma^2}} \cdot e^{\frac{-y'^2}{2\sigma^2}}$$

the profile along the $y'$ axis for any fixed $z'$ value can be seen to be a Gaussian curve in one dimension with the same standard deviation, but a reduced peak value of $e^{\frac{-z'^2}{2\sigma^2}}$. The important property that the standard deviation of the profile is the same for any fixed $z'$ value means that the shape of the Doppler spectrum returning from the whole sample volume is the same as the shape of the spectrum returning from any slice of the sample volume, corresponding to a particular $z'$ value. Each slice, if it could be considered separate, and consequently the whole beam, would give the same mean frequency. Therefore for the Gaussian beam the variation of the beam response in the $z'$ and $z''$ directions need not be considered in deriving an estimate of mean velocity, either in theory or by simulation, and use of a single slice is sufficient. (If an elliptical Gaussian beam (Aldis and Thompson 1992) is used, defined by two standard deviations, this result is still valid provided that the $y'$ direction corresponds to one of the axes of the ellipse. In this case the relevant standard deviation for the following results would be the standard deviation along the $y'$ axis.)

For Gaussian beams of various widths the percentage errors in the estimates IWMB and PIWMB for a parabolic velocity profile (i.e. $n = 2$) are shown by curves A and B* respectively in fig.5.3. Curve A gives the overestimate associated with IWMB, i.e. a positive error. The maximum overestimate is $33\frac{1}{3}\%$ and occurs when the beam is 'thin'. This exact figure is derived in chapter 12, but can be found using (3.2) with $n = 2$ and (3.5) with $t = 0.5$. Use of PIWMB gives an underestimate, i.e. a negative error, which for comparison purposes is inverted to give a positive quantity and plotted as curve B*.

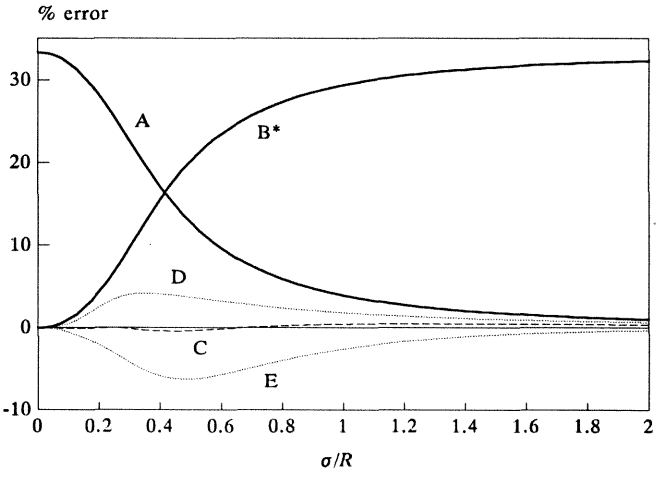


**Fig.5.3 - errors for parabolic flow and a Gaussian beam profile**

The abscissa is the true ratio of the standard deviation of the Gaussian curve to the radius. It is seen that PIWMB performs very much better than IWMB for ratios less than 0.2, and they have a similar degree of error when the ratio is approximately 0.4. This crossover ratio slowly increases as the profile becomes more blunt, i.e. as $n$ increases.

The degree of overestimation associated with IWMB decreases to zero as the beam becomes broader. By contrast PIWMB is correct for a 'thin' beam, but otherwise underestimates the true value, and moreso as the beam broadens. This suggests that the true value could be better estimated by a weighted sum of these two statistics than by either of the statistics individually. This **combined** statistic is denoted by CIWMB. The sum would be of the form

$$\text{CIWMB} = \alpha \cdot \text{IWMB} + (1-\alpha)\,\text{PIWMB} \tag{5.1}$$

where $\alpha$ is a proportion that is equal to zero when the beamwidth is infinitesimal, equal to 1 when the beam uniformly insonates the vessel, and is expected to vary with both velocity profile and beam profile. It was observed that the combined estimate CIWMB was close to the true value over a wide range of beamwidths (and velocity profiles) if $\alpha$ was chosen to be

$$\alpha = \frac{8.5\left(\frac{\sigma}{R}\right)^{2.5}}{\left(1+8.5\left(\frac{\sigma}{R}\right)^{2.5}\right)} \tag{5.2}$$

The percentage error incurred by estimating the true value by CIWMB, where $\alpha$ has the above form, is shown on fig.5.3 by the dashed curve, C. However using this equation presupposes knowledge of the beamwidth and vessel radius (in which case IWMB or PIWMB could be used with a known correction factor anyway). The beam dimensions may be poorly known, and the vessel radius changes throughout the cycle (over a range of the order of 10% for a carotid artery), so that this small level of error is not appropriate. Rather it is more realistic to suggest that the estimate of $\sigma/R$ used in (5.2) may be in error from the true value by a certain quantity. The upper dotted curve, D, is the error in CIWMB if the estimate of $\sigma/R$ used in (5.2) is 25% above the true half-beamwidth to radius ratio. Similarly the lower dotted curve, E, is the error in CIWMB if the estimate used is 25% below the true ratio, so that the region between the dotted curves represents the error range if the estimate of the half-beamwidth to radius ratio is accurate to within $\pm$ 25 % of the true value.

It is perhaps more valuable to consider the variation in error over a range of profiles for a fixed beam dimension. The resulting curves are given in fig.5.4(a)(b) and (c) where the ratios of standard deviation to vessel radius are 0.2, 0.4 and 0.6 respectively. In each case the vertical error scale is the same though the position of the origin may differ. Curve A as before gives the error in the use of IWMB. Curves C,D and E correspond to the same statistics as used in fig.5.3. Curve B shows the underestimate of PIWMB as a negative error (i.e. without inversion) and is now preferred to the previously used curve B*. It should be remembered that only profiles with $n \geq 2$ are regarded as being physiologically meaningful.

For the case where the standard deviation to radius ratio is 0.1 (not shown) curves B,C,D and E are, as expected, all close to the x-axis. Clearly when the beam has a standard deviation of less than 0.2 of the vessel radius PIWMB estimates the true mean frequency much more closely than IWMB throughout the range of velocity profiles. IWMB becomes in general a better estimator than PIWMB when the ratio increases to above 0.4. The dashed and dotted curves are bound by the solid curves for all beamwidths as the quantities $\alpha$ and $(1-\alpha)$ are bound between 0 and 1. It appears that the mean velocity estimation is improved by the use of (5.1) and (5.2) even if the beamwidth ratio estimate is $\pm$25% in error, especially so for ratios in the 'transition' area of 0.4. As curve E is bound to be closer to the x-axis than curve B, the value of CIWMB will always be closer to the true mean frequency than PIWMB if the beamwidth ratio is underestimated. Curve D on the other hand is bound to be closer than curve A and not curve B, so that for large overestimates of beamwidth CIWMB may not perform as well as PIWMB. In the case of a parabolic velocity profile this occurs when the overestimate is greater than approximately 40%.

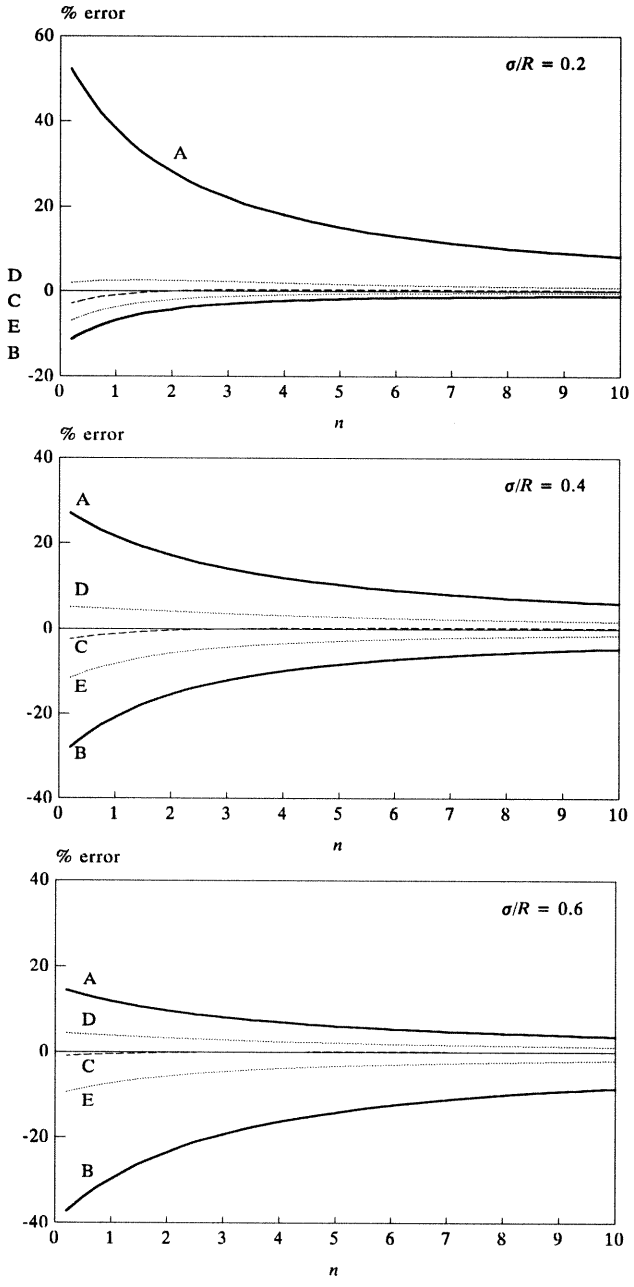


**Fig.5.4a,b,c - errors for Gaussian beam profiles with standard deviation to radius ratios of 0.2, 0.4, 0.6**

## A practical example

For the 7.5 MHz linear array transducer of a Diasonics Spectra ultrasound scanner an approximate value for the standard deviation of a relevant Gaussian curve was obtained. The markers shown in fig.5.5 show the voltage of a signal observed at a hydrophone as it was moved in the Doppler beam. Because the voltage at the hydrophone is proportional to the amplitude of the pressure fluctuations, the intensity profile at the hydrophone is the square of this curve. A Gaussian curve has a form proportional to

$$\exp\left(-\frac{y'^2}{2\sigma^2}\right)$$

and fig.5.5 shows that the main lobe is easily contained within a Gaussian curve with a standard deviation of 0.8 mm, given approximately by the solid line. Squaring this gives another Gaussian curve with the standard deviation reduced by $\sqrt{2}$, i.e. a standard deviation of 0.6 mm. (As stated earlier the distribution of intensity received *at the transducer elements* tends to be more peaked still. For example, according to the principle of reciprocity, the standard deviation is further reduced by a factor of $\sqrt{2}$ if the transmit and receive focussing are the same.) For a 6 mm diameter vessel such as might be a carotid artery this standard deviation of 0.6 mm corresponds to a ratio of standard deviation to radius of 0.2. So for this example beam and an artery of 6 mm diameter PIWMB is theoretically superior to IWMB.

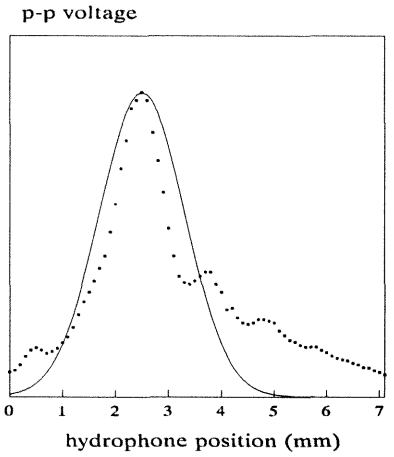


**Fig.5.5 - the amplitude profile of an actual beam and a Gaussian approximation**

## Rectangular beam

The simpler case of a beam with a rectangular profile can also be considered using a single cross section. Again IWMB leads to an overestimate of mean velocity and PIWMB to an underestimate. The half-beamwidth is denoted by $b$. The percentage errors in IWMB and PIWMB against the half-beamwidth to radius ratio $b/R$ for a parabolic velocity profile are shown by curves A and B* respectively in fig.5.6, as in fig.5.3. PIWMB performs much better than IWMB when the ratio of half-beamwidth to radius is less than approximately 0.4. The degrees of error are approximately equal when the ratio is 0.65.

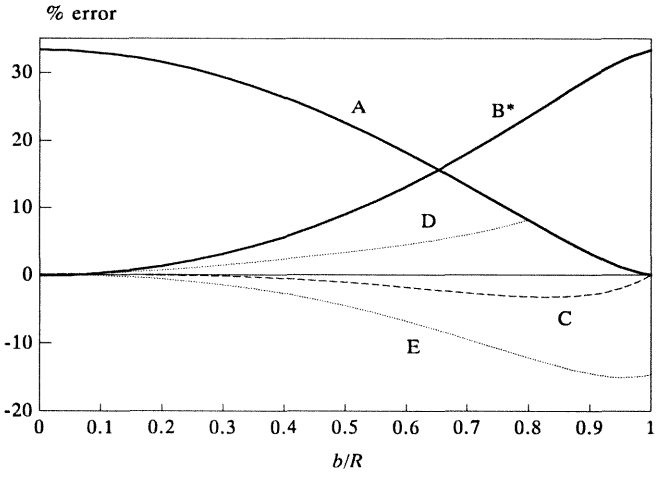


**Fig.5.6 - errors for parabolic flow and rectangular beam profile**

In this rectangular beam case, for parabolic and for other velocity profiles, it was observed that CIWMB was close to the true value over a wide range of beamwidths if $\alpha$ was simply chosen to be

$$\alpha = \left(\frac{b}{R}\right)^2 \tag{5.3}$$

Curves C, D and E in fig.5.6 are also defined as in fig.5.3, except that $\alpha$ is now given by this equation (5.3) and curves D and E relate to 25% over- and underestimates of the ratio $b/R$.

## Summary

If a centrally placed sample volume has a finite width less than the vessel diameter and the velocities are larger nearer the vessel axis then, other factors aside, PIWMB leads to an underestimate of mean blood velocity and IWMB leads to an overestimate. For Gaussian beam profiles with a standard deviation to vessel radius ratio of less than 0.4, PIWMB performs better over a wide range of velocity profiles than IWMB, and very much better when the ratio is less than 0.2. If the beam is modelled as having a rectangular profile then PIWMB performs better for half-beamwidth to radius ratios less than approximately 0.65 and very much better for ratios less than 0.4. It is suggested that in many situations, especially with linear and phased array transducers the beam may be better approximated as being of infinitesimal width than as insonating uniformly. If a sensible estimate of the beamwidth to radius ratio can be made a further improvement can be achieved by obtaining a combined estimate CIWMB, which is a weighted mean of the two estimates.

## Notation for this chapter

| | |
|---|---|
| $b$ | half the width of a beam with a rectangular intensity profile |
| CIWMB | an estimator of mean frequency bin number, being a weighted sum of IWMB and PIWMB |
| $y'$ | perpendicular distance from the axis of a Gaussian beam in the plane of the circular vessel cross section |
| $z'$ | perpendicular distance from the axis of a Gaussian beam in a direction perpendicular to $y'$ |
| $z''$ | (distance in) a direction parallel to the vessel axis |
| $\alpha$ | proportion of the estimate IWMB in the weighted estimate CIWMB |
| $\sigma$ | standard deviation of the intensity response for a Gaussian shaped Doppler beam |

# CHAPTER 6 - MISALIGNMENT OF THE BEAM

No matter what the shape of the ultrasound beam, it is likely that its preferred alignment is such that its axis passes through the axis of the vessel. (A situation is described briefly in chapter 12, and more fully in appendix B, where it might be desirable for this not to be the case.) Correct alignment relies on operator skill and the absence of lateral motion of the vessel beneath the probe. This chapter discusses the effects on IWMF and PIWMF, and by implication on the deterministic forms of IWMB and PIWMB, when the beam axis does not pass through the centre of the vessel.

## Error in IWMF

The effect of such a misalignment on IWMF, with a beam which when correctly aligned is 'wide', is obviously linked to the actual beamwidth. Cobbold et al. (1983), using computer simulation, investigated the effect on IWMF of a rectangular or Gaussian shaped Doppler beam being displaced from the centre of the vessel, and, as already seen in chapter 2, suggested that, "when the beam width is roughly equal to the vessel diameter the estimated mean velocity is not a sensitive function of beam profile and position". Clearly if the beam is wide enough so that the vessel falls *comfortably* in a region of uniform intensity insonation then a small lateral movement of beam or vessel will produce no change in IWMF. Conversely the maximum sensitivity to displacement of an otherwise 'wide' beam occurs when the beamwidth is equal to the diameter, the beam has a rectangular intensity profile, and the velocity profile is as peaked as possible, i.e. when it is parabolic if we allow only the profiles of (3.1) with $n \geq 2$. As the beam becomes displaced the slower scatterers at the periphery are missed so that IWMF overestimates. Results in agreement with the work of Cobbold et al. were obtained when computer simulation was applied to this worst case. The greatest amount of overestimate is approximately 9% and is observed when the displacement is approximately 0.6 radii. This worst case error is only appropriate in the unrealistic case that the beam is rectangular with the minimum width, i.e. one vessel diameter. In the more realistic case that the intensity profile is curved, a beam that insonates the vessel more or less uniformly would have a width *significantly greater* than the diameter, and the error with beam displacement would be considerably less.

## Error in PIWMF

Attention is now given to the misalignment of a beam which otherwise would be 'thin'. If a sample volume of negligible width is displaced then the high frequencies associated with scatterers at the centre of the vessel are absent from the observed spectrum. So intuitively using PIWMF produces an underestimate of the mean velocity. The degree of underestimation is shown here to be small for typical displacement values if the profile

follows (3.1). The geometry is given in fig.6.1. As in chapter 2, $x$ is measured along the sample volume from the point opposite the vessel centre. The beam displacement is given by $y$.

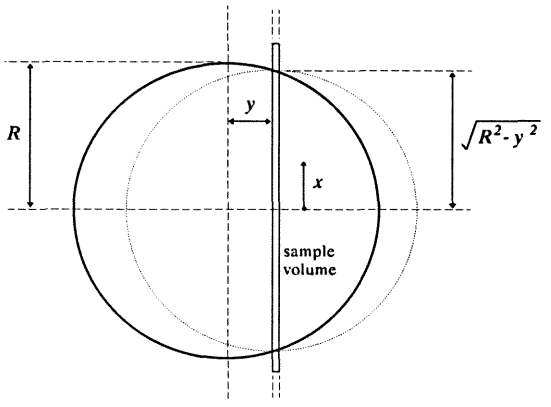


**Fig.6.1 - a displaced beam of negligible width**

If the velocity profile is given by (3.1) then the velocity at a point ($x$, $y$) in the sample volume is

$$v = v_m\left(1-\left(\frac{x^2+y^2}{R^2}\right)^{n/2}\right) \qquad \text{for} \qquad x \le \sqrt{R^2-y^2} \tag{6.1}$$

and is zero otherwise. For a fixed value of $y$ this is a monotonic function of $x$. Evaluating PIWMF from the deterministic spectrum leads to the velocity that would be the mean velocity if the sample volume passed through the centre of the vessel and if the velocity profile along the sample volume was monotonic and axi-symmetric. So the mean velocity estimate calculated from PIWMF for the given displacement, $y$, can be found by integrating over the dotted disc of radius $\sqrt{R^2-y^2}$ in fig.6.1, where the profile across its diameter is given by equation (6.1). Using $r^*$ as the radial distance variable in this disc, so that the circumference of the lamina at this distance is $2\pi r^*$, the calculated mean velocity, $\bar{v}'$ is given by

$$\bar{v}' = \frac{\int_0^{\sqrt{R^2-y^2}} 2\pi r^* v_m\left(1-\left(\frac{r^{*2}+y^2}{R^2}\right)^{n/2}\right)dr^*}{\int_0^{\sqrt{R^2-y^2}} 2\pi r^* dr^*}$$

which leads to

$$\bar{v}' = v_m\left(1 - \frac{2}{n+2}\left[\frac{1-\left(y/R\right)^{n+2}}{1-\left(y/R\right)^{2}}\right]\right) \tag{6.2}$$

The derivation of this result is given in appendix F. The true mean velocity, $\bar{v}$, is given by (3.2) but can also be found here by setting $y$ equal to zero, and is

$$\bar{v} = v_m\left(1 - \frac{2}{n+2}\right) = v_m\left(\frac{n}{n+2}\right)$$

As $n$ is positive the quantity in the square bracket of (6.2) is greater than 1 so that the estimate of mean velocity with a displaced beam, $\bar{v}'$, underestimates the true mean velocity, $\bar{v}$. The percentage error due to the beam displacement, $E_{\text{PIWMF}}$, is negative and is

$$\begin{aligned} E_{\text{PIWMF}} &\equiv \frac{\bar{v}' - \bar{v}}{\bar{v}} \times 100\% \\ &= 100 \cdot \frac{2}{n} \cdot \left(1 - \left[\frac{1-\left(y/R\right)^{n+2}}{1-\left(y/R\right)^{2}}\right]\right)\% \end{aligned} \tag{6.3}$$

This function is zero for plug flow, i.e. where $n = \infty$, and is monotonic in $n$. Therefore, for profiles with forms between parabolic and plug, the error is bound between zero and the function resulting when the flow is parabolic. Putting $n = 2$ into (6.3) and changing to the inequality gives

$$-100\left(y/R\right)^{2}\ \% \le E_{\text{PIWMF}} \le 0 \tag{6.4}$$

The error is therefore small for typical displacements. For example, if the displacement is 10% or 20% of the radius the true mean velocity is underestimated by at most only 1% or 4% respectively.

## Summary

This chapter has considered the errors incurred by the use of IWMF with an otherwise 'wide' beam, or PIWMF with an otherwise 'thin' beam, when the beam is displaced from the vessel centre. The results are obviously applicable to the deterministic forms of IWMB and PIWMB. Analysis of the maximum error in IWMF if a uniformly insonating beam is misaligned requires the assumption of a very unrealistic beam profile. A uniformly insonating beam would tend to be much broader than the vessel so that errors due to misalignment would in fact be small. Errors are greater the more peaked the velocity profile, so that for flows ranging from plug to parabolic the worst errors in IWMF and PIWMF are observed when the profile is parabolic. For these flows, if a beam of negligible width is displaced from the vessel centre then PIWMF underestimates the true mean velocity, and the error is bound by equation (6.4). The errors are small for realistic displacements and these idealised profile shapes, so that even if some misalignment occurs both IWMF and PIWMF are still valid estimators with their appropriate beams.

## Notation for this chapter

| | |
|---|---|
| $x$ | distance along sample volume from point opposite the vessel centre |
| $y$ | displacement of beam from vessel centre |
| $r^*$ | position variable in imagined circle |

# CHAPTER 7 - SPECTRAL BROADENING

The derivations of IWMF and PIWMF have required the Doppler spectrum to accurately mirror the velocity distribution of scatterers in the sample volume. In general the Doppler spectrum is a broadened form of this desired spectrum, and subsequent velocity estimation may be in error. The vast majority of this chapter is concerned with the effect on IWMF and PIWMF of the broadening associated with the finite geometry of both the transducer and sample volume. Such broadening is called geometrical spectral broadening and is intrinsic to the measuring system. A less influential source of spectral broadening is discrete Fourier analysis of the signal, which is also briefly discussed. A third source of effective spectral broadening described is a change in the velocity distribution during the interval over which the signal is recorded. This is equivalent to the Doppler signal not being stationary over this interval.

It is shown that if the broadening of a frequency *component* is such that its mean frequency, weighted by intensity, is maintained then analysis with IWMF and a 'wide' beam still leads to the correct mean velocity. In contrast, for any such broadening, analysis using PIWMF and a 'thin' beam produces an underestimate of the mean velocity.

## Geometry of insonation

If the transmitter and receiver are coincident point objects then an insonated group of particles moving with a single velocity, $v$, in one direction produces a Doppler spectrum consisting of a single spike at a frequency, $f_\theta$, given by equation (1.2), which is expressed here as

$$f_\theta = \frac{2 F v \cos\theta}{c} \tag{7.1}$$

A group of particles with a range of velocities would produce a range of frequency components. If the appropriate representative frequency, $f_{rep}$, is found then the mean particle velocity, $\bar{v}$, is obtained from a rearrangement of the form of (7.1) where the velocity and frequency are these values, i.e.

$$\bar{v} = \frac{f_{rep}\, c}{2F \cos\theta} \tag{7.2}$$

For a 'wide' beam the representative frequency is IWMF, i.e. $f_{rep} = \bar{f}$, and for a 'thin' beam the representative frequency is PIWMF, i.e. $f_{rep} = \hat{f}$. So the mean velocity is recovered from the spectrum by calculation of the correct representative frequency and the assumption of the single angle $\theta$.

In practice the ideal spectrum corresponding to a single velocity component is broadened by the finite size of the transducer aperture and the sample volume, as no unique Doppler angle is appropriate. In other words a particle moving with a fixed velocity will give a Doppler signal with a finite bandwidth. This effect has been called geometrical spectral broadening and is recognised in both Doppler ultrasound (Newhouse et al. 1980) and laser fields. It is especially apparent if a large number of elements in an array transducer are activated when transmitting and receiving the Doppler signal.

As no single Doppler angle exists, the angle used in (7.2) to calculate mean velocity should be representative of the geometry of the beam and the motion of the particles. The identity of this angle, and some associated sources of error, have already been discussed in chapter 4. This current chapter is primarily concerned with the effects of the range of angles, and not the choice of a single angle. The nominal Doppler angle used might be the angle, called $\theta$, between the direction of motion and the line bisecting the *length* of the transducer drawn through the centre of the sample volume, as in chapter 4. (The angle $\theta$ is defined in this way when the transducer has a finite length.) Alternatively the angle used might be the bisector, called $\kappa$, of the range of *angles* of insonation, also as in chapter 4. If the dimensions of the sample volume are very small compared to the transducer length, the sample volume can be thought of as a point target, as in fig.7.1. This is the same diagram as fig.4.2 but with $\theta$ defined unambiguously. At the target is a group of particles moving with a single velocity $v$.

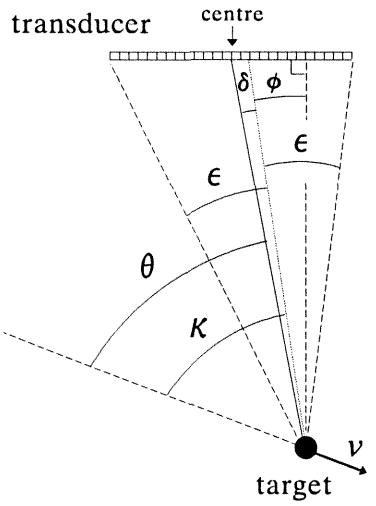


**Fig.7.1 -the geometry of a finite aperture transducer and a moving point target**

The transducer is regarded as being narrow in comparison in the dimension into the page so that the relevant geometry is described in the two dimensions of the page. The angle $\kappa$ bisects the angle $2\varepsilon$ subtended by the transducer at the target, and the tranducer elements lie at angles to the direction of motion between $\kappa-\varepsilon$ and $\kappa+\varepsilon$ . The maximum and minimum frequencies observed in the Doppler spectrum are found by substituting these angles into (7.1) so that provided $\kappa \geq \varepsilon$ the Doppler spectrum will have a bandwidth, $w$, of

$$w = \frac{2Fv}{c}\left(\cos(\kappa-\varepsilon)-\cos(\kappa+\varepsilon)\right) \tag{7.3}$$

The idealised spectral spike is therefore broadened to extend over a frequency range of $w$, an extent which is seen to be proportional to the velocity of the group of particles, and dependent on the direction of motion.

As stated in chapter 4, the angle $\delta$ is approximately equal to $\varepsilon^2\phi$ and is in general very small. So because $\kappa = \theta+\delta$ the frequency of the desired spike corresponding to the velocity $v$ might be defined either by $f_\theta$ according to (7.1), or by the frequency, $f_\kappa$ , which is analogously

$$f_\kappa = \frac{2Fv}{c}\cos\kappa$$

These frequencies are representative of the location of the broadened spectrum. If $f_\kappa$ is used then the fractional bandwidth of the received Doppler signal is given by

$$\begin{aligned}
\frac{w}{f_\kappa} &= \frac{\cos(\kappa-\varepsilon)-\cos(\kappa+\varepsilon)}{\cos\kappa} \\
&= \frac{(\cos\kappa\cos\varepsilon+\sin\kappa\sin\varepsilon)-(\cos\kappa\cos\varepsilon-\sin\kappa\sin\varepsilon)}{\cos\kappa} \\
&= \frac{2\sin\varepsilon\sin\kappa}{\cos\kappa} \\
&\approx 2\varepsilon\tan\kappa
\end{aligned}$$

which agrees with a result of Newhouse et al. (1980), and is a good approximation for $\varepsilon < 0.25$ $(\approx 15°)$ . As $\delta$ is very small $\kappa$ can be replaced by $\theta$ in this approximate result, i.e.

$$\frac{w}{f_\theta} \approx 2\varepsilon\tan\theta \tag{7.4}$$

For a given transducer the extent of the broadened spike is therefore minimised by minimising the Doppler angle $\theta$. As explained in chapter 4, a low $\theta$ is generally sought anyway to improve the accuracy of the frequency/velocity scale factor.

The work of Newhouse et al. was primarily concerned with determining the bandwidth of the Doppler signal returning from particles of a single velocity. In the context of continuous wave insonation they also point out that this geometrical spectral broadening is equivalent to the effect of the particles moving through the *sides* of the sample volume, i.e. 'transit time broadening' where the transit time is not limited by the *ends* of the sample volume. The upper extreme of the broadened spectrum is also relevant in the determination of the *maximum* blood velocity. Knowledge of the maximum frequency returning from the blood sample and the minimum Doppler angle enables the maximum particle velocity present in the sample volume to be estimated. This principle has been used in commercially available scanners for maximum velocity measurement. However the estimation of *mean* velocity in the sample volume requires knowledge of the *shape*, as well as the extent and location, of the broadened spike from any single velocity component.

The shape of the broadened spike (or broadening function) depends on the relative power recorded at each receiver element. This is affected by transducer/target geometry, beam intensity profile, attenuation and transducer element weightings. The shape, not extent, is the same for each velocity present in the sample of scatterers, and the resulting spectrum is the sum of the broadenings of each velocity component. (The total spectrum cannot be thought of as a convolution of the theoretical signal with a single broadening function. This is because the width of the function is not the same for each component, being proportional to the velocity of that component as (7.3) has shown.)

## The effect on IWMF

If the beam is 'wide', and the power spectrum $p_s(f)$, as introduced in chapter 3, is proportional to the number density of insonated scatterers moving with the corresponding velocity, then IWMF is proportional to mean blood velocity. The IWMF for this theoretical spectrum is denoted by $\bar{f}_s$, and for a single-sided spectrum is defined according to (2.10) and is

$$\bar{f}_s = \frac{\int_0^\infty f\, p_s(f) df}{\int_0^\infty p_s(f) df} \tag{7.5}$$

This spectrum, $p_s(f)$, is that which would be observed if there was a single angle, say $\theta$, between the transducer and the motion. The correct mean velocity would be found from (7.2) using this mean frequency $\bar{f}_s$ and the angle $\theta$. The observed spectrum, which is

broadened in practice, is given by $p(f)$. The corresponding IWMF is denoted by $\bar{f}$ and is defined by (2.10) which is restated here

$$\bar{f} = \frac{\int_0^\infty f\, p(f) df}{\int_0^\infty p(f) df} \tag{7.6}$$

This frequency estimates the desired IWMF, $\bar{f}_s$. In relating $\bar{f}$ to $\bar{f}_s$ it is first noted that the denominators of (7.5) and (7.6) are equal. This is because the broadening of a spike preserves power and so the total power in the spectrum is conserved.

Each velocity component corresponds to an idealised spike which is subject to a broadening function with a fixed shape. An example for a spike of frequency $f_1$ is shown by the solid line of fig.7.2. The nominal frequency $f_1$ is the frequency that would correspond to the velocity if $\theta$ was the single Doppler angle.

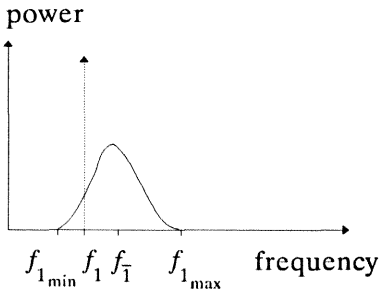


**Fig.7.2 -a general broadening function**

The resulting frequency extremes, $f_{1_{min}}$ and $f_{1_{max}}$, are proportional to the nominal frequency $f_1$, e.g. for the insonation of fig.7.1

$$f_{1_{min}} = \frac{\cos(\kappa+\varepsilon)}{\cos\theta}\cdot f_1 \qquad \text{and} \qquad f_{1_{max}} = \frac{\cos(\kappa-\varepsilon)}{\cos\theta}\cdot f_1$$

which are easily shown using (7.1) with the extreme angles $\kappa+\varepsilon$ and $\kappa-\varepsilon$, and the nominal angle $\theta$. This means that the IWMF of the broadened spike, $f_{\bar{1}}$, is also related to $f_1$ by a third constant factor, say $k$, i.e. $f_{\bar{1}} = k f_1$. Furthermore as the power of each spike is conserved in the broadening process, and as the individual broadened components add linearly to obtain the total spectrum, $p(f)$, and the numerators of (7.5) and (7.6) are linear

in $p_S(f)$ and $p(f)$, this same constant factor, $k$, must relate $\bar{f}$ to $\bar{f}_S$, i.e. $\bar{f} = k\,\bar{f}_S$. At no point does this result depend on the form of the theoretical spectrum, so this factor is independent of the blood velocity profile. However because the broadening function depends on the orientation of the artery, as suggested by (7.3) and (7.4), this factor is dependent on the orientation of the artery. This factor is the correction factor needed if the calculation of mean velocity is made using the angle $\theta$. No correction is needed if $\bar{f}_S$ is equal to $\bar{f}$, which is only true if the IWMF of a broadened spike is equal to its nominal frequency, i.e. if $f_{\bar{1}} = f_1$. In this case the measured mean velocity using (7.2) based on $\bar{f}$ and $\theta$ would be correct for any velocity distribution of scatterers. Note that the broadening function need not be symmetric.

More generally an angle $\theta_{\text{eff}}$ exists such that

$$\frac{\cos\theta_{\text{eff}}}{\cos\theta} = k \equiv \frac{\bar{f}}{\bar{f}_S} \tag{7.7}$$

which is the desired correction factor. So $\theta_{\text{eff}}$ can be thought of as the effective Doppler angle, and the correct mean velocity can be found using $\bar{f}$ in (7.2) with $\theta_{\text{eff}}$ in place of $\theta$. Therefore, no matter what the velocity distribution of scatterers, for any **fixed** geometry of the artery, transducer and beam there exists an 'equivalent' Doppler angle, $\theta_{\text{eff}}$, for use in (7.2), such that the calculated mean velocity using the IWMF, $\bar{f}$, is correct, despite the spectral broadening.

(The above analysis would show that these results are also valid for double-sided spectra where (7.5) and (7.6) would then have lower limits of integration of -∞.)

## The effect on PIWMF

If the beam is 'thin' then PIWMF evaluated from $p_S(f)$ is proportional to mean blood velocity. The PIWMF for this theoretical spectrum is $\hat{f}_S$ and is defined according to (2.11) by

$$\hat{f}_S = \frac{2\int_0^{f_m} f \cdot p_S(f)\left(\int_f^{f_m} p_S(u)\,du\right)df}{\left(\int_0^{f_m} p_S(f)\right)^2} \tag{7.8}$$

where the maximum frequency in the spectrum is $f_m$. Under the above assumptions, this frequency, $\hat{f}_S$, should be used in (7.2) to find mean velocity.

With the observed spectrum, $p(f)$, the PIWMF, $\hat{f}$, is given by

$$\hat{f} = \frac{2\int_0^{f_{max}} f \cdot p(f)\left(\int_f^{f_{max}} p(u)\,du\right)df}{\left(\int_0^{f_{max}} p(f)\right)^2} \qquad (7.9)$$

where $f_{max}$ is the maximum frequency present in the broadened spectrum, and is therefore higher than the maximum frequency in the ideal spectrum $f_m$. It is seen that the numerators of (7.8) and (7.9) are non-linear in the spectral densities $p_s(f)$ and $p(f)$. An effect of this is that the ratio of $\hat{f}$ to the desired value $\hat{f}_s$, which is the required correction factor, is different for different velocity profiles. This is shown in more detail in succeeding paragraphs. In particular it is demonstrated that if the broadening function is symmetric about the nominal Doppler shift frequency then $\hat{f}$ underestimates the desired value $\hat{f}_s$. (Qualitatively this can be inferred from the fact that, with PIWMF, the 'half' of any ideal frequency component spread to be below its nominal frequency is weighted more than the 'half' spread above. As already seen, this unequal weighting is because lower frequencies in the signal are deemed to originate from scatterers further from the vessel axis, and hence to be representative of laminae of greater circumference and area.)

Again the family of velocity profiles given by (3.1) is considered. The corresponding normalised spectra are given by (3.4), which is restated here

$$p_s(f) = \frac{t}{f_m}\left(1 - \frac{f}{f_m}\right)^{t-1} \qquad 0 \le f \le f_m \qquad (7.10)$$

where $t \equiv 2/n$ if the beam is 'wide' and $t \equiv 1/n$ if the beam is 'thin'. Such a spectrum is uniform between zero and $f_m$ when $t = 1$, i.e. for parabolic flow and a 'wide' beam. It is intuitive that a given amount of broadening has less effect on the form of a uniform spectrum than the form of any other, as the broadening primarily affects the uniform nature at the 'edges' of the spectrum. So the broadening has least effect when the spectrum is as uniform as possible, which, restricting the flow to be between plug and parabolic forms, occurs for parabolic flow. In contrast, with plug flow $t = 0$, the spectrum is a spike at the maximum frequency $f_m$, and the effect of the spreading on the form of the spectrum is maximised. So for a given amount of broadening, the amount of underestimate incurred by calculating PIWMF from the broadened spectrum, $p(f)$, will be a maximum for plug flow and will decrease monotonically as $t$ increases, towards parabolic flow.

*Forms of the broadening function*

Consider the two spectral broadening functions shown in fig.7.3. These are where a spike at a nominal frequency $u$, shown by the dotted line, is smoothed to give either a rectangular or an isosceles triangular spectrum with a mean frequency of $bu$ and a width of $abu$. The extent of the broadening as a fraction of the resulting mean is described by $a$, and the extent of the broadening as a fraction of the nominal frequency is described by the product $ab$. These rectangular and triangular broadening functions are idealised forms for mathematical description and manipulation, and are shown by the dashed and solid lines respectively. As suggested above the dimensionless parameters $a$ and $b$ are fixed by the geometry relating the artery, transducer and beam. The functions are scaled so that in each case the area beneath them is 1. The nominal frequency $u$ is the frequency that would be present for a fixed target velocity if the transducer was a point transmitter/receiver at a position corresponding to the assumed Doppler angle. In cases where $b = 1$ the broadened spike has an intensity weighted mean frequency equal to the nominal frequency $u$ and, as discussed above, IWMF is unaffected by the spectral broadening.

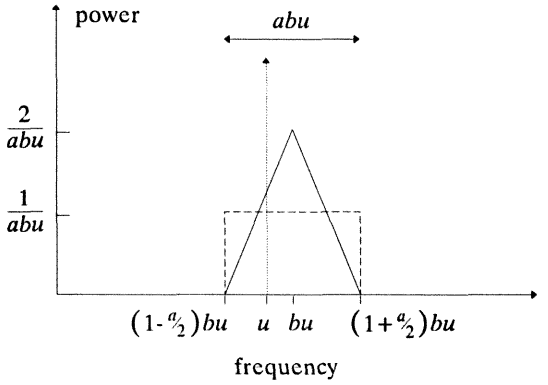


**Fig.7.3 - a theoretical spike and two idealised broadening functions representing the spectrum arising from scatterers of a single velocity - (dashed line for rectangular broadening and solid line for triangular broadening)**

The triangular broadening function approximates the function observed in practice, an example of which is given in fig.7.4. Theoretical justification for the use of a triangular form is given later in this chapter and in more detail in appendix E. The attractiveness of the rectangular broadening form is its mathematical simplicity.

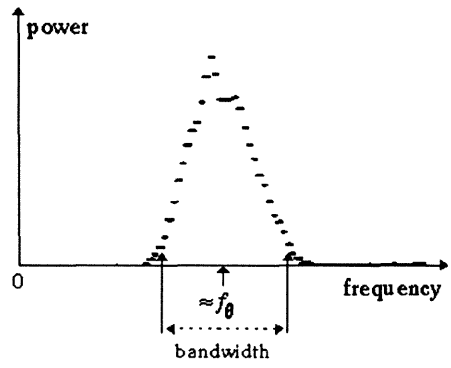


**Fig.7.4 - a spectrum observed with a modern linear array transducer, from the insonation of a straight section of a rubber O-loop moving with a constant velocity at a nominal Doppler angle of 59°.**

For both the rectangular and triangular broadening functions the observed spectrum, $p(f)$, is found from the ideal spectrum, $p_S(f)$, as follows. A nominal frequency component, say at $u$, contributes to the observed spectrum between the frequencies $(1-\frac{a}{2})bu$ and $(1+\frac{a}{2})bu$. Therefore the observed power at $f$ is contributed to by nominal frequency components between $\frac{f}{b(1+\frac{a}{2})}$ and $\frac{f}{b(1-\frac{a}{2})}$. So the broadened spectrum can be written as

$$p(f) = \int_{f/b(1+a/2)}^{f/b(1-a/2)} T(u,f)\,p_S(u)\,du \qquad (7.11)$$

where $T(u,f)$ is the fractional contribution of the nominal component at $u$ to the observed spectrum at $f$, and is consequently zero outside these limits of integration. $T(u,f)$ is in fact the broadening function, so that, within these limits,

for the rectangular broadening of fig.7.3 $\quad T(u,f) = \dfrac{1}{abu}$

and for the triangular broadening $\quad T(u,f) = \dfrac{2}{abu}\cdot\left(1-\dfrac{2|f-bu|}{abu}\right)$.

The maximum frequency in the broadened spectrum is given by $f_{max} = (1+a/2)b\,f_m$.

*Plug flow - Rectangular broadening*

For plug flow $v = v_m$ at all positions in the vessel, so that the theoretical Doppler spectrum is a spike at $f = f_m$, This can be scaled to have a total power of 1, and without requiring (7.11) the observed spectrum can be seen to be

$$p(f) = \frac{1}{a\,b\,f_m} \qquad \left(1 - a/2\right) b f_m < f < \left(1 + a/2\right) b f_m \tag{7.12}$$

and zero elsewhere. If $u$ is replaced by $f_m$ in the annotation to fig.7.3 then the spike and the observed spectrum (dashed line) are shown in this figure. Substitution of this spectrum into (7.9) leads to an expression for the observed PIWMF of

$$\hat{f} = \left(1 - \frac{a}{6}\right) b f_m \tag{7.13}$$

A derivation of this result is given in appendix F.

The percentage error due to spectral broadening incurred using PIWMF is defined by

$$E_{\text{PIWMF}} \equiv \left( \frac{\hat{f} - \hat{f}_S}{\hat{f}_S} \right) \times 100\%$$

In the absence of broadening PIWMF is the frequency of the spike, i.e. $\hat{f}_S = f_m$ . So the percentage error in the case of plug flow is

$$E_{\text{PIWMF}} = \left[ b\left(1 - \frac{a}{6}\right) - 1 \right] \times 100\% \tag{7.14}$$

This error is shown as the dashed straight line in fig.7.5 for various values of $a$ in the case where the broadening does not alter the IWMF, i.e. where $b = 1$.

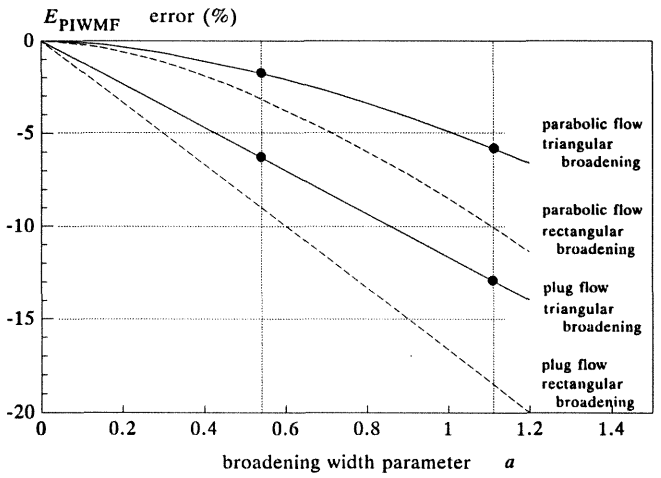


**Fig.7.5 - errors in PIWMF for plug and parabolic flows arising from rectangular and triangular broadening where the IWMF is unaltered, i.e. where $b$=1.**

*Plug flow - Triangular broadening*

For the same ideal spike spectrum the observed spectrum after triangular broadening can be seen, again without using (7.11), to be

$$p(f)=\frac{2}{abf_m}\left(1-\frac{2|f-bf_m|}{abf_m}\right) \qquad \left(1-a/2\right)bf_m < f < \left(1+a/2\right)bf_m \tag{7.15}$$

and zero elsewhere. The observed spectrum (solid line) is shown in fig.7.3 if again $u$ is taken to be $f_m$. Substitution of this into (7.9) leads to an expression for the observed PIWMF

$$\hat{f}=\left(1-\frac{7a}{60}\right)bf_m \tag{7.16}$$

A derivation of this result also is given in appendix F. The corresponding percentage error is

$$E_{PIWMF}=\left[b\left(1-\frac{7a}{60}\right)-1\right]\times 100\% \tag{7.17}$$

This is shown as the solid straight line in fig.7.5 for various values of $a$ with $b=1$.

*Parabolic flow*

In the case of parabolic flow the theoretical power spectrum from a 'thin' beam, scaled to give a numerical total power of 1, is found by putting $t = 0.5$ into (7.10). This is shown by the dotted line of fig.7.6. The PIWMF in the absence of broadening is given by (3.6) and is $\hat{f}_S = \frac{f_m}{2t+1}$, so for parabolic flow is $\hat{f}_S = \frac{f_m}{2}$. For both rectangular and triangular broadening the calculation of the observed spectrum from (7.11) is possible, and leads to piecewise expressions involving inverse hyberbolic tangents of simple functions of frequency. (An example is given in fig.7.6 where the dashed line gives the result of rectangular broadening of the dotted theoretical spectrum with $b = 1$ and $a = 0.4$.) However the substitution of these expressions into (7.9) to solve for PIWMF is difficult. The PIWMF of the broadened spectrum was therefore calculated by computer simulation where the continuous theoretical spectrum was treated as comprising 1000 discrete intervals, and where the mean in each interval was taken to avoid the problem that the theoretical spectral density is undefined at $f = f_m$. For the case where $b = 1$, the resulting percentage errors due to the spectral broadening are shown against $a$ by the curved lines in fig.7.5 for rectangular (dashed line) and triangular (solid line) broadening. As suggested earlier, the errors with parabolic flow are smaller in magnitude than the corresponding errors with plug flow.

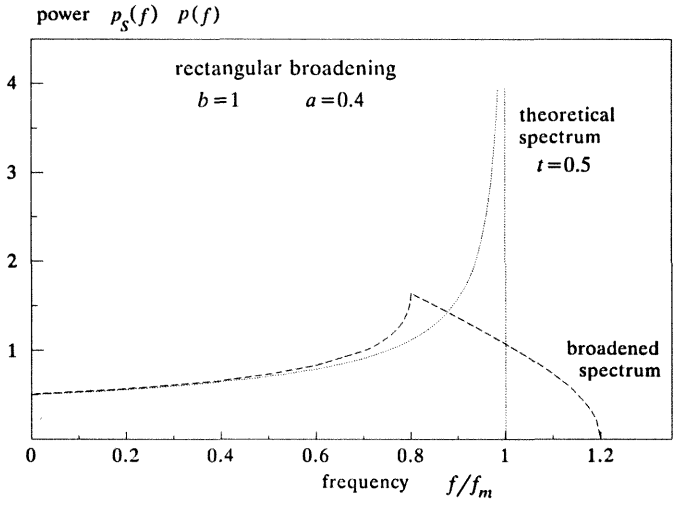


**Fig.7.6 - the theoretical spectrum (dotted line) for a 'thin' beam and a parabolic velocity profile, and the corresponding spectrum (dashed line) resulting from rectangular broadening with $b=1$ and $a=0.4$.**

*Some practical results*

In an experiment performed with a Diasonics Spectra scanner, equipped with a 7.5 MHz linear array probe, the spectrum returning from a straight section of a rubber O-loop moving with a constant velocity showed an approximately triangular form. An example of this has already been seen in fig.7.4. This broadening function can be treated as having a mean frequency which, to a first approximation, is equal to $f_\theta$, the spike frequency expected in assuming the single nominal angle $\theta$. Therefore $b = 1$ and the ratio of bandwidth to $f_\theta$ is equal to $a$. So according to (7.4) we can write

$$a = \frac{w}{f_\theta} \approx 2\varepsilon \tan\theta \qquad (7.18)$$

An estimate of the bandwidth was made for several angles and different speeds by finding the frequency difference between the points where the tails of the spectrum commenced, as defined by a visually noted change in the derivative of the spectrum, e.g. at the frequencies marked with the larger arrows on fig.7.4. In each case the 'average' Doppler frequency $f_\theta$ was also estimated. For the example given in fig.7.4, the ratio of the bandwidth, defined by the larger arrows, to the average frequency is $w/f_\theta \approx 0.62$, and the nominal angle is 59° (be it $\theta$ or $\kappa$ - the difference is small). Applying (7.18) gives an estimate of $\varepsilon$ of 11° (0.19 rad) from this single example. The results for this and other examples appeared consistent with a value of $\varepsilon \approx 13°$ (0.225 rad) for the linear array. This angle of $\varepsilon \approx 13°$ had previously been measured visually from the screen of the scanner, by noting the marked directions of the extreme rays insonating the sample volume. Therefore for the linear array putting $\varepsilon \approx 0.225$ in (7.18) gives

$$a \approx 0.45 \tan\theta$$

So for example nominal angles of $\theta = 50°$ and $\theta = 68°$ we have $a \approx 0.54$ and $a \approx 1.11$ respectively. (The angle of 68° represents the highest for which the scanner displays a calculated velocity scale in preference to a raw frequency scale, as conversion to velocity is thought to be too prone to error at higher angles.) These values of $a$ are marked by the vertical lines on fig.7.5. The broadening function in practice is approximately described by the triangular form and the appropriate points of error on fig.7.5 are marked. It is seen that for profiles between parabolic and plug, with an example Doppler angle of 50° PIWMF underestimates the value with no broadening, $\hat{f}_S$, by between 2% and 6% approximately, and with an angle of 68° by between 6% and 13% approximately, the smaller error in both cases being for parabolic flow.

## Theoretical form of the broadening function

For a long thin transducer with each point (or element) equally active, and a sample volume which by comparison is small in extent an approximately triangular form is expected. This is suggested by considering the insonation and particle motion shown in fig.7.1. The highest Doppler shifted frequencies observed result from energy transmitted and received by the leftmost transducer elements, and the lowest frequencies from energy transmitted and received by the rightmost elements. Middle frequencies are favoured because they arise not only from energy transmitted and received by middle elements, but also from energy transmitted by a left-hand element and received on the right, and vice versa. The result is a near symmetric single-peaked spectrum.

A more detailed treatment is given in appendix E, where it is suggested that the broadening function for scatterers at the point target, or in the practical case near the centre of the sample volume, is more closely represented by the square of an isosceles triangular form, so that the halves of the function are parabolic. A triangular form and a squared triangular form are shown by the dashed and solid lines of fig.7.7 respectively. Both these forms approximate the observed spectrum shown in fig7.4.

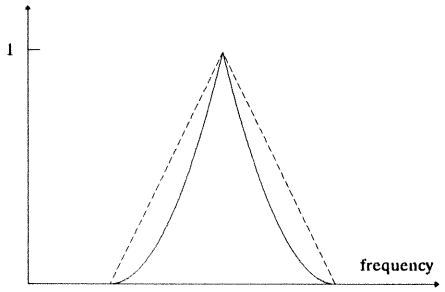


**Fig.7.7 - theoretical triangular and squared triangular broadening forms**

## Discussion

The errors read from the *dashed* lines of fig.7.5, appropriate for the rectangular broadening form, are unrealistically large. This is because the broadening observed with the linear array transducer was much more triangular than rectangular, which is not surprising if the array has each element equally active. In addition, if triangular broadening is assumed and $a$ is estimated from the extremes of the broadening function, then the errors given by the *solid* lines in fig.7.5 are perhaps worst-case results. This is firstly because the theory in appendix E favours the more peaked 'squared triangular' form of fig.7.7, and secondly because if some elements were favoured they would naturally be those at the centre of the

array, e.g. Gaussian 'apodization', and so the form of the resulting broadening function would be even more peaked than the approximate squared triangle. Against this however is the effect of the finite width of the sample volume, and the effect of the beam not being uniform throughout this width. The Doppler spectrum is therefore made up of different strength signals from different positions along the section of the moving rubber loop. The result is an approximate convolution of the 'squared triangular' form with the beam profile across the sample volume, and so is more uniform than the 'squared triangle'. The tail structure observed in fig.7.4 is thus reinforced, and the spectrum is broader to some degree than that which would arise from a point sample volume.

It is not necessarily correct to regard the broadening as maintaining the intensity weighted mean frequency of each nominal component. That is, in practice the broadening function would have $b \neq 1$ and so IWMF and a 'wide' beam would also lead to an error in mean velocity. For IWMF, the **form** of the function, and hence $a$, have no effect on accuracy. Equations (7.14) and (7.17) therefore suggest that the error incurred by IWMF is

$$E_{\mathrm{IWMF}} = (b-1) \times 100\%$$

which also follows from recognising that the idealised factor $b$ can be identified with the practical factor $k$ in (7.7).

## Spectral broadening from Fourier analysis

Only spectral broadening due to the finite dimensions of the transducer and sample volume has been discussed so far. Another source of spectral broadening is the leakage of power at any one frequency into neighbouring bins when analysis is performed by discrete Fourier transform. This leakage is not entirely symmetric and is reduced by the application of a window function. So the Fourier analysis itself introduces broadening which generally affects IWMF very slightly and PIWMF more. In this form of broadening the resulting bandwidth of a single low frequency component is as much as that of a high frequency component, and so the broadening models of fig.7.3 where the resulting bandwidths are proportional to the nominal frequency $u$ are not appropriate. The result is that this broadening may affect the spectrum at low frequencies as much as the geometrical broadening, but will not in general affect the spectrum as much at higher frequencies. For example, the spectrum of a pure sinusoid analysed by a 256 point Fast Fourier Transform using a Hanning window is, to a first approximation, an isosceles triangle with a bandwidth of 4 frequency bins. So for a component at the 10'th bin say the equivalent value of $a$ is approximately 0.4, and is comparable with the values of $a$ suggested as typical above. If the signal occupies the whole frequency range of 128 bins then, for a high frequency component, the equivalent value of $a$ is only approximately 0.03. At low frequencies a spectrum following (7.10) is relatively flat and is therefore largely unaffected by broadening

even if the value of $a$ is large. In the peaked high-frequency region the form of such a spectrum is susceptible to broadening, but as seen the appropriate value of $a$ is small. So it is suggested that if the spectrum occupies a large number of the available bins the effects on IWMF and PIWMF of spectral broadening due to the Fourier analysis are small.

## Spectral broadening due to non-stationarity of the Doppler signal

Changes in the velocity distribution of scatterers during the recording of the data segment will appear as a 'broadening' of the spectrum - a rectangular broadening if the accelerations are constant. This non-stationary behaviour of the Doppler signal would only give values of $a$ comparable with the typical values above if the velocity scale changed by approximately 50% during the recording time, which is typically 10 milliseconds. The effect is therefore negligible except perhaps at the onset of systole. A more detailed discussion of the effect of non-stationarity is given in appendix D. The mean velocity estimated no longer is an 'instantaneous' value but is the average mean velocity during the collection of the data segment. It is suggested in appendix D that such 'broadening' does not introduce error into the theoretical estimate of mean velocity made from IWMF, but does affect the validity of PIWMF in the way described in this chapter.

## Summary

Owing to the finite dimensions of the transducer and sample volume the Doppler spectrum received from scatterers moving with a unique velocity is in reality broad, and not a spike. The extent and form of this spectrum is also dependent on the angle between the direction of motion and the beam. If this broadened spike has an IWMF, which when combined with the assumed Doppler angle gives the correct unique velocity, then for any velocity distribution of scatterers in a 'wide' beam the IWMF when used with this angle will give the correct mean velocity. However the presence of non-linear terms in the expression for PIWMF means that this estimator is affected by any spectral broadening. For a broadening function which is symmetric and leaves IWMF unaltered, PIWMF underestimates the value found in the absence of broadening by an amount that depends on the velocity profile and the nature of the broadening function. The extent of the underestimate is increased if the theoretical spectrum becomes more peaked or if the broadening function widens which happens if the Doppler angle is increased. The broadening effect is then least when the Doppler angle is minimised, which is generally desired anyway. If velocity profiles following (3.1) between plug and parabolic forms are considered then the error is least when the flow is parabolic and greatest with plug flow.

The results of this chapter therefore lend support to the use of a 'wide' beam for mean velocity estimation, in preference to a 'thin' beam, as IWMF does not suffer from this broadening error.

## Notation for this chapter

| | |
|---|---|
| $a,b$ | parameters defining the idealised broadening functions |
| $f_{rep}$ | a frequency representative of the mean blood velocity |
| $g(a,V)$ | an error incurred by PIWMF due to the extent of broadening defined by the parameter $a$ and related to the velocity profile $V$ |
| $V$ | the function describing the velocity profile |
| $w$ | bandwidth of the Doppler spectrum of a single velocity component |
| $\delta$ | the difference in angle between the bisector of the length subtended by the transducer and the bisector of the angle subtended by the transducer, i.e. the difference between $\theta$ and $\kappa$ |
| $\varepsilon$ | half of the angular extent of the transducer at the target point |
| $\kappa$ | the angle at the target between the direction of motion and the angle bisector of the transducer |
| $\theta$ | the angle at the target between the direction of motion and the line to the centre of the transducer |
| $\theta_{eff}$ | the unique angle that would lead to the correct value of IWMF |

# CHAPTER 8 - NOISE IN THE DOPPLER SIGNAL

The effect on IWMF and PIWMF of failures of the assumptions about the beam have been studied in the previous three chapters. Another source of corruption of the theoretical spectrum is the presence of noise in the Doppler signal. In this chapter the errors incurred by IWMF and PIWMF in the presence of additive noise are found and compared. The analysis takes no account of the stochastic nature of the spectral estimates observed in practice, but is appropriate for deterministic spectra.

The model studied is that of a theoretical Doppler signal with a single-sided power spectrum of $p_S(f)$, as introduced in chapter 3, contaminated by additive noise with a power spectrum of $p_N(f)$. So the power spectrum of the total signal, $p(f)$, is the sum of the spectra of the signal and noise independently, i.e. $p(f) \equiv p_S(f) + p_N(f)$. The symbols $S$ and $N$ denote the total powers in the signal and noise respectively, i.e.

$$S = \int_0^\infty p_S(f)\,df$$

and

$$N = \int_0^\infty p_N(f)\,df$$

so that the ratio $S/N$ can be thought of as a signal to noise ratio (snr).

## The effect of noise on IWMF

The result for IWMF is known and can be derived as follows. From (2.10) the IWMF of the signal spectrum, $\bar{f}_S$, is

$$\bar{f}_S = \frac{\int_0^\infty f\, p_S(f)\,df}{S}$$

and the IWMF of the noise spectrum, $\bar{f}_N$, is

$$\bar{f}_N = \frac{\int_0^\infty f\, p_N(f)\,df}{N}$$

The IWMF of the observed spectrum, $\bar{f}$ , can then be written as

$$\begin{aligned}\bar{f} &= \frac{\int_0^\infty f\left(p_S(f)+p_N(f)\right)df}{S+N} \\ &= \frac{\int_0^\infty f\, p_S(f)df}{S\left(1+N/S\right)} + \frac{\int_0^\infty f\, p_N(f)df}{N\left(1+S/N\right)} \\ &= \frac{\bar{f}_S}{1+\mathrm{snr}^{-1}} + \frac{\bar{f}_N}{1+\mathrm{snr}}\end{aligned}$$

If the definition of $\bar{f}$ in (2.10), and consequently the above expressions for $\bar{f}_S$ and $\bar{f}_N$, are extended to be valid for a double-sided spectrum by moving the lower limit of integration to -∞ then the same result is obtained, so that this equation is applicable to both single- and double-sided spectra. This equation is also the result of Gerzberg and Meindl (1977) and Gill (1979). The IWMF is therefore a weighted mean of the IWMF values of the signal and noise spectra, with the weighting determined by the signal to noise ratio. This equation can be expressed as

$$\begin{aligned}\bar{f} &= \frac{\bar{f}_S + \mathrm{snr}^{-1}\bar{f}_N}{1+\mathrm{snr}^{-1}} \\ &= \left(\bar{f}_S + \mathrm{snr}^{-1}\bar{f}_N\right)\left(1-\mathrm{snr}^{-1}+\mathrm{snr}^{-2}\ldots\right)\end{aligned}$$

If $\bar{f}_S$ and $\bar{f}_N$ are of the same order and snr is high (ie. $\mathrm{snr} >> 1$ so $\mathrm{snr}^{-1} >> \mathrm{snr}^{-2}$) then terms in $\mathrm{snr}^{-2}$ and smaller can be removed to give an approximation for the absolute effect of the noise

$$\bar{f} \approx \bar{f}_S + \mathrm{snr}^{-1}\left(\bar{f}_N - \bar{f}_S\right) \qquad \text{(8.1a)}$$

The IWMF is seen to be shifted by an amount equal to the signal to noise ratio multiplied by the difference in the intensity weighted mean frequencies of the noise and signal spectra. The fractional effect is then given by

$$\bar{f} \approx \bar{f}_S\left[1+\mathrm{snr}^{-1}\left(\bar{f}_N/\bar{f}_S - 1\right)\right] \qquad \text{(8.1b)}$$

## The effect of noise on PIWMF

*Low and high frequency noise*

Some basic principles about the effect on PIWMF can be established by considering the effects of low- and high-frequency noise. Because low frequencies, attributed to scatterers further from the vessel axis, are weighted more in PIWMB than in IWMB, low-frequency noise will affect PIWMB more than IWMB. The opposite is true for high-frequency noise. These principles, which are clearly valid for PIWMF and IWMF too, can be illustrated quantitatively by considering a discrete deterministic theoretical signal spectrum completely contained between the $L$'th bin and the $H$'th bin inclusive, and scaled to have a total power of 1. Therefore $\sum_{i=L}^{H} \tilde{p}_i = 1$. The IWMB and PIWMB of this uncorrupted spectrum are denoted by $\overline{B}_{DS}$ and $\hat{B}_{DS}$. From (2.1b) and (2.9b) they are therefore given by

$$\overline{B}_{DS} = \sum_{i=L}^{H} i\tilde{p}_i \tag{8.2}$$

and

$$\hat{B}_{DS} = \sum_{i=L}^{H} i\tilde{p}_i \left( 2\sum_{j=i+1}^{H} \tilde{p}_j + \tilde{p}_i \right) \tag{8.3}$$

respectively. If a low-frequency noise component of mean power $\tilde{x}$ is introduced into the $a$'th bin, where $\tilde{x} << 1$ and $a < L$, giving the situation of fig.8.1a, then (2.9b) becomes

$$\hat{B}_D = \frac{a.\tilde{x}(2+\tilde{x}) + \hat{B}_{DS}}{(1+\tilde{x})^2}$$

using (8.3), where the new term in the numerator is the contribution of the $a$'th bin in the main summation. Using $(1+\tilde{x})^{-2} = (1-2\tilde{x}+3\tilde{x}^2-\ldots)$, discarding terms in $\tilde{x}^2$ and smaller, and recognising that the signal to noise ratio is $1/\tilde{x}$ gives

$$\hat{B}_D \approx \hat{B}_{DS} - 2\mathrm{snr}^{-1}\left(\hat{B}_{DS} - a\right) \tag{8.4}$$

Equation (8.1a) for IWMB in this case becomes

$$\overline{B}_D \approx \overline{B}_{DS} - \mathrm{snr}^{-1}\left(\overline{B}_{DS} - a\right) \tag{8.5}$$

so the effect of the low-frequency noise on PIWMB is of the order of twice as much as the effect on IWMB, and is negative as is expected.

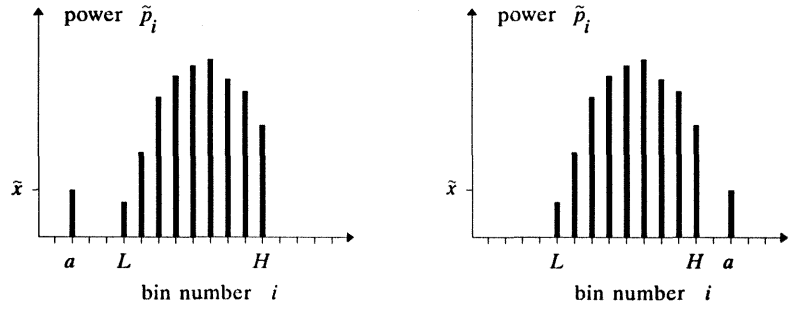


**Fig.8.1 - examples of noise below and above a signal spectrum**

Similarly if a high frequency noise component of power $\tilde{x}$ is introduced into the $a$'th bin, where $a > H$, giving the situation of fig.8.1b, then (2.9b) becomes

$$\hat{B}_D = \frac{\hat{B}_{DS} + \sum_{i=L}^{H} i\tilde{p}_i . 2\tilde{x} + a.\tilde{x}^2}{(1+\tilde{x})^2}$$

using (8.3). Again terms in $\tilde{x}^2 \equiv \text{snr}^{-2}$ and smaller are discarded to give

$$\hat{B}_D \approx \hat{B}_{DS} + 2\text{snr}^{-1}\left(\overline{B}_{DS} - \hat{B}_{DS}\right) \qquad (8.6)$$

using (8.2). From (2.12) $\overline{B}_{DS} \geq \hat{B}_{DS}$ , so the high frequency noise raises PIWMB as would be expected. The frequency $a$ of the noise would appear only in terms in $\text{snr}^{-2}$ and smaller so that when compared with (8.5), which again is appropriate for IWMB, it is seen that very high frequency noise affects PIWMB less than IWMB. The effect on PIWMB is linked more to the difference between $\overline{B}_{DS}$ and $\hat{B}_{DS}$ , which increases with a greater low-frequency emphasis in the signal spectrum, than to the location, $a$, of the high frequency noise.

Figs. 8.1a and 8.1b represent simple extreme cases, and show that noise of a frequency below the signal has of the order of twice the effect on PIWMF as on IWMF, and noise of a frequency above the signal tends to have less effect on PIWMF than on IWMF. In the typical case where the signal and noise bands overlap, e.g. in the case of the white noise discussed in the next section, the effect on PIWMF for a given signal to noise ratio will be between the above extremes.

*White noise and theoretical spectra*

A situation of interest is where the noise is white (i.e. of uniform power density) up to a maximum frequency, say $f_e$, which might for example be the Nyquist limit corresponding to the highest bin. To facilitate analysis the signal is assumed to correspond to a velocity profile following (3.1). The corresponding theoretical spectrum normalised to have total power of 1 has been derived as equation (3.4), which is restated here.

$$p_S(f) = \frac{t}{f_m}\left(1 - \frac{f}{f_m}\right)^{t-1} \qquad 0 \le f \le f_m \tag{8.7}$$

For the 'wide' beam $t \equiv 2/n$ and for the 'thin' beam $t \equiv 1/n$ . For such a spectrum the IWMF, $\bar{f}_S$ , and the PIWMF, $\hat{f}_S$ , have been found to be

$$\bar{f}_S = \frac{f_m}{t+1} \tag{8.8}$$

and

$$\hat{f}_S = \frac{f_m}{2t+1} \tag{8.9}$$

which are equations (3.5) and (3.6) restated. An example of the relationship of the signal and noise bands is given in fig.8.2. The signal spectrum is given by the dotted line and is that for $t = 0.5$. In this case it occupies approximately 70% of the noise band, the spectrum of which is given by the dashed line.

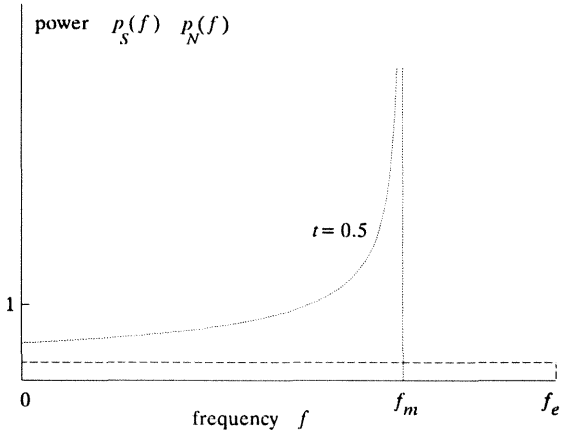


**Fig.8.2 - a theoretical spectrum with $t$=0.5 (dotted line) in relation to white noise (dashed line)**

From (2.11) the PIWMF for the signal alone, $\hat{f}_S$ , would be

$$\hat{f}_S = \frac{2\int_0^{f_m} f\, p_S(f)\left(\int_f^{f_m} p_S(u)\,du\right)df}{S^2} \tag{8.10}$$

the PIWMF for the noise alone, $\hat{f}_N$ , would be

$$\hat{f}_N = \frac{2\int_0^{f_e} f\, p_N(f)\left(\int_f^{f_e} p_N(u)\,du\right)df}{N^2} \tag{8.11}$$

and the PIWMF for the total signal is

$$\hat{f} = \frac{2}{(S+N)^2}\int_0^{f_e} f\left(p_S(f)+p_N(f)\right)\left[\int_f^{f_e}\left(p_S(u)+p_N(u)\right)du\right]df \ .$$

The total signal is divided into its components, and regions of integration where the signal is zero are ignored. So this last equation can be rewritten as

$$\begin{aligned}\frac{(S+N)^2}{2}\hat{f} = &\int_0^{f_m} f\, p_S(f)\left[\int_f^{f_m} p_S(u)du\right]df \\ &+\int_0^{f_m} f\, p_S(f)\left[\int_f^{f_e} p_N(u)du\right]df + \int_0^{f_m} f\, p_N(f)\left[\int_f^{f_m} p_S(u)du\right]df \\ &+\int_0^{f_e} f\, p_N(f)\left[\int_f^{f_e} p_N(u)du\right]df\end{aligned} \tag{8.12}$$

The first line of the right hand side can be seen from (8.10) to be equal to $\frac{1}{2}S^2\hat{f}_S$ and the third line, from (8.11), to be equal to $\frac{1}{2}N^2\hat{f}_N$ . The more difficult terms are the 'cross-integral' terms making up the second line. For a signal with total power $S$ the spectrum of (8.7), which has unit power, is multiplied by $S$. The noise spectrum is a constant, between 0 and $f_e$, given by $p_N(f) = N/f_e$ , so that the second line is given by

$$\text{second line} = \int_0^{f_m} f\,\frac{St}{f_m}\left(1-{}^{f}\!/_{f_m}\right)^{t-1}\frac{N}{f_e}(f_e-f)df + \int_0^{f_m} f\,\frac{N}{f_e}\left[\int_f^{f_m}\frac{St}{f_m}\left(1-{}^{u}\!/_{f_m}\right)^{t-1}du\right]df$$

It is useful to define the proportion of the noise band occupied by the signal as $m$, i.e. $m \equiv \frac{f_m}{f_e}$. The integrations are performed by making the substitutions $x = 1 - f/f_m$ and $y = 1 - u/f_m$. Using (8.8) gives the result

$$\text{second line} = SN\left(1 - \frac{m}{t+2}\right)\bar{f}_S \tag{8.13}$$

The derivation of this result is given in appendix F. Substituting for the three lines of the right hand side of (8.12) gives

$$\frac{(S+N)^2}{2}\hat{f} = \frac{S^2}{2}\hat{f}_S + SN\left(1 - \frac{m}{t+2}\right)\bar{f}_S + \frac{N^2}{2}\hat{f}_N$$

Therefore

$$\hat{f} = \frac{1}{\left(1+N/S\right)^2}\hat{f}_S + \frac{2\left(1-\frac{m}{t+2}\right)}{\left(1+N/S\right)\left(1+S/N\right)}\bar{f}_S + \frac{1}{\left(1+S/N\right)^2}\hat{f}_N$$

which simply becomes

$$\hat{f} = \frac{\hat{f}_S + 2\,\mathrm{snr}^{-1}\left(1-\frac{m}{t+2}\right)\bar{f}_S + \mathrm{snr}^{-2}\hat{f}_N}{\left(1+\mathrm{snr}^{-1}\right)^2}$$

Furthermore again ignoring terms in $\mathrm{snr}^{-2}$ gives the approximation for the absolute effect of the noise

$$\hat{f} \approx \hat{f}_S + 2\,\mathrm{snr}^{-1}\left(\left(1-\frac{m}{t+2}\right)\bar{f}_S - \hat{f}_S\right) \tag{8.14a}$$

This reduces to the form of (8.6) for a continuous spectrum when $m$ is small, which is as expected as this corresponds to a noise spectrum effectively of frequencies all higher than the signal. The fractional effect of the noise is therefore given by

$$\hat{f} \approx \hat{f}_S\left[1 + 2\,\mathrm{snr}^{-1}\left(\left(1-\frac{m}{t+2}\right)\frac{\bar{f}_S}{\hat{f}_S} - 1\right)\right] \tag{8.14b}$$

## Comparison of noise immunity

The most useful comparison between the effects of white noise on IWMF and PIWMF for such spectra is made by considering (8.1) and (8.14). These equations are appropriate if the signal to noise ratio is high enough so that terms in $\text{snr}^{-2}$ can be ignored. We consider the fractional effects, called $E_{\text{IWMF}}$ and $E_{\text{PIWMF}}$, which are the second terms in the square brackets of (8.1b) and (8.14b) respectively. That is

$$E_{\text{IWMF}} \approx \text{snr}^{-1}\left(\bar{f}_N \big/ \bar{f}_S - 1\right) \qquad \text{and} \qquad E_{\text{PIWMF}} \approx 2\text{snr}^{-1}\left(\left(1-\frac{m}{t+2}\right)\frac{\bar{f}_S}{\hat{f}_S} - 1\right)$$

Making use of the fact that equations (8.8) and (8.9) are valid for any scale factor $S$, and also the obvious fact that $\bar{f}_N = \frac{f_e}{2} \equiv \frac{f_m}{2m}$, leads to

$$E_{\text{IWMF}} \approx \text{snr}^{-1}\left(\frac{t+1}{2m} - 1\right) \qquad \text{and} \qquad E_{\text{PIWMF}} \approx 2\text{snr}^{-1}\left(\left(1-\frac{m}{t+2}\right)\left(1+\frac{t}{t+1}\right) - 1\right)$$

These fractional effects are plotted in fig.8.3 for the uniform spectrum given by $t = 1$ (solid lines), the spectrum of fig.8.2 given by $t = 0.5$ (dotted lines) and the spike spectrum given by $t = 0$ (dashed lines). It is noted that $m$ is bound between 0 and 1. Also, for flows between plug and parabolic, $t$ is bound between 0 and 1 for a 'wide' beam and between 0 and 0.5 for a 'thin' beam.

A number of conclusions can be drawn from these equations and fig.8.3. Firstly, if the snr is large, so that we are justified in ignoring terms in $\text{snr}^{-2}$ and smaller, the fractional effect of the noise on each estimator can be regarded as being proportional to $\text{snr}^{-1}$. Secondly the magnitude of the effect on PIWMF is less than or equal to $\text{snr}^{-1}$. Thirdly for IWMF, because curves A, B and C are asymptotic to the y-axis at $m \approx 0$, there is no limit to the effect of the noise as the signal frequency band becomes lower relative to the noise. The worst negative effect is $-50 \times \text{snr}^{-1}\%$ when the spectrum is a spike at the maximum noise frequency.

The effects on IWMF and PIWMF may be compared in two ways. Firstly the comparison may be made for a given spectrum, defined by $t$. This might be appropriate if the width of the beam is fixed and is such that neither IWMF nor PIWMF is obviously superior. In these cases the spectrum will generally not follow (8.7). In particular it is unlikely to be nearly uniform because, when the beamwidth is less than the diameter of the vessel, a uniform spectrum implies that $n < 2$. However, such comparison of curves A and D shows

that for a uniform spectrum the fractional effect on PIWMF is less than or equal to the effect on IWMF. Comparison of curves C and F shows that for a spike spectrum the modulus of the fractional effect on PIWMF is less in magnitude than the effect on IWMF only if the spike is at a frequency less than approximately 0.35 of the highest noise frequency, i.e. $m <\approx 0.35$. The point of equal error magnitude is marked on fig.8.3.

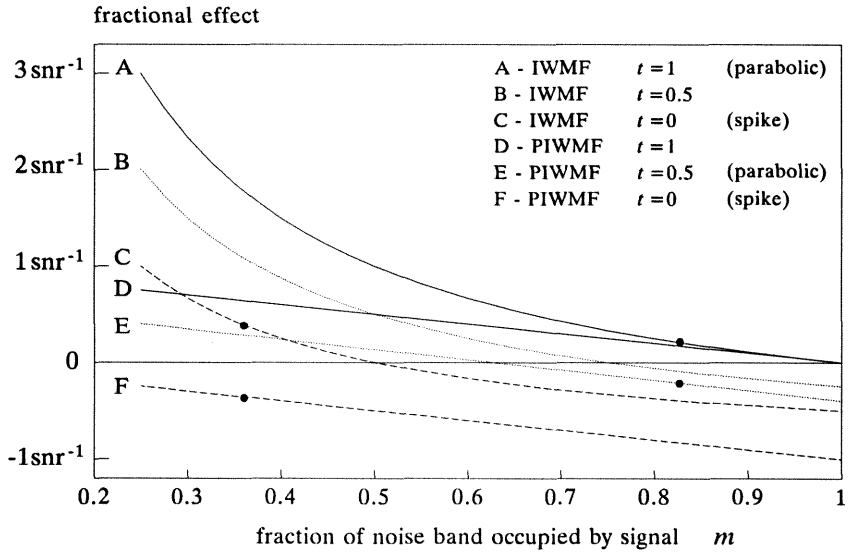


**Fig.8.3 - fractional errors in the estimators IWMF and PIWMF for white noise and three theoretical spectra**

Secondly a comparison can be made for a given velocity profile, defined by $n$, where it is assumed that IWMF is used when the beam is 'wide' so that $t \equiv 2/n$ , and PIWMF is used when the beam can be thought of as 'thin' so that $t \equiv 1/n$ . As the estimators are being used with the beams for which, other factors allowing, they are accurate the 'effect' of the noise, plotted and described above, can be thought of as the 'error'. For parabolic flow $n = 2$ and curve A is compared with curve E. This shows that the magnitude of the fractional error in PIWMF is less than in IWMF when the highest signal frequency is less than approximately 0.8 of the highest noise frequency, i.e. $m <\approx 0.8$. Again the point of equal error size is marked on fig.8.3. For plug flow both beams give a spike spectrum and curves C and F are again to be compared.

These results support the previous observations that high-frequency noise tends to have less effect on PIWMF than on IWMF, and that low-frequency noise has more effect on PIWMF than on IWMF.

## Summary

Comparison between the effects of noise on IWMF and PIWMF can firstly be made for a given Doppler spectrum, which might be appropriate for a beam falling between the ideals of being of 'wide' or 'thin'. In this case, as shown in chapter 5, neither estimator is accurate, and the effect of the noise is to alter the actual error in the mean velocity estimate. Secondly comparison can be made for a given velocity profile. If each estimator is then used with its appropriate beam, so that, other factors aside, each is accurate, then the effects of the noise described here are the errors in the velocity estimates.

The basic principle affecting a comparison is the notion that for a given signal spectrum high-frequency perturbations tend to have less effect on PIWMF than on IWMF, but low-frequency perturbations have more effect. This is because high frequencies are interpreted by PIWMF as originating from scatterers nearer the centre of the vessel, (i.e. coming from radial positions contributing proportionately less to the cross-sectional area,) and low frequencies are interpreted as originating from nearer the vessel walls.

If the signal to noise ratio is large the errors in each estimator are approximately proportional to the inverse of this ratio. PIWMF is affected to the order of twice as much as IWMF by perturbations in a given spectrum at frequencies below the minimum signal frequency, but tends to be affected less than IWMF by perturbations above the highest frequency. With white noise, a theoretical spectrum derived from the family of velocity profiles defined by (3.1), and a large signal to noise ratio, the modulus of the fractional effect on PIWMF is less than the inverse of the signal to noise ratio. There is no bound on the possible fractional increase in IWMF caused by the noise, but the greatest fractional decrease possible is half the inverse of the signal to noise ratio.

## Notation for this chapter

| | |
|---|---|
| $a$ | bin number of an idealised noise component |
| $\overline{B}_{DS}$ , $\hat{B}_{DS}$ | IWMB and PIWMB of the deterministic signal in the absence of noise |
| $f_e$ | upper limit of white noise band |
| $\overline{f}_N$ , $\hat{f}_N$ | IWMF and PIWMF of noise spectrum |
| $H$ | the index of the highest frequency bin with non-zero spectral power |
| $L$ | the index of the lowest frequency bin with non-zero spectral power |
| $m$ | ratio of maximum signal frequency to maximum noise frequency |
| $N$ | total noise power |
| $p_N(f)$ | power spectrum of noise |
| $S$ | total power in signal |
| snr | signal to noise ratio |
| $\tilde{x}$ | mean power of an idealised noise component |

# CHAPTER 9 - HIGH-PASS FILTERING OF THE DOPPLER SIGNAL

For both 'wide' and 'thin' beams the sample volume needs to be sufficiently long to insonate the scatterers adjacent to the vessel walls. A consequence of this is that added to the scattered signal from the blood are echoes from the relatively highly reflective, slowly moving vessel walls. If a high-pass filter was not applied this would cause an unwanted, high-amplitude low-frequency component in the Doppler signal. The removal of this unwanted component means however that the low-frequency components of the Doppler spectrum from the flowing blood are also removed. Intuitively this results in overestimation of the representative frequency of the Doppler spectrum and consequent overestimation of the mean blood velocity. The quantitative effect of such filtering on both IWMF and PIWMF can be found if the velocity profile and filter characteristics are idealised. In this chapter the familiar velocity profiles given by (3.1) are used to derive expressions for the errors in IWMF and PIWMF with the ideal high-pass, i.e. brick wall, filter. This is implied to be the form of the filter leading to the greatest errors. Also the effects of a gradual ramp-shaped filter are discussed.

For a profile of (3.1) the equations (3.4), (3.5) and (3.6) relevant to the corresponding normalised theoretical spectrum are restated. The spectrum is

$$p_S(f) = \frac{t}{f_m}\left(1 - \frac{f}{f_m}\right)^{t-1} \qquad 0 \le f \le f_m \tag{9.1}$$

where for the 'wide' beam $t \equiv 2/n$ and for the 'thin' beam $t \equiv 1/n$. The IWMF is

$$\bar{f}_S = \frac{f_m}{t+1} \tag{9.2}$$

and the PIWMF is

$$\hat{f}_S = \frac{f_m}{2t+1} \tag{9.3}$$

These equations therefore define the 'correct' values of IWMF and PIWMF, i.e. the values that would be observed if there was no low-frequency component from the wall motion and no filter was applied.

## Ideal high-pass filter model

The filter model chosen defines the response to be zero below a cut-off (*brick* wall) frequency, $f_b$, and uniform above this frequency at least to above the maximum frequency in the signal, $f_m$. This step function is an ideal high-pass filter, and was used, in effect, by

Gill (1979) for the case where a 'wide' beam is assumed. Gill considered velocity profiles given by (3.1) which, as seen above, give rise to normalised Doppler spectra, according to (9.1). An example of the filter transfer function, in relation to such a spectrum, is given by the solid line of fig.9.1.

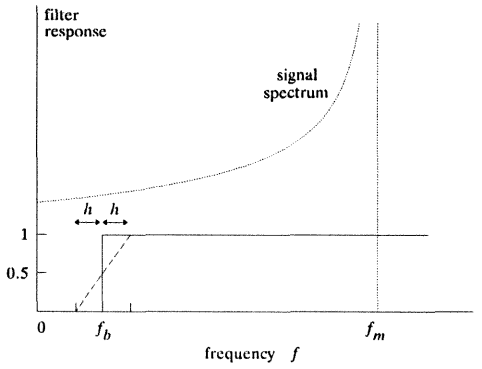


**Fig.9.1 - an ideal high-pass filter (solid line) and a corresponding 'ramp' filter (dashed line) in relation to a spectrum following equation (9.1)**

The spectrum after filtering is given by (9.1) for frequencies greater than $f_b$, and is zero below $f_b$. The relationship of the filter to the theoretical spectrum is characterised by the ratio of the cut-off frequency to the highest signal frequency. This ratio is denoted by $b$, i.e. $b \equiv f_b / f_m$ .

## The effect on IWMF

The IWMF of the signal is defined by (2.10) and in the absence of the filter is $\bar{f}_s$ . The IWMF after the filtering is the observed value $\bar{f}$. If the unfiltered spectrum follows (9.1) then this IWMF is given by

$$\bar{f} = \frac{\int_{f_b}^{f_m} f \cdot \frac{t}{f_m}\left(1 - f/f_m\right)^{t-1} df}{\int_{f_b}^{f_m} \frac{t}{f_m}\left(1 - f/f_m\right)^{t-1} df} \qquad (9.4)$$

$$= f_m\left(\frac{1}{t+1} + \frac{tb}{t+1}\right)$$

The derivation of this result is given in appendix F.

Using (9.2) gives for the multiplicative effect of the filter

$$\bar{f} = \bar{f}_S(1+tb) \tag{9.5a}$$

and using the definition of $b$ gives for the additive effect of the filter

$$\bar{f} = \bar{f}_S + f_b\left(\frac{t}{t+1}\right) \tag{9.5b}$$

The effect of the filter, for a given value of $t$, is to introduce a positive fixed absolute offset to the IWMF. This is true with any value of the maximum frequency $f_m$, provided $f_m > f_b$ of course. Using the forms of equations (9.1), (9.2) and (9.5b) for uniform insonation (i.e. where $t \equiv 2/n$ ) Gill reached the same conclusion about the effect of this filter on the intensity weighted mean frequency.

## The effect on PIWMF

The PIWMF is defined by (2.11) and in the absence of a filter is $\hat{f}_S$ . The observed PIWMF is $\hat{f}$. So if the unfiltered spectrum follows (9.1) this PIWMF is

$$\begin{aligned}\hat{f} &= \frac{2\int_{f_b}^{f_m} f \cdot \frac{t}{f_m}\left(1-f/f_m\right)^{t-1}\left[\int_f^{f_m}\frac{t}{f_m}\left(1-u/f_m\right)^{t-1}du\right]df}{\left(\int_{f_b}^{f_m}\frac{t}{f_m}\left(1-f/f_m\right)^{t-1}df\right)^2} \\ &= f_m\left(\frac{1}{2t+1}+\frac{2tb}{2t+1}\right)\end{aligned} \tag{9.6}$$

The derivation of this result also is given in appendix F. The correct PIWMF is given by (9.3) so that the multiplicative effect of the filter is

$$\hat{f} = \hat{f}_S(1+2tb) \tag{9.7a}$$

and using the definition of $b$ gives the additive effect

$$\hat{f} = \hat{f}_S + f_b\left(\frac{2t}{2t+1}\right) \tag{9.7b}$$

As with IWMF, for a given value of $t$, the filter produces a fixed offset to the measured frequency estimator.

## Comparison of immunity to filtering

As with the effects of noise discussed in the previous chapter, the comparison of the effects of filtering on IWMF and PIWMF can either be made for a given spectrum, or for a given profile with the appropriate beams assumed.

*(i) comparison for the same spectrum*

If the comparison is made for a given spectrum, defined by $t$, then (9.5a) and (9.7a) show that the fractional effect of a filter on PIWMF is twice the effect on IWMF. From (9.5b) and (9.7b) the absolute effect on PIWMF is a factor of $\frac{2t+2}{2t+1}$ times as large as the effect on IWMF. Therefore when applied to a common signal PIWMF is affected more by the ideal high-pass filter than IWMF. The results for a uniform spectrum are found by putting $t=1$. Putting $t=0$ gives the trivial case of a spectrum which is a spike at $f=f_m$, and the spectrum and the estimators are unaffected by the filter.

*(ii) comparison for the same profile*

If the comparison is made for a given velocity profile, and IWMF is used with a 'wide' beam, i.e. $t \equiv 2/n$, and PIWMF with a 'thin' beam, i.e. $t \equiv 1/n$, then (9.5a) and (9.7a) become $\bar{f} = \bar{f}_S\left(1+\frac{2b}{n}\right)$ and $\hat{f} = \hat{f}_S\left(1+\frac{2b}{n}\right)$. Thus the fractional effect of the filter is the same on both estimators. Also with these appropriate beams the 'mean' frequencies, $\bar{f}_S$ and $\hat{f}_S$, given by (9.2) and (9.3), must be equal. So the absolute effects of the filter are also equal. This can alternatively be seen by noting that (9.5b) and (9.7b) become $\bar{f} = \bar{f}_S + f_b\left(\frac{2}{2+n}\right)$ and $\hat{f} = \hat{f}_S + f_b\left(\frac{2}{2+n}\right)$. Therefore, when applied to signals derived from beams for which they are appropriate, IWMF and PIWMF are affected equally by the simple high-pass filter described. This is a sensible conclusion as perfect removal of low frequencies corresponds to ignoring the scatterers further than a particular distance from the vessel axis. In effect the estimators after the filtering both provide correct measures of the mean velocity through this reduced but still circular cross section, with a truncated but still monotonic profile, and so they will be equal. For a parabolic velocity profile the results are found by putting $n=2$. For plug flow $n=\infty$, the spectrum is a spike as above, and the error due to the filter is zero.

## Discussion

For both estimators the fractional effect of such a filter is proportional to $b$ which is the ratio of the cut-off frequency $f_b$ to the maximum frequency in the Doppler spectrum, $f_m$. The maximum frequency is representative of the velocity scale so the fractional effect of the filter is smaller at peak systole and greater during diastole, as might be expected. The absolute effect in both cases is proportional to the filter cut-off frequency, and is not dependent on the maximum signal frequency. As is intuitive, in every case the effect of the filter is to produce an overestimate of mean blood velocity.

If the filter is adjustable the error will be minimised when $f_b$ is equal to (i.e. just above) the highest frequency in the unwanted high-amplitude signal component. If we assume this component is due entirely to motion of the vessel walls perpendicular to the vessel axis then, given knowledge of the maximum speed of the vessel wall, denoted by $v_{wmax}$, this minimum filter frequency can be found. Using the Doppler equation (1.2) the minimum filter frequency, $f_{b_{min}}$, can be seen to be

$$f_{b_{min}} \approx \frac{2F v_{wmax} \sin\theta}{c} \tag{9.8}$$

where $\sin\theta$ replaces the normal $\cos\theta$ as the vessel wall motion is perpendicular to the vessel axis. So another advantage of reducing the Doppler angle becomes evident, as with a smaller angle the filter frequency required is also reduced. Applying the Doppler equation to calculate $f_m$ from $v_m$, i.e.

$$f_m \approx \frac{2F v_m \cos\theta}{c}$$

leads to an expression for the lowest possible value of $b$, which is

$$b_{min} \equiv \frac{f_{b_{min}}}{f_m} = \frac{v_{wmax}}{v_m} \cdot \tan\theta$$

If the filter is adjustable the fractional error incurred is therefore proportional to the tangent of the Doppler angle.

It is implied in the previous chapter in equations (8.4) and (8.5) that fractionally PIWMF is approximately twice as sensitive as IWMF to additive noise of near-zero frequency. By implication this is true also for a subtractive effect. So it is not surprising that when comparing results for a given spectrum the factor 2 appears in the relative sizes of the fractional effects on PIWMF and IWMF with the ideal high-pass filter, which is an example of a perturbation in the spectrum affecting only the lower frequencies.

Other results in the previous chapter, i.e. comparison of (8.6) and (8.5), and fig.8.3, indicate that as the frequency of the perturbation becomes higher relative to the signal band the relative effect on PIWMF with respect to the effect on IWMF decreases, eventually becoming less than 1. So a filter without the sharp step at a well-defined frequency, because it would attenuate some higher frequencies partially without attenuating lower frequencies completely, would cause a fractional effect on PIWMF *less* than twice the fractional effect on IWMF. Therefore, for a given spectrum, if this measure of relative performance of PIWMF to IWMF is used, the ideal high-pass filter form gives the most unfavourable results.

## Ramp Filter

A simple example of a filter without the step is the 'ramp' filter given by the dashed line in fig.9.1. This ramp is based around the same frequency $f_b$. After the ideal high-pass filter this would be the first approximation to an actual filter characteristic. For a ramp with an extent, $2h$, which is small, the ramp filter performs like the ideal filter already described. Furthermore as $h$ increases the ramp becomes more horizontal until in the absurd limit it would be uniform with a value of 0.5, in which case it is obvious that both IWMF and PIWMF would be unaffected. Because it is intuitive that the effect of the filter on each estimator is monotonic decreasing with increasing $h$ it follows that the effect on IWMF or PIWMF is greatest when the filter is of the ideal high-pass form.

## Summary

When applied to a given spectrum a high-pass filter affects PIWMF more than IWMF because it alters the low frequency content of the signal, which with PIWMF is weighted more heavily. For a velocity profile following (3.1), the ratio of the fractional effect on PIWMF to that on IWMF is at its maximum value of 2 when the filter is of the ideal high-pass form, i.e. when the response is a step function. However if the estimators are each applied to beams for which they are accurate then, for a given velocity profile, the same ideal high-pass filter causes the same error in each estimator.

If, in the place of an ideal high-pass filter, a ramp filter is used, with the ramp positioned to extend equally either side of the position of the response step, both estimators incur less error. By implication the ideal high-pass is the form of the filter leading to the greatest errors.

## Notation for this chapter

| | |
|---|---|
| $b$ | ratio of cut-off frequency of ideal filter to maximum frequency in signal |
| $f_b$ | cut-off frequency in ideal high-pass (step) filter |
| $h$ | half the frequency width of the ramp in 'ramp' filter |

# CHAPTER 10 - BIAS AND VARIANCE IN THE MEAN VELOCITY ESTIMATES

Estimation of mean blood velocity is based on the principle that, for a fixed incident intensity, the expected power of the Doppler signal in the $i$'th bin, $\tilde{p}_i$, is proportional to the number of scatterers in the sample volume with velocities in the corresponding range. In the actual case the stochastic nature of the signal dictates that the observed results of spectral analysis are random estimates, $p_i$, of these $\tilde{p}_i$ values, with these random values being dependent on the spatial distribution of the relevant scatterers. An example of a deterministic, i.e. expected, spectrum and a stochastic equivalent are given in fig.10.1.

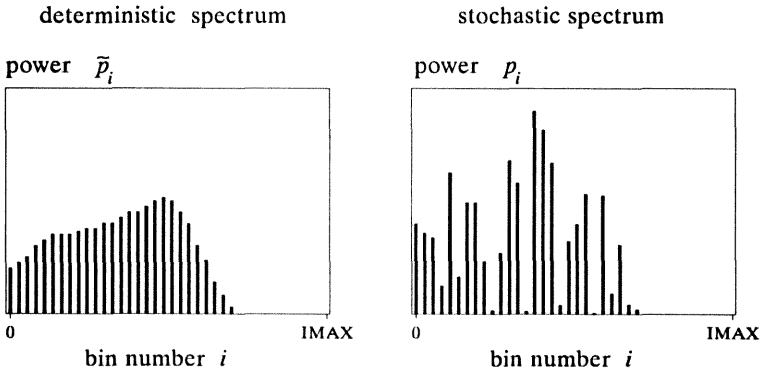


**Fig.10.1 - examples of deterministic and stochastic spectra**

So another source of error in mean velocity measurement is found in the random nature of the Doppler signal, which can be thought of as non-white noise. The spectral power estimates, $p_i$, are random quantities, so that the mean velocity estimates themselves are random variables. This chapter presents a theoretical and computational analysis of the associated bias and variance in IWMB and PIWMB.

## Definition of IWMB

The IWMB if there was no randomness in the Doppler signal is the deterministic value $\overline{B}_D$ given by

$$\overline{B}_D = \frac{\sum_{i=0}^{IMAX} i\,\tilde{p}_i}{\sum_{i=0}^{IMAX} \tilde{p}_i} \qquad (10.1)$$

but the observed IWMB, $\overline{B}$, is

$$\overline{B} = \frac{\sum_{i=0}^{\text{IMAX}} i\, p_i}{\sum_{i=0}^{\text{IMAX}} p_i} \qquad (10.2)$$

These equations have already been introduced as (2.1a) and (2.1b). By definition $p_i$ is an unbiased estimator of $\tilde{p}_i$ , i.e. $\tilde{p}_i \equiv E[p_i]$ where $E[\ ]$ is the expectation operator. Therefore, being linear, the numerator and denominator of (10.2) are unbiased random estimates of the numerator and denominator of (10.1). However this is not necessarily so for the quotient. So in addition to the obvious non-zero variance the possibility remains that the mean velocity estimate found from (10.2) has non-zero bias.

Some work has previously been performed to investigate the statistical properties of estimators used for 'wide' beam mean velocity estimation. Gerzberg and Meindl (1980) gave an expression for the variance of the (intensity weighted) mean frequency by expressing both the numerator and denominator in terms of their mean values and fractional deviations. To evaluate this generally the covariance of the numerator and denominator needs to be known. This was reduced to a more simple form if the numerator and denominator were uncorrelated, which is not expected because both numerator and denominator are derived from the same spectral estimates, or if the estimator was unbiased. Angelsen (1981) obtained the variance of (intensity weighted) mean frequency estimators derived without complete spectral analysis, and found that the variability of the estimators was inversely related to the duration of the signal analysed, and that the relative uncertainty in the mean frequency estimate was approximately inversely proportional to the square root of the true mean frequency.

## Definition of PIWMB

The deterministic form of PIWMB is appropriate for a 'thin' beam. It is denoted by $\hat{B}_D$ and is defined by

$$\hat{B}_D = \frac{\sum_{i=0}^{\text{IMAX}} i\, \tilde{p}_i \left( \sum_{j=i+1}^{\text{IMAX}} 2\tilde{p}_j + \tilde{p}_i \right)}{\left( \sum_{i=0}^{\text{IMAX}} \tilde{p}_i \right)^2} \qquad (10.3)$$

The observed form of PIWMB is the statistic $\hat{B}$ which is

$$\hat{B} = \frac{\sum_{i=0}^{IMAX} i\, p_i \left( \sum_{j=i+1}^{IMAX} 2p_j + p_i \right)}{\left( \sum_{i=0}^{IMAX} p_i \right)^2} \qquad (10.4)$$

These equations have previously been seen as (2.9a) and (2.9b).

## Distribution of the spectral estimates

To find the bias and variance of these mean velocity statistics, $\overline{B}$ and $\hat{B}$, the distributions of the spectral power estimates, $p_i$, need to be known.

*The nature of the signal*

The Doppler signal can be regarded as a Gaussian random process (Angelsen 1980) (Mo and Cobbold 1992) which is band-limited, i.e. non-white Gaussian 'noise'. This follows from noting the uniformly random phases of the signals from a large number of uncorrelated 'scatterers' randomly distributed in the same small target area, and considering the superposition of these contributions. This is appropriate for several different models proposed for the scattering from blood. An early model was to treat the individual scatterers as being independently distributed red blood cells. In this context the work of Brody (1972) has been cited. A more advanced model, taking into account interdependence of the cell positions that was known to exist, was given by Angelsen (1980) who treated the independent scatterers as being fluctuations in cell concentration in a continuous medium of blood. Mo and Cobbold (1986a) regarded the scatterers as being groups of blood particles with random sizes, and positions.

*The nature of the estimates*

In the simple case where a rectangular data window is applied to the sampled continuous Doppler signal, the spectral estimates are equally spaced ordinates of the periodogram, which is the squared modulus of the Fourier transform of the data. For a Gaussian white noise signal these estimates are uncorrelated, and except for those in the highest and lowest frequency bins, each such estimate has a variance equal to the square of its mean value, if there is a typically large number of points in the data segment. These results for Gaussian white noise hold approximately for non-white Gaussian signals, and qualititatively for a rather wide variety of signals following other distributions (Oppenheim and Schafer 1975). A more complete treatment (Priestley 1981) gives the result that for a zero-mean purely

random Gaussian process (i.e. Gaussian white noise) the estimates, other than for the highest and lowest bins, are independently distributed and follow the form of the $\chi^2$ distribution with 2 degrees of freedom (2d.f.), and each has a variance equal to the square of its mean. For the extreme bins, corresponding to the constant component and the frequency component at the Nyquist frequency, the means are unchanged but the variance is doubled, and the distribution follows $\chi^2$ (1d.f.).

Therefore, although the Doppler signals modelled are non-white noise, for the purposes below all the spectral estimates $p_i$ are assumed to be independent and distributed such that the statistic $2p_i/\tilde{p}_i$ follows the $\chi^2$ distribution (2d.f.), or $p_i = \frac{1}{2}\tilde{p}_i \chi_2^2$ . Both the mean and the standard deviation of $p_i$ are equal to $\tilde{p}_i$ . As there are ideally a large number of bins the different distributions of the estimates of the extreme bins mentioned above can be ignored. Under these assumptions it is possible to find the biases and variances of IWMB and PIWMB.

The probability density function of the $\chi^2$ (2d.f.) distribution, denoted by $g(x)$, is an extremely simple exponential function, being $g(x) = \frac{1}{2}e^{-x/2}$ for $x > 0$. The power in a spectral component being distributed in this way is equivalent to the amplitude of the component following what is known as the Rayleigh distribution.

*Further justification of the statistical model*

This description of the distribution of the spectral estimates is supported by the results of Mo and Cobbold (1992). Earlier Mo and Cobbold (1986b) gave a theoretical basis for the modelling of a Doppler signal from the summation of closely spaced sinusoidal components with powers following such a $\chi^2$ (2d.f.) distribution, and with random phases. They also estimated the power spectral density function (equivalent to the $\tilde{p}_i$ values) at peak systole from actual signals, and then synthesised Doppler signals which appeared similar in both the time and frequency domains to actual Doppler signals at peak systole.

The central limit theorem and the large number of contributions from independent scatterers to the Doppler signal suggest that the Gaussian distribution for the Doppler signal is theoretically appropriate (Mo and Cobbold 1986b). Anyway, because the spectral estimates from the Fourier analysis, $p_i$ , are based on linear combinations of the signal values, departures from a Gaussian distribution will have little effect on the distribution of the spectral estimates when the number of sample points is large.

When the number of bins making significant contributions to (10.2) is large (say >50) the assumption of the $\chi^2(2\,\mathrm{d.f.})$ *form* of the underlying distribution of these spectral estimates

becomes unnecessary. In this case only the mean and variance of the $p_i$ values need to be known as with a large number of independent bins both numerator and denominator of (10.2) are approximately normally distributed. It is suggested that the same principle holds for (10.4) also.

## Velocity profiles and Doppler spectra

Again use is made of the standard family of monotonic, axi-symmetric velocity profiles given by (3.1). If there is no spectral broadening the frequency spectrum mirrors the velocity distribution, and the corresponding Doppler power spectrum, $p_S(f)$, is given by (3.4) which is

$$p_S(f) = \frac{t}{f_m}\left(1 - f/f_m\right)^{t-1} \qquad 0 \le f \le f_m \qquad (10.5)$$

and zero elsewhere, where $t \equiv 2/n$ when the beam is 'wide' and $t \equiv 1/n$ when the beam is 'thin'.

The following sections give derivations of the biases and variances in the two estimators in the mathematically attractive case where $t = 1$ and so the expected spectrum is uniform. For a 'wide' beam this spectrum corresponds to the useful parabolic velocity profile, i.e. $n = 2$, but for a 'thin' beam this corresponds to the less realistic case of the triangular profile given by $n = 1$. When $t = 0$, the flow is of the plug form for both 'wide' and 'thin' beams, and the spectrum is a delta function, so that all the spectral power resides in one bin. Therefore for plug flow the biases will be less than the bin quantization error and the variances will be zero. Results for the more complex intermediate spectra where $0 < t < 1$ required the computational approach described later.

## Bias in IWMB

For any symmetric mean spectrum, and hence for a uniform mean spectrum, the bias in IWMB is zero. This can be inferred by noting that (10.2) is linear in both numerator and denominator, and the spectrum is symmetric about the deterministic IWMB. So the spectrum could be translated along the frequency axis to set the deterministic IWMB to zero without altering the *absolute* bias, which by symmetry must then be zero. For the uniform mean spectrum a more mathematical derivation of this result is given in appendix E.

## Bias in PIWMB

To find the bias in PIWMB we make use of the fact that the spectrum can be scaled so that the total mean power in the signal is 1, without altering any representative frequency. If the signal occupies $M$ of the available IMAX bins, (so $M = H+1$ where $H$ is the index of the highest bin with non-zero power as in chapter 1,) and if each bin estimate $p_i$ is thought of as being its mean value $\tilde{p}_i$ plus a deviation, $e_i$, then, using $(1+x)^{-2} = 1-2x+3x^2-\ldots$, equation (10.4) gives

$$\hat{B} = \frac{\sum_{i=0}^{M-1} i(\tilde{p}_i + e_i)\left[2\sum_{j=i+1}^{M-1}(\tilde{p}_j + e_j) + (\tilde{p}_i + e_i)\right]}{\left(1+\sum_{i=0}^{M-1} e_i\right)^2}$$

$$= \left(1-2\sum_{i=0}^{M-1} e_i + 3\left(\sum_{i=0}^{M-1} e_i\right)^2 - \ldots\right) \times \left(\sum_{i=0}^{M-1} i\tilde{p}_i\left[2\sum_{j=i+1}^{M-1}\tilde{p}_j + \tilde{p}_i\right] + \right.$$
$$\left. \sum_{i=0}^{M-1} ie_i\left[2\sum_{j=i+1}^{M-1}\tilde{p}_j + \tilde{p}_i\right] + \sum_{i=0}^{M-1} i\tilde{p}_i\left[2\sum_{j=i+1}^{M-1} e_j + e_i\right] + \sum_{i=0}^{M-1} ie_i\left[2\sum_{j=i+1}^{M-1} e_j + e_i\right]\right)$$

which is true for all spectra. The first of the four terms of the second factor is recognised from (10.3) as $\hat{B}_D$. For simplicity in the following description the other terms in this equation are relabelled, in the order in which they appear, to give

$$\hat{B} = (1-\alpha_1+\alpha_2-\ldots)\times\left(\hat{B}_D+\beta_1+\beta_2+\beta_3\right) \qquad (10.6)$$

By definition $E[e_i] = 0$, and as the $p_i$ values are independent $E[e_i e_j] = 0$ if $i \neq j$. Here and elsewhere in this chapter use is made of these equalities and the equalities

$$\sum_{i=0}^{M-1} i = \frac{(M-1)M}{2} \qquad \text{and} \qquad \sum_{i=0}^{M-1} i^2 = \frac{(M-1)M(2M-1)}{6}$$

Also in the case of the uniform spectrum, $\tilde{p}_i = 1/M$ and $E[e_i^2] \equiv \text{var}\, p_i = 1/M^2$, according to the statistical model. Furthermore considering the third moment of the $\chi_2^2$ distribution leads to a result proven in appendix E, namely

$$E[e_i^3] = 2\tilde{p}_i^3 = 2/M^3. \qquad (10.7)$$

**These give**

$$E[\alpha_1] = E\left[2\sum_{i=0}^{M-1} e_i\right] = 0$$

$$E[\alpha_2] = E\left[3\sum_{i=0}^{M-1} e_i^2\right] = 3M\,E\left[e_i^2\right] = \frac{3}{M}$$

$$\begin{aligned}
\hat{B}_D &= \sum_{i=0}^{M-1} i\tilde{p}_i\left[2\sum_{j=i+1}^{M-1}\tilde{p}_j + \tilde{p}_i\right] \\
&= \sum_{i=0}^{M-1} i\cdot\frac{1}{M}\cdot\left[\frac{2M-1-2i}{M}\right] \\
&= \frac{1}{M^2}\left((2M-1)\sum_{i=0}^{M-1} i \;-\; 2\sum_{i=0}^{M-1} i^2\right) \\
&= \frac{1}{M^2}\left((2M-1)\frac{(M-1)M}{2} \;-\; 2\frac{(M-1)M(2M-1)}{6}\right) \\
&= \frac{(M-1)(2M-1)}{6M} \\
&= \frac{M}{3} - \frac{1}{2} + \frac{1}{6M}
\end{aligned}$$

$$E[\beta_1] = E\left[\sum_{i=0}^{M-1} ie_i\left(2\sum_{j=i+1}^{M-1}\tilde{p}_j + \tilde{p}_i\right)\right] = 0$$

$$E[\beta_2] = E\left[\sum_{i=0}^{M-1} i\tilde{p}_i\left(2\sum_{j=i+1}^{M-1} e_j + e_i\right)\right] = 0$$

$$E[\beta_3] = E\left[\sum_{i=0}^{M-1} ie_i\left(2\sum_{j=i+1}^{M-1} e_j + e_i\right)\right] = \sum_{i=0}^{M-1} iE\left[e_i{}^2\right] = \frac{1}{M^2}\sum_{i=0}^{M-1} i = \frac{M-1}{2M}$$

$$E[\alpha_1\beta_1] = E\left[2\sum_{i=0}^{M-1} e_i \cdot \sum_{i=0}^{M-1} ie_i\left(2\sum_{j=i+1}^{M-1}\tilde{p}_j + \tilde{p}_i\right)\right]$$

$$= 2\sum_{i=0}^{M-1} iE\left[e_i^2\right]\left(\frac{2M-1-2i}{M}\right)$$

$$= \frac{2}{M^3}\left((2M-1)\sum_{i=0}^{M-1} i - 2\sum_{i=0}^{M-1} i^2\right)$$

$$= \frac{(M-1)(2M-1)}{3M^2}$$

Also, as analysis given in appendix F shows,

$$E[\alpha_1\beta_2] = E\left[2\sum_{i=0}^{M-1} e_i \cdot \sum_{i=0}^{M-1} i\tilde{p}_i\left(2\sum_{j=i+1}^{M-1} e_j + e_i\right)\right] = \frac{(M-1)(2M-1)}{3M^2} \qquad (10.8)$$

The expansion of $\alpha_1\beta_3$ includes terms of the form $e_i e_j e_k$ where $i \neq j \neq k$, and terms of the form $e_i^2 e_j$ where $i \neq j$, which both have zero expectation. The only other terms are of the form $e_i^3$, so

$$E[\alpha_1\beta_3] = E\left[2\sum_{i=0}^{M-1} ie_i^3\right] = \frac{4}{M^3}\sum_{i=0}^{M-1} i = \frac{2(M-1)}{M^2}$$

The expectations of terms not evaluated in the expansion of (10.6) e.g. $E[\alpha_2\beta_1]$, $E[\alpha_2\beta_2]$ and $E[\alpha_2\beta_3]$ are of the order of $M^{-1}$ or smaller. The dominant term, $\hat{B}_D$, is of the order of $M^1$, and the only terms of the order of $M^0$ are $\hat{B}_D \times E[\alpha_2]$, $E[\beta_3]$, $-E[\alpha_1\beta_1]$ and $-E[\alpha_1\beta_2]$. Using these terms only in the expectation of (10.6) gives, correct to terms of order $M^0$,

$$E\left[\hat{B}\right] \approx \hat{B}_D + \left(\hat{B}_D \times E[\alpha_2]\right) + E[\beta_3] - E[\alpha_1\beta_1] - E[\alpha_1\beta_2]$$

The bias is therefore of order $M^0$ and is

$$\text{bias} \approx \left(\hat{B}_D \times E[\alpha_2]\right) + E[\beta_3] - E[\alpha_1\beta_1] - E[\alpha_1\beta_2]$$

Considering only the contributions to these terms of the order of $M^0$ gives

$$\text{bias} \approx \left(\frac{M}{3} \times \frac{3}{M}\right) + \frac{M}{2M} - \frac{2M^2}{3M^2} - \frac{2M^2}{3M^2} = \frac{1}{6}$$

So

$$E\left[\hat{B}\right] \approx \hat{B}_D + \frac{1}{6}$$

Thus the expected value of PIWMB is larger than the true value by the small amount of approximately 1/6 of a bin unit. It follows that the relative bias in PIWMB correct to terms in $M^{-1}$ is

$$\frac{E\left[\hat{B}\right] - \hat{B}_D}{\hat{B}_D} \approx \frac{1}{2M} \tag{10.9}$$

and this is also the relative bias in the mean velocity estimate. So the mean velocity estimate from PIWMB for the uniform spectrum is asymptotically unbiased for large $M$. As an example, with a signal occupying 50 bins the bias is 1%.

## Variance of IWMB

To derive the variance of IWMB the spectrum is again scaled to have a total mean power of 1, and we again define $p_i \equiv \tilde{p}_i + e_i$ . The numerator of (10.2) can be regarded as being made up of its expected value, which is seen to be the deterministic IWMB value $\overline{B}_D = \sum_{i=0}^{M-1} i\tilde{p}_i$ , plus a deviation defined by $\Delta C = \sum_{i=0}^{M-1} ie_i$ . The denominator can be regarded as being its expected value, i.e. 1, plus deviation defined by $\Delta D = \sum_{i=0}^{M-1} e_i$. Therefore

$$\begin{aligned}
\overline{B} &= \frac{\overline{B}_D + \Delta C}{1 + \Delta D} \\
&= \left(\overline{B}_D + \Delta C\right)\left(1 - \Delta D + (\Delta D)^2 - \ldots\right) \\
&\approx \left(\overline{B}_D + \Delta C - \overline{B}_D \Delta D\right)
\end{aligned}$$

where terms of the second order in the deviations $\Delta C$ or $\Delta D$ have been ignored. So the variance of $\overline{B}$ is

$$\text{var}\,\overline{B} \approx \text{var}\,\Delta C + \overline{B}_D{}^2\,\text{var}\,\Delta D - 2\overline{B}_D\,\text{cov}\left[\Delta C, \Delta D\right] \tag{10.10}$$

This result is applicable to all spectra. For the uniform spectrum $\overline{B}_D = (M-1)/2$ and, making use of the equalities stated earlier, the variance terms simplify to

$$\begin{aligned}\text{var}\,\Delta C &= \text{var}\sum_{i=0}^{M-1} ie_i & \text{var}\,\Delta D &= \text{var}\sum_{i=0}^{M-1} e_i \\ &= \sum_{i=0}^{M-1} i^2\,\text{var}\,e_i & &= \sum_{i=0}^{M-1}\text{var}\,e_i \\ &= \frac{1}{M^2}\sum_{i=0}^{M-1} i^2 & &= M\cdot\frac{1}{M^2} \\ &= \frac{(M-1)(2M-1)}{6M} & &= \frac{1}{M}\end{aligned}$$

As $\Delta C$ and $\Delta D$ are deviations with zero mean

$$\begin{aligned}\text{cov}[\Delta C, \Delta D] &= E[\Delta C \Delta D] \\ &= E\left[\sum_0^{M-1} ie_i \sum_0^{M-1} e_i\right] \\ &= E\left[\sum_0^{M-1} ie_i^2\right] \\ &= E\left[e_i^2\right]\sum_0^{M-1} i \\ &= \frac{1}{M^2}\cdot\frac{M(M-1)}{2} \\ &= \frac{(M-1)}{2M}\end{aligned}$$

Making these substitutions in (10.10) gives

$$\text{var}\,\overline{B} \approx \frac{(M-1)(2M-1)}{6M} + \frac{(M-1)^2}{4}\cdot\frac{1}{M} - 2\cdot\frac{M-1}{2}\cdot\frac{M-1}{2M}$$

and keeping only the terms in $M^1$ as $M >> 1$ gives

$$\text{var}\,\overline{B} \approx \frac{M}{3} + \frac{M}{4} - \frac{M}{2} = \frac{M}{12} \qquad (10.11)$$

In relative terms the variability of IWMB is best expressed as a ratio of standard deviation to expected value. This measure of fractional variability is called the 'relative uncertainty' (r.u.). The statistic $\overline{B}$ is unbiased so, under the approximation to terms in $M^1$,

$$E[\overline{B}] = \overline{B}_D \approx \frac{M}{2}$$

and the r.u. is

$$\text{r.u.}_{\text{IWMB}} \equiv \frac{\sqrt{\text{var}\,\overline{B}}}{E[\overline{B}]} \approx \frac{\sqrt{M/12}}{M/2} = \frac{1}{\sqrt{3M}} \qquad (10.12)$$

If the same approximations are made, (10.12) is in agreement with the result derived from the expression of Gerzberg and Meindl (1980) where the estimator is unbiased. Also as $M$ is proportional to the frequency scale of the spectrum this is in agreement with Angelsen's result (1981) that the r.u. is approximately inversely proportional to the square root of the mean frequency.

## Variance of PIWMB

Derivation of the variability of PIWMB using the same technique as used above for IWMB is difficult. However a less rigorous approach can be used. Scaling the spectrum again to have a total power of 1, we consider the effect on (10.3) of a variation in a **single** spectral estimate, say in the $k$'th bin, of $+e_k$ . The observed statistic becomes

$$\hat{B} = \frac{\sum_{i=0}^{M-1} i\,\tilde{p}_i \left( 2\sum_{j=i+1}^{M-1} \tilde{p}_j + \tilde{p}_i \right) + 2e_k \sum_{i=0}^{k-1} i\,\tilde{p}_i + k e_k \left( 2\sum_{j=k}^{M-1} \tilde{p}_j + e_k \right)}{(1+e_k)^2} \qquad (10.13)$$

A derivation of this equation is given in appendix F. The first term in the numerator is the deterministic value $\hat{B}_D$. The second is the added effect on the numerator of (10.3) corresponding to the bins below $k$ in the main summation, and the third is the added effect corresponding to the $k$'th bin. The contributions from bins above $k$ are unaffected. In the statistical model described above $e_k$ is of the order of $\tilde{p}_k$ . So if the number of bins $M$ is large enough and the spectrum smooth enough $e_k << 1$. The division is alternatively

multiplication by $(1+e_k)^{-2} = (1-2e_k+3e_k^2-\ldots)$. So approximating by neglecting terms in $e_k^2$ and smaller leads to

$$\hat{B} \approx \hat{B}_D + 2e_k\left[\sum_{i=0}^{k-1} i\,\tilde{p}_i + k\left(\sum_{j=k}^{M-1}\tilde{p}_j\right) - \hat{B}_D\right]$$

Therefore the mean square error (mse) caused by this variation $e_k$ is the mean square of the second term, i.e.

$$\text{mse} = 4\left[\sum_{i=0}^{k-1} i\,\tilde{p}_i + k\left(\sum_{j=k}^{M-1}\tilde{p}_j\right) - \hat{B}_D\right]^2 E\left[e_k^2\right]$$

In this statistical model $\text{var}\, p_k \equiv E\left[e_k^2\right] = \tilde{p}_k^2$, so as $\tilde{p}_k$ is small the mean square error caused by $e_k$ is small. Therefore, as the spectral estimates are independent, an approximation to the total mean squared error (tmse) if there was a variation in every bin is simply the sum of the small mean square errors due to variations in individual bins. That is

$$\text{tmse} \approx 4\sum_{k=0}^{M-1}\left(\tilde{p}_k^2\left[\sum_{i=0}^{k-1} i\,\tilde{p}_i + k\left(\sum_{j=k}^{M-1}\tilde{p}_j\right) - \hat{B}_D\right]^2\right)$$

which is valid for all spectra. If again the mean spectrum is uniform, so that $\tilde{p}_k = 1/M$ and from above $\hat{B}_D = \frac{M}{3} - \frac{1}{2} - \frac{1}{6M}$, this becomes

$$\begin{aligned}
\text{tmse} &\approx \frac{4}{M^2}\sum_{k=0}^{M-1}\left[\frac{1}{M}\sum_{i=0}^{M-1} i + \frac{k}{M}\sum_{i=0}^{M-1} 1 - \left(\frac{M}{3} - \frac{1}{2} - \frac{1}{6M}\right)\right]^2 \\
&= \frac{4}{M^2}\sum_{k=0}^{M-1}\left[\frac{1}{M}\cdot\frac{(k-1)k}{2} + \frac{k}{M}(M-k) - \left(\frac{M}{3} - \frac{1}{2} - \frac{1}{6M}\right)\right]^2 \\
&= \frac{4}{M^2}\sum_{k=0}^{M-1}\left[-\frac{k}{2M} + k - \frac{k^2}{2M} - \frac{M}{3} + \frac{1}{2} + \frac{1}{6M}\right]^2
\end{aligned}$$

As $k$ is of the order of $M^1$ the 2nd 3rd and 4'th terms in the bracket are the largest, being of the order of $M^1$. Retaining these and squaring gives terms in $M^2$ , i.e.

$$\begin{aligned}\text{tmse} &\approx \frac{4}{M^2}\sum_{k=0}^{M-1}\left[k-\frac{k^2}{2M}-\frac{M}{3}\right]^2 \\ &= \frac{4}{M^2}\sum_{k=0}^{M-1}\left[k^2-\frac{k^3}{M}-\frac{2kM}{3}+\frac{k^4}{4M^2}+\frac{k^2}{3}+\frac{M^2}{9}\right] \\ &= \frac{4}{M^2}\left[\frac{M^2}{9}\sum_{k=0}^{M-1}1-\frac{2M}{3}\sum_{k=0}^{M-1}k+\frac{4}{3}\sum_{k=0}^{M-1}k^2-\frac{1}{M}\sum_{k=0}^{M-1}k^3+\frac{1}{4M^2}\sum_{k=0}^{M-1}k^4\right]\end{aligned}$$

If the previous summation identities, and the further identities

$$\sum_{k=1}^{x}k^3=\frac{x^2(x+1)^2}{4} \qquad \text{and} \qquad \sum_{k=1}^{x}k^4=\frac{x(x+1)(2x+1)(3x^2+3x-1)}{30}$$

are written as

$$\sum_{k=0}^{x}k^b \approx \int_0^x k^b=\frac{x^{b+1}}{b+1} \qquad\qquad b=1\ldots 4$$

which is correct to the highest order, then the terms in the square bracket all become proportional to $M^3$ and

$$\text{tmse} \approx \frac{4}{M^2}\left[\frac{M^3}{9}-\frac{M\cdot M^2}{3}+\frac{4M^3}{9}-\frac{M^4}{4M}+\frac{M^5}{20M^2}\right]=\frac{4M}{45}$$

Furthermore the mean square error is the sum of the variance and the squared bias. From above, the order of the squared bias in $\hat{B}$ is only $M^0$. Therefore for the uniform spectrum, correct to terms in $M^1$,

$$\text{var}\,\hat{B} \approx \frac{4M}{45} \qquad (10.14)$$

This is only marginally more than the variance of $M/12$ for $\overline{B}$ with the uniform spectrum, given by (10.11). The r.u. of PIWMB is then

$$\text{r.u.}_{\text{PIWMB}} \equiv \frac{\sqrt{\text{var}\,\hat{B}}}{E\left[\hat{B}\right]} \approx \frac{\sqrt{4M/45}}{M/3}=\frac{2}{\sqrt{5M}} \qquad (10.15)$$

which is larger than the r.u. of IWMB primarily because the expected value is smaller. Again the r.u. is approximately inversely proportional to the square root of $M$ and so to the mean frequency.

As suggested this method of derivation is less rigorous than the derivation of the variance of IWMB, var $\overline{B}$. However, as shown in appendix E, when var $\overline{B}$ is derived this way the correct result, i.e. $M/12$, is obtained, which supports the use of this method.

## Variability expressed in terms of the underlying parameters

It is possible to describe the r.u.'s and variances in terms other than of the number of bins in the spectrum. The bin width in discrete Fourier analysis, which is the frequency resolution and is denoted by $\Delta f$, is equal to the reciprocal of the duration of the data segment, denoted by $\Delta\tau$.

$$\Delta f = 1/\Delta\tau$$

However this bin width is also the maximum frequency in the signal, $f_m$, divided by $M$. So

$$M = f_m \Delta\tau$$

and therefore from the Doppler equation (1.2) we can write

$$M \approx \frac{2F v_m \Delta\tau \cos\theta}{c} \tag{10.16}$$

The notation $\overline{v}'(\overline{B})$ denotes the estimate of true mean velocity $\overline{v}$ made using IWMB, $\overline{B}$. With a 'wide' beam (3.5) implies that with a uniform spectrum $v_m = 2\overline{v}$ . So, substituting for $M$ in (10.12), the relative uncertainty in the estimate of mean velocity is therefore

$$\text{r.u.}_{\overline{v}'(\overline{B})} \equiv \text{r.u.}_{\text{IWMB}} \approx \sqrt{\frac{c}{12F\Delta\tau\cos\theta\,\overline{v}}} \tag{10.17}$$

Similarly $\overline{v}'(\hat{B})$ denotes the mean velocity estimate made using PIWMB, $\hat{B}$. With a 'thin' beam and a uniform spectrum (3.6) implies that $v_m = 3\overline{v}$ and so from (10.15)

$$\text{r.u.}_{\overline{v}'(\hat{B})} \equiv \text{r.u.}_{\text{PIWMB}} \approx \sqrt{\frac{2c}{15F\Delta\tau\cos\theta\,\overline{v}}} \tag{10.18}$$

The fractional precision of either mean velocity estimator is improved when any of the terms in the denominators becomes larger, for instance when the Doppler angle is reduced, the duration of the data segment is increased, or during systole when the velocities are greater.

The variance of the mean velocity estimate $\overline{v}'(\overline{B})$ can be found by multiplying (10.17) by its expected value, which is $\overline{v}$ as the estimate is unbiased, and then squaring. Therefore

$$\text{var } \overline{v}'(\overline{B}) \approx \frac{c}{12F\ \Delta\tau \cos\theta} \cdot \overline{v} \qquad (10.19)$$

Similarly with $\overline{v}'(\hat{B})$ and (10.18)

$$\text{var } \overline{v}'(\hat{B}) \approx \frac{2c}{15F\ \Delta\tau \cos\theta} \cdot \overline{v} \qquad (10.20)$$

## A limit on the available precision

The variance of a final estimate of mean velocity could be reduced by finding the mean value of a number of independent estimates of $\overline{B}$ or $\hat{B}$. If $N$ such estimates were made giving mean values of $\grave{}\overline{B}$ or $\grave{}\hat{B}$ say then the variances would be reduced by a factor of $N$, and using (10.12) and (10.15) the relative uncertainties of $\grave{}\overline{B}$ and $\grave{}\hat{B}$ would be

$$\frac{\sqrt{\text{var}\,\grave{}\overline{B}}}{E\left[\grave{}\overline{B}\right]} \approx \frac{1}{\sqrt{3NM}} \qquad \text{and} \qquad \frac{\sqrt{\text{var}\,\grave{}\hat{B}}}{E\left[\grave{}\hat{B}\right]} \approx \frac{2}{\sqrt{5NM}}$$

Therefore the variability of the velocity estimate is a function of the product $NM$. But from (10.16) $M$ is proportional to the duration of each individual segment, $\Delta\tau$, so the product $NM$ is proportional to the total duration of the segments. No reduction in estimator variance could be obtained by subdividing a single segment into $N$ independent contiguous sub-segments (if possible) as the product $NM$ would not alter. Neither would increasing the sampling frequency be helpful as it would only introduce frequency bins with zero contents above the maximum frequency in the signal, and the number of bins, $M$, making a non-zero contribution to the equations above would stay the same. It is evident that, if the spectral analysis is performed by Fourier transform, the precision of the mean velocity estimate is limited by the maximum allowable value of $N\Delta\tau$, which is often taken to be the maximum length of time the Doppler signal can be thought of as being stationary.

## Variance of IWMB in an example practical situation

As an example of the precision in practice consider the case where the velocity profile is parabolic so that for a 'wide' beam the mean spectrum is uniform. The transmit frequency, $F$, is 6 MHz and the Doppler angle, $\theta$, is 50°. The velocity of sound in blood, $c$, is taken as 1580 m.s$^{-1}$ and the velocity at the vessel axis as 0.4 m.s$^{-1}$. If the interval in which the signal can be regarded as stationary is 10 milliseconds, and this interval is chosen as a single data segment, i.e. $\Delta\tau = 10^{-2}$ s, then (10.16) shows that the Doppler signal occupies only 20 frequency bins, i.e. $M \approx 20$. Though $M$ is not large here we still use equation (10.12), or alternatively (10.17), found for large $M$, to find that the r.u. of the appropriate estimator of mean velocity is

$$\text{r.u.}_{\overline{v}'(\overline{B})} \equiv \text{r.u.}_{\text{IWMB}} \approx 0.13$$

If $\overline{B}$ is treated as being normally distributed, it follows that, as the bias is zero, an approximate 95% confidence interval for the true mean velocity is within ±26% of the measured value.

As mentioned above Angelsen (1981) also found the variance to be affected by the duration of the contributing signal. For 10 milliseconds of a signal with a uniform (mean) spectrum and a maximum frequency of 4 kHz, the estimators he studied had r.u. values of ≈0.084 and ≈0.09 . Applying (10.12) in this case gives ≈0.09 indicating good agreement.

## More general spectra and spectral broadening

Results have been derived above for the biases and variances in IWMB and PIWMB when the spectrum is uniform, i.e. where $t = 1$ in (10.5). More generally the spectrum is peaked towards $f_m$, i.e. $t < 1$, and theoretical derivations of the biases and variances are more difficult. For the general spectrum computer simulation was used to investigate the biases and variances over a wide range of velocity profiles and frequency bin widths. To provide more useful results the spectra were broadened by the triangular geometrical spectral broadening function of chapter 7.

For a value of $t < 1$ the spectrum of (10.5) becomes undefined as $f$ approaches $f_m$. To provide a more manageable form the spectrum was smoothed to simulate the collection of power in discrete bins. The width in frequency of each bin is $\Delta f$, and so the smoothed spectrum, $p'(f)$, is

$$p'(f) = \frac{1}{\Delta f} \int_{f - \Delta f/2}^{f + \Delta f/2} p_S(f)\, df \qquad (10.21)$$

which is nowhere undefined. This spectrum was then broadened numerically according to the triangular function of chapter 7 with the parameter $a$ variable and the parameter $b$ set equal to 1. Using (7.10) and (7.14) gives the smoothed and broadened spectrum $p(f)$ for the simulation,

$$p(f) = \int_{f/(1-a/2)}^{f/(1+a/2)} \frac{2}{au}\left(1 - \frac{2|f-u|}{au}\right) \cdot p'(u)\, du \qquad (10.22)$$

The broadening ideally should have been applied before the smoothing. However, as the theoretical spectrum of (10.5) is undefined at $f = f_m$ it is not suitable for broadening by numerical means, whereas the spectrum of (10.21) is. This reversal of order is justified for spectra with $n > 2$, i.e. between parabolic and plug, as the broadening has much greater effect than the smoothing on the rapidly varying portion of the spectrum, i.e. the high-frequency end near $f_m$. If the unbroadened spectrum occupies $M^*$ bins then the width of each bin is $\Delta f \equiv f_m / M^*$ and in this high-frequency region the smoothing over one bin described is similar to a broadening with a parameter of approximately $1/M^*$. The sum of the broadening and smoothing is therefore approximately a broadening with parameter $a + (1/M^*)$, where $M^*$ is not generally small and, as seen in chapter 7, $a$ is of the order of 0.5. So the broadening dominates the smoothing, and the reversal of the order of application is justified. The resulting spectrum of (10.22) occupies $M$ bins, which is a larger number than $M^*$.

## Computer simulation

For various combinations of $n$, $a$ and $M^*$ the mean values, $\tilde{p}_i$ , of the spectral estimates were found by the numerical evaluation of (10.22) at frequencies corresponding to the centres of bins of width $\Delta f$. Independent random $p_i$ values for each bin were generated such that the quantity $2p_i/\tilde{p}_i$ followed a $\chi^2$ (2 d.f.) distribution. These $p_i$ values were used in (10.2) to calculate $\overline{B}$. This was repeated 10 000 times to allow the variance of $\overline{B}$ and its bias with respect to $\overline{B}_D$ to be measured. As such a large sample was used the population mean and variance of $\overline{B}$ were able to be very closely approximated by the sample mean and variance. This process was also carried out to examine the bias and variance of $\hat{B}$ as defined by (10.4).

*Results - bias*

For the uniform spectrum given by a 'wide' beam with $n = 2$ and $a = 0$, the bias observed in IWMB was zero within statistical variation, as predicted by the theory above. Similarly for the uniform spectrum given by a 'thin' beam with $n = 1$ and $a = 0$, the bias in PIWMB was consistent with the value predicted by (10.9).

For fixed $a$ and $M^*$ values, as $n$ was made larger the expected velocity estimates became less than the deterministic values, with the biases being maximised at levels and $n$ values dependent on the amount of spectral broadening. An example of this is illustrated in fig.10.2 where the triangular symbols show the biases, expressed in terms of the ratios $E[\overline{B}]/\overline{B}_D$ and $E[\hat{B}]/\hat{B}_D$, for various values of $n$ where $a = 0.1$ and $M^* = 50$.

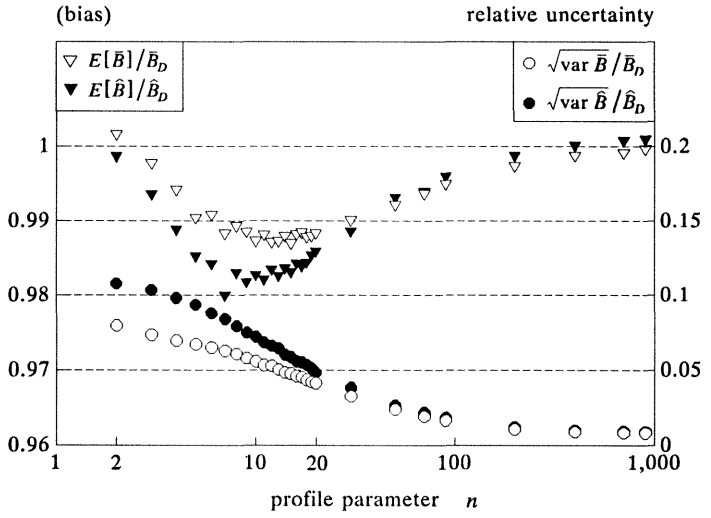


**Fig.10.2 - A measure of the bias and the relative uncertainty observed in IWMB and PIWMB for different velocity profiles defined by $n$, where the amount of spectral broadening is given by $a$=0.1 and the number of bins in the unbroadened spectrum by $M^*$=50.**

Considering the greatest bias for flows between parabolic and plug, i.e. for $n \geq 2$, gave an indication of the worst-case bias throughout a cardiac cycle where $n$ may fluctuate. For example with $a = 0.1$ and $M^* = 50$ as seen in fig.10.2 the worst biases in IWMB and PIWMB were approximately $-1\frac{1}{4}\%$ and $-1\frac{3}{4}\%$. Fig.10.3 shows the worst biases for various amounts of broadening of spectra occupying $M^*$ = 25, 50, 100 and 200 bins, against $M$. As in fig.10.2, the hollow markers are for IWMB, and the solid markers for PIWMB. The large square markers correspond to $a = 0$, i.e. where only the smoothing is applied. The diamond markers correspond to $a = 0.1$, which is a small amount of broadening, and the small square markers to $a = 0.5$, which is perhaps more typical for a linear array transducer. The worst bias is reduced as the signal occupies an increasing

number of bins and is reduced quickly as broadening is introduced. The worst bias in both IWMB and PIWMB is smaller than −1% when the broadening has the more typical value of $a \approx 0.5$. To conclude, the biases in the IWMB and PIWMB statistics introduced by the stochastic nature of the Doppler signal are very small for typical amounts of spectral broadening, and can be ignored in comparison with the variability discussed below, and also with other sources of error in the mean velocity estimate.

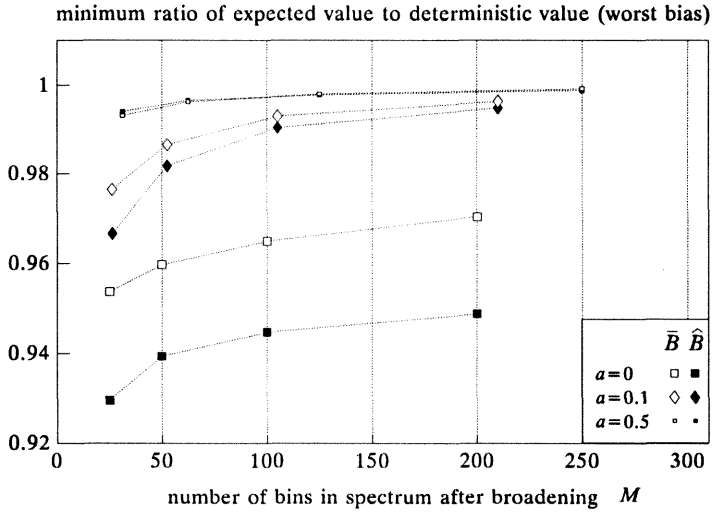


**Fig.10.3 - The worst observed biases in IWMB and PIWMB with profiles of $n \geq 2$, for various numbers of bins and various amounts of spectral broadening**

It should be noted that the biases discussed here are calculated with respect to $\overline{B}_D$ and $\hat{B}_D$, and so are only true biases if these deterministic values are accurate estimators of mean velocity. There are many reasons why this should not be so. Indeed, as shown in chapter 7, the very presence of such a broadening function means that $\hat{B}_D$ tends to underestimate the true velocity.

*Results - variance*

Similarly for fixed values of $a$ and $M^*$ the maximum relative uncertainty (m.r.u.) was found for profiles between parabolic and plug. An example of the effect of changing $n$ on r.u. is given by the octagonal symbols of fig.10.2 where again $M^* = 50$ and $a = 0.1$. In this case the m.r.u. values for both IWMB and PIWMB are observed with parabolic flow, i.e. $n = 2$.

The observed m.r.u. results for various values of $a$ and $M^*$, plotted against $M$ can be seen in fig.10.4 with the markers used as in fig.10.3. Results for the additional case of $a = 1$ are given by the 'plus' sign markers. The dashed line represents the r.u. values for IWMB with a uniform spectrum predicted by (10.12), and is associated with the hollow markers. If a small or a typical amount of broadening is present all the spectra with $n \geq 2$ are spread sufficiently for the m.r.u. to be observed when the profile is parabolic, as in fig.10.2, and the results lie close to the dashed line.

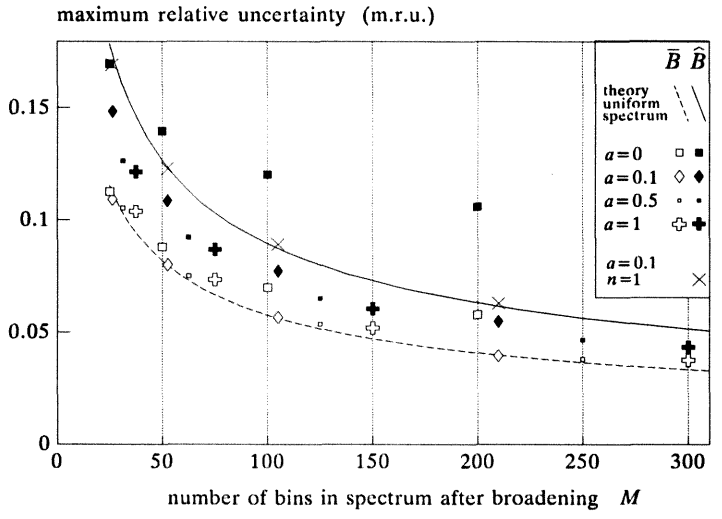


**Fig.10.4 - The worst observed relative uncertainties in IWMB and PIWMB with profiles of $n \geq 2$, for various numbers of bins and various amounts of spectral broadening**

The solid line represents the r.u. values for PIWMB with a uniform spectrum predicted by equation (10.15), and is associated with the solid markers. Again with more than a very small amount of broadening the m.r.u., for flow between parabolic and plug, is observed for parabolic flow, but in this case it does not correspond to the uniform spectrum, which would be when $n = 1$. If the profile given by $n = 1$ is included, the results for more than a little broadening lie close to the solid line, as shown by the × markers for $a = 0.1$.

Comparison of the solid with the hollow markers shows that for realistic amounts of spectral broadening the maximum relative uncertainty of the velocity estimate PIWMB is somewhat greater than that of IWMB. With such broadening these variabilities are approximated by the theoretical equations (10.15) and (10.12) respectively.

## The effect of windowing

Typically a symmetric non-rectangular data window is applied which forces the data segment to zero at both ends, and so prevents discontinuities caused by the assumption of periodicity inherent in the use of the Discrete (or Fast) Fourier Transform. The effect of applying such a window is to convolve the complex transform outputs with the transform of the window shape, which is symmetric. The spectral estimates are then the squared magnitudes of the complex results. This introduces correlation between neighbouring $p_i$ estimates, in which case the theoretical treatment above for the uniform spectrum is inappropriate. The qualitative effects on the variances of IWMB and PIWMB can be inferred by noting that after applying the window the data points near the ends are weighted lowly while those near the centre are favoured. So the effective number of contributing data points is reduced. Thus the effect on the variance is similar to the effect of a reduction in data segment duration, namely an increase in variance.

This was demonstrated by calculating the Fourier transforms of 2000 sets of 256 zero-mean random variables, generated to follow an approximate Gaussian distribution, with various windows applied. The 'signal' was therefore approximately Gaussian white noise, with a uniform spectrum encompassing a frequency range of $M = 128$ bins. From the resulting $p_i$ values the observed means and variances of $\overline{B}$ and $\hat{B}$ were calculated.

The effect of a non-rectangular window on the mean value of $\overline{B}$ seemed to be to increase it by the very small amount of ~0.1 bins (i.e. ~0.2%), so that $\overline{B}$ is biased by this negligible amount if such a window is applied. The effect on the mean value of $\hat{B}$ was to increase it by an amount of the order of twice that much (~0.2 bins) so that, instead of the theoretical bias of 1/6 of a bin derived earlier, the bias in $\hat{B}$ with such a window is closer to 1/3 of a bin.

The variances are more interesting and are tabulated in table 10.1. If $\overline{B}$ and $\hat{B}$ are normally distributed then the recorded variances in all but the top row have approximate standard errors of 3%. The variances where no window is applied (i.e. in effect with a rectangular window) were found from the average results of 5 sets of 2000 and are slightly larger than the previously derived theoretical values of $M/12 = 10.67$ for $\overline{B}$, and $4M/45 = 11.38$ for $\hat{B}$. Little attention is given to this seeming discrepancy as the random variables followed a Gaussian distribution only approximately, and the variances are themselves random variables with, in this case a standard error of approximately 1½%. The important point is that with non-rectangular windows the variances are increased as suggested above.

| window | var $\overline{B}$ | var $\hat{B}$ | $K$ 50% o'lap | $K$ 75% o'lap |
|---|---|---|---|---|
| none (rectangular) | 11.0 | 11.8 | 50 % | 75 % |
| cos | 16.1 | 17.4 | 31.8 % | 75.5 % |
| triangular | 19.3 | 20.6 | 25 % | 71.9 % |
| $\cos^2$ (Hanning) | 20.6 | 22.1 | 16.7 % | 65.9 % |
| $\cos^3$ | 23.3 | 25.5 | 8.5 % | 56.7 % |
| $\cos^4$ | 27.3 | 29.3 | 4.3 % | 48.6 % |

**Table 10.1 - variances of mean bin numbers for different data windows applied to sections of near-Gaussian white noise data with a spectrum occupying 128 bins. The correlation data is taken from Harris (1978).**

However another effect of the reduction in effective data length is that overlapped data segments can be treated as independent. This overlapping is desirable anyway to avoid wasting the data weighted lightly by the window at the end of each segment. Harris (1978), discussing the 'degree of correlation of the random components in successive transforms', computed a correlation coefficient, here called $K$, for various windows with the commonly used amounts of overlap of 50% and 75%. Some of his results are shown in table 10.1. As might be expected, the variances with the different windows are inversely related to the correlations, which themselves are clearly related to the window 'widths'. Harris notes that 'for good windows... transforms taken with 50-percent overlap are essentially independent.' So, if a window and overlapped segments are used, independent mean frequency estimates have greater variance but can be made more often. For example with the Hanning window the variance approximately doubles, but with a 50% overlap the number of independent estimates that can be made from a given amount of data also doubles. The result is that the variance of the overall estimate of a mean frequency from that data stays approximately the same. The suggestion is that use of a window on overlapped segments does not greatly affect the precision of a mean blood velocity estimate.

For non-uniform spectra the effects of different windows were not calculated. The results given by the treatment of the $p_i$ values as independent $\chi^2$ (2d.f.) variables, (i.e where the data window is rectangular) are suggested as useful guides to the behaviour of IWMB and PIWMB statistics in practice.

## Summary

In this chapter the spectral estimates in each frequency bin are modelled as being independent, with standard deviations equal to their means, and distributed according to the form of a $\chi^2$ distribution with 2 degrees of freedom. With velocity profiles between parabolic and plug forms, the biases in IWMB and PIWMB due to the random nature of the spectral estimates have been shown to be small (<1%) in the presence of typical amounts of spectral broadening. For realistic amounts of spectral broadening the maximum variability of IWMB or PIWMB occurs when the profile is parabolic. Approximate expressions for the maximum fractional variabilities are those derived for uniform spectra, namely equations (10.12) and (10.17) for IWMB, and (10.15) and (10.18) for PIWMB. The fractional variability is inversely proportional to the square root of the maximum frequency in the Doppler signal, so precision is improved if the velocity of the blood increases, the Doppler angle is made smaller or the transmit frequency larger. These factors aside, the limitation on the precision of an estimate of mean blood velocity is the maximum time interval over which the Doppler signal is recorded. This is often thought of as the maximum interval over which the signal can be regarded as stationary. Estimates made where a non-rectangular spectral window is applied to the data have larger variance. However the use of such a window permits the overlapping of data segments and so estimates can be made more often. The variance of the overall estimate of mean velocity is not greatly altered. With typical parameters the ratio of the standard deviation to the expected value of the mean velocity estimate might easily be greater than 10%. The stochastic nature of the spectral estimates therefore contributes a negligible bias but considerable variance to IWMB and PIWMB as estimators of mean blood velocity.

## Notation for this chapter

| | |
|---|---|
| $a$ | width parameter of triangular broadening function, as in chapter 7 |
| $\overline{B}$ | mean of a sample of IWMB measurements |
| $\hat{B}$ | mean of a sample of PIWMB measurements |
| $e_i$ | deviation from the mean power in the $i$'th bin |
| $E[\ ]$ | expectation operator |
| $\Delta f$ | width of each frequency bin |
| $K$ | correlation figure for overlapped and windowed data segments |
| $M^*$ | number of bins in the unbroadened spectrum |
| $M$ | number of bins in the observed, i.e. broadened spectrum |
| $\bar{v}'(\overline{B}), \bar{v}'(\hat{B})$ | estimates of mean velocity made from IWMB and PIWMB |
| $\alpha_1, \alpha_2, \beta_1, \beta_2, \beta_3$ | temporary notation for more complex expressions |
| $\Delta\tau$ | duration of each data segment |

# CHAPTER 11 - A DEFINITION OF PIWMB FOR MIXED FLOW

In this chapter the assumption of monotonicity introduced in chapter 2 is relaxed to include profiles which consist of a central, forward (positive), monotonically increasing component surrounded by a single region of reverse (negative) flow. The whole profile is symmetric about the vessel axis. It is shown that if the profile in the reverse flow region can itself be assumed symmetric about the point of greatest negative velocity then the previous derivation of PIWMB can be extended to give the correct mean velocity. An example of a profile satisfying these criteria is illustrated in fig.11.1.

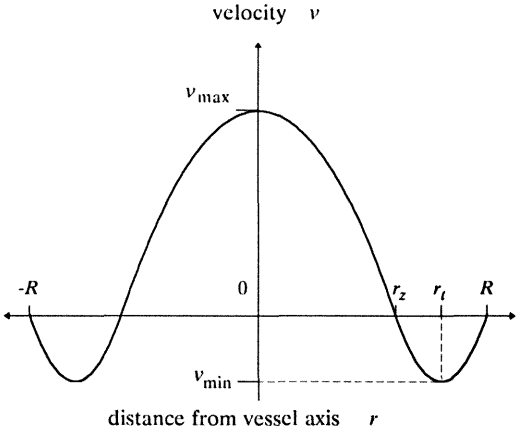


**Fig.11.1 - a profile with a symmetric reverse flow component**

The turning point in the negative velocity region is denoted by $r_t$ , and the profile in the region of negative velocity is assumed to be symmetric about this point. The velocity is zero at a radial distance denoted by $r_z$. Throughout this chapter, because flow in two directions is considered, the notation $v_m$ for maximum velocity is replaced by $v_{max}$ with the corresponding frequency being $f_{max}$ , and the notations $v_{min}$ and $f_{min}$ are introduced for the minimum velocity and the corresponding minimum frequency, which are both negative quantities.

Consider minus IMIN frequency bins corresponding to the range of negative velocities. (Note that IMIN is a negative number). These bins are numbered IMIN to -1, where the IMIN'th bin includes the most negative velocities able to be measured. The range of positive and negative velocity components is then represented by three subsets of the total set of bins. Bins numbered 1 to IMAX represent increasing positive velocity. Bins numbered -1 to IMIN represent negative velocities increasing in magnitude. The zero'th

bin represents both positive and negative velocities with magnitudes small enough to be contained in this bin.

## General IWMB statistic

The single-sided definitions of IWMB given by (2.1a) and (2.1b) are simply replaced by

$$\overline{B}_D^* = \frac{\sum_{i=\mathrm{IMIN}}^{\mathrm{IMAX}} i\,\tilde{p}_i}{\sum_{i=\mathrm{IMIN}}^{\mathrm{IMAX}} \tilde{p}_i} \qquad (11.1a)$$

and

$$\overline{B}^* = \frac{\sum_{i=\mathrm{IMIN}}^{\mathrm{IMAX}} i\,p_i}{\sum_{i=\mathrm{IMIN}}^{\mathrm{IMAX}} p_i} \qquad (11.1b)$$

respectively, where the * signifies a double-sided spectrum.

## Development of the more general PIWMB statistic

For the single-sided case, equation (2.7) expressed PIWMB in terms of the sum, over all bins, of contributions weighted by the areas of the corresponding rings of cross section, and normalised by the total area. When there is a region of symmetric negative flow the appropriate equation for PIWMB will be of a similar form, with once again the areas being found from rings bounded by known values, once again denoted by $s_i$ . In this case the deterministic statistic is denoted by $\hat{B}_D^*$ and can be written as

$$\hat{B}_D^* = \frac{C_+ + C_- + C_0}{R^2} \qquad (11.2)$$

where $C_+$ is a contribution from bins above the zero'th bin, $C_-$ is a contribution from bins below the zero'th bin and $C_0$ is a contribution from the zero'th bin itself. The total expected power $\tilde{P}$ with this double-sided spectrum is

$$\tilde{P} = \sum_{i=\mathrm{IMIN}}^{\mathrm{IMAX}} \tilde{p}_i \qquad (11.3)$$

Note that this expression for $\tilde{P}$ is different to that for the monotonic case given by (2.2).

*Positive bins*

Consider the positive component, $C_+$, represented by the bins above the zero'th bin. The derivation of the $s_i$ values for $i > 0$ is the same as that in chapter 2. That is, from (2.3)

$$s_i = \frac{R}{\tilde{P}} \sum_{j=i}^{\text{IMAX}} \tilde{p}_j \qquad 1 < i \le \text{IMAX}$$

where now $\tilde{P}$ is defined by (11.3). As in chapter 2, $s_{\text{IMAX+1}}$ is defined to be zero, and the mean frequency in bin units, $i'$, is replaced by $i$, and so the contribution from the bins above the carrier bin is

$$C_+ = \sum_{i=1}^{\text{IMAX}} i\,(s_i^2 - s_{i+1}^2)$$

so that, by making the same steps as in the derivation of (2.9a) from (2.7)

$$C_+ = \frac{R^2}{\tilde{P}^2} \sum_{i=1}^{\text{IMAX}} i\,\tilde{p}_i \left( 2 \sum_{j=i}^{\text{IMAX}} \tilde{p}_j - \tilde{p}_i \right). \qquad (11.4)$$

*Negative bins*

Next the contribution, $C_-$, from bins below the carrier frequency is considered. Fig.11.2 shows only the negative portion of the profile and the region close to the zero'th bin, with the corresponding sector of the cross section above. As in chapter 8, the lowest indexed bin with non-zero contents is called the $L$'th bin. In this chapter however $L$ must be zero or negative. So scatterers with the most negative velocity present contribute to bin $L$, and $\tilde{p}_i = 0$ for $\text{IMIN} \le i < L$.

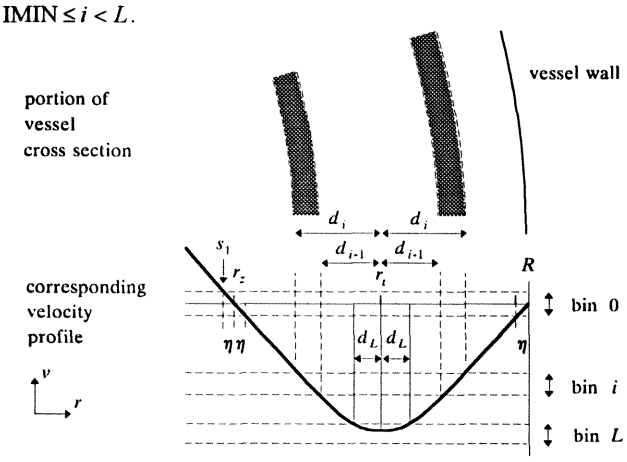


**Fig.11.2 - the reverse flow region of the cross section and profile**

First, expressions are derived for the radial positions $r_z$ and $r_t$. The velocities corresponding to frequencies in the zero'th bin are bounded by the top pair of dotted lines. Because the profile is smooth and the bin width is small it is reasonable to approximate the profile around the point $r_z$ between these dotted lines by a straight line segment passing through zero at $r_z$. Therefore the section of the sample volume occupied by the scatterers of the zero'th bin, giving a mean received power of $\tilde{p}_0$, is a region extending an equal distance $\eta$ either side of $r_z$, and, by the symmetry assumption, a region extending the same distance $\eta$ in from the vessel wall, giving in total a distance $3\eta$ along the radius. As in chapter 2 the constant of proportionality relating the length (along the radius) of a section of the sample volume to the received power is $R/\tilde{P}$. Therefore

$$\eta = \frac{R}{\tilde{P}} \cdot \frac{\tilde{p}_0}{3}$$

Because the position $r_z - \eta$ is the position of the outer extent of the ring for the 1'st bin, $s_1$, the position of the zero velocity point, $r_z$, is

$$\begin{aligned} r_z &= s_1 + \frac{R}{\tilde{P}} \cdot \frac{\tilde{p}_0}{3} \\ &= \frac{R}{\tilde{P}} \left( \sum_{j=1}^{\mathrm{IMAX}} \tilde{p}_j + \frac{\tilde{p}_0}{3} \right) \end{aligned}$$

and from the symmetry $r_t$ must be midway between $R$ and $r_z$, so

$$\begin{aligned} r_t &= \frac{R + r_z}{2} \\ &= \frac{R}{2\tilde{P}} \left( \tilde{P} + \sum_{j=1}^{\mathrm{IMAX}} \tilde{p}_j + \frac{\tilde{p}_0}{3} \right) \end{aligned} \qquad (11.5)$$

The group of scatterers with the most negative velocities, i.e. the scatterers of the $L$'th bin, must occupy a ring including this circle of radial distance $r_t$. The symmetry assumption means that the limits of this ring are equal distances in front of and beyond the radius $r_t$ as is shown in fig.11.2. The ring for the $L$'th bin is defined by the limits $r_t + d_L$ and $r_t - d_L$. In general the regions of the cross section with scatterers of a velocity appropriate to the $i$'th bin are rings bounded by $r_t + d_i$ and $r_t + d_{i-1}$, and by $r_t - d_{i-1}$ and $r_t - d_i$, as shown in fig.11.2. This is true for all bins below the zero'th bin, including the $L$'th bin and

any lower empty bins if we define $d_i = 0$ for IMIN $\le i < L$. The combined area, $A_i$, of these two rings, without the $\pi$ factor is

$$\begin{aligned} A_i &= \left[(r_t + d_i)^2 - (r_t + d_{i-1})^2\right] + \left[(r_t - d_{i-1})^2 - (r_t - d_i)^2\right] \\ &= \left(r_t^2 + 2r_t d_i + d_i^2\right) - \left(r_t^2 + 2r_t d_{i-1} + d_{i-1}^2\right) + \left(r_t^2 - 2r_t d_{i-1} + d_{i-1}^2\right) - \left(r_t^2 - 2r_t d_i + d_i^2\right) \\ &= 4r_t (d_i - d_{i-1}) \end{aligned}$$

IMIN $\le i < 0$

In the sample volume the section of length $d_i - d_{i-1}$, being half the section of the radius for the $i$'th bin, contains $\tilde{p}_i/2$ scatterers so that

$$d_i - d_{i-1} = \frac{R}{\tilde{P}} \cdot \frac{\tilde{p}_i}{2}$$

and therefore

$$A_i = 2r_t \frac{R}{\tilde{P}} \tilde{p}_i \qquad \text{IMIN} \le i < 0$$

The contribution from the bins below the carrier frequency is

$$\begin{aligned} C_- &= \sum_{i=\text{IMIN}}^{-1} i\, A_i \\ &= 2r_t \frac{R}{\tilde{P}} \sum_{i=\text{IMIN}}^{-1} i\, \tilde{p}_i \end{aligned}$$

where again $i$ is used to replace the more correct $i'$. Analogously to the case of positive bins described in chapter 2, the lower limit of the summation is chosen to be the fixed quantity IMIN and not the variable $L$ as the terms for bins below $L$ are all zero and contribute nothing to the summation. So, making use of the expression for $r_t$ in (11.5), the contribution to the numerator of (11.2) from the bins with negative indices is

$$C_- = \frac{R^2}{\tilde{P}^2} \left( \tilde{P} + \sum_{i=1}^{\text{IMAX}} \tilde{p}_i + \frac{\tilde{p}_0}{3} \right) \sum_{i=\text{IMIN}}^{-1} i\, \tilde{p}_i \qquad (11.6)$$

*Zero'th bin*

Lastly the contribution to the numerator from the zero'th bin itself is considered. This is zero as $i'$ is approximated by $i$ which is zero. That is $C_0 = 0$.

*The resulting statistic*

When substituting for the non-zero terms $C_+$ and $C_-$ in (11.2) the $R^2$ factors in (11.4) and (11.6) cancel with the denominator to give

$$\hat{B}_D^* = \frac{\sum_{i=1}^{\text{IMAX}} i\,\tilde{p}_i\left(2\sum_{j=i}^{\text{IMAX}}\tilde{p}_j - \tilde{p}_i\right) + \left(\tilde{P} + \sum_{i=1}^{\text{IMAX}}\tilde{p}_i + \frac{\tilde{p}_0}{3}\right)\sum_{i=\text{IMIN}}^{-1} i\,\tilde{p}_i}{\tilde{P}^2} \qquad (11.7a)$$

Substitution of the summation for $\tilde{P}$, simplification and changing to the observed, i.e. stochastic, form give

$$\hat{B}^* = \frac{\sum_{i=1}^{\text{IMAX}} i\,p_i\left(2\sum_{j=i}^{\text{IMAX}}p_j - p_i\right) + \left(\sum_{i=\text{IMIN}}^{0}p_i + 2\sum_{i=1}^{\text{IMAX}}p_i + \frac{p_0}{3}\right)\sum_{i=\text{IMIN}}^{-1} i\,p_i}{\left(\sum_{i=\text{IMIN}}^{\text{IMAX}}p_i\right)^2} \qquad (11.7b)$$

An alternative estimate of mean velocity is therefore available despite the presence of this symmetric area of negative flow outside the monotonic region of positive flow. The validity of this equation has been verified by the computer simulation technique.

The integral form of (11.7a) expressed as a PIWMF is

$$\hat{f}^* = \frac{2\int_0^{f_{\max}} f p(f)\left(\int_f^{f_{\max}} p(u)\,du\right)df + \left(\int_{f_{\min}}^{0} p(f)\,df + 2\int_0^{f_{\max}} p(f)\,df\right)\cdot\int_{f_{\min}}^{0} f\,p(f)\,df}{\left(\int_{f_{\min}}^{f_{\max}} p(f)\,df\right)^2} \qquad (11.8)$$

which follows from increasing the number of bins without limit. The term related to the zero'th bin therefore vanishes.

## Properties of the PIWMB statistic

(i)

In the case where there is no *negative* flow the bins below the zero frequency are empty, i.e.

$$p_i = 0 \qquad \text{IMIN} \le i < 0$$

and the second term in the numerator of (11.7b) is zero. The summation in the first term can be extended to start at $i = 0$ without changing the result, to give

$$\hat{B}^* = \frac{\sum_{i=0}^{\text{IMAX}} i\, p_i \left( 2 \sum_{j=i}^{\text{IMAX}} p_j - p_i \right)}{\left( \sum_{i=0}^{\text{IMAX}} p_i \right)^2} = \hat{B}$$

showing that the more complex expression for both positive and negative components collapses to the result for positive flow only. Equation (2.9b) then is a special case of the more general (11.7b).

(ii)

Consider the case where there is no flow in the *positive* direction. The first term in the numerator of (11.7b) is therefore zero, as is the second term in the second bracket in the numerator. The term $p_0/3$ is also not relevant as it corresponds to the signal from scatterers with positive velocities but too small to be above the zero'th bin. In this case (11.7b) collapses to become

$$\hat{B}^* = \frac{\sum_{i=\text{IMIN}}^{-1} i\, p_i}{\sum_{i=\text{IMIN}}^{-1} p_i} = \overline{B}^*$$

using (11.1b). So if there is no forward flow, and the negative portion of each half of the velocity profile is itself symmetric, then PIWMB is equal to IWMB. This is a consequence of the extra symmetry allowing all the scatterers to be effectively positioned at $r_t$.

(iii)

The positive flow component through the circle of radius $r_z$, shown in fig.11.3a, has a mean velocity denoted by $\hat{B}_{D+}$ which must be the deterministic PIWMB evaluated from the positive frequencies only. In addition, the result of paragraph (ii) above does not rely on there being a central mass of fluid, such as is absent from the symmetric negative flow through the remainder of the vessel illustrated in fig.11.3b. So this symmetric negative flow has a mean velocity which can be found from the corresponding IWMB called $\overline{B}_{D-}$ .

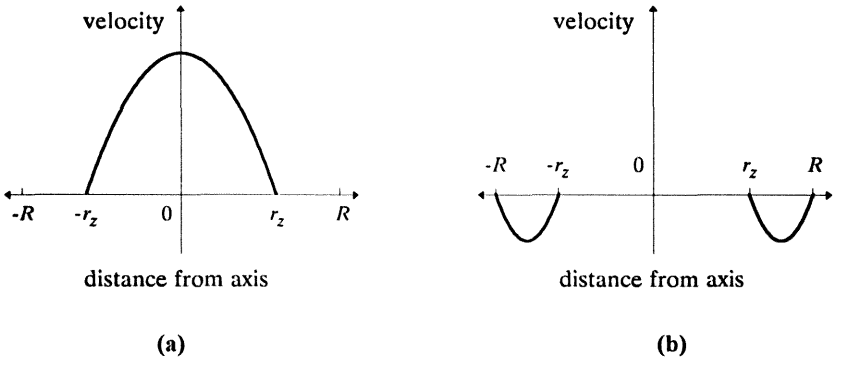


**Fig.11.3 - positive and negative flow components**

The relative weights for these mean velocities are the cross-sectional areas through which they flow. The total mean velocity is proportional to $\hat{B}_D^*$ , which is given by (11.7a) but can therefore also be given by

$$\hat{B}_D^* = \left(\frac{r_z}{R}\right)^2 \hat{B}_{D+} + \left(1 - \left(\frac{r_z}{R}\right)^2\right) \overline{B}_{D-} \qquad \text{(11.9a)}$$

The observed form of this is

$$\hat{B}^* = \left(\frac{P_+}{P}\right)^2 \hat{B}_+ + \left(1 - \left(\frac{P_+}{P}\right)^2\right) \overline{B}_- \qquad \text{(11.9b)}$$

where $P \equiv \sum_{i=\text{IMIN}}^{\text{IMAX}} p_i$ is the total observed power in the spectrum, $P_+ \equiv \sum_{i=1}^{\text{IMAX}} p_i + p_0/3$ is the total observed power in frequencies corresponding to positive velocities, and $\hat{B}_+$ and $\overline{B}_-$ are the observed forms of $\hat{B}_{D+}$ and $\overline{B}_{D-}$. In effect the two terms of (11.9b) are the two

terms of (11.7b). So if the cross section primarily contains forward flow, i.e. $r_z \approx R$, then $\hat{B}^*$ as defined by (11.7b) behaves like its less general form $\hat{B}$ defined by (2.9b). If the cross section is primarily filled with the negative flow, i.e. $r_z \approx 0$, then $\hat{B}^*$ behaves like the simple intensity weighted form, $\overline{B}^*$, defined by (11.1b). These principles are useful when the phenomena studied in chapters 7-10, namely the effects of spectral broadening, noise, filtering and statistical fluctuations are considered in the context of the accuracy of (11.7b).

## Errors in PIWMB

As indicated above errors in $\hat{B}^*$ may arise from several sources. As the amount of negative flow increases, e.g. as the point $r_z$ moves from $R$ towards the vessel centre, the actual mean velocity gets smaller. No matter what the source, the percentage error in PIWMB (or in IWMB) is large if the mean velocity is itself small.

*(i) beam misalignment*

Consider an axi-symmetric 'monotonic' flow and a corresponding mixed flow with profiles along the diameter given by the solid lines of fig.11.4a and fig.11.4b respectively. The reverse flow region in the mixed flow case is comparatively small. If the beam is 'thin' there is no error in PIWMB, but if the beam is of negligible width and is offset slightly from the vessel axis, then the profiles along the chords insonated will be like the dashed lines. In the monotonic case of fig.11.4a the resulting spectrum is 'shrunk' and is located at lower frequencies, so PIWMB underestimates the true mean velocity as suggested in chapter 6. In the mixed case of fig.11.4b the positive velocity components are similarly affected, but the negative velocity region of the profile is not altered in the same way, and instead occupies a greater proportion of the chord. The result is that PIWMB underestimates the true mean velocity by a larger absolute amount than in the monotonic case. Because the true mean velocity becomes less as the reverse flow region gets larger the amount of underestimate as a percentage must also be larger.

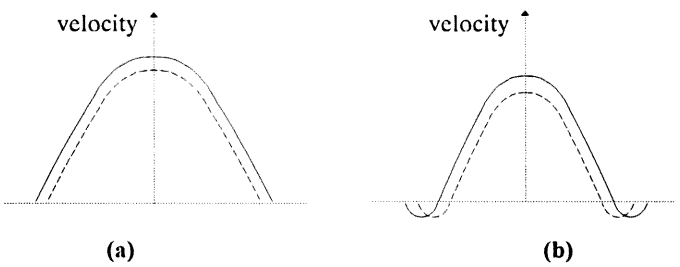


**Fig.11.4 - (a) a monotonic profile and (b) a mixed profile interrogated by a narrow beam which is correctly aligned (solid line) and offset (dashed line)**

*(ii) finite beamwidth*

Referring again to fig.11.4, if the beam is centrally positioned but has finite width, then both the diameter and neighbouring chords are insonated. So the 'profile' inferred from the $p_i$ values is an 'average' of the solid line and neighbouring dashed lines, the concepts of the previous paragraph are again applicable, and the same conclusion can be drawn. Therefore, if the beamwidth is finite, PIWMB incurs more error, both absolutely and fractionally, when the profile has a moderate reverse component than in the monotonic case.

*(iii) spectral broadening*

If a symmetric spectral broadening is assumed, e.g. where $b = 1$ in chapter 7, then the results of chapter 7 show that the statistic $\overline{B}_{D-}$ will be correct for the mean velocity in the flow component of fig.11.3b. However the statistic $\hat{B}_{D+}$ will underestimate the value of the mean velocity in the flow component of fig.11.3a. The result is that overall statistic $\hat{B}_D^*$ of (11.9a) gives an estimate of mean velocity that is less positive, or more negative, than the true value, unless there is no forward flow.

*(iv) noise*

The principles of chapter 8 suggest that the effect of white noise on $\hat{B}^*$ will depend upon the fraction of the total negative frequency range occupied by the negative frequencies, and the fraction of the positive frequencies occupied by the positive frequencies. Altering the number of available positive and negative bins, e.g. by altering a baseline frequency if applicable, will therefore affect the error in $\hat{B}^*$ in the presence of this noise.

*(v) filtering*

If the signal is subject to an ideal high-pass filter with a cut-off frequency less than both $f_{\max}$ and $|f_{\min}|$ then $\overline{B}_{D-}$ will be less negative than is correct, and $\hat{B}_{D+}$ will be more positive than is correct. The effect on $\hat{B}^*$ depends on the relative amounts of forward and reverse flow.

*(vi) statistical fluctuation*

The results of chapter 10 showed that the biases in $\overline{B}$ and $\hat{B}$ are small. An implication is that the bias of $\hat{B}^*$ in (11.9b) will also be small. To derive an approximate value for the variance in $\hat{B}^*$ we make use of the results for uniform single-sided spectra obtained in chapter 10, i.e. that if the spectrum occupies $M$ bins then the variances of $\overline{B}$ and $\hat{B}$ are $M/12$ and $4M/45$ from (10.11) and (10.14) respectively. These variances are very similar, and, as suggested in chapter 10, the variance results for uniform spectra hold approximately for some other spectra if there is a small amount of spectral broadening.

So the variance of (11.9b) can be approximated by the variance of

$$\left(\frac{P_+}{P}\right)^2 \overline{B}_+ + \left(1-\left(\frac{P_+}{P}\right)^2\right) \overline{B}_-$$

where the observed IWMB for the positive flow component, $\overline{B}_+$, has replaced the observed PIWMB, $\hat{B}_+$. The quantity given by this expression is equal to the IWMB of the total observed spectrum, $\overline{B}^*$, as it is the correctly weighted sum of the IWMB values of the two component flows. Furthermore translating the spectrum by a frequency of $|f_{min}|$ to become single-sided can not affect the *variance* of a linear frequency estimator. So the variance of (11.9b) can be approximated by the variance of a uniform single-sided spectrum of width $f_{max} - f_{min}$. The number of bins occupied is then found from the frequency bin width $\Delta f$. Therefore, from (10.11), the variance of PIWMB with this form of reverse flow is

$$\text{var}\,\hat{B}^* \approx \frac{f_{max} - f_{min}}{12\ \Delta f} \qquad \text{or alternatively} \qquad \text{var}\,\hat{B}^* \approx \frac{H - L + 1}{12}$$

where, as before, $H$ is the highest non-empty bin and $L$ is the lowest non-empty bin, and it is remembered that $f_{min}$ and $L$ are negative.

## Discussion

The following chapter suggests that if there is a triphasic mean velocity waveform, the velocity profile in the portion of the cycle where the mean velocity crosses zero going negative can be modelled as being monotonic with a symmetric reverse flow component. This is because the reverse flow near the vessel walls leads the reverse flow in the centre of the artery. An example of the evolution of the profile for such a waveform is seen in fig.11.5.

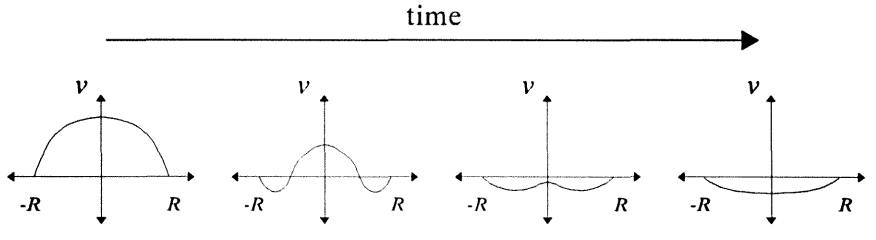


**Fig.11.5 - evolution of a profile with reverse flow**

So the instantaneous mean velocity in the first two stages shown can be correctly measured with the deterministic general form of PIWMB, i.e. (11.7a). Only if the reverse flow components become asymmetric, or if the entire flow becomes reverse as in the third stage

shown will (11.7a) lead to error. This suggests that the instantaneous spatial mean velocity measured using (11.7b) will be appropriate for more than just the systolic phase of such a cycle. The fourth stage shows a case where the flow is monotonic and reverse, so that if the positive bins were considered negative, and vice versa, (11.7a) would again give the correct velocity. The accuracy of PIWMB throughout the cardiac cycle where the velocity profile changes in such a way is relevant to the question of the measurement of volumetric blood flow. This is the subject of the next chapter.

## Summary

If outside a region of monotonic positive flow there is a region of negative flow symmetric about its own centre then PIWMB and PIWMF have more general forms and are accurate, other factors allowing. These forms are given by (11.7b) and (11.8) respectively.

## Notation for this chapter

| | |
|---|---|
| $\overline{B}_D^*, \hat{B}_D^*$ | IWMB and PIWMB as defined by their more general forms with a deterministic spectrum |
| $\overline{B}^*, \hat{B}^*$ | observed IWMB and observed PIWMB as defined by their more general forms |
| $\overline{B}_+, \hat{B}_+, \hat{B}_{D+}$ | observed IWMB, observed PIWMB and deterministic PIWMB for the component flow with positive velocities only |
| $\overline{B}_-, \overline{B}_{D-}$ | observed IWMB and deterministic IWMB for the component flow with negative velocities only |
| $\hat{f}^*$ | PIWMF as defined by its more general form |
| $f_{\min}$ | minimum signal frequency, corresponding to a scatterer with velocity $v_{\min}$ |
| $\Delta f$ | width of each frequency bin |
| $H$ | the index of the highest frequency bin with non-zero spectral power |
| $i'$ | frequency equivalent to the mean velocity of scatterers in the ring corresponding to the $i$'th bin, as in chapter 1 |
| IMIN | minus the number of available bins corresponding to negative velocities (a negative quantity) |
| $L$ | the index of the lowest frequency bin with non-zero spectral power |
| $P_+$ | total observed power in frequencies corresponding to positive velocities |
| $r_z$ | position of lamina of zero velocity |
| $r_t$ | position of lamina with most negative velocity |
| $s_i$ | calculated extent of radial position of scatterers with velocities in the $i$'th bin and above with a 'thin' beam |
| $v_{\max}$ | maximum blood velocity (a positive quantity) $\equiv v_m$ |
| $v_{\min}$ | minimum blood velocity (a negative quantity) |

# CHAPTER 12 - VOLUMETRIC MEASUREMENT USING A MODEL OF PULSATILE FLOW

Prior to chapter 11 the only velocity profiles considered were both axi-symmetric and monotonic and often were idealised to follow (3.1). In this chapter more realistic profiles are derived from a theoretical model of flow throughout the cardiac cycle, and the resulting errors in volumetric flow measurements using IWMB and PIWMB are estimated. First however some theoretical results, more fully described in appendices B and C, about departures from symmetry or monotonicity are given.

(i) A profile which is not axi-symmetric might be expected with flow near changes in vessel geometry. A simple model of such a profile can be obtained by allowing the point, E, of maximum velocity to be a distance, $e$, from the vessel centre, C, as in fig.12.1 and modifying (3.1) to be

$$v = v_m\left(1-\left(\frac{s}{S}\right)^n\right) \qquad (12.1)$$

where $v$ is the velocity a distance $s$ from E, and $S$ is the distance from E to the vessel wall along the same line.

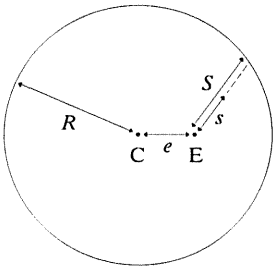


**Fig.12.1 - geometry for an asymmetric velocity profile**

The form of the profile is defined by the parameters $n$ and $e/R$ and the scale by the maximum velocity $v_m$. Appendix B discusses the effects of this model of profile asymmetry on mean velocity measurement with PIWMB, but it is worth stating the surprising main results here, namely that the true mean velocity is independent of $e$ and is therefore given by (3.2), and that if the beam has negligible width and passes throught the point of maximum velocity E then using the deterministic value of PIWMB incurs no error.

(ii) In pulsatile flow the velocity profile might be expected to be non-monotonic at various stages of the cycle. As seen in chapter 11 a more general equation for

PIWMB exists for when the non-monotonicity has a certain form involving some reverse flow. The situation of a non-monotonic but completely positive profile is discussed in appendix C. The main principle with such a profile can be inferred from fig.12.2. Using PIWMB assumes that the particles with higher velocities are closer to the vessel centre. The result is that if such non-monotonicity exists then some of the higher velocities are underweighted, and some lower velocities overweighted, so that PIWMB underestimates the true mean velocity.

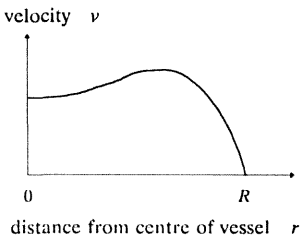


**Fig.12.2 - a positive non-monotonic profile**

The remainder of this chapter shows how the form of the velocity profile at any point in the cycle can be modelled from the mean velocity waveform. Actual estimates of mean velocity waveforms are then used to produce more realistic profiles appropriate to different points of the cycle. These profiles, both monotonic and non-monotonic are used to examine the errors in mean velocity estimates made using the general form of IWMB defined by (11.1a) and the general form of PIWMB given by (11.7a). Volumetric flow measurements are primarily of use when made over an integral number of cardiac cycles. By summing mean velocity errors throughout the cycle estimates of error in volumetric flow are made.

## Steady flow

The starting point is Poiseuille's equation for steady flow of a Newtonian fluid in a rigid pipe, a long way from the entrance. A fluid is Newtonian if its viscosity is independent of velocity gradient. Blood is not Newtonian, but in major arteries, as the velocity scale and diameter are relatively large, the 'asymptotic' viscosity can be used, i.e. the viscosity at high velocity gradients (Evans et al. 1989). Poiseuille's work gives

$$Q = \frac{\pi A R^4}{8\mu}$$

where $Q$ is the volume flow per unit time, $R$ is the internal radius of the pipe, $\mu$ is the viscosity of the liquid, and $A$ is the constant pressure difference per unit length of the pipe, i.e. the pressure gradient. If the radial position is described by the dimensionless parameter

$y \equiv r/R$, where $r = 0$ at the vessel axis, then the velocity profile associated with this equation is the parabolic profile

$$u(y) = \frac{AR^2}{4\mu} \cdot (1 - y^2) \tag{12.2}$$

which is the familiar equation (3.1) with $v = u$, $n = 2$ and $v_m$ identified.

## Sinusoidal flow

A more general case is where the pressure difference fluctuates sinusoidally, i.e. where the pressure gradient is given by the real part of $Ae^{j\omega\tau}$ where $j$ is the square root of $-1$, $\omega$ is the angular frequency and as before $\tau$ is a time variable. The resulting profile equation is attributed to many authors by McDonald (1974), who makes particular reference to work of Womersley (1955, 1957). A dimensionless parameter, $\alpha$, can be defined by $\alpha \equiv R(\omega\rho/\mu)^{1/2} \equiv R(\omega/\nu)^{1/2}$ where $\rho$ is the density of the fluid, and $\nu \equiv \mu/\rho$ is the kinematic viscosity. As a result of a sinusoidal pressure gradient with angular frequency $\omega$, the varying velocity of fluid in the lamina defined by $y$ is the real part of

$$\grave{u}(\omega, y, \tau) = \frac{-AR^2}{\mu} \cdot \frac{1}{j^3\alpha^2} \left( 1 - \frac{J_0(y\alpha j^{3/2})}{J_0(\alpha j^{3/2})} \right) \cdot e^{j\omega\tau} \tag{12.3}$$

where the 'preceding prime' notation, e.g. $\grave{u}$, is used here to indicate a complex velocity, and where $J_0(\cdot)$ is the Bessel function of the first kind of order 0, which in this case has complex arguments. It is seen that, as the time dependence is in the last term only, a sinusoidal pressure gradient gives rise to a sinusoidal fluctuation in the velocity at each point in the pipe, with the same frequency. The form of the velocity profile resulting from this pressure gradient is given by the term in the large parentheses. If $\alpha$ is equal to zero, i.e. if the pipe radius is infinitesimal or the fluid has limitless viscosity, or the angular frequency is zero, this becomes the parabolic profile of (12.2) and there is flow according to Poiseuille's theory.

The instantaneous spatial mean velocity can be found by integrating over all the laminae in the pipe and dividing by the cross-sectional area of the pipe, $\pi R^2$, and is the real part of

$$\grave{\bar{u}}(\omega, \tau) = \frac{-AR^2}{\mu} \cdot \frac{1}{j^3\alpha^2} \cdot \left( 1 - \frac{2J_1(\alpha j^{3/2})}{\alpha j^{3/2} J_0(\alpha j^{3/2})} \right) \cdot e^{j\omega\tau} \tag{12.4}$$

where $J_1(\cdot)$ is the Bessel function of the first kind of order 1. Equations (12.3) and (12.4)

can be combined to give the velocity in any lamina in terms of the spatial mean velocity, i.e.

$$\grave{u}(\omega, y, \tau) = \grave{\bar{u}}(\omega, \tau) \cdot \left( \frac{\alpha j^{3/2} J_0\left(\alpha j^{3/2}\right) - \alpha j^{3/2} J_0\left(y \alpha j^{3/2}\right)}{\alpha j^{3/2} J_0\left(\alpha j^{3/2}\right) - 2 J_1\left(\alpha j^{3/2}\right)} \right) \tag{12.5}$$

remembering that $\alpha$ is a function of $\omega$. The term in the large bracket is complex and can be called $\psi(\alpha, y)$, having magnitude $|\psi(\alpha, y)|$ and phase $\zeta(\alpha, y)$ which for various values of $\alpha$ have been plotted by Evans (1982b). This term contains the only reference to $y$, and so defines the form of the velocity profile produced by the pressure gradient. The scale of the profile given by (12.5) is related to the other term, which is the spatial mean velocity.

## Actual flow

In practice the pressure gradient will not be sinusoidal, but will be a waveform definable by a set of $A_k$ values, where $A_k$ is a complex number describing the amplitude and phase of the $k$'th harmonic. However each of its harmonics will give rise to a separate case of equation (12.4), each with its own amplitude and phase, and $\omega$ and $\alpha$ values. In considering the complete pressure gradient these equations can simply be summed because the theory leading to (12.3) involving the viscosity is linear in the associated velocity gradient *du/dy* and hence in $u$, which is the real part of $\grave{u}$. In this way McDonald (1974) applied the theory to the calculation of profiles from a pressure gradient made up of several frequency components. Evans (1982b) extended the theory to the calculation of profiles by Fourier analysis of the associated flow, or spatial mean velocity, waveform. If the observed mean velocity waveform, $\bar{v}'(\tau)$, is decomposed into its harmonic components, $\bar{u}_k \cos(k\omega_1 \tau + \phi_k)$, where $k$ is the number of the harmonic, $\omega_1$ is the angular frequency of the fundamental, and $\bar{u}_k$ and $\phi_k$ are the results of the Fourier analysis, then

$$\bar{v}'(\tau) = \sum_{k=0}^{\infty} \bar{u}_k \cos(k\omega_1 \tau + \phi_k) \tag{12.6}$$

The component $\bar{u}_k \cos(k\omega_1 \tau + \phi_k)$ is therefore the real part of the complex term $\grave{\bar{u}}(k\omega_1, \tau)$ in the relevant evaluation of (12.4) or (12.5). With these equations a single value of $\alpha$ is not appropriate for the different components. The definition of $\alpha_k$ for the $k$'th harmonic is therefore

$$\alpha_k \equiv R(k\omega_1 \rho/\mu)^{1/2} \tag{12.7a}$$

The value for the fundamental is $\alpha_1$ and it is clear that

$$\alpha_k = \sqrt{k} \cdot \alpha_1 \tag{12.7b}$$

Therefore from (12.5) and (12.6) the instantaneous real-valued velocity profile estimate, $v'(y,\tau)$, is given by

$$v'(y,\tau) = \sum_{k=0}^{\infty} \overline{u}_k \cdot \left|\psi(\alpha_k, y)\right| \cdot \cos\left(k\omega_1 \tau + \phi_k + \zeta(\alpha_k, y)\right)$$

So from Fourier analysis of an estimate of the mean velocity waveform, $\overline{v}'(\tau)$, and knowledge of the 'scaled profile' terms $\psi(\alpha_k, y)$, instantaneous velocity profiles can be constructed. It is important to note that the theory is based on the asumption that the site of investigation is far enough from any change in the geometry of the tube for the flow components to be established. That is, for a given pressure gradient, the velocity profile can be thought of as being independent of the axial position in the tube. It is apparent also that the theory fails to model the actual expansion and contraction of the arterial cross section, and allows no curvature in the artery.

## Data collection and analysis

Examples of approximate mean velocity waveforms from various arterial sites were obtained from healthy volunteers. The mean velocity was assumed to be proportional to the IWMB of the Doppler signal received using a sector scanner, calculated from (2.1b). The sector scanner was chosen primarily because its separate Doppler beam was broader than the beam of our linear array transducer, and so would insonate more uniformly the vessel cross section, thus improving the accuracy of IWMB. These waveforms were used to estimate the instantaneous profiles according to the theory above, and so to test the accuracy of PIWMB as a means of flow calculation at these sites.

Mean velocity waveforms of single cardiac cycles were obtained from both the common and superficial femoral arteries of 13 young, healthy volunteers $(\text{age} \le 45)$. In addition some examples of internal carotid, common carotid, brachial and radial mean velocity waveforms were obtained from the same group of subjects. Fourier analysis was performed on these waveforms, which were noisy and generally had a region(s) of zeroes where the high-pass filter (nominally 200 Hz) had removed a large amount of the signal power. The constant component and the first 10 harmonics were retained to reconstruct a representative waveform, and were also used to derive the changing velocity profiles predicted by the theory above. For each of these profiles, computer simulation of insonation by a 'thin' beam allowed PIWMB as defined by (11.7a) to be calculated. Such a calculation was made at 60 points uniformly spaced throughout the cycle (i.e. every 6° of phase). Using the model assumption of an unchanging cross-sectional area, this led to a proportional estimate of volumetric flow. This was compared with the 'correct' value

appropriate to the reconstructed waveform to find the error incurred through use of PIWMB.

## Results

In most cases only one waveform from each site of each volunteer was analysed. For the few volunteers where more than one was analysed the result presented is that with the largest error magnitude.

*Common femoral artery*

As shown in fig.12.3 the errors for the flows in the common femoral arteries ranged from +3.0% to -2.4% , though only two of the errors were more negative than +1.4%. This suggests that accurate flow measurement in the common femoral artery may be possible with PIWMB despite the triphasic nature of the flow at this site.

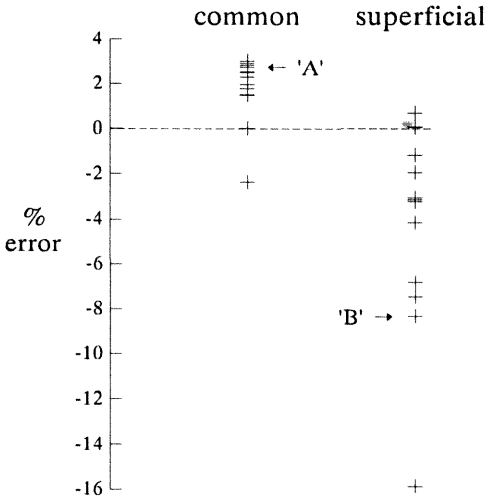


**Fig.12.3 - errors in volumetric flow for single cycles from common and superficial femoral artery recordings**

The source of the typical 2½% overestimation can be seen by considering the waveform which gave rise to an error of +2.7% marked 'A' on fig.12.3. The relative amplitudes and phases of the first 10 harmonics of this waveform are listed in table 12.1. Also tabulated are the relevant $\alpha_k$ values calculated from the vessel diameter and period according to (12.7).

Waveform 'A' Heart rate (based on this single cycle) = 82 bpm
Estimated diameter = 10mm

Assumed kinematic viscosity = 0.038 St $\equiv 3.8 \times 10^{-6}\ m^2 s^{-1}$ (Evans et al. 1989)

| Harmonic ($k$) | Amplitude $(\overline{u}_k / \overline{u}_0)$ | Phase $(\phi_k)°$ | $\alpha_k$ |
|---|---|---|---|
| 0 | 1 | 0 | 0 |
| 1 | 1.120 | 2.5 | 7.5 |
| 2 | 2.262 | 60.8 | 10.6 |
| 3 | 1.173 | 120.9 | 13.0 |
| 4 | 0.212 | 157.1 | 15.0 |
| 5 | 0.249 | 129.2 | 16.8 |
| 6 | 0.249 | 129.0 | 18.4 |
| 7 | 0.188 | 120.9 | 19.9 |
| 8 | 0.242 | 188.3 | 21.3 |
| 9 | 0.092 | 232.0 | 22.6 |
| 10 | 0.113 | 144.7 | 23.8 |

**Table 12.1 - parameters of waveform 'A'**

The appropriate reconstructed waveform, called waveform 'A', is shown by the solid line of fig.12.4, and the estimate using PIWMB is given by the dashed line, which for the majority of the cycle is virtually coincident with the solid line. The overestimate of flow is seen to be caused almost entirely by PIWMB being less negative than the correct value during the phase of the cycle with negative mean velocity. The error in this region can be understood by making reference to fig.12.5 which shows some of the corresponding profiles predicted by the theory. For clarity the profiles shown are spaced at intervals of 18°, i.e. at intervals of every 3 sample points. (The steplike nature of each profile is a reproduction artifact.) Consider, as an example, the profile at the 90° point. The negative flow regions are not symmetric but are skewed considerably towards the vessel wall. Using PIWMB in such a case assumes symmetry and therefore treats the most negative velocities as being present closer to the vessel centre. This assignment of the largest velocities to laminae which contribute less to the total cross-sectional area leads to a value of PIWMB which is numerically too small, i.e. in this case not negative enough. (The profiles not shown before 36° are positive and monotonic, and the profiles towards the end of the cycle are small and contribute little to the volumetric flow. Such small profiles correspond to the late periods of small fluctuation in the reconstructed mean velocity waveform of fig.12.4. These fluctuations, which are more evident in the waveform of fig.12.6 to be introduced shortly, are artificially created by the truncation of the sequence of Fourier coefficients.)

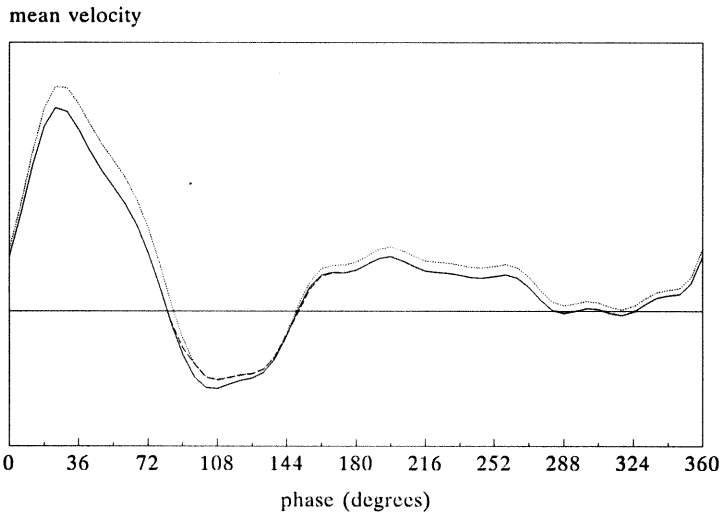


**Fig.12.4 - The solid line shows waveform 'A', which is the reconstruction of the mean velocity recorded in a common femoral artery throughout a cardiac cycle. The corresponding mean velocity estimated using PIWMB with a 'thin' beam is given by the dashed line. The dotted line gives the estimate using IWMB with a 'thin' beam, discussed later in the text.**

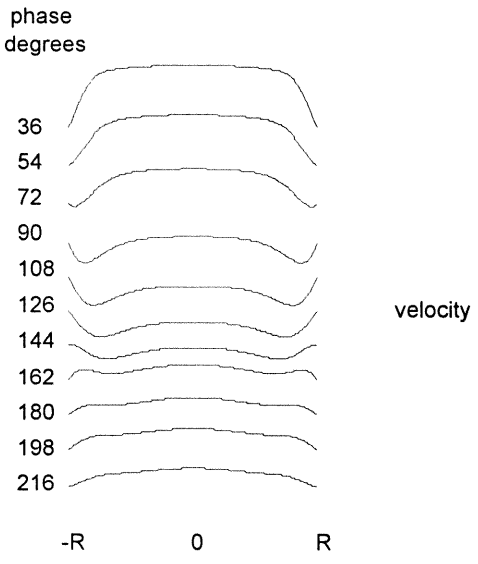


**Fig.12.5 - velocity profiles during the cycle for waveform 'A'**

*Superficial femoral artery*

As shown in fig.12.3 the errors for the flows in the superficial femoral arteries ranged from +0.7% to -8.3% with a single extreme value at -15.9%. So it would appear that PIWMB is less accurate in determining volumetric flow at this site than in the common femoral artery. The source of the underestimation typically observed is suggested when considering the waveform for the only female volunteer, which gave the error of -8.3% marked 'B' on fig.12.3. The relevant Fourier amplitudes, phases and $\alpha_k$ values are given in table 12.2.

Waveform 'B' Heart rate (based on this single cycle) = 83 bpm
Estimated diameter = 4.2 mm

Assumed kinematic viscosity = 0.038 St $\equiv 3.8 \times 10^{-6}\ m^2 s^{-1}$ (Evans et al. 1989)

| Harmonic ($k$) | Amplitude $(\overline{u}_k/\overline{u}_0)$ | Phase $(\phi_k)°$ | $\alpha_k$ |
|---|---|---|---|
| 0 | 1 | 0 | 0 |
| 1 | 1.794 | 23.9 | 3.17 |
| 2 | 2.618 | 73.0 | 4.49 |
| 3 | 1.400 | 148.1 | 5.49 |
| 4 | 0.573 | 140.7 | 6.34 |
| 5 | 0.291 | 203.7 | 7.09 |
| 6 | 0.178 | 112.6 | 7.77 |
| 7 | 0.246 | 140.9 | 8.39 |
| 8 | 0.123 | 208.4 | 8.97 |
| 9 | 0.103 | 165.8 | 9.51 |
| 10 | 0.083 | 23.2 | 10.03 |

**Table 12.2 - parameters of waveform 'B'**

The appropriate reconstructed waveform, called waveform 'B', is shown by the solid line of fig.12.6, and the estimate of PIWMB is given by the dashed line. The waveform is seen to be 'more pulsatile' than waveform 'A' in that the mean velocity descends from its maximum value more rapidly, and the reverse flow region occupies a greater proportion of the cycle. As with waveform 'A' PIWMB is not negative enough at approximately 90°, but this effect is swamped by the fact that between 108° and 196° PIWMB records a value that is too negative. Making reference to fig.12.7, which is as in fig.12.5 but corresponds to waveform 'B', the greater pulsatile nature is seen in that beyond 108° the profile actually becomes monotonic in the reverse direction. In the absence of any positive flow PIWMB then treats the profile as being made up of two symmetric reverse regions with the greatest velocities midway between the axis and the vessel wall. In this way the most negative velocities are overweighted and so PIWMB is too negative.

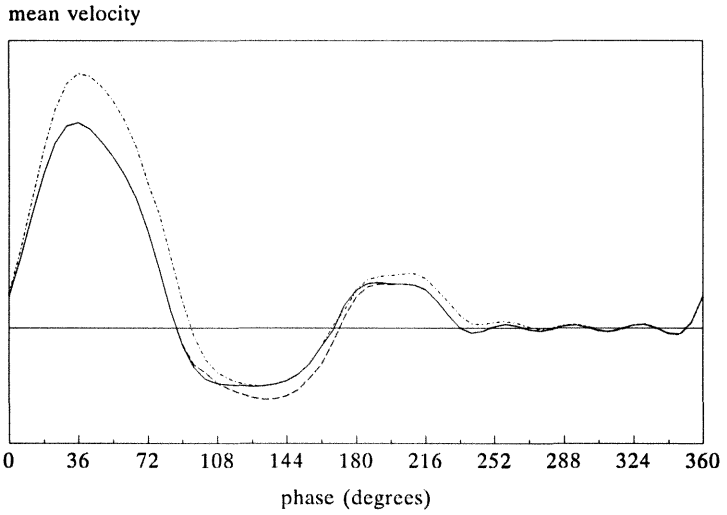


**Fig.12.6 - The solid line shows waveform 'B', which is the reconstruction of the mean velocity recorded in a superficial femoral artery throughout a cardiac cycle. The corresponding mean velocity estimated using PIWMB with a 'thin' beam is given by the dashed line. The dash-dot line shows the estimate of the 'backwards' form of PIWMB discussed later in the text.**

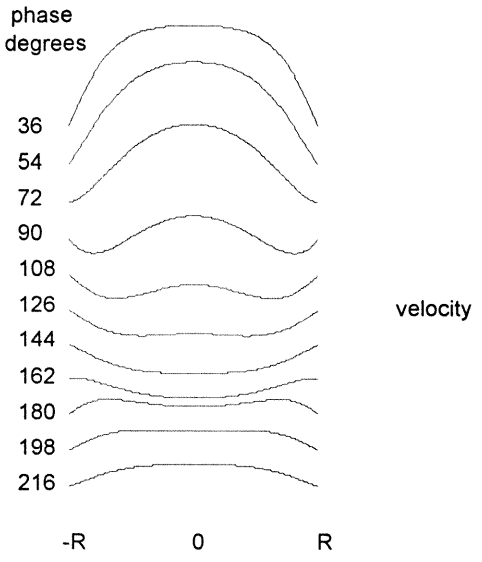


**Fig.12.7 - velocity profiles during the cycle for waveform 'B'**

*Other sites*

The example internal carotid, common carotid, radial and brachial artery waveforms (7 in total) all gave velocity profiles which visually were positive and monotonic at almost every stage of the cycle. The resulting flow errors measured were of the order of 0.001%. Fewer examples of waveforms from these sites were taken as it was quickly apparent that the error was zero or negligible. The very small departures from monotonicity observed were in the form of small regions of reverse flow near the vessel walls. So it would seem that, with this model, this form of non-monotonicity occurs more easily than a non-monotonicity in a completely positive profile. The implication is that PIWMB could be used without error at sites where flow is entirely forward, i.e. where the spectrum is single-sided.

*Comments*

The error in PIWMB is linked to the 'pulsatility' of the waveform. Because their waveforms tend to be pulsatile, a group of young, healthy volunteers represent a worst-case sample, and so the errors in the recorded values of PIWMB are likely to be relatively large.

It is interesting to note that the extreme negative result of -2.4% for the common femoral artery and the extreme result of -15.9% for the superficial femoral artery were recorded from the same volunteer. From the same original recordings for this subject, other waveforms from single cycles were obtained giving results of -1.6% and -0.2% for the common femoral artery, and -15.7% , -14.5% and -13.8% for the superficial femoral artery, so that there was a considerable degree of repeatability in the extremeness of these results.

## Entrance length effects

As suggested earlier the validity of the results depends on the degree to which the flow profile components can be regarded as being established at the site of measurement. If the profile is taken as being of the plug form when the section of the artery is entered then an approximate expression for the length required in the vessel before the constant component of flow gives rise to the parabolic profile is

$$X_0 \approx 0.03 d N_R \qquad (12.8)$$

(Caro et al. 1978) where $d$ is the vessel diameter, and $N_R$ is the Reynolds number of the

flow. The Reynolds number $N_R$ for a given flow is

$$N_R = \frac{UL}{\nu}$$

where $U$ and $L$ are representative velocity and length scales of the system respectively. For flow in a tube the Reynolds number can be defined by

$$N_R = \frac{\bar{s}d}{\nu} \tag{12.9}$$

where $\bar{s}$ is the spatial mean velocity. If a large reservoir feeds into a narrow tube then $\bar{s}$ will be the single velocity at the entrance to the tube. In practice the relevant distance may be the distance from the site of measurement to the previous major bifurcation, and the profile (2 diameters) downstream from this 'entrance' point will not have a plug form but may have an asymmetric M shape, with the highest velocities being on the side of the inner vessel wall. The distance required for the parabolic flow to be re-established after this bifurcation is comparable to the entrance length in the case of plug flow (Caro et al. 1978).

For an oscillating component with angular frequency $\omega$ (in our case $\omega \equiv k\omega_1$) the instantaneous entrance length, if the initial flow is of the plug form, can be described by

$$X_{ki} \approx \frac{3.4 s_{ki}}{\omega}$$

(Caro et al. 1978) where $s_{ki}$ is the instantaneous core velocity. Throughout the cycle the largest value of this length is therefore given by

$$X_k \approx \frac{3.4 s_k}{\omega} \tag{12.10}$$

where $s_k$ is the maximum core velocity. It is assumed below that the developments of the mean component and the various oscillating components do not affect each other so that (12.8) and (12.10) can be applied to the results of the Fourier analysis independently.

For waveform 'A' the mean velocity of the constant component was estimated, using knowledge of the Doppler angle (which was 39°), to be $\bar{u}_0 \approx 8.1$ cm.s$^{-1}$. This is the value of $\bar{s}$ for use in (12.9). So with $d \approx 10$mm and $\nu \approx 3.8 \times 10^{-6}$ m$^2$s$^{-1}$ the Reynolds number is $\approx 200$, and using (12.8) the entrance length, $X_0$, for the constant flow component is approximately 6 cm. The site of the recording of waveform 'A' was approximately 2 cm

above the femoral bifurcation, and consequently was a long way from the previous bifurcation. So the constant forward component of the velocity profile could be regarded as being established at the site at which waveform 'A' was recorded.

For the $k$'th harmonic the maximum core velocity $s_k$ is proportional to $\overline{u}_k$ . In addition, with a parabolic profile the velocity observed at the core of the vessel is twice the mean velocity, as can be seen from (3.2) with $n=2$. From the plots of $|\psi(\alpha,y)|$ given by Evans (1982b) and referred to above, the velocity profiles associated with the oscillating components can be seen to be blunter than parabolic, so therefore the maximum central velocity cannot be greater than the quantity $2\times\overline{u}_k$. So from (12.10) an upper bound for the entrance length for the $k$'th harmonic is given by

$$X_k <\approx \frac{6.8\ \overline{u}_k}{k\omega_1}$$

For this artery this length is largest for the second harmonic and is approximately 7 cm. Therefore being only a few centimetres away, the site was too close to the bifurcation for all the oscillating components to be regarded as established at all phases of the cycle. At least 10 of the other 12 common femoral recordings were made at sites in the region of 5 cm above the femoral bifurcation. However these tended to have larger maximum values of $X_k$. As indicated in fig.12.3 several of these recordings gave similar errors to waveform 'A'. Their similar waveforms, and consequently similar profiles, incurring error in the same way, mean that although waveform 'A' was recorded at a site closer to the bifurcation it is regarded as an appropriate example.

Waveform 'B' was obtained at a site approximately 20 cm distal to the femoral bifurcation. Similar calculations to those performed for waveform 'A' above show that the entrance lengths for the constant and oscillating profile components of waveform 'B' are given by $X_0 \approx 1\text{cm}$ and $X_k <\approx 7\text{cm}$. Therefore at this site flow is regarded as being established. The other recordings from the superficial femoral arteries were made from sites approximately 15 cm (or more) from the femoral bifurcation.

## Errors in IWMB

The errors associated with incomplete insonation in the use of IWMB to estimate volumetric flow have been shown to depend only on the form of the constant component of the velocity profile (Evans 1985). This can be understood by considering that each oscillating component by its time-symmetry contributes no net flow throughout the cycle, and no net contribution to the measured flow no matter what the shape of the beam. If the actual flow followed the theoretical model above then, as each component of the flow is

assumed to be established, the constant component of the velocity profile would have a parabolic form. This profile can simply be expressed by

$$v = v_m\left(1 - y^2\right)$$

which is (3.1) with $y \equiv r/R$ and $n = 2$. Estimating mean velocity using IWMB and a 'thin' beam is equivalent to finding the mean value of $v$ along the diameter from $y = -1$ to $y = 1$. So the estimate found would be

$$\bar{v}_{\text{IWMB}} = \tfrac{1}{2}\int_{-1}^{1} v_m\left(1 - y^2\right)dy = \tfrac{2}{3}\, v_m$$

which is 33⅓% larger than the correct mean velocity of $\frac{1}{2}\, v_m$ found from (3.2). (This value of $\frac{2}{3} v_m$ follows also from (3.5) with $t = 0.5$.) Therefore, no matter how pulsatile the mean velocity waveform, with this flow model and with a 'thin' beam, use of IWMB would introduce a systematic error of +33⅓% which could be corrected for. In practice the beamwidth is finite, so that the percentage error would be less than this but would still be independent of the mean velocity waveform. Similarly, departures of the constant component from the parabolic form predicted by the model would alter the error. A correction factor therefore could only be accurately applied if the time-averaged velocity profile and the beam intensity profile were known.

For waveform 'A' the value of IWMB with a 'thin' beam, also calculated by computer simulation, is shown as the dotted line on fig.12.4. As expected IWMB overestimates the mean velocity throughout most (in this case all) of the cycle, leading to the overall flow error of +33⅓% as demonstrated above.

## Relevance of the flow model

The flow model above has been put forward to derive approximate values for the errors that might be incurred using PIWMB for the estimation of volumetric flow. If this model accurately described the actual flow then, as seen in the previous section, the statistic IWMB might be used with a correction factor, and there would in fact be no advantage in using PIWMB, even if the beam was 'thin'. So, in the context of flow estimation, the usefulness of PIWMB is linked to the inadequacies of the flow model. As seen above one such inadequacy might be that at the site of investigation the flow may not be established. A second, as mentioned, is that the theory is for flow in a tube which is rigid. If the model was in fact able to take into account the changes of cross-sectional area during the cycle, the flow errors derived would still be approximate. This is because, in the subsequent

calculations, PIWMB was assumed to be proportional to the instantaneous flow, which is only true if the cross-sectional area is constant. Thirdly, as stated, the model also allows no curvature of the artery. The presence of local curvature would tend to violate the assumption of axi-symmetry necessary for the validity of PIWMB. Lastly, if the site of measurement was not far from a bifurcation, in addition to uncertainty about the form of the unestablished profile, some asymmetry might remain from the asymmetry introduced at the bifurcation.

## Finite beamwidth and/or displaced beam

In the practical case the beam fails to satisfy the assumption of infinitesimal width, and may be displaced from the centre of the vessel. In either case, with an axi-symmetric monotonic profile, the estimate of the mean velocity made using PIWMB is below the true value, as shown in chapters 5 and 6. So, for example, as the profile is typically positive and monotonic throughout a significant proportion of the cycle, the error with waveform 'B' might be expected to be more negative than the recorded -8.3%. Computer simulation was used to find the percentage errors in volumetric flow measurement with beams which are of finite width and/or which are displaced. The results are shown in table 12.3. The ultrasound beam is deemed to have a Gaussian shape which, in the same way as in chapter 5, is defined by the ratio of standard deviation of the intensity response *upon reception* to the radius, denoted by $\sigma/R$. The displacement of the centre of the beam from the vessel axis is given as a fraction of the radius. So the results for the 'thin' beam are very close to those given in the first row, where the beamwith is very small and the displacement is zero, and the results for a 'wide' beam are approximately given by the row for $\sigma/R = 10$. The errors tabulated are those incurred by the use of PIWMB for waveforms 'A' and 'B' and for constant flow as given by a constant parabolic profile, and those incurred by IWMB for any mean velocity waveform. The bracketed values are the exact theoretical values found from (6.4) and give an indication of the uncertainty in the values in the table.

The additional errors due to a finite beamwidth or a beam displacement are seen to be similar for waveforms 'A' and 'B' and the constant flow, and can be treated as being equal to a good approximation when these effects are small. For example with a centrally placed beam with $\sigma/R = 0.2$ the additional errors with 'A' and 'B' respectively are

$$(-1.9\%)-(+2.7\%) = -4.6\% \qquad \text{and} \qquad (-12.7\%)-(-8.3\%) = -4.4\%$$

which are both close to the value of -4.3% for the constant flow. Similarly for a beam of negligible width but displaced from the centre by 0.2 radii the extra errors for 'A' and 'B' are both approximately -4% which is the value for the constant flow. Also, for small beamwidths and displacements, the individual errors can be treated as additive, as indicated

by the row with beamwidth ratio = 0.2 and offset = 0.2. Comparison can also be made with the performance of IWMB which gives the same results for any mean velocity waveform, as only the shape of the constant velocity profile component is relevant, and these are all taken to be parabolic. For IWMB the errors are given in the last column of table 12.3. The most meaningful comparison between PIWMB and IWMB is made for a beam of finite width. As with the monotonic case in chapter 5, PIWMB performs considerably better than IWMB if the beam has a standard deviation to radius ratio of 0.2 or less. In chapter 5 a ratio of approximately 0.2 was suggested as being appropriate for our transducer and a 6 mm diameter vessel.

| | beamwidth ($\sigma/R$) | offset (radii) | waveform 'A' PIWMB | waveform 'B' PIWMB | constant flow PIWMB | any waveform IWMB |
|---|---|---|---|---|---|---|
| 'thin' | $\approx 0$ | 0 | +2.7 | -8.3 | 0.0 | +33.3 |
| finite width | 0.2 | 0 | -1.9 | -12.7 | -4.3 | +28.3 |
| | 0.5 | 0 | -19.1 | -29.6 | -20.2 | +12.8 |
| | 10 | 0 | -34.2 | -43.7 | -33.3 | + 0.1 |
| offset | $\approx 0$ | 0.2 | -1.4 | -12.1 | -3.8 (-4) | +28.1 |
| | $\approx 0$ | 0.4 | -15.1 | -24.5 | -16.0 (-16) | +12.0 |
| both | 0.2 | 0.2 | -6.6 | -17.3 | -8.7 | +23.4 |
| | 0.5 | 0.4 | -25.6 | -35.8 | -25.9 | +7.2 |

**Table 12.3 - Percentage errors in volumetric flow measurement for beams which are displaced and/or have Gaussian intensity profiles of finite width**

## Redefining the forward direction

The fact that the profile in the case of waveform 'B', shown in fig.12.7, becomes monotonic and reverse, e.g. at 144°, suggests that at this point in the cycle if the sense of direction of the frequency axis was reversed the resulting value of PIWMB would accurately give the instantaneous mean velocity. This could simply be achieved by calling the negative frequency bins positive, and vice versa, then applying (11.7a) and multiplying the final velocity by -1. However an alternative is not to renumber the bins, but to change the

defining equation to produce the same effect. The resulting 'backwards' stochastic estimate, $\hat{B}_B^*$, would therefore be

$$\hat{B}_B^* = \frac{\sum_{i=\mathrm{IMIN}}^{-1} i\,p_i\left(2\sum_{m=\mathrm{IMIN}}^{-1} p_m - p_i\right) + \left(\sum_{i=0}^{\mathrm{IMAX}} p_i + 2\sum_{i=\mathrm{IMIN}}^{-1} p_i + \frac{p_0}{3}\right)\sum_{i=1}^{\mathrm{IMAX}} i\,p_i}{\left(\sum_{i=\mathrm{IMIN}}^{\mathrm{IMAX}} p_i\right)^2} \qquad (12.11)$$

where the index $m$ is used, as the usual $j$ or $k$ have other definitions in this chapter. The implication is that at some points in the cycle, in this example most notably in between 126° and 180°, this 'backwards' form of PIWMB follows the true mean velocity more accurately than the 'forwards' form. This is seen on the corresponding fig.12.6 where the value of the deterministic form of (12.11) is given by the dash-dot line. If a procedure was available to detect such a region(s) in the cycle the estimate of volumetric flow could be improved. In this way a simple algorithm was developed which reduced the error in this example of waveform 'B' from -8.3% to +0.4%, but increased the error for some other waveforms. If such an algorithm were to be useful it would need to be robust enough to offer improvement with all typical waveforms, and with signals 'corrupted' by spectral broadening, noise, filtering and statistical fluctuation.

It is noticeable in fig.12.6 that the 'backwards' estimator is greater than the 'forwards' estimator at all points of the cycle. It is demonstrated in appendix E is that this is necessarily true for their continuous frequency forms. This suggests the result that, in every case

$$\hat{B}_B^* \geq \hat{B}^* \qquad (12.12)$$

## Summary

The instantaneous velocity profiles for the testing of the more general form of PIWMB given by (11.7a) were derived from experimental mean velocity data, and the theory of pulsatile flow of a Newtonian fluid in a rigid tube. If this theory gives a useful approximation to the actual flow then the results imply that PIWMB as defined by (11.7b) can be used to estimate volumetric flow at sites where the flow has a low degree of pulsatility, e.g. the carotid, radial and brachial arteries, without incurring error due to invalid assumptions about the velocity profiles. In the common femoral artery the small positive error, with little variation between subjects, also supports the validity of PIWMB for volumetric flow measurements. PIWMB should be used with more caution in the superficial femoral artery as the errors measured at this site showed greater magnitude and greater variance.

## Notation for this chapter

| | |
|---|---|
| $\hat{B}^*$ | PIWMB as defined by its more general form, (11.7b) |
| $\hat{B}_B^*$ | PIWMB when frequency axis is reversed |
| $j$ | square root of -1 |
| $J_0(\cdot), J_1(\cdot)$ | Bessel functions of the first kind of order 0 and 1 |
| $k$ | harmonic index number |
| $N_R$ | Reynolds number |
| $\overline{u}_k$ | amplitude of $k$'th harmonic component of mean velocity waveform |
| $\grave{u}(\omega, y, \tau)$ | complex velocity profile due to sinusoidal pressure gradient with frequency $\omega$ |
| $\grave{\overline{u}}(\omega, \tau)$ | complex spatial mean velocity with a sinusoidal pressure gradient with frequency $\omega$ |
| $v(y, \tau)$ | total velocity profile |
| $\overline{v}(\tau)$ | spatial mean velocity waveform |
| $y$ | fractional radial position ($\equiv r/R$) |
| $X_0, X_k$ | entrance lengths for constant profile component, $k$'th harmonic component |
| $\alpha, \alpha_k$ | parameter defining profile form for the ($k$'th) harmonic pressure gradient |
| $\phi_k$ | phase of $k$'th harmonic component in mean velocity waveform |
| $\mu$ | viscosity of blood |
| $\nu$ | kinematic viscosity of blood ($\equiv \mu/\rho$) |
| $\rho$ | density of blood |
| $\sigma$ | standard deviation of the intensity response for a Gaussian shaped beam |
| $\omega$ | angular frequency |
| $\omega_1$ | fundamental angular frequency of the mean velocity waveform |
| $\psi(\alpha, y)$ | complex profile form for the pressure gradient associated with $\alpha$ |
| $\zeta(\alpha, y)$ | phase of the complex function $\psi(\alpha, y)$ |

# CHAPTER 13 - ERROR COMPARISON IN VOLUMETRIC FLOW MEASUREMENT

Previous chapters, chapter 12 apart, have concentrated on the accuracy of IWMB and PIWMB for the measurement of instantaneous mean blood velocity. However such velocity measurement is most useful in the context of examining the total volumetric flow in a period of time, for example during an integral number of cardiac cycles. The usefulness of the estimators are therefore best considered by integrating the relevant instantaneous errors throughout the cycle. The object of this final chapter is to provide a feel for the typical errors in volumetric flow measurements made using IWMB and PIWMB, and to suggest the factor(s) most affecting their accuracy.

Clearly there are many parameters and variables defining the accuracy, and it is necessary to assign example values to these to obtain quantitative results. In particular the flow throughout the cycle needs to be assumed. Therefore we consider the example mean velocity waveform given in fig.13.1, which is an actual waveform recorded in the carotid artery in the same way as those given in chapter 12. It is therefore only an approximate representation of the true mean velocity waveform, being liable to errors, notably those due to non-uniformity of insonation and high-pass filtering. As the mean velocity is at all points considerably positive, it might be justified to consider the velocity profile to be parabolic at all points in time. The form of the spectrum is therefore regarded as being constant throughout the cycle, and the scale of the spectrum is proportional to the mean velocity which, from (3.2), is at all times equal to half the maximum velocity.

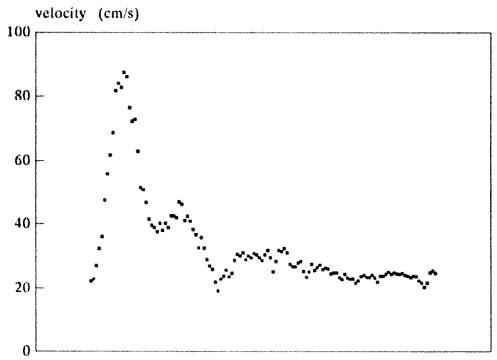


**Fig.13.1 - example of a 'mean' velocity waveform**

The error sources of chapters 4 - 10 are considered separately, with example parameter values chosen to give a guide to the sizes of the errors involved. To a poor first approximation these errors can be considered additive. The accuracy of such addition is improved the smaller the errors involved.

## Errors with an example beam

As suggested in chapter 5, with our transducer and a 6 mm diameter vessel the beam intensity response profile can be approximated as being Gaussian, with a width defined by the ratio $\sigma/R$~0.2. For comparison of the accuracies of IWMB and PIWMB both estimators are assessed for this beam. The figures derived are tabulated in table13.1.

*Angle measurement - chapter 4*

The work of chapter 4 shows that for both IWMB and PIWMB a 2° error in the estimation of a Doppler angle of 50° leads to an error in mean velocity measurement of $\pm 4\frac{1}{2}\%$. This percentage is unaffected by the changing value of the true mean velocity throughout the cycle, so it would also be the percentage error in volumetric flow.

*Finite beamwidth - chapter 5*

From fig.3.3 the error in IWMB for mean velocity estimation with this beam is approximately +29% and the error in PIWMB is approximately -4%. These percentages are constant throughout the cycle, so these are also the percentage errors in volumetric flow.

*Displaced beam - chapter 6*

If a uniformly insonating beam with a realistic shape was offset from the vessel centre by the reasonable amount of 20% of the radius then IWMF would incur little or no error. However if this much thinner example beam was displaced by the same amount then, because of the parabolic profile, the centre of the beam insonates a maximum velocity

| chapter no. | error source | % errors in volumetric flow using example beam | |
|---|---|---|---|
| | | IWMB | PIWMB |
| **4** | **angle measurement** | **±4½** | **±4½** |
| 5 | finite beamwidth | +29 | -4 |
| **6** | **displaced beam** | **-4 to 0** | **-4 to 0** |
| 7 | spectral broadening | 0 | -2 |
| 8 | white noise | +2.5 | < ±1 |
| 9 | high-pass filter | +5 | +7 |
| **10** | **stochastic signal** | **±2** | **±2½** |
| **12** | **non-monotonicity** | **0** | **-8, +2** |

**Table 13.1 - example errors in volumetric flow measurement using IWMB and PIWMB**

reduced by 4%, and the spectrum as a whole could be thought of as being reduced in frequency by approximately this amount. So IWMB would incur an error of approximately −4%, offsetting in some part the large +29% error associated with the beamwidth itself. If a beam of negligible width was misaligned to the same extent, then according to (6.4) PIWMF incurs an error of −4%. This figure will be similar for the example beam. If the correct radius is used these percentages will be the same when considering volume flow, and they will be smaller for smaller beam displacements. If however the radius is estimated from a related B-mode image, and the plane of this image is also misaligned with the vessel axis to the same extent, then the radius estimated will tend to be the quantity $\sqrt{R^2 - y^2}$ indicated in fig.6.1. The cross-sectional area calculated will then be equal to $\left(1-\left(y/R\right)^2\right)$ multiplied by the correct value. The resulting percentage error in area is $-100\left(y/R\right)^2\%$. For small displacements this will add to the percentage error in the mean velocity estimate. With a parabolic profile the flow errors using either IWMF or PIWMF are thus doubled.

*Spectral broadening - chapter 7*

As shown in chapter 7, if our transducer is used with a Doppler angle of 50° then the broadening function is approximately triangular with $a \approx 0.54$. If the broadening is such that $b = 1$ then IWMF is unaffected and fig.7.5 shows that PIWMF with this value of $a$ is reduced by 2%. Again this percentage is not dependent on the mean velocity so that this percentage is appropriate to volume flow also.

*White noise - chapter 8*

If there is white noise throughout the frequency range then for IWMF the relevant curve is curve B of fig.8.3, as the parabolic profile and the near 'thin' beam lead to a spectrum approximated by $t = 0.5$. If the frequency range is chosen so that at peak systole the signal occupies 90% of the available bins, i.e. where $m \approx 0.9$, then fig.13.1 suggests that at diastole the signal occupies approximately 20% of the frequency range, i.e. $m \approx 0.2$. So at systole the error is small and negative, and at diastole the error is large and positive. The waveform of fig.13.1 can be roughly thought of as comprising a 'systolic' segment contributing half of the total flow and occupying the first third of the waveform, and a 'diastolic' segment contributing the other half of the flow in the remaining two thirds of the cycle. So the error due to noise in the first third of the cycle can be ignored, and, from fig.8.3 with $m \approx 0.2$, the error incurred in the remainder is approximately $+2.5\ \text{snr}^{-1} \times 100\%$. This represents an average error of $+1.25\ \text{snr}^{-1} \times 100\%$ over the two 'halves' of the flow so that for a signal to noise ratio of 50 this corresponds to an error in volumetric flow using IWMF of +2.5%.

Curve E of fig.8.3 shows that the error in PIWMF at any point in the cycle is in the range of $-0.5\ \text{snr}^{-1} \times 100\%$ to $+0.5\ \text{snr}^{-1} \times 100\%$. So, considering the whole cycle, the overall error must also be within this range. For a signal to noise ratio of 50 this corresponds to an error in volumetric flow of less than ±1% which is small. Furthermore the instantaneous errors will partially cancel over the whole cycle so even this small figure overestimates the error magnitude.

*High-pass filter - chapter 9*

Equation (9.5b) shows that the ideal high-pass filter introduces a fixed absolute error to IWMF, which is equal to $+f_b/3$ when $t = 0.5$, as is approximately so for a parabolic profile and a near 'thin' beam. This results in an absolute error in instantaneous mean velocity which remains the same throughout the cycle, so that the absolute error in the mean velocity averaged over the whole cycle is also the same. The percentage error in volumetric flow is then given by

$$+\frac{f_b}{3f_{\bar{v}_{ave}}} \times 100\%$$

where $f_{\bar{v}_{ave}}$ is the frequency corresponding to this spatially and temporally averaged velocity, $\bar{v}_{ave}$. In practice a filter with a quoted (corner) frequency of 200 Hz might be used, so we take $f_b \approx 200$ Hz. In the example of fig.13.1 $\bar{v}_{ave} \approx 0.34\ \text{m s}^{-1}$ so that with a transmit frequency of 6 MHz, a Doppler angle of 50°, and a speed of sound in blood of $1580\ \text{m s}^{-1}$, the corresponding frequency from the Doppler equation is $f_{\bar{v}_{ave}} \approx 1600$ Hz and the error in volumetric flow incurred using IWMF is therefore approximately +5%.

Equation (9.7b) shows that the ideal high-pass filter introduces a fixed absolute error to PIWMF, which is equal to $+f_b/2$ when $t = 0.5$. Analogously to the case of IWMF, the percentage error in volumetric flow is then given by

$$+\frac{f_b}{2f_{\bar{v}_{ave}}} \times 100\%$$

and so for the example parameters is +7%.

Application of (9.8) to the data above suggests that this figure of $f_b \approx 200$ Hz is sufficient to remove wall motions with velocities less than approximately $3\ \text{cm s}^{-1}$.

*Statistical fluctuation - chapter 10*

The amount of blood passing through a cross section of a vessel of radius $R$ in a small time $\Delta\tau$ can be given by

$$\pi R^2 \bar{v} \Delta\tau$$

where $\bar{v}$ is the spatial mean velocity appropriate throughout that small time interval. The average rate of flow of blood by volume, $Q_{\text{ave}}$ , throughout a cardiac cycle made up of $N$ contiguous time intervals each of duration $\Delta\tau$ can therefore be given by

$$Q_{\text{ave}} = \frac{1}{N\Delta\tau} \sum_{j=1}^{N} \pi R_j^2 \bar{v}_j \Delta\tau$$

where the $j$ subscript indices indicate variables appropriate to the $j$'th such time interval. Assuming a constant radius $R$ we can then write

$$Q_{\text{ave}} = \frac{\pi R^2}{N} \sum_{j=1}^{N} \bar{v}_j$$

So if the spatial mean velocities $\bar{v}_j$ are estimated using IWMB, and the estimates are denoted by $\bar{v}_j'(\bar{B})$ , then the resulting estimate of volumetric flow rate, $Q'_{\text{ave}}(\bar{B})$, has a variance given by

$$\text{var}\, Q'_{\text{ave}}(\bar{B}) = \frac{\pi^2 R^4}{N^2} \sum_{j=1}^{N} \text{var}\, \bar{v}_j'(\bar{B})$$

if the $\bar{v}_j'(\bar{B})$ estimates are independent. From (10.19) we have the working relationship that an estimate $\bar{v}_j'(\bar{B})$ has a variance that can be given by

$$\text{var}\, \bar{v}_j'(\bar{B}) \approx \frac{c}{12 F \Delta\tau \cos\theta} \cdot \bar{v}_j$$

Defining the period of the cycle to be $T \equiv N\Delta\tau$ , it follows simply that

$$\text{var}\, Q'_{\text{ave}}(\bar{B}) \approx \frac{c\pi^2 R^4}{12 F \cos\theta\, T} \cdot \left( \frac{1}{N} \sum_{j=1}^{N} \bar{v}_j \right)$$

The bracketed term in the limit of large $N$ is the true spatial and temporal mean velocity throughout the cycle, $\overline{v}_{ave}$. So

$$\text{var}\, Q'_{ave}\left(\overline{B}\right) \approx \frac{c\,\pi^2 R^4}{12 F \cos\theta\, T} \cdot \overline{v}_{ave}$$

Taking $Q'_{ave}\left(\overline{B}\right)$ to be unbiased, as from chapter 10 the $\overline{v}'_j\left(\overline{B}\right)$ values are regarded as unbiased, and recognising that the true flow rate is given by $Q_{ave} = \pi R^2 \overline{v}_{ave}$ the relative uncertainty of the estimate of flow, $\text{r.u.}_{Q'_{ave}\left(\overline{B}\right)}$, is expressed by

$$\text{r.u.}_{Q'_{ave}\left(\overline{B}\right)} \equiv \frac{\sqrt{\text{var}\, Q'_{ave}\left(\overline{B}\right)}}{Q_{ave}} \approx \sqrt{\frac{c}{12 F \cos\theta\, T}} \cdot \sqrt{\frac{1}{\overline{v}_{ave}}}$$

So, for a given transducer, geometry of insonation and velocity scale, the limiting factor on the precision of the estimate of flow rate is the duration of the cardiac cycle, $T$. This is an improvement on the situation of chapter 10 where the precision of an individual estimate of 'instantaneous' spatial mean velocity was limited by the duration of the data segment, $\Delta\tau$. This precision could further be improved by measuring over more than one cycle. Putting $F = 6$ MHz, $c = 1580$ ms$^{-1}$, $\theta = 50°$, $T = 1$ s, and, as in the example of fig.13.1, $\overline{v}_{ave} \approx 0.34$ m s$^{-1}$ gives $\text{r.u.}_{Q'_{ave}\left(\overline{B}\right)} \approx 0.010 \equiv 1.0\%$. Allowing two standard deviations of departure from the mean, an appropriate measure of the random error in the estimate of flow rate in this example is therefore ±2%.

An analogous derivation using (10.20) gives the relative uncertainty in the estimate of flow rate using PIWMB, $Q'_{ave}\left(\hat{B}\right)$, as

$$\text{r.u.}_{Q'_{ave}\left(\hat{B}\right)} \equiv \frac{\sqrt{\text{var}\, Q'_{ave}\left(\hat{B}\right)}}{Q_{ave}} \approx \sqrt{\frac{2c}{15 F \cos\theta\, T}} \cdot \sqrt{\frac{1}{\overline{v}_{ave}}}$$

which with the parameter values used above gives $\text{r.u.}_{Q'_{ave}\left(\hat{B}\right)} \approx 0.013 \equiv 1.3\%$. The appropriate uncertainty in the estimate of flow rate is therefore approximately ±2½%.

*Chapter 12 - non-monotonic flow at other sites*

The assumption that the example carotid waveform of fig.13.1 has at all times a parabolic profile precludes the possibility of the profile being non-monotonic, so there is no associated error in volumetric flow. If the beam is 'wide' IWMF is not affected by non-monotonicity in the profile anyway. Even with this example thinner beam no extra error is incurred with IWMF if the profile throughout the cycle is sometimes non-monotonic because, as stated in chapter 12, the relevant velocity profile is the time-averaged profile, which is thought to be monotonic and parabolic. A guide to the error with PIWMF with this near 'thin' beam in the actual case of pulsatile waveforms is given by the results of chapter 12, e.g. +2% and -8% in the common and superficial femoral arteries respectively.

*Discussion*

The errors of table 13.1 are rough guides and can only be compared accordingly. The dominant error in the use of IWMB is clearly that caused by the wrong assumption of the beamwidth. However, with knowledge of the true beamwidth and vessel radius, this may be compensated for if, as in the example, the average velocity profile throughout the cycle can be assumed to have a particular axi-symmetric form. PIWMB is subject to more sources of error, and none is dominant. The negative errors due to the beam not being ideal, i.e. the errors of chapters 5, 6 and 7, cancel in part with the necessarily positive error due to filtering. Some knowledge of the physical parameters of the system might reasonably be held, and so some errors could be predicted and therefore in part compensated for. This is of course true for IWMB also. In particular the beam intensity profile, the spectral broadening characteristics, and the filter characteristics may all be known. It may also be appropriate to assume a certain noise level. Even if these parameters are not known they will remain constant from one examination to the next so that these errors need not affect the results of a flow comparison before and after administration of a drug, for example. The remaining sources of error might therefore be considered more troublesome, and so are highlighted in bold script in table 13.1. These are the uncertainties of the angle measurement and the positioning of the beam, the random nature of the Doppler signal and a departure from ideal behaviour of the velocity profile.

## Error comparison with beams of ideal widths

Another comparison might be made if the estimators are used with beams of the appropriate widths. In this case there are some differences to the errors tabulated in table 13.1. If the beam insonates uniformly, the error in IWMB corresponding to chapter 5 is zero, and if the beam is broad enough the error due to it being displaced is also zero. However the relevant curve on fig.8.3 for IWMF is now curve A with an increase in the error due to the noise to around +4%. If the beam has a negligible beamwidth then the error in PIWMB corresponding to chapter 5 is zero.

## Concluding remarks

The statistic PIWMB has been presented for use in the calculation of spatial mean blood velocity, and hence for measurement of volumetric flow, when the ultrasound beam is better described as being of negligible width compared to the vessel radius than as insonating the vessel uniformly. The validity of this statistic relies upon assumptions about the velocity profile which are invalid near to vessel bifurcations and at various stages of the cardiac cycle in highly pulsatile flow. Nevertheless if the beam is better modelled as 'thin' than as 'wide' then using PIWMB avoids the large error associated with IWMB, the statistic valid with uniform insonation. PIWMB suffers in the same way as IWMB from the well-known problems of uncertainty in the measurement of the Doppler angle, and the necessary high-pass filtering of the Doppler signal. In addition, PIWMB when used with a narrow beam is susceptible to sources of error not affecting IWMB when used with a broad beam, e.g. departures from the ideal profile forms, misalignment of the beam and geometrical spectral broadening. The suggestion therefore is that mean velocity and volumetric flow estimation are better carried out with a broad beam than with a narrow beam. However in duplex systems that use the same crystals for transmission of both the imaging and Doppler beams, the beam is not thought to be broad enough to uniformly insonate sizeable blood vessels and might be better modelled as 'thin'.

## Notation for this chapter

| | |
|---|---|
| $a,b$ | parameters defining the idealised broadening functions as in chapter 7 |
| $f_b$ | cut-off frequency in ideal high-pass (brick-wall) filter as in chapter 9 |
| $m$ | ratio of maximum signal frequency to maximum noise frequency as in chapter 8 |
| $N$ | number of time intervals in the cardiac cycle |
| $Q_{\text{ave}}$ | average rate of volumetric flow in the cardiac cycle |
| $Q'_{\text{ave}}(\overline{B}), Q'_{\text{ave}}(\hat{B})$ | estimates of the average rate of volumetric flow in a cardiac cycle made using IWMB and PIWMB |
| snr | signal to noise ratio as in chapter 8 |
| $T$ | period of the cardiac cycle |
| $\overline{v}_{\text{ave}}$ | mean velocity averaged both spatially and temporally |
| $\overline{v}_j$ | spatial mean velocity in the $j$'th time interval |
| $\overline{v}'_j(\overline{B})$ | estimate of the spatial mean velocity in the $j$'th time interval made using IWMB |
| $\sigma$ | standard deviation of the intensity response for a Gaussian shaped Doppler beam as in chapter 5 |
| $\Delta\tau$ | duration of each time interval |

# APPENDIX A - REAL-TIME DIAMETER AND FLOW MEASUREMENT

Prior to the detailed study of PIWMB the general intention of this project was to improve the accuracy of volumetric flow measurements by taking into account the changing cross-sectional area of the blood vessel. On the assumption of circularity of this cross section this is equivalent to evaluating the more correct equation

$$Q'_{ave} = \frac{\pi}{T} \int_{\tau}^{\tau+T} R'^2(\tau)\, \bar{v}'(\tau)\, d\tau \qquad \text{(A.1)}$$

instead of the commonly used equation

$$Q'_{ave} = \frac{\pi R''^2}{T} \int_{\tau}^{\tau+T} \bar{v}'(\tau) d\tau \qquad \text{(A.2)}$$

where $R''$ is the single representative estimate of the true changing radius $R(\tau)$ throughout the cycle. These equations have previously been given as (1.6b) and (1.7b). The approach taken was to modify the duplex method described in chapter 1 in order to find corresponding changing radius and mean velocity estimates, $R'(\tau)$ and $\bar{v}'(\tau)$, with particular emphasis being given to the measurement of the changing radius. This appendix therefore primarily describes the measurement of the changing radius, to produce an estimate $R'(\tau)$ appropriate in time to the estimate of mean velocity, $\bar{v}'(\tau)$. The body of the thesis has considered in some detail the measurement of the mean velocity.

## Flow estimation by simultaneous velocity and diameter measurement

As described in chapter 1 velocity estimation using the duplex method is achieved by manipulating the sample volume to be at the correct position and of the correct size, as indicated on the B-mode images, and then switching off the imaging mode to allow all the machine time to be devoted to velocity measurement. Typically a single estimate of the arterial radius, $R''$, is found from one or several frozen images, and so, with the mean velocity estimate $\bar{v}'(\tau)$, an estimate of volumetric flow is given by (A.2). This estimate is therefore in error to the extent that $R''^2$ is not representative of the instanteous true value $R(\tau)^2$ throughout the cycle.

It is suggested that, to overcome this problem, future estimates of volumetric flow may be performed by the pseudo-simultaneous measurement of vessel diameter and velocity, and their combination according to (A.1). The technique used would differ from the duplex

method described in chapter 1 in that, as well as the Doppler operation, the B-mode imaging would be 'continuous' in order to obtain instantaneous estimates of vessel diameter. The term 'pseudo-simultaneous' is used to indicate that, if time-sharing in the scanner is necessary to provide both dynamic imaging and Doppler signals, then 'corresponding' diameter and velocity data are not strictly measured simultaneously.

Assuming circularity, as is common, the problem of real-time flow measurement can then be broken down into three components, i.e. the measurement of continuous instantaneous spatial mean velocity, the measurement of the continuous instantantaneous internal diameter of the artery, and the accurate referencing in time of these two quantities. These have been attempted by processing the audio output of the scanner carrying the Doppler signal and the video output of the scanner carrying the image information, and combining the results. Without going into great detail some principles, problems and conclusions are stated in this appendix.

## Summary of system operation

The processing of the Doppler signal is performed in a digital signal processor purpose-built for Doppler signal analysis (Schlindwein et al. 1988) and the results sent to a personal computer (Research Machines Nimbus) which has an Intel 80186 microprocessor. The image information is transferred via a digital frame store designed for real-time image acquisition (Bush et al.) into the personal computer, where it is analysed to provide the diameter information. The time registration and combination of the velocity and diameter estimates are performed in the personal computer to make available the real-time estimates of volumetric flow.

## Measurement of spatial mean velocity

In this appendix the method of calculation of $\overline{v}'(\tau)$ is not relevant, that being the subject of the main body of this thesis. It is sufficient to say that, with the help of the Doppler equation (1.2), a real-time estimate of mean velocity throughout a vessel cross section can be made by processing the spectrum of the audio signal, which ideally is the uncorrupted Doppler signal. This real-time spectral analysis is performed on a segment of the Doppler signal, and enables a mean velocity estimate to be made which is representative of the interval over which the signal segment is acquired. In our system (Schlindwein et al. 1988) the spectral analysis was performed using a Fast Fourier Transform algorithm with a Hanning spectral window applied to segments of 256 data points sampled at either 1.28, 2.56, 5.12 or 10.24 kHz. By overlapping successive data segments the required amount, a new estimate of mean velocity was available 160 times every second.

## Measurement of arterial diameter

Previous studies of the diameter of the pulsating vessel have concentrated on the precise measurement not of absolute arterial diameter but of *changes* in diameter. Examples involve the measurement of the time delay before the wall echo is received by amplitude (Hokanson et al. 1970) and phase-lock (Hokanson et al. 1972) techniques, the analysis in a multi-gate pulsed Doppler system of the low-frequency Doppler signal reflected from the moving arterial walls (Hoeks et al. 1985), and the updating of the data window position at the lumen/vessel wall boundary by the tracking of the phase of the reflected radio-frequency (RF) wave (Hoeks et al. 1990). The approach described in this appendix has more similarities to the work of Wilson et al. (1990), who 'averaged' and smoothed the A-lines through the region of interest in the image and used edge detection by differentiation to locate and track the vessel boundary and orientation, at a rate of 4 images per second.

The temporal and spatial resolution of a system based on the processing of B-mode images, such as the system described in this appendix, are poorer than in other systems due to the limited frame update rate, the discarding of the RF echo information in envelope detection, and other processing of the information making up the image.

Estimation of an absolute change in diameter, $\Delta D$, requires no knowledge of the true diameter, whereas estimation of the relative change of diameter $\Delta D/D$, given that the maximum changes are of the order of 10%, requires a first approximation to the diameter only. Determination of the diameter itself is a different question. Not only must the relevant echoes somehow be tracked throughout the cycle, but the echoes chosen must be identifiable in terms of the structure of the vessel wall. For flow studies the statistic of interest is the lumen diameter, which is the internal diameter of the blood vessel. This is the boundary between the lumen and the intimal layer of the vessel wall. If the vessel is insonated from near to the perpendicular then this boundary may appear as a line on the B-mode image distinct from, and less bright than, the line representing the boundary between the media and adventitia of the vessel wall. The identification of these lines as representing these boundaries is due to Pignoli et al. (1986), who correlated the distance between these lines with a histologically determined thickness of the intima and neighbouring media. These lines are clearly visible in the distal (i.e. lower) wall on fig.A.1, where the reproduction fails to show that the shallower echo is duller than the main echo. The line structure of the proximal wall in the image is less well pronounced, as is typical. Measurement of diameter therefore consists fundamentally of measuring the distance across the lumen between the two inner lines.

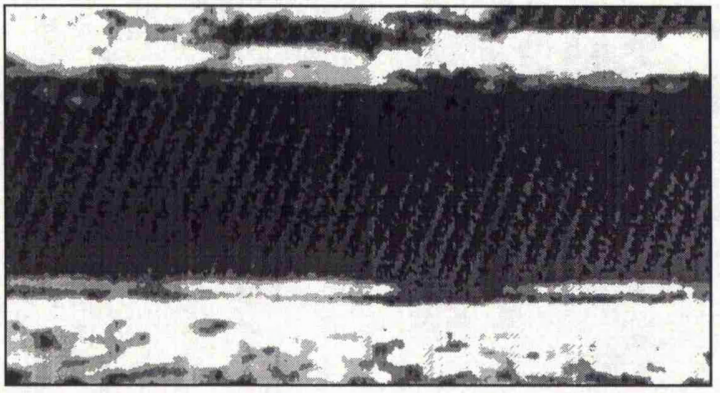

**Fig.A.1 - an example image of an arterial segment showing the distinct lumen/intima and media/adventitia boundaries sometimes observable in high resolution systems**

*Image processing*

The fact that the boundary of interest provides a significant echo and is adjacent to the lowly echogenic blood is useful for diameter measurement by B-mode image processing. With an image of an artery orientated substantially across the screen the distal lumen/intima boundary can be flagged by locating the depth at which the echo level begins to exceed the very low level of echo from the blood. It is therefore not necessary for the lumen/intima and media/adventitia boundaries to be resolved. The proximal lumen/intima boundary may be flagged in the same way by starting in the lumen and processing up the image. A quantitative measure of lumen diameter can be made by calibrating the image scales and recognising that, due to the finite duration of the echo pulse, the true diameter exceeds the distance measured between the two flagged depths by approximately the extent in the vertical direction of the point spread function. This correction to the raw distance is essentially the same as that applied by Li et al. (1993) in their study of the accuracy of internal tube diameter measurements made using the on-screen calipers.

In practice image smoothing was applied in the direction of the artery axis by considering the mean of 7 adjacent pixels. The shape of this 'bar' of 7 pixels was such that it conformed in angle to the orientation of the artery, calculated from a set of images acquired before the real-time process began. The walls of the artery were located by moving this bar either side of a starting point in the lumen, in a direction perpendicular to the artery axis, until the relevant thresholds were exceeded. The thresholds were calculated from a linear function which took into account estimates of the variability and (small) trend in the image brightness in the lumen to avoid falsely assigning the position of a wall to the lumen region. A schematic example of the brightness profile as a bar of 7 pixels traverses through an artery such as that shown in fig.A.1 is given in fig.A.2. The diameter is measured from the points where the profile exceeds the threshold line, which is calculated to not intersect the profile in the lumen region.

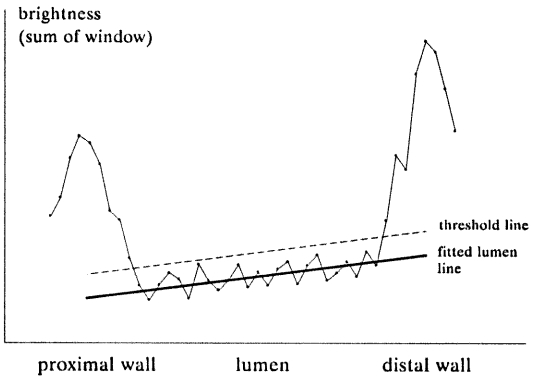


**Fig.A.2 - a schematic of an image brightness profile perpendicular to the artery axis**

As stated before, the distal lumen/intima boundary generally appears more pronounced than the proximal one. This is seen in fig.A.2, where at the distal wall this boundary is represented by the initial small maximum but at the proximal wall this boundary only appears as a change in the derivative of the slope of the main echo. There are several reasons why this is observed, one important one being that the echo pulse has a steeper leading edge than trailing edge so that the shallower edge of an image line is better defined.

*Image calibration*

The production of an absolute estimate of diameter requires calibration factors for the image extent in both screen dimensions. The fixed sampling rate of the digital frame store means that the image acquisition introduces an aspect ratio of approximately 4:3 to any redisplayed digital image. For diameter measurement accurate calibration is more important in the vertical dimension because the vessel is primarily orientated horizontally across the screen. Vertical calibration is achievable using a signal injection system which generates bright bands on the image separated by a distance corresponding to a known time interval. Even though the image is made up of a finite number of discrete rows, applying the quadratic interpolation process outlined in the '*Image resolution*' section below, and averaging over many frames enables a calibration factor to be found with an uncertainty that might be better than ±1%. A high proportion of this uncertainty is due to the uncertainty of the velocity of sound in blood. The velocity is dependent on the haematocrit which shows considerable variation among both males and females, and has different means for the genders. The calibration in the horizontal dimension can be achieved using test objects of thin wires separated by a known distance. This method of calibration is not generally as precise, but because the vessel is primarily orientated horizontally this is of limited importance.

## Time referencing

Having made a diameter measurement, the volumetric flow rate follows from (A.1) using the measurement of mean velocity appropriate to the time at which the image of the artery was created. So the temporal resolution of such a system for measuring volumetric flow is limited by the available image update rate when in time-sharing mode. With our current scanner a rate of 17 image frames per second (fps) is achievable. Even if this could be increased, unless the normal format of transfer of video information is superceded the maximum frame rate for our system running in real time is 25 fps, or 50 fps if the interleaving video lines are regarded as constituting a separate image.

In essence a lot of the problem of time referencing in our system could be put down to the presence of three asynchronous cycles needing to be accommodated, that is the image update rate of 17 fps (Hz), the video transfer rate of 25 fps (Hz) and the rate of acquisition of mean velocity information of 160 Hz.

*Discarding redundant frames*

A consequence of the images being created at a rate lower than the video transfer rate of 25 fps is that the data in the region of interest of the frame may not have been updated between the transfer of successive images. The relevant data in one digitised frame might therefore be a copy of the data of the preceding frame. With a refresh rate of 17 fps this happens approximately every third digitised frame. To achieve a linear time scale these copied frames must be discarded. This can be achieved by the digital subtraction of the region of interest of one frame from that of the previous frame. Relying upon the presence of noise or moving 'speckle' in successive created images, and the motion of stronger scatterers such as the pulsating vessel walls, the region of interest is rejected as being a copy of the previous one if the results of the pixel-by-pixel subtraction show too little variance.

*Time delay adjustments*

With the above image generation rate of 17 fps, video information displayed at any one time may be approximately 60 ms old, depending on the phase relationship between the asynchronous creation and transfer of fresh video data. The accurate synchronization of the diameter and velocity information needs to take continual account of this and any other 'delays' such as the time difference between the transfer of video data at the top and bottom of the image, the time required to acquire the digital images and the duration of the data segment from which the mean velocity estimate is made. Furthermore there may be hidden delays in the time registration of the video and audio outputs of a commercial machine as synchronization to the degree of accuracy desired may not have been a design consideration.

*Pseudo-simultaneity and Doppler signal synthesis*

It is thought that, by considering factors such as those in the preceding paragraphs, the problem of relative time registration of the audio and video information has been solved to approximately 10 ms. However even if the video and audio signals are referenced well in time an error exists as the B-mode and Doppler operation are not strictly simultaneous. Both modes of insonation use the same linear or phased array transducer and so the available time is shared. In practice the Doppler signal corresponding to the time spent during creation of an image might be synthesised by extra/interpolation from adjacent data. A trade-off exists between the two modes of insonation so that if the number of images created per second is maximised, such extrapolation of the Doppler signal is required more often and overall quality is reduced. It is ironic that, after solving the difficult problem of synchronization, the section of the audio signal corresponding to the time a diameter measurement is made is found to be extra/interpolated, and hence to be an approximation. Furthermore the 'true' Doppler signal corresponding to time when the images were not being created is discarded. A more sensible approach might be to use a 'true' portion of the Doppler signal and interpolate between diameter measurements, or accept a small error in time registration.

## Factors affecting image and audio signal quality

*Beam width*

The use of electronic array transducers has considerably improved the rate at which successive images are created. The pulsed Doppler beam for the velocity measurement can also be generated from the same array of transducers. However there are at least two trades-off between image and Doppler signal quality when insonating blood vessels. Firstly the optimum B-mode beam is 'thin', with the dimension in question being the dimension of the width of the transducer. In this way the vessel walls are clearly defined in the image and not smeared. This is illustrated in fig.A.3a. However the ideal Doppler beam is regarded as being 'wide', as in fig.A.3b, so that each scatterer in the cross section contributes to the Doppler signal equally. This then is a problem if the same array is used for both purposes as there is generally no control over beam focusing in this dimension. The determination of mean blood velocity when the beam is 'thin', thus providing a solution to this problem, has been the main subject of this thesis.

*Beam angles*

The quality of the images of the vessel walls deteriorates as the transducer is tilted on the skin surface because the vessel wall is no longer insonated perpendicularly and specular reflection is not observed by the transducer. (In this case the two lines of Pignoli visible in fig.A.1 generally become indistinct, although this in itself is not a problem.) However this

tilting is necessary with our linear array to produce an acceptable Doppler angle for the quantitative measurement of blood velocity. The ability to steer the beam electronically is not sufficient in itself to produce a low enough angle. This would not be a problem it there were separate imaging and Doppler transducers as might be found with a mechanical sector scanner. Our sector scanner however has a duplex image update rate of only 4 fps, and the mechanical rocking of the crystal producing the image causes interference in the Doppler signal.

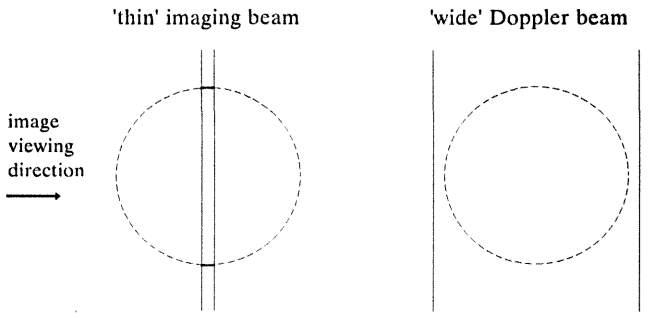


**Fig.A.3a - a 'thin' imaging beam is optimal to avoid smearing of the artery walls in the image**

**Fig.A.3b - a 'wide' Doppler beam is optimal to insonate equally the red blood cells passing through any point in the cross section**

*Doppler cursors*

Diameter measurement in the cross section of the vessel intersected by the Doppler beam is complicated by the overlaying on the image of the cursors defining the Doppler beam direction and the sample volume extent. If these cursors cannot be removed, a solution is to measure the diameter through a point on the image a short distance from where the mean velocity is measured, and assume that the measured diameter is accurate.

*Image resolution*

It might be thought that the image resolution is limited by the pixel scale. Typically the pixel-to-pixel distance in the depth dimension might be ~0.2 mm. For example, in any one column of an image, the depth where the echo amplitude exceeds a certain threshold might

be taken to be the shallowest row where the pixel brightness exceeds the required value. However linear interpolation from the pixel value in the row above can simply be used to determine more accurately the depth at which the threshold is exceeded, as in fig.A.4a. This depth will be represented by a fractional number of rows, $x$. Such interpolation effectively improves this depth 'resolution'. The algorithm for the location of the vessel walls used a similar technique.

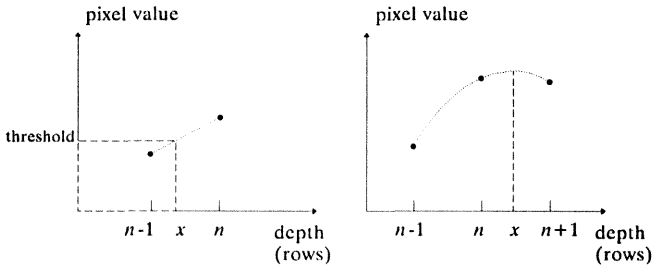


**Fig.A.4a - determination of depth, $x$, where a threshold is exceeded by linear interpolation back from the first row where a higher value is observed, $n$.**

**Fig.A.4b - quadratic interpolation to determine the depth of maximum response, $x$, from the highest observed value (i.e. at row $n$) and those above and below**

Alternatively it might be desirable to locate the depth of maximum echo amplitude in a column. An obvious estimate of this depth is simply the row co-ordinate of the pixel with the greatest value. However an improvement can be made on this by considering the values of the pixels immediately above and below this brightest pixel. A quadratic function can easily be fitted to the three points, and the position of the turning point found. This gives a fractional number of rows which is a more accurate estimate of the depth of maximum response. This is illustrated in fig.A.4b. This quadratic interpolation method was tested by following the path of (the brightest point of) an object boundary as the object sank smoothly in a water bath. The motion of the object was measured to be much smoother when the interpolation was applied than when the simple brightest row method was employed. So, as with the linear interpolation above, this quadratic interpolation improves the depth 'resolution'. It can easily be applied to locate the depth of maximum *rate of change* of brightness, by first taking the row-to-row differences.

*Image interpretation*

The simplest, and perhaps best, image processing is performed without assuming that the pixel values lie on a scale with physical meaning. To suggest, for example, that the digitised brightness scale is linear with the echo amplitude implies that the enveloping of the echo signals is understood, that the transfer function chosen for the generation of the video signal is linear (whereas the default setting may be of a sigmoidal form), and that the A/D conversion in the image transfer is linear.

*Audio response*

The audio output of the scanner is ideally a true representation of the Doppler signal. At least two important factors affect the fidelity of the audio output with respect to the displayed 'sonogram' summarizing the Doppler signal. The sonogram may have the ability to be baseline adjusted, e.g. positive frequencies above the Nyquist limit can be correctly displayed on the sonogram by lowering the baseline. The sonogram frequency range is therefore equal to the value of the sampling frequency. However frequencies above the Nyquist limit do not appear correctly in the audio signal and are aliased. So, for example, high frequencies at systole may be seen on the sonogram using the baseline adjustment, but may not be heard in the audio signal. The appropriate technique is therefore to allow no baseline adjustment in the sonogram, and instead increase the Pulse Repetition Frequency if the maximum velocity is seen to correspond to frequencies above the Nyquist limit. Secondly the audio output must not have been internally filtered. The use of a variable frequency, fixed intensity, signal injection source allowed the audio-output transfer function to be examined. The extent to which this transfer function departed from uniformity in our scanner was alarming. Clearly errors in mean velocity measurement will result if this audio signal is assumed to be the true Doppler signal.

## Summary

On-line and real-time volumetric flow measurements may well be performed in future by simultaneous B-mode image and Doppler signal processing. A real-time system based around a personal computer with an 80186 microprocessor, digital signal processor and digital frame store has been developed with some success in principle. However a robust system would require more processing power and better quality image data, as provided for example if the artery can be orientated horizontally on the image. Such orientation would require greater flexibility in the steering of the Doppler beam. A major limitation is the rate at which fresh B-mode images are created when operating in duplex mode, and/or

transferred to the computer. With our scanner images are available at a maximum of only 17 frames per second, and with our frame store images are transferred at 25 frames per second.

An intermediate step or approximation to this approach may be to treat the diameter measurement and mean velocity measurement problems one after the other. For example the changing diameter throughout an average cardiac cycle could be found with a horizontally orientated artery before the duplex operation was commenced. This would provide greater accuracy and higher temporal resolution in the diameter measurements. Subsequently the probe is tilted, the imaging rate is minimised subject to the need to monitor any global motion of the artery, and the Doppler operation is performed. The velocity data and diameter data could be combined by matching points in the average cardiac cycles, according to (A.1). Alternatively a single time-averaged diameter estimate might be calculated for use in (A.2), in accordance with the small error reported by Eriksen (1992) and described in chapter 1.

## Notation for this appendix

| | |
|---|---|
| $Q_{ave}$ , $Q'_{ave}$ | average volumetric flow rate in one cardiac cycle, and its estimate |
| $R(\tau), R'(\tau)$ | instantaneous internal radius of blood vessel, and its estimate |
| $R''$ | a single estimate of internal radius |
| $T$ | period of cardiac cycle |
| $\bar{v}'(\tau)$ | estimate of instantaneous spatial mean velocity |

# APPENDIX B - A MODEL OF ASYMMETRY IN THE VELOCITY PROFILE

When the beam is 'thin' the estimator PIWMF has been shown to be accurate for monotonic axi-symmetric velocity profiles. The family of monotonic axi-symmetric velocity profiles given by (3.1) has been used in the context of quantifying the errors from various individual sources. This profile equation is restated here.

$$v = v_m\left(1-\left(\frac{r}{R}\right)^n\right) \qquad \text{(B.1)}$$

Errors in PIWMF will in general also arise if the velocity profile is asymmetric. This appendix describes the effect on the accuracy of PIWMF if the profile has an asymmetric form related to the form of (B.1). This asymmetric profile form was briefly introduced in chapter 12.

## Model of asymmetry

If the point, E, of maximum velocity, $v_m$, is a distance, $e$, from the centre of the vessel, C, as in fig.B.1, an asymmetric form of (B.1) is

$$v = v_m\left(1-\left(\frac{s}{S}\right)^n\right) \qquad \text{(B.2)}$$

where $v$ is the velocity a distance $s$ from E, and $S$ is the distance from E to the vessel wall along the same line. Fig.B.1 and equation (B.2) can be seen to be the same as fig.12.1 and equation (12.1).

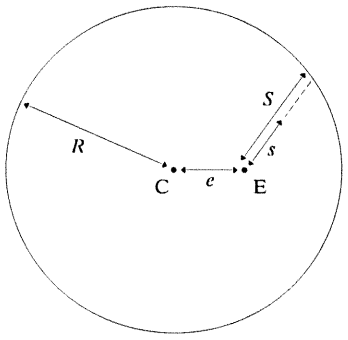


**Fig.B.1 - geometry for an asymmetric velocity profile**

Clearly $S$ varies with the position around the vessel circumference, and with the displacement $e$, so that the profile is not axi-symmetric, but the profile is still monotonic, and is symmetric about the line joining C and E. The form of (B.2) is defined by $n$ and the fraction $e/R$, and the scale by $v_m$. For $n>1$ this asymmetric profile surface is continuous and has a derivative continuous at every point in the cross section. The equation describing the surface in Cartesian coordinates is derived later. An example of the profile surface with $e=0.4R$ and $n=2$ is shown in fig.B.2a and the corresponding velocity contour plot is given in fig.B.2b. The contours of velocity are seen to be non-concentric circles as discussed below.

It follows from (B.2) that the profile along any chord passing through the maximal point is piecewise and consists of two 'halves', each of the form defined by the single value of $n$, but with different length scales. It is debatable how well this approximates profiles observed in practice. While the profile along any one line from E to the circumference might be definable by a single value of $n$ it is presumptuous to assume that the same value of $n$ describes the profile along every such line, in particular the line in the opposite direction.

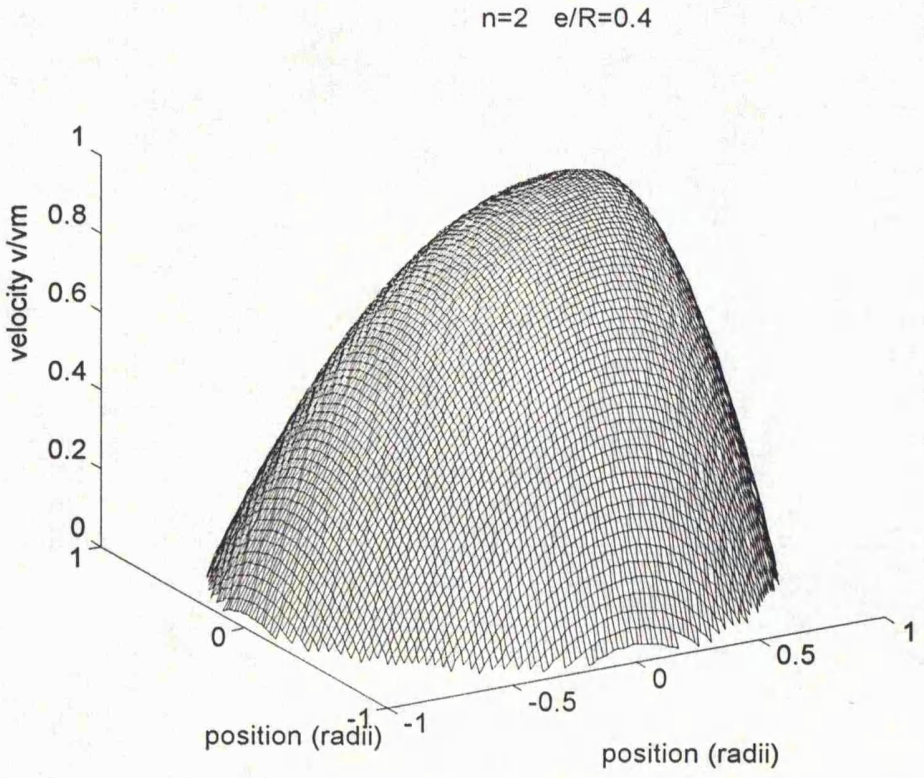


**Fig.B.2a - an asymmetric profile**

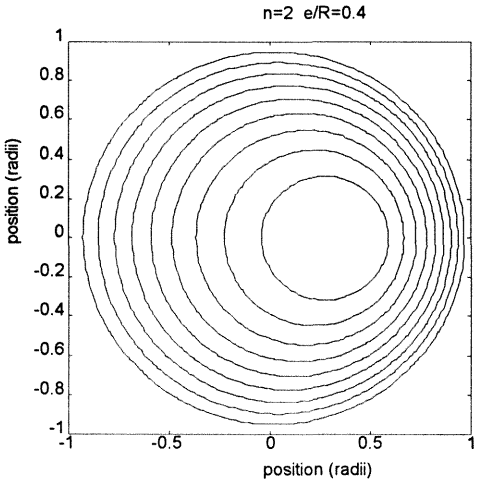


**Fig.B.2b - the corresponding velocity contour plot**

## Mean velocity with the asymmetric profile

The first step in an analysis of mean velocity is to derive the equation of the velocity contour defined by a fixed value of the ratio $\beta \equiv s/S$. The velocity is then given by $v = v_m(1-\beta^n)$. The locus of the contour must be an enlargement of the circle of radius $R$ about the fixed point E, with an enlargement factor of $\beta$. The contour is therefore a circle of radius $\beta R$, which obviously has an area independent of $e$. This is shown in fig.B.3 where in this example $\beta \approx 0.7$.

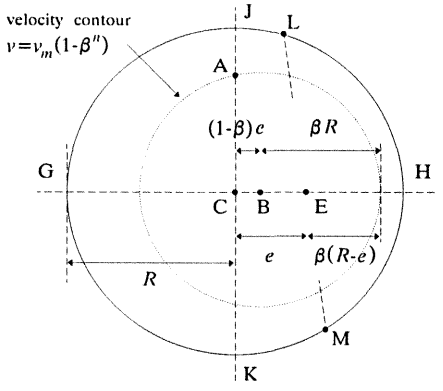


**Fig.B.3 - a circular velocity contour in the vessel cross section**

By symmetry the centre, B, of this contour circle is on the line joining C and E and can be found from known distances, i.e.

$$|\mathrm{CB}| = e + \beta(R-e) - \beta R = (1-\beta)e \qquad \textbf{(B.3)}$$

Velocity contours cannot intersect each other so that the area between the velocity contours defined by two different values of $\beta$ is the difference in the areas of the corresponding circles, even though the circles are not concentric. It follows that the proportion of the cross section containing scatterers with velocities between these contour values is also independent of $e$, and so must be equal to the proportion found when $e = 0$, i.e. when the profile is axi-symmetric as in (B.1). This result means that any amount of this form of asymmetry does not alter the mean blood velocity through the cross section, provided the maximum velocity $v_m$ stays the same. The mean velocity for the profile of (B.1) has been found to be given by equation (3.2) and is

$$\overline{v} = v_m \cdot \frac{n}{n+2} \qquad \textbf{(B.4)}$$

and this is therefore also the mean velocity for any profile given by (B.2). This result has been previously stated in chapter 12.

## General surface equation

The equation in Cartesian coordinates of the general asymmetric profile, defined by $e/R$, $n$, and $v_m$, can be found with the help of fig.B.4.

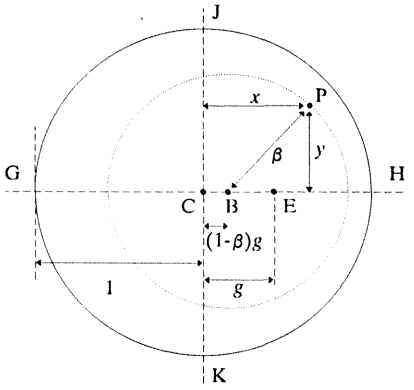


**Fig.B.4 - the geometry for the derivation of the surface equation in Cartesian co-ordinates**

This shows the cross section scaled in units of radii, so that the dimensionless displacements $x$ and $y$ are bound between -1 and 1. The asymmetry is defined by the dimensionless parameter $g \equiv e/R$, which is between 0 and 1. The points C, B and E have the same meaning as above. The velocity at a general point P defined by $x$ and $y$ is calculated by finding $\beta$ which is $|\mathrm{PB}|$. This is achieved by applying the 'cosine' rule to the lengths of the sides of the triangle PCB and the angle PCB, which states that

$$\beta^2 = \left(\sqrt{x^2+y^2}\right)^2 + (1-\beta)^2 g^2 - 2\sqrt{x^2+y^2}\cdot(1-\beta)g\cdot\cos(\angle \mathrm{PCB})$$

but this cosine is

$$\cos(\angle \mathrm{PCB}) = \frac{x}{\sqrt{x^2+y^2}}$$

and therefore

$$\beta^2 = x^2 + y^2 + (1-\beta)^2 g^2 - 2gx(1-\beta)$$

which becomes the quadratic equation

$$\beta^2(1-g^2) + \beta(2g)(g-x) + \left(-y^2 - (g-x)^2\right) = 0. \qquad \text{(B.5)}$$

Solving this, for $g \neq 1$, gives

$$\beta = \frac{g(x-g) \pm \sqrt{(x-g)^2 + y^2(1-g^2)}}{1-g^2}.$$

As $y^2(1-g^2)$ is non-negative the square root quantity must be not less than $|x-g|$ which is not less than $g(x-g)$ as $0 \le g \le 1$. Therefore only the positive square root gives a positive value of $\beta$. The velocity at the general point defined by $x$ and $y$ for the profile defined by $n$, $g$ and $v_m$ is $v = v_m(1-\beta^n)$, and is therefore

$$v = v_m\left[1 - \left(\frac{g(x-g) + \sqrt{(x-g)^2 + y^2(1-g^2)}}{1-g^2}\right)^n\right] \qquad \text{(B.6a)}$$

For $g = 1$ solving (B.5) gives

$$\beta = 1 - x + \frac{y^2}{2(1-x)}$$

so that for $g = 1$ the profile is

$$v = v_m\left[1-\left(1-x+\frac{y^2}{2(1-x)}\right)^n\right] \qquad \text{(B.6b)}$$

which must be the limiting form of (B.6a) as $g \to 1$. So, remembering that $x$, $y$ and $g$ are displacements normalised to the radius, the asymmetric profile equation expressed in Cartesian co-ordinates can be found from (B.6a) and (B.6b).

## Errors incurred by PIWMF

Refer again to fig.B.3 or fig.B.4. When the beam is 'thin', i.e. is of negligible width *and passes through the vessel centre* C, it is suggested that the highest value of PIWMF will be found when the beam is along the line GH and the lowest value when it is along JK. This might be intuitive but has been too difficult to prove.

*The maximum value of PIWMF*

An example profile along the diameter GH is shown in fig.B.5 where the values of the parameters are the same as in fig.B.2, i.e. $e = 0.4R$ and $n = 2$. The 'halves' of the profile

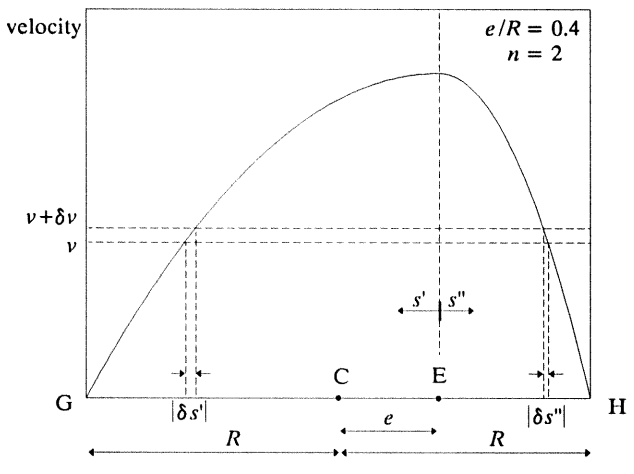


**Fig.B.5 - the asymmetric profile along the diameter GH**

have the same form, defined by $n$, but the half between G and E is extended over the length $R+e$ and is given by the equation

$$v = v_m\left(1-\left(\frac{s'}{R+e}\right)^n\right)$$

and the half between E and H is extends over $R-e$ and is given by the equation

$$v = v_m\left(1-\left(\frac{s''}{R-e}\right)^n\right)$$

where $s'$ and $s''$ are measured from E. From these equations it follows simply, using similar steps to that applied when manipulating (3.1) in chapter 3, that

$$\left|\frac{ds'}{dv}\right| = \frac{(R+e)}{nv_m}\cdot\left(1-\frac{v}{v_m}\right)^{\frac{1}{n}-1} \qquad \text{and} \qquad \left|\frac{ds''}{dv}\right| = \frac{(R-e)}{nv_m}\cdot\left(1-\frac{v}{v_m}\right)^{\frac{1}{n}-1}$$

If the sample volume with the 'thin' beam is this diameter GH then the fraction of the sample volume occupied by scatterers with velocities between $v$ and $v+\delta v$ where $\delta v$ is very small is

$$\begin{aligned}\left|\frac{\delta s'}{R}\right|+\left|\frac{\delta s''}{R}\right| &= \left|\frac{ds'}{dv}\right|\frac{\delta v}{R} + \left|\frac{ds''}{dv}\right|\frac{\delta v}{R} \\ &= \frac{2\delta v}{nv_m}\cdot\left(1-\frac{v}{v_m}\right)^{\frac{1}{n}-1}\end{aligned} \qquad \text{(B.7)}$$

which is independent of $e$, so the velocity distribution of scatterers in the sample volume is the same as it would be if $e$ was equal to zero, i.e. the same as it would be in the axi-symmetric case. Therefore the spectrum from insonation along GH is the same as that for the axi-symmetric profile with the same maximum velocity. This leads to the same value of PIWMF, which must be the correct value as it has been seen that the true mean velocity is not affected by $e$. Therefore, whatever the amount of asymmetry, the error incurred by PIWMF when the beam is along GH is zero. It is therefore suggested that the maximum observed value of PIWMF for a 'thin' beam is the correct value.

Furthermore (B.7) is independent of the length of the diameter $R$. A similar analysis can be performed for any chord passing through E, e.g. $\overline{\mathrm{LM}}$ on fig.B.3, to give the same equation, which is independent of $e$ and the length of the chord. This follows from redefining the directions $s'$ and $s''$ to be along the chord $\overline{\mathrm{LM}}$ and replacing $R+e$ and $R-e$ by $|\mathrm{LE}|$ and $|\mathrm{EM}|$ respectively. Therefore there is the interesting result, already given in chapter 12, that for any beam of negligible width passing through the point of maximum velocity E the estimator PIWMF incurs no error. It is suggested without proof that a beam that does not pass through E must give a lower PIWMF. A proof is available for beams not passing between C and E.

*The minimum value of PIWMF*

It follows that if PIWMF is in error it must be in the form of an underestimate. With reference to fig.B.3 or fig.B.4, the worst underestimate for a 'thin' beam would appear to be when the beam is along JK, as suggested earlier. Furthermore the profile is most peaked, and therefore the error at its greatest, when $n$ is at its minimum value. The symmetric profiles of (B.1) considered have often had $n \geq 2$. In the asymmetric case it is reasonable also to choose the minimum value of $n$ to be 2. Therefore the equation of the profile along this diameter leading to the minimum value of PIWMF is given by (B.6) with $x = 0$ and $n = 2$, and is

$$v(y) = v_m \left[ 1 - \left( \frac{\sqrt{g^2 + y^2(1-g^2)} - g^2}{1-g^2} \right)^2 \right] \tag{B.8}$$

So the mean velocity estimate corresponding to this minimum value of PIWMF, denoted by $\overline{v}'\left(\hat{f}_{\min}\right)$, would be the mean velocity if this monotonic profile along the diameter was axi-symmetric about C. This velocity could be found by integrating over the cross section and normalizing. Therefore if this axi-symmetric profile is $v(r)$

$$\overline{v}'\left(\hat{f}_{\min}\right) = \frac{\int_0^R 2\pi r \cdot v(r)\, dr}{\int_0^R 2\pi r\, dr} = \frac{\int_0^R 2r \cdot v(r)\, dr}{R^2}$$

Using $y \equiv r/R$ this becomes

$$\overline{v}'\left(\hat{f}_{\min}\right) = \int_0^1 2y \cdot v(y)\, dy \tag{B.9}$$

which in combination with (B.8) yields

$$\overline{v}'\left(\hat{f}_{\min}\right)=\frac{v_m}{2}\cdot\frac{1}{\left(1-g^2\right)^2}\cdot\left(1-\frac{7g^2}{3}+\frac{8g^4}{3(1+g)}\right) \tag{B.10}$$

The analysis leading to this result is given at the end of this appendix. As the true mean velocity with $n=2$ is $\overline{v}=v_m/2$ the percentage error is

$$\begin{aligned} E_{\overline{v}'\left(\hat{f}_{\min}\right)}(g) &\equiv \left(\frac{\overline{v}'\left(\hat{f}_{\min}\right)}{\overline{v}}-1\right)\times 100\% \\ &= \left[\frac{1}{\left(1-g^2\right)^2}\times\left(1-\frac{7g^2}{3}+\frac{8g^4}{3(1+g)}\right)-1\right]\times 100\% \end{aligned} \tag{B.11}$$

This error is tabulated for various values of $g$ in table B.1. The tabulated value when $g=1$ is the limiting value of (B.11). Alternatively it is evident that (B.6b), which is true for $g=1$, gives $\beta=\left(y^2+1\right)/2$ when $x=0$. Subsequent substitution of $v=v_m\left(1-\beta^2\right)$ into (B.9) leads to the tabulated value, which is exact.

| $g$ | 0 | 0.1 | 0.2 | 0.3 | 0.4 | 0.5 | 0.6 | 0.7 | 0.8 | 0.9 | 1.0 |
|---|---|---|---|---|---|---|---|---|---|---|---|
| $E_{\overline{v}'\left(\hat{f}_{\min}\right)}(g)$ | 0 | -0.3 | -1.2 | -2.6 | -4.3 | -6.2 | -8.2 | -10.3 | -12.4 | -14.6 | $-16\frac{2}{3}$ |

**Table B.1 - the largest negative percentage error in PIWMF for an asymmetric profile with $n\geq 2$ if the beam is 'thin'.**

*Summary error expression*

The error bounds for PIWMF and a 'thin' beam are then given by combining (B.11) with the suggested result that the error is never positive. This can be stated as

$$E_{\overline{v}'\left(\hat{f}_{\min}\right)}(g)\leq E_{\text{PIWMF}}\leq 0 \tag{B.12}$$

The greatest negative error $E_{\overline{v}'\left(\hat{f}_{\min}\right)}(g)$ can be found from (B.11) or read from table B.1.

## Summary

Based around the often used family of symmetric blood velocity profiles given by (B.1), a family of asymmetric profiles can be defined by (B.2) with reference to fig.B.1. The point of maximum velocity is displaced a distance $e$ from the centre of the vessel of radius $R$, and the form of the profile is defined by the parameters $n$ and $g \equiv e/R$ . If a beam which is of negligible width compared to the radius of the vessel passes through the point of maximum velocity the value of PIWMF is an accurate proportional measure of spatial mean blood velocity. It is suggested that evaluating PIWMF for any other position of such a beam would give an underestimate. In particular if the beam is 'thin', i.e. it also passes through the centre of the vessel, the error is bound according to (B.12) for profiles with $n \geq 2$.

## Notation for this appendix

| | |
|---|---|
| $e$ | displacement of the point of maximum velocity from the centre of vessel |
| $g$ | displacement of the point of maximum velocity from the centre of vessel as a fraction of the radius, i.e. $g \equiv e/R$. |
| $s$ | displacement from the point of maximum velocity |
| $s'$,$s''$ | displacements from the point of maximum velocity along the line through the centre of the vessel |
| $S$ | the distance from point of maximum velocity to the circumference |
| $x$ | horizontal displacement from the centre of the vessel as a fraction of the radius |
| $y$ | vertical displacement from the centre of the vessel as a fraction of the radius |
| $\beta$ | fraction of the distance from the point of maximum velocity to the circumference, i.e. $\beta = s/S$ |

## Derivation of equation (B.10)

We can rearrange (B.8) to give

$$(1-g^2)^2\frac{v(y)}{v_m} = (1-g^2)^2 - \left(\sqrt{g^2+y^2(1-g^2)} - g^2\right)^2$$

$$= \left(1-2g^2+g^4\right) - \left(g^2+y^2(1-g^2) - 2g^2\sqrt{g^2+y^2(1-g^2)} + g^4\right)$$

$$= (1-3g^2) - (1-g^2)y^2 + 2g^2\sqrt{g^2+y^2(1-g^2)}$$

Therefore (B.9) can be written as

$$2(1-g^2)^2\frac{\hat{v}'_{\min}}{v_m} = 4(1-3g^2)\int_0^1 y\,dy - 4(1-g^2)\int_0^1 y^3\,dy + 8g^2\int_0^1 y\sqrt{g^2+y^2(1-g^2)}\,dy$$

$$= 4(1-3g^2)\left[\frac{y^2}{2}\right]_0^1 - 4(1-g^2)\left[\frac{y^4}{4}\right]_0^1 + 8g^2\left[\frac{\sqrt{1-g^2}}{3}\left(y^2+\frac{g^2}{(1-g^2)}\right)^{\frac{3}{2}}\right]_0^1$$

$$= 2(1-3g^2) - (1-g^2) + \frac{8g^2\sqrt{1-g^2}}{3}\left[\left(\frac{1}{(1-g^2)}\right)^{\frac{3}{2}} - \left(\frac{g^2}{(1-g^2)}\right)^{\frac{3}{2}}\right]$$

$$= 1 - 5g^2 + \frac{8g^2\sqrt{1-g^2}}{3(1-g^2)^{\frac{3}{2}}}\left[1^{\frac{3}{2}} - (g^2)^{\frac{3}{2}}\right]$$

$$= 1 - 5g^2 + \frac{8g^2(1-g^3)}{3(1-g^2)}$$

$$= 1 - 5g^2 + \frac{8g^2(1-g)(1+g+g^2)}{3(1-g)(1+g)}$$

$$= 1 - 5g^2 + \frac{8g^2}{3}\cdot\left(1+\frac{g^2}{1+g}\right)$$

$$= 1 - \frac{7g^2}{3} + \frac{8g^4}{3(1+g)}$$

which leads directly to the desired result (B.10).

# APPENDIX C - DEPARTURE FROM A MONOTONIC PROFILE

A possible source of error in the mean velocity calculated from PIWMF is the presence of one or more sections in the velocity profile where the velocity is not monotonically increasing from the vessel wall to the centre. This appendix investigates the error incurred by PIWMF in cases where there is flow in only one direction but the profile is not monotonic.

## Generalised non-monotonic profile

An example of a velocity profile which is at all points positive, and is monotonic except in a known region, is shown in fig.C.1. The limits of this region are $r=b$ and $r=a$ where $r$ is measured from the vessel centre. (Between these limits there may be any number of sections of non-monotonicity so that within the corresponding dotted rectangle the velocity profile can take any form.)

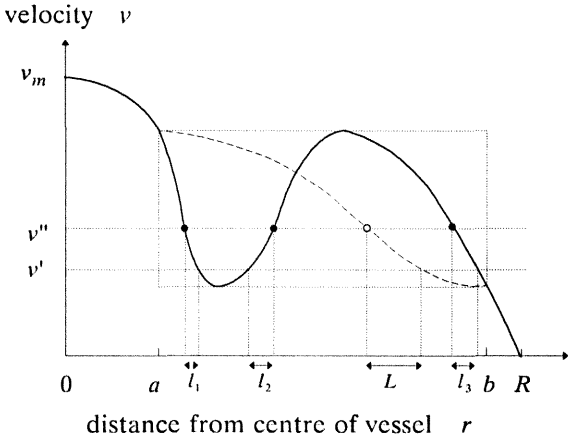


**Fig.C.1 - an axi-symmetric non-monotonic unidirectional profile**

The use of PIWMF to calculate the mean flow assumes that the particles with higher velocities are closer to the vessel centre. So, for a 'thin' beam, if the velocity profile is given by the solid line then the calculated PIWMF will give the mean flow appropriate to the profile given by the dashed line, where both profiles give the same Doppler spectrum. The result is that if non-monotonicity exists the higher velocities are underweighted, and so PIWMF underestimates the true mean velocity. This is the principle stated in chapter 12.

As any frequency range in the Doppler signal has a corresponding velocity range, and as both the solid and dashed profiles give the same spectrum, it follows that the fraction of the radius occupied by the dashed line between any two velocities, $v'$ and $v''$, is equal to the fraction of the radius occupied by the solid line between these velocities, that is $L = l_1 + l_2 + l_3$ . It was shown in chapter 3 using (3.3) that the power spectrum $p(f)$ for an axi-symmetric profile and a 'thin' beam is such that

$$p(f) \propto \left|\frac{dr}{dv}\right| \qquad \text{(C.1)}$$

So the dashed line can be 'constructed' from the true profile by noting that on this line at any velocity $v''$ say, marked by the hollow circle, the modulus of the derivative $dr/dv$, which is proportional to the power at the corresponding Doppler frequency, must be equal to the sum of the moduli of the derivatives $dr/dv$ at each of the points in the true profile where the velocity is $v''$, marked by the solid circles.

## An extreme form

Given a region of non-monotonicity between $r = b$ and $r = a$, the worst departure from monotonicity, leading to the greatest error in PIWMF, will be when the profile has velocities as high as possible close to $r = b$ and as low as possible close to $r = a$. This unrealistic 'rectangular' form is given by the solid line of fig.C.2. Obviously $w$ is a length less than $(b - a)$. The velocity at $r = a^-$ is $v_a$ and the velocity at $r = b^+$ is $v_b$.

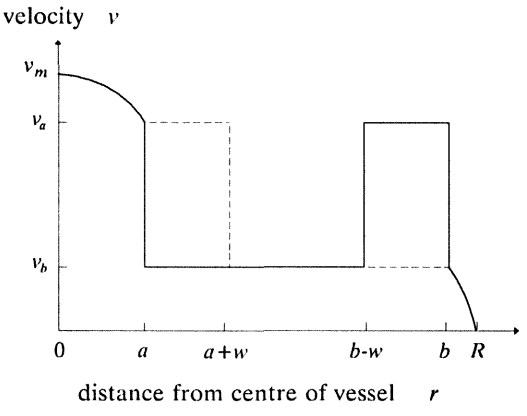


**Fig.C.2 - 'rectangular' form between the known values**

The true mean velocity, $\bar{v}$, for an axi-symmetric velocity profile $v(r)$ is

$$\bar{v} = \frac{\int_0^R 2\pi r.v(r)\,dr}{\pi R^2} \qquad \text{(C.2)}$$

Once again using PIWMF gives the mean velocity that would be the case if the profile followed the dashed line. Therefore for the true (solid) and false (dashed) profiles of fig.C.2, with the monotonic sections cancelling, the difference in the true and false mean velocities, $\bar{v}$ and $\bar{v}'$, is

$$\begin{aligned}\bar{v} - \bar{v}' &= \frac{1}{R^2}\left[\left(\int_{b-w}^{b} 2rv_a\,dr + \int_a^{a+w} 2rv_b\,dr\right) - \left(\int_{b-w}^{b} 2rv_b\,dr + \int_a^{a+w} 2rv_a\,dr\right)\right] \\ &= \frac{1}{R^2}\left[2w(v_a - v_b)(b-a-w)\right]\end{aligned} \qquad \text{(C.3)}$$

This is a positive quantity so, as suggested above for the general case, PIWMF underestimates the true value in the presence of this departure from monotonicity. Differentiating (C.3) with respect to $w$ shows that the difference between the true and estimated mean velocities is maximised when

$$w = \frac{b-a}{2}$$

and so the maximum difference is

$$\left(\bar{v} - \bar{v}'\right)_{\max} = \frac{(b-a)^2(v_a - v_b)}{2R^2}$$

*Worst case form*

In particular the least favourable case is where $b=R$, $a=0$ and $v_b = 0$ as shown in fig.C.3 where $v_a$ is relabelled as the maximum velocity $v_m$. Equation (C.3) becomes

$$\bar{v} - \bar{v}' = \frac{v_m}{R^2}\left(2wR - 2w^2\right)$$

which is maximised when $w = R/2$ to give

$$\left(\bar{v} - \bar{v}'\right)_{\max} = \frac{v_m}{2}$$

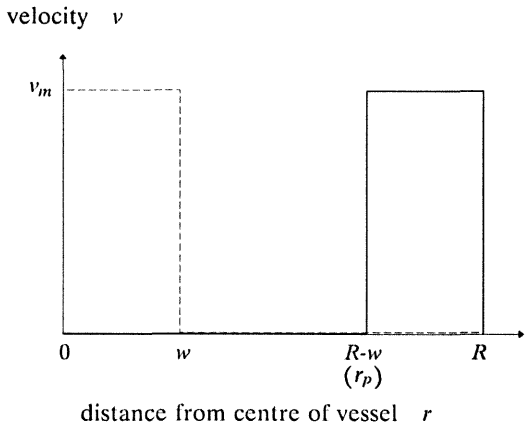


**Fig.C.3 - worst case unidirectional profile**

The true mean velocity is

$$\begin{aligned}\overline{v} &= \frac{1}{R^2}\int_{R-w}^{R} 2r\, v_m\, dr \\ &= \frac{2v_m}{R^2}\left(\frac{R^2}{2} - \frac{(R-w)^2}{2}\right) \\ &= \frac{v_m}{R^2}\left(2wR - w^2\right)\end{aligned}$$

so that the percentage error using PIWMF is

$$\begin{aligned}E_{\text{PIWMF}} &\equiv \frac{\overline{v}' - \overline{v}}{\overline{v}} \times 100\% \\ &= -\frac{2R-2w}{2R-w} \times 100\%\end{aligned} \qquad \text{(C.4)}$$

If the radial distance where the profile departs from monotonicity and starts to decrease towards the vessel centre is denoted by $r_p$ then with this rectangular shaped profile $r_p = R - w$, as marked on fig.C.3.

The error given by (C.4) can then be expressed as

$$E_{\text{PIWMF}} = \frac{-2(r_p/R)}{1+(r_p/R)} \times 100\%$$

This percentage error is plotted against $r_p/R$ on fig.C.4 and is shown by the dashed curve. (The solid curves are described later). As $r_p$ approaches 0, the error approaches 0. As $r_p$ approaches $R$ this error approaches the worst value of -100%. This corresponds to the unrealistic case of the extreme outer lamina being the only moving layer of blood. As seen above the absolute underestimate is greatest and equal to $v_m/2$ when $r_p/R = 0.5$.

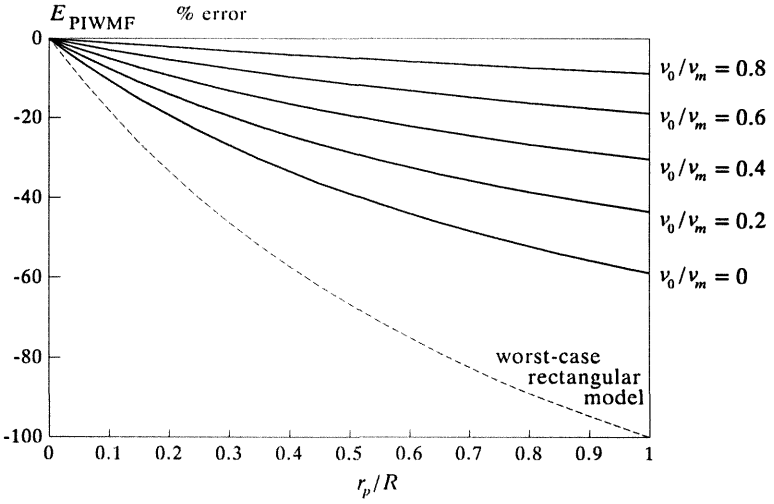


**Fig.C.4 - error in PIWMF with a non-monotonic unidirectional profile**
**- dashed line - worst-case rectangular model (see text above)**
**- solid lines - parabolic model (see text below)**

## 'Parabolic' profile model

The 'rectangular' velocity profiles above represent unrealistic extreme cases. An idealised example of a more sensible profile with no negative flow but with a large departure from monotonicity is given in fig.C.5. The function describing the profile is piecewise and comprises sections of three parabolae, labelled A, B and C, with each section having as one end point the vertex of its parabola. The derivative of the function is continuous, and sections A and B are rotationally symmetric about their joining point. The velocity at the centre of the vessel is $v_0$. The point $r_p$ is as defined above, and is now the unique point of maximum velocity. The sections are described by

$$v = v_0 + 2(v_m - v_0)\left(\frac{r}{r_p}\right)^2 \qquad 0 < r \le \frac{r_p}{2} \qquad \text{Section A} \qquad \text{(C.5)}$$

and

$$v = v_m - 2(v_m - v_0)\left(\frac{r - r_p}{r_p}\right)^2 \qquad \frac{r_p}{2} < r \le r_p \qquad \text{Section B} \qquad \text{(C.6)}$$

and

$$v = v_m\left(1 - \left(\frac{r - r_p}{R - r_p}\right)^2\right) \qquad r_p < r \le R \qquad \text{Section C} \qquad \text{(C.7)}$$

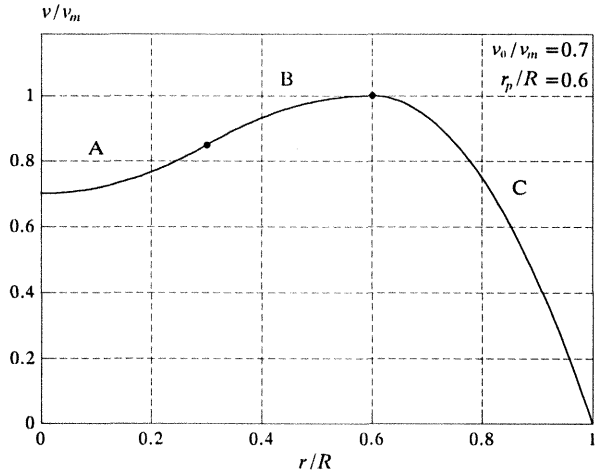


**Fig.C.5 - a velocity profile made up of parabolic segments**

The maximum velocity and radius are scale factors so that the form of the profile is completely defined by the parameters $v_0/v_m$ and $r_p/R$. The example profile of fig.C.5 corresponds to the parameter values of $v_0/v_m$ = 0.7 and $r_p/R$ = 0.6. The profile is not dissimilar to the theoretical profile shown in fig.12.7 at a phase of 180°, which was derived from actual experimental data.

Using the velocity profile the true mean flow, $\bar{v}$, was numerically estimated from (C.2) by treating the profile as being made up of 2000 steps of equal radial extent for various values of these parameters. The measured mean velocity, $\bar{v}'$, was found from the form of the spectrum, according to (C.1). (For mean velocity calculations the scale of the spectrum is irrelevant.) The quantity $dr/dv$ can be found by differentiating the velocity profile $v(r)$ and taking the reciprocal. The relative magnitude of the spectral densities from the three individual sections of the profile, (C.5),(C.6) and (C.7), are found to be

$$p_A(f) = \frac{\sqrt{2}\,r_p}{R} \cdot \frac{f_m}{\sqrt{f_m - f_0}\sqrt{f - f_0}} \qquad f_0 < f \le \frac{f_0 + f_m}{2} \qquad \text{Section A}$$

$$p_B(f) = \frac{\sqrt{2}\,r_p}{R} \cdot \frac{f_m}{\sqrt{f_m - f}\sqrt{f_m - f_0}} \qquad \frac{f_0 + f_m}{2} < f < f_m \qquad \text{Section B}$$

$$p_C(f) = \frac{2(R - r_p)}{R} \cdot \frac{f_m}{\sqrt{f_m}\sqrt{f_m - f}} \qquad 0 \le f < f_m \qquad \text{Section C}$$

where $f$ and $f_m$ are the Doppler frequencies corresponding to $v$ and $v_m$, and each spectrum has zero density outside the limits given. The total spectrum is the sum of the spectra from the three regions, i.e.

$$p(f) = p_A(f) + p_B(f) + p_C(f)$$

From its definition in (2.11) PIWMF is given by

$$\text{PIWMF} = \frac{2\int_0^{f_m} f \cdot p(f)\left(\int_f^{f_m} p(u)\,du\right)df}{\left(\int_0^{f_m} p(f)\right)^2} \qquad \text{(C.8)}$$

and the estimate of mean velocity, $\bar{v}'$, is calculated simply by conversion back from frequency to velocity. This velocity estimate was also evaluated numerically from (C.8) where the continuous spectrum was approximated by 2000 equally spaced frequency bins.

The simulation was made for various values of the parameters $v_0/v_m$ and $r_p/R$. The resulting percentage errors $E_{\text{PIWMF}}$ are given by the solid lines of fig.C.4. Clearly as $r_p$ approaches zero or as $v_0$ approaches $v_m$ the error becomes zero.

It is instructive to compare the curve where $v_0/v_m = 0$ with the dotted curve which corresponds to the rectangular profile of fig.C.3. In both these cases the non-monotonicity is such that the velocity is zero at the vessel centre. The effect of introducing the parabolic model is that for the same value of $r_p$ the error is reduced to about 60% of that if the profile were rectangular. This figure of approximately two thirds is not surprising given that the area beneath a parabolic segment, $y = kx^2$, with one end as its turning point is one third of the enclosing rectangle, i.e. in fig.C.6 the shaded area is one third of the rectangle.

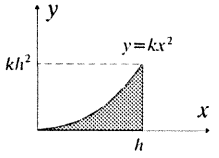


$$\int_0^h kx^2\,dx = \frac{h \cdot kh^2}{3}$$

**Fig.C.6 - parabolic segment as two thirds of a step function**

Inverting this parabolic curve in the enclosing dashed rectangle gives a parabolic segment which 'according to this measure' is two thirds of the enclosing step function.

## Summary

In the presence of an axi-symmetric velocity profile that is positive but not monotonically increasing from the vessel wall to the vessel centre, use of PIWMF leads to an underestimate of the true mean velocity. The amount of error depends on the form and extent of the non-monotonicity. If the fraction of the radius over which the profile is problematic is known, and if the limits of the velocities in this radial range are known an upper bound can be put on the amount of error incurred. This upper bound is not approached in practice as it corresponds to the case of a profile with an unrealistic form. A guide to a more realistic estimate of the error incurred by a region of non-monotonicity, based on a profile model of parabolic segments, would be 2/3 of the value incurred if the region had the least favourable, i.e. rectangular, form.

## Notation for this appendix

| | |
|---|---|
| $a,b$ | boundaries of region of non-monotonicity |
| $r_p$ | radial position where velocity starts to decrease towards vessel centre |
| $w$ | width of rectangular perturbation in velocity profile |

# APPENDIX D - NON-STATIONARITY OF THE DOPPLER SIGNAL

The meaning of a spatial mean velocity estimate is compromised if the segment duration is longer than the time over which the Doppler signal has a fixed frequency content, as no single 'instantaneous' mean velocity is appropriate. This interval of 'stationarity' is also usually regarded as being the longest interval appropriate for Fourier analysis because of the theoretical basis of the analysis. As suggested in chapter 7, non-stationarity of the signal, in the form of a change in the underlying power spectrum representing a change in the velocity distribution of scatterers, is manifested as a type of spectral 'broadening' in the single spectrum observed from this period. The relevant mean velocity is not appropriate to any instant but is clearly the average mean velocity throughout this period. The nature of the 'broadened' spectrum appears to be such that an estimate of this mean velocity can legitimately be made using IWMB, but not using PIWMB. This is supported by the following non-rigorous demonstration.

## Theoretical analysis

Consider a zero-mean semi-infinite stationary signal $A(\tau)$, as in fig.D.1a. This can be represented as a sequence of equally spaced samples $A_j$ where the sampling rate can be increased without limit. The autocovariance function of this sequence is denoted by $\gamma_{AA}(m)$ and is

$$\gamma_{AA}(m) = E\left[A_j A_{j+m}\right]$$

where $m$ is an integer shift parameter, and the expectation, $E[\ ]$, is found by considering all values of $j$. Similarly a second zero-mean semi-infinite stationary signal $B(\tau)$, as in fig.D.1b, has an autocovariance function of

$$\gamma_{BB}(m) = E\left[B_j B_{j+m}\right]$$

These signals can be placed back to back to create one zero-mean non-stationary signal of infinite length $C(\tau)$, as in fig.D.1c, with an autocovariance function of

$$\gamma_{CC}(m) = E\left[C_j C_{j+m}\right]$$

where $-\infty < j < \infty$ and we define $j = 0$ where the signals are joined.

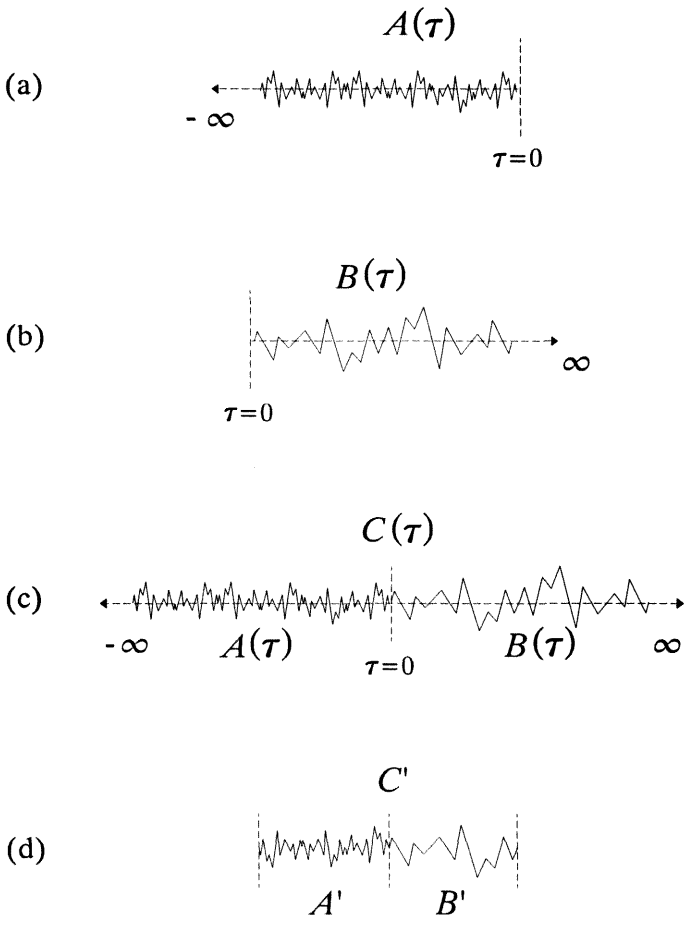


**Fig.D.1 - stationary and non-stationary signals**

If we choose $C_0$ to be equal to $B_0$ then the value of this last function for any shift $m$ is

$$\begin{aligned}\gamma_{CC}(m) &= \lim_{N\to\infty}\left(\frac{1}{2N+m}\right)\left(\sum_{j=-N}^{-m-1} C_j C_{j+m} + \sum_{j=-m}^{-1} C_j C_{j+m} + \sum_{j=0}^{N} C_j C_{j+m}\right) \\ &= \lim_{N\to\infty}\left(\frac{1}{2N+m}\right)\left(\sum_{j=-N}^{-m-1} A_j A_{j+m} + \sum_{j=-m}^{-1} A_j B_{j+m} + \sum_{j=0}^{N} B_j B_{j+m}\right) \\ &= \frac{1}{2}\left(\gamma_{AA}(m) + \gamma_{BB}(m)\right)\end{aligned}$$

recognising that the second summation term has only a finite number, $m$, of contributions and so vanishes in the limit, and the first and third terms, divided by $N$, in the limit are the individual autocovariances.

The power spectra of the stationary signals $A(\tau)$ and $B(\tau)$ are denoted by $p_A(f)$ and $p_B(f)$. For a stationary signal the power spectrum is defined as the Fourier transform of the autocovariance function. If the 'power spectrum' of the non-stationary signal $C$, $p_C(f)$, is defined similarly then if follows that

$$p_C(f) = \tfrac{1}{2}\left(p_A(f) + p_B(f)\right)$$

as the Fourier transformation is distributive and scalable. So the power spectrum of the infinite signal is the average of the power spectra of the semi-infinite 'halves'. The implication of this is that, as a finite signal segment $A'$ can be used to estimate the power spectrum of $A$, and an equal length finite segment $B'$ can be used to estimate the power spectrum of $B$, so a segment $C'$ made up of $A'$ and $B'$ back to back, as seen in fig.D.1d, can be used to estimate the mean power spectrum of $A$ and $B$. Because IWMF is linear in the spectral intensities, if follows that the IWMF of the segment $C'$ can be used to estimate the weighted mean IWMF of $A$ and $B$. If the IWMF of a (semi-) infinite signal is proportional to the corresponding mean blood velocity during this time, as in the case of a 'wide' beam, then the IWMF found from the segment $C'$ can be used to estimate the overall mean blood velocity. The same can not be said for PIWMF because PIWMF is not linear in the spectral intensities and so using the *mean* spectra found from $C'$ leads to errors. It is reasonable to extend these suggestions to the more general case where $A'$ and $B'$ are of different lengths, so that $C'$ provides an estimate of the *weighted* mean power spectrum of $A$ and $B$. The estimate of mean blood velocity resulting from the IWMF of $C'$ is then an estimate of the mean blood velocity in the time interval from which the segment was taken.

In chapter 10 it was seen that the IWMF of $A'$ can generally be thought of as an unbiased estimator of the IWMF of $A$, and likewise for $B'$ and $B$. However the analyses leading to the results of chapter 10 assumed a stationary signal. It is therefore not possible to state that the IWMF resulting from $C'$ leads to an unbiased estimator of the overall mean velocity.

## A simple example

The suggestion is that non-stationarity of the signal does not invalidate an estimate of mean blood velocity made from IWMF, yet does for an estimate made from PIWMF. A simple idealised example can help to illustrate this. Consider the Doppler signal resulting from a scatterer moving with constant velocity $v$ throughout an interval of 'stationarity' $\Delta\tau$. At the end of this interval the scatterer accelerates immediately to $5v$, and remains at this speed throughout another interval of the same duration $\Delta\tau$. The cycle is then repeated. The overall mean velocity is clearly $3v$. The Doppler signal in one period of length $2\Delta\tau$ can be idealised as the concatenation of two sinusoidal segments, with the appropriate frequency ratio of 1:5, shown in fig.D.2.

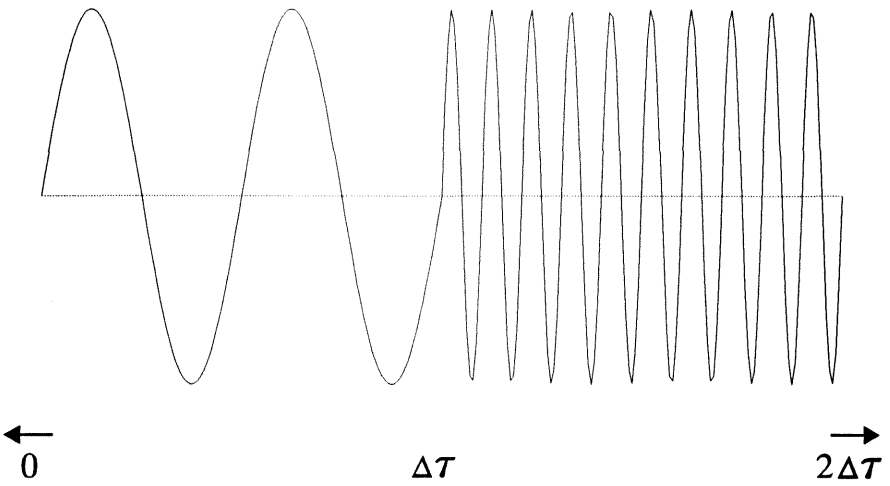


**Fig.D.2 - the idealised Doppler signal returning from a single scatterer with a change in velocity**

If discrete Fourier analysis is applied to this signal of length $2\Delta\tau$ and no modifying window is applied, and if the sampling rate is $256/\Delta\tau$ and the frequency corresponding to $v$ is $10/\Delta\tau$, then the half of the power spectrum below the Nyquist frequency is shown in fig.D.3.

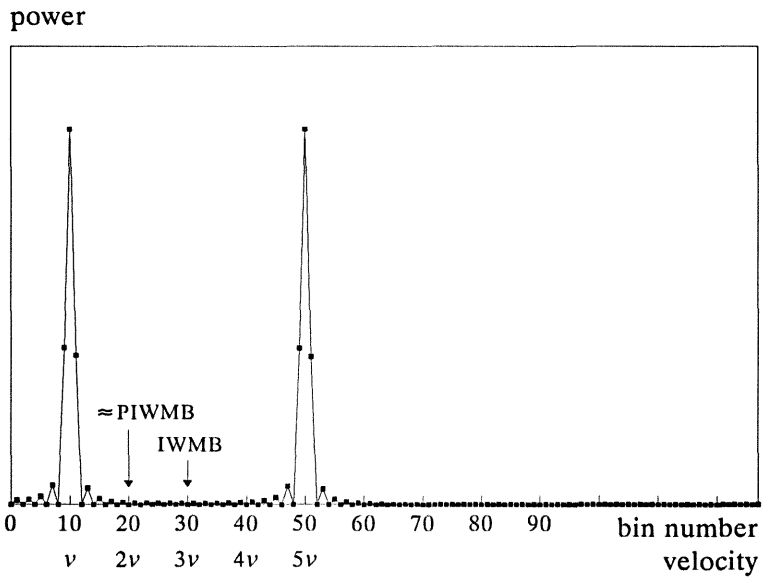


**Fig.D.3 - the power spectrum resulting from the single scatterer with the change in velocity**

The mean velocity calculated from the IWMB of the spectrum is $2.99v$, which is very close to the true value of $3v$. (The error is in part due to the finite nature of the power spectrum at the edge of the spectrum near zero frequency.) In the context of estimation using PIWMB, the spectrum can be approximated by two spikes of equal power at frequencies corresponding to $v$ and $5v$. Application of (2.9b) then shows that the estimate of mean velocity following from PIWMB is approximately $2v$ as marked, giving a large negative error. This near accuracy of IWMB and large error in PIWMB can be explained by noting that the variation in time of the velocity of the scatterer has appeared in the spectrum as a 'broadening' of the spectrum, in this case the addition of another spike. These spikes in reality correspond to 'scatterings' which are *coincident in their axial distance from the transducer* but are *separated in time*. However use of IWMB and PIWMB assumes these 'scatterings' are *coincident in time* but *separated in space*, i.e. separated throughout a vessel cross section. IWMB weights these spikes appropriately despite this, but PIWMB assigns a lower weight to the higher velocity as it treats this velocity as being appropriate to scatterers nearer the vessel axis.

## Discussion

The non-stationarity of the signal is due to different velocities being appropriate to the same point in the sample volume at different times during the recorded time interval. The amount of error in PIWMB will be dependent on the extent of this variation of velocity as a fraction of the average velocity at that point in the cross section. A rectangular broadening function representing a steady change in velocity would be a rough approximation to the spectral broadening introduced, and this fraction could be thought of as an effective value of the parameter $a$ defined in chapter 7. For this fraction $a$ to be in the region of 0.5, leading to a negative error of a few percent as described in chapter 7, large relative changes in velocity would have to occur within the time interval. Typically the data segment might correspond to 10 milliseconds of the signal. Large velocity changes in such an interval might occur at the onset of systole, but for the rest of the cardiac cycle $a$ will be very small and so PIWMB, as well as IWMB, can be thought of as incurring negligible error.

## Summary

If the velocity distribution of the scatterers changes during the time interval over which the Doppler signal is recorded then the relevant mean velocity is the average spatial mean velocity in that time interval, and the data segment can not be regarded as being sampled from a stationary source. Spectral analysis by Fourier transform is usually performed under the assumption that the signal is stationary. However even if non-stationarity exists IWMB with a 'wide' beam could be used to estimate the mean velocity with only a negligible error. The nature of the changing velocity distribution as a source of spectral broadening means that use of PIWMB with a non-stationary signal, even with a 'thin' beam, incurs some error in the manner described in chapter 7, but this error is small.

## Notation for this appendix

| | |
|---|---|
| $E[\ ]$ | expectation operator |
| $j$ | index of sample in time series - an integer |
| $m$ | shift parameter - an integer |

# APPENDIX E - JUSTIFICATIONS OF RESULTS IN THE TEXT

Some peripheral results in the text have merely been stated, and reference has been made to this appendix for their justification. They are treated here in the order in which they appear in the text. For each section the symbol notation is that of the relevant chapter, unless it is new in which case it is listed at the end of this appendix.

## Bounds on PIWMB - equations (2.12) and (2.13)

In chapter 2 bounds on PIWMB and PIWMF were given in relation to IWMB and IWMF and the highest signal frequency. The results stated were

$$\frac{\overline{B}^2}{H} \le \hat{B} \le \overline{B} \qquad \text{and analogously} \qquad \frac{\bar{f}^2}{f_{\max}} < \hat{f} \le \bar{f}$$

which are (2.12) and (2.13) respectively. The first of these results is stated in terms of the observed statistics $\overline{B}$ and $\hat{B}$ but can also be written using their deterministic forms, $\overline{B}_D$ and $\hat{B}_D$, simply by considering $\tilde{p}_i$ instead of $p_i$ throughout. To prove both these results consider the statistic PIWMB, $\hat{B}$.

*Upper bound*

PIWMB assumes that the profile is monotonic, and so weights the low-frequency components more, i.e. those from the scatterers near the vessel walls. So an upper bound for PIWMB must be the value of IWMB. This can be proven analytically by noting that, if summation without limits means summing over all the bins, alternative expressions for IWMB and PIWMB are

$$\overline{B} = \frac{\sum ip_i}{\sum p_i} \qquad \text{and} \qquad \hat{B} = \frac{\sum ip_i\left(2\sum_{j>i} p_j + p_i\right)}{\left(\sum p_i\right)^2}$$

The two are equal only if all the power in the spectrum is contained in one frequency bin, corresponding to the presence of a single velocity among the blood cells. This can be proven by examining the ratio

$$\frac{\hat{B}}{\overline{B}} = \frac{\sum ip_i\left(2\sum_{j>i} p_j + p_i\right)}{\sum ip_i \cdot \sum p_i} = \frac{\sum ip_i^2 + \sum_{j>i} ip_ip_j + \sum_{j>i} ip_ip_j}{\sum ip_i^2 + \sum_{j>i} ip_ip_j + \sum_{j<i} ip_ip_j}$$

where the numerator and denominator have been retained and expanded. The only difference between the numerator and denominator are in the third terms. Both these terms contain one and only one term of each possible combination $p_i p_j$ where $i \neq j$. In both cases these combinations are multiplied by the index $i$, but in the numerator $i$ is the lower index and in the denominator $i$ is the larger index so that, as each $i$ and each $p_i$ value are non-negative, the numerator can not be larger than the denominator. Therefore $\hat{B} \leq \overline{B}$. The numerator and denominator are equal, and hence PIWMB and IWMB are equal, if and only if $p_i p_j = 0$ for all possibilities of $i \neq j$. This is the case only if all the power is contained in one frequency bin as described above. This argument is valid for any total number of frequency bins and with the $\tilde{p}_i$ values replacing the $p_i$ values, so that the result must be true for the continuous estimators PIWMF and IWMF also. So $\bar{f} \leq \hat{f}$ , and these are equal only if the spectrum is a spike. These relationships are consequences of the proportionately lower weighting given to high Doppler frequencies if the beam is considered 'thin'.

*Lower bound*

If, as in chapter 2, $H$ is the index of the highest bin with non-zero observed power then a lower bound for the observed PIWMB statistic is given by

$$\hat{B} \geq \frac{\overline{B}^2}{H} . \tag{E.1}$$

To prove this it is helpful to denote the total observed power by $P$, i.e.

$$P = \sum_{i=0}^{\mathrm{IMAX}} p_i$$

whereupon both sides of the inequality (E.1) can be multiplied by the non-negative quantity $P^2/H$ to give the equivalent inequality

$$\left( \frac{P^2 \hat{B}}{H} \right) \geq \left( \frac{P \overline{B}}{H} \right)^2 \tag{E.2}$$

The numerators of the bracketed terms in (E.2) are the numerators of (2.9b) and (2.1b). Furthermore, as the bins above $H$ are empty, the divisions by $H$ can effectively be achieved by defining $i'' = i/H$ and $j'' = j/H$ and using the indices $i''$ and $j''$ summed from 0 to 1, instead of $i$ and $j$ summed to IMAX. So (E.2) can be written as

$$\sum_{i''=0}^{1} i'' p_{i''} \left( 2 \sum_{j''>i''} p_{j''} + p_{i''} \right) \geq \left( \sum_{i''=0}^{1} i'' p_{i''} \right)^2 . \tag{E.3}$$

Consider a spectrum which contains no power below a frequency bin defined by $i'' = b$, and which satisfies (E.3), i.e.

$$\sum_{i''=b}^{1} i'' p_{i''} \left( 2 \sum_{j''>i''} p_{j''} + p_{i''} \right) \geq \left( \sum_{i''=b}^{1} i'' p_{i''} \right)^2 \qquad \text{(E.4)}$$

to which a spectral component of any non-zero power $p_a$ is added to the bin defined by $i'' = a$ below the lowest frequency, i.e. where $a < b$ as in fig.E.1a.

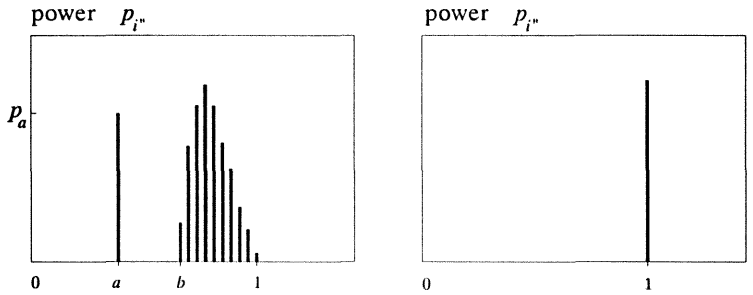


**(a)** **(b)**

**Fig.E.1 - hypothetical spectra**

The inequality which we want to demonstrate is (E.3) which can now be expressed as

$$ap_a \left( 2 \sum_{j''=b}^{1} p_{j''} + p_a \right) + \sum_{i''=b}^{1} i'' p_{i''} \left( 2 \sum_{j''>i''} p_{j''} + p_{i''} \right) \geq \left( ap_a + \sum_{i''=b}^{1} i'' p_{i''} \right)^2$$

$$\Leftrightarrow \; ap_a^2 + 2ap_a \sum_{i''=b}^{1} p_{i''} + \sum_{i''=b}^{1} i'' p_{i''} \left( 2 \sum_{j''>i''} p_{j''} + p_{i''} \right) \geq a^2 p_a^2 + 2ap_a \sum_{i''=b}^{1} i'' p_{i''} + \left( \sum_{i''=b}^{1} i'' p_{i''} \right)^2$$

(E.5)

The last term of the left hand side is greater than or equal to the last term of the right hand side as these are the terms of (E.4). The second term of the left hand side is greater than or equal to the second term of the right hand side as the only difference between these terms is the presence of the $i''$ indices in the right hand term, which are all less than or equal to 1. The first term of the left hand side is greater than the first term of the right hand side if $a \neq 0$ as $a$ is below 1. So the whole inequality is satisfied, and the spectrum resulting from the addition of the component at $a$ must also satisfy (E.3).

Next consider a spectrum that is zero everywhere except the $H$ 'th bin, i.e. except where $i'' = 1$, as shown in fig.E.1b. Equation (E.3) therefore is

$$1 \cdot p_1 \cdot p_1 \geq (1 \cdot p_1)^2$$

which is true as both sides are equal. So this 'spike' spectrum satisfies (E.3), and from the preceding analysis, the subsequent introduction of any component in a bin below the $H$'th bin gives a spectrum which also satisfies (E.3). Furthermore any shaped spectrum can be built by adding the highest frequency components first, so (E.3) and hence (E.1) must be true for any spectrum (of non-negative frequencies). Analysis of (E.5) shows that the sides of the inequality are only equal if $a = 0$ and $b = 1$. So the sides of (E.1) are equal only if the power is shared between just two bins, the zero'th bin and the $H$'th bin, or if the power is entirely in the $H$'th bin.

By considering an infinite number of frequency bins we can draw analogous conclusions for the continuous frequency case. So if $f_{max}$ is the maximum frequency in the signal then

$$\hat{f} \geq \frac{\bar{f}^2}{f_{max}}$$

and there is equality only if the spectrum is a spike at $f = f_{max}$ with or without a spike at $f = 0$.

*Combined bound expression*

Therefore PIWMB is bound in relation to IWMB and the highest bin with non-zero power by

$$\frac{\bar{B}^2}{H} \leq \hat{B} \leq \bar{B}$$

Analogously, as the Doppler shift frequencies are defined to be positive, PIWMF is bound in relation to IWMF and the highest signal frequency by

$$\frac{\bar{f}^2}{f_{max}} \leq \hat{f} \leq \bar{f}$$

and these are the stated results (2.12) and (2.13).

## The correction for the continuous monotonic profile - equation (2.14)

The correction term associated with the treatment of the profile as being piecewise and linear between the $s_i$ values was given in (2.14) by

$$-\frac{1}{6}\sum\frac{\tilde{p}_i^2}{\tilde{P}^2}$$

This result can be shown by starting with the final form of equation (2.6). This gives the mean frequency in bin units over the whole cross section for the monotonic profile, and is

$$\text{mean frequency in bin units} = \frac{\sum_{i=0}^{IMAX} i'(s_i^2 - s_{i+1}^2)}{\sum_{i=0}^{IMAX}(s_i^2 - s_{i+1}^2)} \qquad \text{(E.6)}$$

In the derivation of PIWMB $i$ was subsequently substituted for $i'$, thus introducing a small error. As stated earlier, in general $i' \leq i$. More particularly they are only equal for every bin if the velocity profile has the unrealistic discontinuous form shown in fig.E.2a. In this diagram the ordinate is given in terms of frequency rather than velocity.

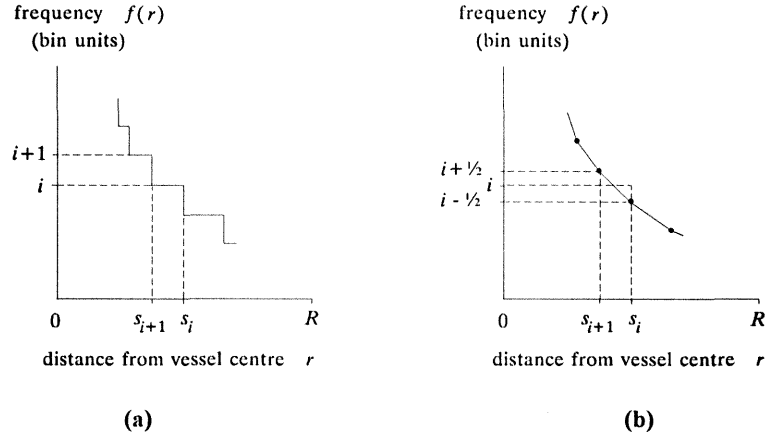


**Fig.E.2 - (a) an unrealistic form and (b) a more realistic form of a velocity (frequency) profile**

A closer approximation to the actual smooth profile is shown in fig.E.2b, and earlier in fig.2.6, where the profile is thought of as being a series of contiguous line segments. For the general value of $i$ this profile passes through the frequency $i-½$ when the radial distance is $s_i$. There are no discontinuities in the profile, and for the $i$'th bin $i$ remains the mean frequency as measured in the sample volume. The ordinate $f(r)$ is a continuous measure of frequency in bin units, so that the mean frequency over the ring corresponding to the $i$'th bin is

$$i' = \frac{\int_{s_{i+1}}^{s_i} 2\pi r f(r)\, dr}{\pi(s_i^2 - s_{i+1}^2)}$$

The frequency $f(r)$ between $s_{i+1}$ and $s_i$, is linear from $i+½$ to $i-½$ , and so is

$$f(r) = i + ½ - \left(\frac{r - s_{i+1}}{s_i - s_{i+1}}\right)$$

so the contribution of the $i$'th bin to the numerator of (E.6) can be written as

$$\begin{aligned} i'(s_i^2 - s_{i+1}^2) &= \int_{s_{i+1}}^{s_i} 2r\left[i + ½ - \left(\frac{r - s_{i+1}}{s_i - s_{i+1}}\right)\right] dr \\ &= \left[i + ½ + \left(\frac{s_{i+1}}{s_i - s_{i+1}}\right)\right] \int_{s_{i+1}}^{s_i} 2r\, dr \;-\; \left(\frac{1}{s_i - s_{i+1}}\right) \int_{s_{i+1}}^{s_i} 2r^2\, dr \\ &= \left[i + ½ + \left(\frac{s_{i+1}}{s_i - s_{i+1}}\right)\right] (s_i^2 - s_{i+1}^2) \;-\; \left(\frac{1}{s_i - s_{i+1}}\right)\left(\frac{2}{3}\right)(s_i^3 - s_{i+1}^3) \end{aligned}$$

Factorising the differences of squares and cubes and simplification leads to

$$\begin{aligned} i'(s_i^2 - s_{i+1}^2) &= i\,(s_i^2 - s_{i+1}^2) + ½\,(s_i^2 - s_{i+1}^2) + (s_i s_{i+1} + s_{i+1}^2) - ⅔\,(s_i^2 + s_i s_{i+1} + s_{i+1}^2) \\ &= i\,(s_i^2 - s_{i+1}^2) - ⅙\,(s_i^2 - 2 s_i s_{i+1} + s_{i+1}^2) \\ &= i\,(s_i^2 - s_{i+1}^2) - ⅙\,(s_i - s_{i+1})^2 \end{aligned}$$

The denominator of (E.6) is equal to $R^2$ so that the contribution to (E.6) of the *i*'th bin is

$$\frac{i'\left(s_i^2 - s_{i+1}^2\right)}{R^2} = \frac{i\left(s_i^2 - s_{i+1}^2\right)}{R^2} - \frac{\frac{1}{6}\left(s_i - s_{i+1}\right)^2}{R^2}$$

The first term is the 'uncorrected' result. The second term, the correction term, is simplified by making the substitution, following from (2.3)

$$s_i - s_{i+1} = \frac{R}{\tilde{P}}\tilde{p}_i$$

so that

$$\frac{i'\left(s_i^2 - s_{i+1}^2\right)}{R^2} = \frac{i\,\tilde{p}_i\left(2\sum_{j=i+1}^{IMAX}\tilde{p}_j + p_i\right)}{\tilde{P}^2} - \frac{1}{6}\cdot\frac{\tilde{p}_i^2}{\tilde{P}^2}$$

This is applicable to every bin contributing to (E.6) except the zero'th bin and the bin containing the highest signal frequencies, as the frequency profile in these two bins will not have the form shown in fig.E.2b. The effect of these extreme bins will however be small. The correction to PIWMB is therefore approximately

$$-\frac{1}{6}\sum_{i=0}^{IMAX}\frac{\tilde{p}_i^2}{\tilde{P}^2}$$

which is the term observed in (2.14).

## An alternative frequency bin configuration - equation (2.15)

Equation (2.15) stated that if the bin configuration was such that the lower edge of the zero'th bin was at the zero frequency point, as in fig.2.4b, then the appropriate estimator of mean blood velocity would be

$$\hat{\hat{B}} = \frac{\sum_{i=0}^{IMAX} i\, p_i\, q_i}{\left(\sum_{i=0}^{IMAX} p_i\right)^2} + \frac{1}{2} \qquad \text{(E.7)}$$

This can be shown mathematically by first noting that with this configuration the frequency in bin units corresponding to the centre of the $i$'th bin is $i + \frac{1}{2}$. Using the $q_i$ substitution of chapter 2, equation (2.9b) in this case becomes

$$\hat{\hat{B}} = \frac{\sum_{i=0}^{IMAX} (i + \frac{1}{2})\, p_i\, q_i}{\left(\sum_{i=0}^{IMAX} p_i\right)^2} = \frac{\sum_{i=0}^{IMAX} i\, p_i\, q_i}{\left(\sum_{i=0}^{IMAX} p_i\right)^2} + \frac{\frac{1}{2}\sum_{i=0}^{IMAX} p_i\, q_i}{\left(\sum_{i=0}^{IMAX} p_i\right)^2} \qquad \text{(E.8)}$$

Now

$$\begin{aligned}\sum_{i=0}^{IMAX} p_i\, q_i &= \sum_{i=0}^{IMAX} p_i \left(2\sum_{j=i+1}^{IMAX} p_j + p_i\right) \\ &= \sum_{i=0}^{IMAX} p_i^{\,2} + 2\sum_{i=0}^{IMAX} p_i \sum_{j=i+1}^{IMAX} p_j \\ &= \left(\sum_{i=0}^{IMAX} p_i\right)^2\end{aligned}$$

so that the second term of the right-hand side of (E.8) is equal to $\frac{1}{2}$. The result (E.7), which is (2.15), follows immediately.

## Theoretical form of the broadening function - chapter 7

As suggested in chapter 7 there is theoretical backing for expecting a broadening function with a form which is the 'square' of an isosceles triangle. This can be demonstrated by again considering a target group of particles with a single velocity $v$ insonated by a transducer with angular extent $2\varepsilon$, as in fig.E.3. The quantities $x$ and $\mu$ are defined to be the distance and angular distance along the transducer of a variable point from the point opposite the target, and $\gamma$ is the Doppler angle appropriate to the point defined by $x$ or $\mu$. Note that $x = L\tan\mu$.

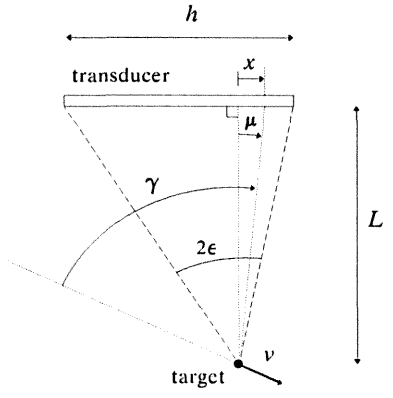


**Fig.E.3 - further geometry of a finite aperture transducer and a moving point target**

If $\Phi(x)$ is the cumulative transmitted power as the points on the transducer are traversed, say from left to right, then allowing each point on the tranducer to be equally active means that between the ends of the transducer $d\Phi(x)/dx = \text{constant}$. Also $d\mu/d\gamma = 1$ and, due to $\varepsilon$ being small, the derivatives $dx/d\mu \equiv L\sec^2\mu$ and $d\gamma/d\cos\gamma \equiv -1/\sin\gamma$ can, to a first approximation, be treated as constants throughout the relevant range of angles. Therefore the quantity

$$\frac{d\Phi(\cos\gamma)}{d\cos\gamma} \equiv \frac{d\Phi(x)}{d\cos\gamma} = \frac{d\Phi(x)}{dx} \cdot \frac{dx}{d\mu} \cdot \frac{d\mu}{d\gamma} \cdot \frac{d\gamma}{d\cos\gamma}$$

which is the power density with cosine, is approximately uniform throughout the range of cosines, as seen if fig.E.4.

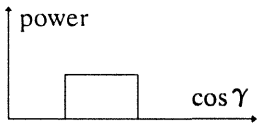


**Fig.E.4 - distribution of cosines for a scattered ray with a single angle of incidence**

So the cosine of the angle of incidence is distributed uniformly with power. Similarly, by the principle of reciprocity, the cosine of angle of reception is distributed uniformly. The power spectrum of transmitted and received radiation is therefore some 'combination' of these uniform distributions.

When a point transmitter insonates a moving target with an angle of incidence of $\alpha_T$ to the motion, and a separated point receiver is situated so that the angle of scattering is $\alpha_R$ to the motion, then the Doppler equation (7.1) becomes

$$f = \frac{Fv}{c}(\cos\alpha_T + \cos\alpha_R)$$

Therefore for the strip transducer of fig.E.3 the power density observed at any particular Doppler shift frequency is found by 'summing' the rays transmitted and scattered at angles such that their cosines add to the same quantity. Consider now the practical case where the sample volume has finite dimensions. At the point of greatest intensity in the sample volume the contributing incident rays are coherent, so that this 'summation' involves adding amplitudes. The result is that the approximate form of the amplitude spectrum is a convolution of these two identical uniform functions, which is an isosceles triangle function. The power spectrum, which is the broadening function, is therefore approximately the square of this triangular form, which is the suggested result. A triangular form and a squared triangular form are shown in fig.E.5 which has already been seen as fig.7.7. The halves of the squared triangular form are parabolic segments.

A more complex theory is given by Newhouse et al. (1987) for a slightly different situation. They consider a focused long strip transducer, with particles moving across its finite width through the focal line in a completely transverse direction. The unimportant difference between this geometry and that described here is that in the dimension not considered their transducer is infinite in extent and in this work the extent is infinitesimal. Further they make the assumption that the finite extent of the transducer is small compared to the

distance to the target, that is, in the terminology of fig.E.3, $h << L$. They consider the diffraction pattern resulting from the superposition of contributions from the points on the transducer face and derive a uniform amplitude/power spectrum for the radiation received by a moving particle, as above, and an isosceles triangular form for the amplitude spectrum received at the transducer, as above if coherent superposition is appropriate. The theory is extended for oblique motion of the particle by Censor et al. (1988), but the same basic result remains.

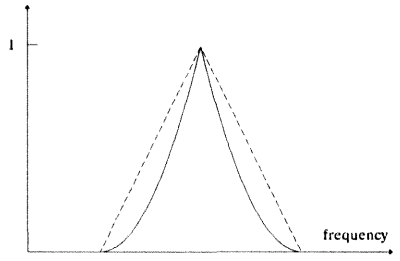


**Fig.E.5 - triangular and squared triangular broadening forms**

In terms of the ray model (and oblique motion) proposed here the addition of *amplitudes* is valid if the received rays are coherent. This is appropriate if the transmit and receive focusing are equivalent and the target is at the point of exact focus so that the phases of the rays from the different elements are the same. If the target is not coincident with this point the received rays will be somewhat out of phase. If the phases are thought of as being distributed randomly and uniformly then the correct convolution would be that of the uniform *power* spectra to give a triangular *power* spectrum. So from particles at the exact focus the received intensity is greatest and the broadening function has the squared triangular form. From particles at other points in the sample volume the contributions are less and the broadening functions are more triangular. This is consistent with the observed broadening function of fig.7.4 showing a form between triangular and squared triangular.

## The unbiasedness of IWMB with a uniform mean spectrum - chapter 10

As stated in chapter 10, for any symmetric mean spectrum, and hence for a uniform mean spectrum, the bias in IWMB is zero. In this section a mathematical proof is given for the case of a uniform spectrum.

The spectrum can be scaled so that the total mean power in the signal is 1 without altering the mean frequency. If the signal occupies $M$ of the available IMAX bins, and if each bin estimate $p_i$ is thought of as its mean value plus deviation, $\tilde{p}_i + e_i$ , then, using $(1+x)^{-1} = 1 - x + x^2 - \ldots$ , the observed value of IWMB in (10.2) is

$$\overline{B} = \frac{\sum i\tilde{p}_i + \sum ie_i}{1 + \sum e_i}$$

$$= \sum i\tilde{p}_i + \sum ie_i - \sum i\tilde{p}_i \left(\sum e_i\right)^1 - \sum ie_i \left(\sum e_i\right)^1 + \sum i\tilde{p}_i \left(\sum e_i\right)^2 + \sum ie_i \left(\sum e_i\right)^2 - \ldots$$

where the summations are over all the non-empty bins, i.e. from 0 to $M$-1. As the total mean power is 1, the first term can be seen to be the deterministic statistic $\overline{B}_D$ . Furthermore when taking the expected value of this expression the second and third terms become zero as the $e_i$ values each have zero mean. Expanding the remaining bracketed summations and multiplying leaves only the terms in $e_i^2$, $e_i^3$ etc. because, as the spectral estimates are uncorrelated, all terms with mixed indices, e.g. $e_i e_j$ if $i \neq j$, have expected value of zero. Up to this point the analysis is valid for all spectra. If the spectrum is uniform $E\left[e_i^2\right]$ and $E\left[e_i^3\right]$ etc. are independent of $i$ and can be taken outside the summations. Recognising that $\sum_{i=0}^{M-1} i = (M-1)M/2$ gives the terms in order

$$E[B] = B_D + 0 - 0 - \frac{(M-1)M}{2} E\left[e_i^2\right] + B_D M E\left[e_i^2\right] + \frac{(M-1)M}{2} E\left[e_i^3\right] - B_D M E\left[e_i^3\right] + \ldots$$

But for this uniform spectrum the deterministic mean statistic $\overline{B}_D$ is clearly the midpoint of the bins occupied by the spectrum, i.e. $\overline{B}_D = (M-1)/2$ , so the 4'th and 5'th terms cancel, as do the 6'th and 7'th etc. The bias in the case of a uniform spectrum is therefore zero.

## The expected value of the cube of the deviation, $e_i$ - equation (10.7)

The deviation of the observed estimate $p_i$ about its mean value of $\tilde{p}_i$ is given by $e_i$ , i.e. $p_i \equiv \tilde{p}_i + e_i$. The expected value of the cube of this deviation, $E\left[e_i^3\right]$ , can be found by considering the moments of the $\chi^2$ distribution with 2 degrees of freedom, which is the form of the distribution of $p_i$ .

*Theory*

For the random variable $X$ the moment-generating function is given by $E\left[e^{yX}\right]$ , and the $a$'th moment about the origin, $E\left[X^a\right]$, is given by

$$E\left[X^a\right] = \left.\frac{d^a E\left[e^{yX}\right]}{dy^a}\right|_{y=0}$$

If $X$ follows the $\chi_2^2$ distribution then the moment-generating function is

$$E\left[e^{yX}\right] = (1-2y)^{-1}$$

These results have been taken from Walpole and Myers (1978).

*Application*

The first moment of the $\chi_2^2$ distribution about the origin is the mean, denoted by $\mu$, and is

$$\begin{aligned}\mu \equiv E[X] &= \left.\frac{d(1-2y)^{-1}}{dy}\right|_{y=0} \\ &= \left.2(1-2y)^{-2}\right|_{y=0} \\ &= 2\end{aligned}$$

where $X$ is again a random variable following the $\chi_2^2$ distribution.

The second moment about the origin is

$$E[X^2] = \left.\frac{d^2(1-2y)^{-1}}{dy^2}\right|_{y=0}$$
$$= \left.8(1-2y)^{-3}\right|_{y=0}$$
$$= 8$$

and the third moment about the origin is

$$E[X^3] = \left.\frac{d^3(1-2y)^{-1}}{dy^3}\right|_{y=0}$$
$$= \left.48(1-2y)^{-4}\right|_{y=0}$$
$$= 48$$

Now the third moment about the mean is

$$E\left[(X-\mu)^3\right] = E\left[X^3 - 3X^2\mu + 3X\mu^2 - \mu^3\right]$$
$$= E[X^3] - 3\mu E[X^2] + 3\mu^2 E[X] - \mu^3$$

which then evaluates simply to

$$E\left[(X-\mu)^3\right] = 16$$

The distribution of $p_i$ is the $\chi_2^2$ distribution scaled such that $p_i = \frac{1}{2}\tilde{p}_i X$ so that the third moment of $p_i$ about its mean $\tilde{p}_i$ is given by

$$E\left[(p_i - \tilde{p}_i)^3\right] = (\tfrac{1}{2}\tilde{p}_i)^3 E\left[(X-\mu)^3\right]$$
$$= 2\tilde{p}_i^{\,3}$$

but $p_i - \tilde{p}_i$ is the deviation $e_i$, and for the uniform spectrum of $M$ bins scaled to have unit total power, $\tilde{p}_i = 1/M$, so equation (10.7) is proved, namely

$$E\left[e_i^{\,3}\right] = 2\tilde{p}_i^{\,3} = 2/M^3.$$

## The variance of PIWMB with a uniform mean spectrum - further justification of equation (10.14)

The method of derivation of the variance of PIWMB, var $\hat{B}$, given by (10.14) is less rigorous than the derivation of the variance of IWMB, var $\overline{B}$, given by (10.11). However, as stated in the text, when var $\overline{B}$ is derived in this less rigorous way the correct result, i.e. $M/12$, is obtained, so supporting the use of this method. This is demonstrated by again setting the total power in the mean spectrum to be 1. The deterministic statistic of (10.1) after a variation in the $k$'th estimate of $+e_k$ becomes an observed statistic of

$$\begin{aligned}\overline{B} &= \frac{\sum_{i=0}^{M-1} i\,\tilde{p}_i + ke_k}{1+e_k} \\ &= \left(\sum_{i=0}^{M-1} i\,\tilde{p}_i + ke_k\right)\left(1 - e_k + {e_k}^2 - \ldots\right) \\ &\approx \sum_{i=0}^{M-1} i\,\tilde{p}_i + ke_k - e_k \sum_{i=0}^{M-1} i\,\tilde{p}_i \\ &= \overline{B}_D + e_k\left(k - \overline{B}_D\right)\end{aligned}$$

where terms in ${e_k}^2$ and smaller have been removed. As $E\left[{e_k}^2\right] = \tilde{p}_k{}^2$ the total mean squared error due to a variation in every bin is

$$\text{tmse} \approx \sum_{k=0}^{M-1} \tilde{p}_k{}^2\left(k - \overline{B}_D\right)^2$$

For a uniform spectrum $\tilde{p}_k = 1/M$ for each bin and $\overline{B}_D = (M-1)/2$ . So

$$\begin{aligned}\text{tmse} &\approx \sum_{k=0}^{M-1}\left(\frac{1}{M}\right)^2\left(k-\frac{M-1}{2}\right)^2 \\ &= \frac{1}{M^2}\sum_{k=0}^{M-1}\left(k^2 - k(M-1) + \frac{(M-1)^2}{4}\right) \\ &= \frac{1}{M^2}\left(\frac{(M-1)M(2M-1)}{6} - \frac{(M-1)M}{2}(M-1) + \frac{M(M-1)^2}{4}\right)\end{aligned}$$

Taking the contributions to the bracket of order $M^3$ and recognising that var $\overline{B} \approx$ tmse, correct to the highest order, gives the result (10.11) derived more rigorously in chapter 10, i.e.

$$\begin{aligned}\text{var}\,\overline{B} &\approx \frac{1}{M^2}\left(\frac{M^3}{3} - \frac{M^3}{2} + \frac{M^3}{4}\right) \\ &= \frac{M}{12}\end{aligned}$$

This supports the validity of (10.14) as the expression for the variance of PIWMB.

## A property of the 'backwards' form of the estimator PIWMB - justification of (12.12)

The form of the estimator PIWMB appropriate when the velocity profile is monotonic but completely negative is denoted by $\hat{B}_B^*$ and given by (12.11). In this section it is shown that this 'backwards' estimator is greater than or equal to the general 'forwards' estimator $\hat{B}^*$ defined by (11.7b), so that the result given as (12.12) is justified.

This is demonstrated by considering their integral forms, denoted by $\hat{f}_B^*$ and $\hat{f}^*$. Using the notation $P$, $P_+$ and $P_-$ for the total powers in the whole spectrum, in the positive frequency and in the negative frequency parts of the spectrum, (which is as in chapter 11 but now in the context of a continuous spectrum,) the integral form of PIWMF $\hat{f}^*$ defined by (11.8) becomes

$$\hat{f}^* = \frac{2\int_0^{f_{max}} fp(f)\left[\int_f^{f_{max}} p(u)du\right]df + (P_- + 2P_+)\cdot\int_{f_{min}}^{0} f\,p(f)df}{P^2} \qquad \text{(E.9)}$$

and the integral form of the backwards estimator (12.11) is

$$\hat{f}_B^* = \frac{2\int_{f_{min}}^{0} fp(f)\left[\int_{f_{min}}^{f} p(u)du\right]df + (P_+ + 2P_-)\cdot\int_0^{f_{max}} f\,p(f)df}{P^2} \qquad \text{(E.10)}$$

If we write $\bar{f}_+$ and $\hat{f}_+$ for the IWMF and PIWMF values that would be calculated from the positive frequency part of the spectrum alone, and $\bar{f}_-$ and $\hat{f}_-$ for the corresponding *negative* values that would be calculated in the 'backwards' fashion from the negative frequency part of the spectrum alone, then from the basic definitions of IWMF and PIWMF, namely (2.10) and (2.11), these equations (E.9) and (E.10) can be written as

$$\begin{aligned} P^2\hat{f}^* &= P_+^2\hat{f}_+ + (P_- + 2P_+)\cdot P_-\bar{f}_- \\ &= P_+^2\hat{f}_+ + (P_-^2 + 2P_+P_-)\bar{f}_- \end{aligned}$$

and

$$\begin{aligned} P^2\hat{f}_B^* &= P_-^2\hat{f}_- + (P_+ + 2P_-)\cdot P_+\bar{f}_+ \\ &= P_-^2\hat{f}_- + (P_+^2 + 2P_+P_-)\bar{f}_+ \end{aligned}$$

so that

$$P^2\left(\hat{f}_B^* - \hat{f}^*\right) = P_-^2\,\hat{f}_- - \left(P_-^2 + 2P_+P_-\right)\bar{f}_- - P_+^2\,\hat{f}_+ + \left(P_+^2 + 2P_+P_-\right)\bar{f}_+$$

However from (2.13) we know that $\hat{f}_+ \le \bar{f}_+$ and consequently $\hat{f}_- \ge \bar{f}_-$ as these are negative. Therefore, removing the terms in $P_+^2$ and in $P_-^2$, we have

$$P^2\left(\hat{f}_B^* - \hat{f}^*\right) \ge 2P_+P_-\left(\bar{f}_+ - \bar{f}_-\right)$$

The right-hand side must be greater than or equal to zero as $\bar{f}_-$ is not greater than zero. So the left-hand side is greater than or equal to zero. This establishes the relationship that

$$\hat{f}_B^* \ge \hat{f}^*$$

It seems reasonable to extend this to the discrete case (especially if there is no power in the ambiguous zero'th bin) to give the result that the analogous deterministic PIWMB values are similarly related. It follows that the corresponding stochastic values satisfy

$$\hat{B}_B^* \ge \hat{B}^*$$

as in this analysis the spectrum $p(f)$ can have any form and the random nature of the signal plays no part . This is the stated result (12.12).

## Notation for this appendix

| | |
|---|---|
| $E[\ ]$ | expectation operator |
| $f(r)$ | the Doppler frequency arising from scatterers a distance $r$ from the centre of the vessel |
| $f_{\min}$ | minimum frequency in observed Doppler signal |
| $\hat{f}^*$ | PIWMF as defined by its more general form, (11.8) |
| $\hat{f}_B^*$ | PIWMF when frequency axis is reversed |
| $\bar{f}_+, \hat{f}_+$ | IWMF and PIWMF calculated from the positive frequencies alone |
| $\bar{f}_-, \hat{f}_-$ | IWMF and PIWMF calculated from the negative frequencies alone |
| $i'', j''$ | bin numbers expressed as fractions of the bin of the highest frequency present |
| $P_+$ | total observed power in the positive frequencies |
| $P_-$ | total observed power in the negative frequencies |
| $\Phi(\cdot)$ | cumulative transmitted power as successive transducer elements are included |

# APPENDIX F - MATHEMATICAL DERIVATIONS OF EQUATIONS

Several equations in the text have been derived from those preceding without the statement of intermediate steps, and reference has been made to this appendix for the necessary proofs. The mathematical derivations are therefore given here. The equations are proved in the order in which they appear in the text. In each equation the notation is that of the relevant chapter.

## Derivation of equation (6.2)

The derivation of (6.2) from the preceding equation is given here. We have

$$\overline{v}' = \frac{\int_0^{\sqrt{R^2-y^2}} 2\pi r^* v_m \left(1-\left(\frac{r^{*2}+y^2}{R^2}\right)^{n/2}\right) dr^*}{\int_0^{\sqrt{R^2-y^2}} 2\pi r^* dr^*}$$

$$= \frac{2\pi v_m \left(\int_0^{\sqrt{R^2-y^2}} r^* dr^* - \int_0^{\sqrt{R^2-y^2}} r^* \left(\frac{r^{*2}+y^2}{R^2}\right)^{n/2} dr^*\right)}{\pi\left(R^2-y^2\right)}$$

The first integration is straightforward. The second can be performed by making the substitution $u = \frac{r^{*2} + y^2}{R^2}$ so that $\frac{du}{dr^*} = \frac{2r^*}{R^2}$ and so

$$\int r^* \left( \frac{r^{*2} + y^2}{R^2} \right)^{n/2} dr^* = \int r^* \, u^{n/2} \, \frac{dr^*}{du} \, du$$

$$= \int \frac{R^2}{2} \, u^{n/2} \, du$$

$$= \frac{R^2}{n+2} \cdot u^{n/2+1} + \text{const}$$

$$= \frac{R^2}{n+2} \cdot \left( \frac{r^{*2} + y^2}{R^2} \right)^{n/2+1} + \text{const}$$

Therefore

$$\overline{v}' = \frac{2v_m}{R^2 - y^2} \cdot \left[ \frac{r^{*2}}{2} \right]_0^{\sqrt{R^2 - y^2}} - \frac{2v_m}{R^2 - y^2} \cdot \left[ \left( \frac{R^2}{n+2} \right) \left( \frac{r^{*2} + y^2}{R^2} \right)^{n/2+1} \right]_0^{\sqrt{R^2 - y^2}}$$

$$= v_m - \frac{2v_m}{n+2} \left( \frac{R^2}{R^2 - y^2} \right) \left\{ 1 - \left( \frac{y^2}{R^2} \right)^{n/2+1} \right\}$$

$$= v_m \left( 1 - \frac{2}{n+2} \left[ \frac{1 - \left( y/R \right)^{n+2}}{1 - \left( y/R \right)^2} \right] \right)$$

which is equation (6.2).

## Derivation of equation (7.13)

The proof of (7.13) is most easily performed by considering the first rectangular spectrum shown on fig.F.1, which has a total power of 1, so that the denominator of (7.9) is 1. The PIWMF of this spectrum is therefore

$$\begin{aligned}
\text{PIWMF} &= 2\int_0^e f \cdot p(f)\left[\int_f^e p(u)\,du\right]df \\
&= 2\int_0^e f \cdot \frac{1}{e}\left[\int_f^e \frac{1}{e}\,du\right]df \\
&= \frac{2}{e^2}\int_0^e f\left[\int_f^e 1\,du\right]df \\
&= \frac{2}{e^2}\int_0^e f(e-f)\,df \\
&= \frac{2}{e^2}\left[\frac{ef^2}{2}-\frac{f^3}{3}\right]_0^e \\
&= \frac{e}{3}
\end{aligned}$$

The broadened spectrum of interest is given by (7.12) and is shown by the second rectangular spectrum. The corresponding result can be found by putting $e = abf_m$ and shifting the spectrum to the right along the frequency axis by $\left(1-\frac{a}{2}\right)bf_m$, which must raise PIWMF by the same amount as (7.9) is linear in $f$. PIWMF for the broadened spectrum is therefore

$$\begin{aligned}
\hat{f} &= \frac{abf_m}{3}+\left(1-\frac{a}{2}\right)bf_m \\
&= \left(1-\frac{a}{6}\right)bf_m
\end{aligned}$$

which is equation (7.13)

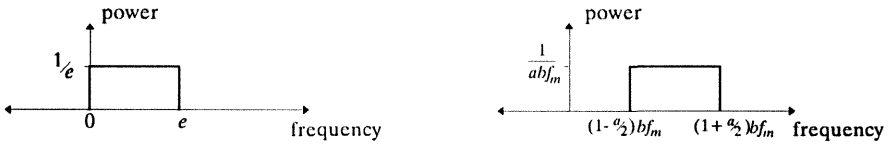


**Fig.F.1 - rectangular broadening**

## Derivation of equation (7.16)

The proof of (7.16) is best achieved by finding the PIWMF for the first triangular spectrum shown on fig.F.2. The total power is again equal to 1, and the spectrum is

$$p(f) = \frac{1}{e} \cdot \frac{e+f}{e} \qquad -e \le f \le 0$$

$$p(f) = \frac{1}{e} \cdot \frac{e-f}{e} \qquad 0 \le f \le e$$

and zero elsewhere. Therefore from (7.9) the PIWMF is

$$\text{PIWMF} = 2\int_{-e}^{e} f \cdot p(f)\left[\int_{f}^{e} p(u)\,du\right]df$$

$$\begin{aligned}
&= 2\int_{-e}^{0} f \cdot p(f)\left[\int_{f}^{0} p(u)\,du\right]df \\
&+2\int_{-e}^{0} f \cdot p(f)\left[\int_{0}^{e} p(u)\,du\right]df \\
&+2\int_{0}^{e} f \cdot p(f)\left[\int_{f}^{e} p(u)\,du\right]df
\end{aligned}$$

$$\begin{aligned}
&= 2\int_{-e}^{0} f \cdot \frac{1}{e} \cdot \frac{e+f}{e}\left[\int_{f}^{0} \frac{1}{e} \cdot \frac{e+u}{e}\,du\right]df \\
&+2\int_{-e}^{0} f \cdot \frac{1}{e} \cdot \frac{e+f}{e}\left[\frac{1}{2}\right]df \\
&+2\int_{0}^{e} f \cdot \frac{1}{e} \cdot \frac{e-f}{e}\left[\int_{f}^{e} \frac{1}{e} \cdot \frac{e-u}{e}\,du\right]df
\end{aligned}$$

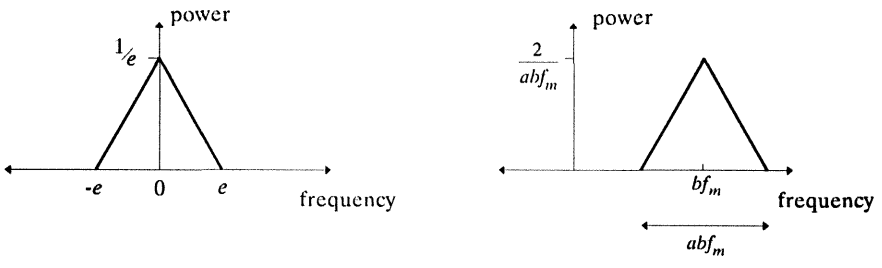


**Fig.F.2 - triangular broadening**

The first of these terms is

$$\begin{aligned}
\text{first term} &= 2\int_{-e}^{0} f\cdot\frac{1}{e}\cdot\frac{e+f}{e}\left[\int_{f}^{0}\frac{1}{e}\cdot\frac{e+u}{e}\,du\right]df \\
&= \frac{2}{e^4}\int_{-e}^{0} f(e+f)\left[\int_{f}^{0}(e+u)\,du\right]df \\
&= \frac{2}{e^4}\int_{-e}^{0}\left(f^2+ef\right)\left[eu+\frac{u^2}{2}\right]_{f}^{0}df \\
&= \frac{1}{e^4}\int_{-e}^{0}\left(f^2+ef\right)\left(-2ef-f^2\right)df \\
&= \frac{1}{e^4}\int_{-e}^{0}\left(-f^4-3ef^3-2e^2f^2\right)df \\
&= \frac{1}{e^4}\left[-\frac{f^5}{5}-\frac{3ef^4}{4}-\frac{2e^2f^3}{3}\right]_{-e}^{0} \\
&= \frac{1}{e^4}\left(-\frac{e^5}{5}+\frac{3e^5}{4}-\frac{2e^5}{3}\right) \\
&= e\left(-\frac{12}{60}+\frac{45}{60}-\frac{40}{60}\right) \\
&= \frac{-7e}{60}
\end{aligned}$$

The second term is

$$\begin{aligned}
\text{second term} &= 2\int_{-e}^{0} f\cdot\frac{1}{e}\cdot\frac{e+f}{e}\left[\frac{1}{2}\right]df \\
&= \frac{1}{e^2}\int_{-e}^{0} f(e+f)\,df \\
&= \frac{1}{e^2}\left[\frac{ef^2}{2}+\frac{f^3}{3}\right]_{-e}^{0} \\
&= \frac{1}{e^2}\left[-\frac{e^3}{2}+\frac{e^3}{3}\right]_{-e}^{0} \\
&= -\frac{e}{6}
\end{aligned}$$

The third term is

$$\begin{aligned}
\text{third term} &= 2\int_0^e f\cdot\frac{1}{e}\cdot\frac{e-f}{e}\left[\int_f^e\frac{1}{e}\cdot\frac{e-u}{e}du\right]df \\
&= \frac{2}{e^4}\int_0^e f(e-f)\left[\int_f^e(e-u)du\right]df \\
&= \frac{2}{e^4}\int_0^e f(e-f)\left[eu-\frac{u^2}{2}\right]_f^e df \\
&= \frac{2}{e^4}\int_0^e f(e-f)\left(\frac{e^2}{2}-ef+\frac{f^2}{2}\right)df \\
&= \frac{1}{e^4}\int_0^e f(e-f)^3 df \\
&= \frac{1}{e^4}\int_0^e\left(e^3f-3e^2f^2+3ef^3-f^4\right)df \\
&= \frac{1}{e^4}\left[\frac{e^3f^2}{2}-e^2f^3+\frac{3ef^4}{4}-\frac{f^5}{5}\right]_0^e \\
&= \frac{1}{e^4}\left(\frac{e^5}{2}-e^5+\frac{3e^5}{4}-\frac{e^5}{5}\right) \\
&= e\left(\frac{10}{20}-\frac{20}{20}+\frac{15}{20}-\frac{4}{20}\right) \\
&= \frac{e}{20}
\end{aligned}$$

Adding these terms shows that PIWMF is

$$\text{PIWMF} = -\frac{7e}{60}-\frac{e}{6}+\frac{e}{20} = -\frac{7e}{60}-\frac{10e}{60}+\frac{3e}{60} = -\frac{7e}{30}$$

The spectrum resulting from triangular broadening is given by (7.15) and is shown by the second spectrum in fig.F.2. The corresponding result can be found by putting $e=\frac{abf_m}{2}$, and shifting the spectrum to the right along the frequency axis by $bf_m$ which must increase the PIWMF by the same amount as (7.9) is linear in $f$. Therefore

$$\begin{aligned}
\hat{f} &= \left(\frac{-7}{30}\cdot\frac{abf_m}{2}\right)+bf_m \\
&= \left(1-\frac{7a}{60}\right)bf_m
\end{aligned}$$

which is equation (7.16).

## Derivation of equation (8.13)

The expression to be simplified is

$$\text{second line} = \int_0^{f_m} f \frac{St}{f_m}\left(1-{}^{f}\!/_{f_m}\right)^{t-1} \frac{N}{f_e}(f_e - f)\, df + \int_0^{f_m} f \frac{N}{f_e}\left[\int_f^{f_m} \frac{St}{f_m}\left(1-{}^{u}\!/_{f_m}\right)^{t-1} du\right] df$$

The proportion of the frequency range occupied by the signal is defined to be $m \equiv \frac{f_m}{f_e}$,

Making the substitutions $x = 1-{}^{f}\!/_{f_m}$ so that $f = f_m(1-x)$ and ${}^{df}\!/_{dx} = -f_m$ , and $y = 1-{}^{u}\!/_{f_m}$ so that ${}^{du}\!/_{dy} = -f_m$ gives

$$\text{second line} = -\int_1^0 f_m(1-x)Stx^{t-1} \frac{N}{f_e} f_m\left({}^{1}\!/_{m} - 1 + x\right) dx - \int_1^0 f_m{}^2(1-x)\frac{N}{f_e}\left[-\int_x^0 Sty^{t-1} dy\right] dx$$

$$= \int_0^1 f_m(1-x)Stx^{t-1} \frac{N}{f_e} f_m\left({}^{1}\!/_{m} - 1 + x\right) dx + \int_0^1 f_m{}^2(1-x)\frac{N}{f_e}\left[\int_0^x Sty^{t-1} dy\right] dx$$

The first term of this expression is

$$\text{first term} = \int_0^1 f_m(1-x)Stx^{t-1} \frac{N}{f_e} f_m\left({}^{1}\!/_{m} - 1 + x\right) dx$$

$$= Sf_m{}^2 \frac{N}{f_e}\int_0^1 \left({}^{1}\!/_{m} - 1 + \left(2 - {}^{1}\!/_{m}\right)x - x^2\right) tx^{t-1}\, dx$$

$$= Sf_m{}^2 \frac{N}{f_e}\left[\left({}^{1}\!/_{m} - 1\right)x^t + \left(2 - {}^{1}\!/_{m}\right)\frac{t}{t+1}x^{t+1} - \frac{t}{t+2}x^{t+2}\right]_0^1$$

$$= Sf_m{}^2 \frac{N}{f_e}\left(\left({}^{1}\!/_{m} - 1\right) + \left(2 - {}^{1}\!/_{m}\right)\frac{t}{t+1} - \frac{t}{t+2}\right)$$

and the second term is

$$\text{second term} = \int_0^1 f_m^{\,2}(1-x)\frac{N}{f_e}\left[\int_0^x Sty^{t-1}dy\right]dx$$

$$= \int_0^1 Sf_m^{\,2}(1-x)\frac{N}{f_e}x^t\,dx$$

$$= Sf_m^{\,2}\frac{N}{f_e}\int_0^1(1-x)x^t\,dx$$

$$= Sf_m^{\,2}\frac{N}{f_e}\left[\frac{x^{t+1}}{t+1}-\frac{x^{t+2}}{t+2}\right]_0^1$$

$$= Sf_m^{\,2}\frac{N}{f_e}\left(\frac{1}{t+1}-\frac{1}{t+2}\right)$$

Adding these terms gives

$$\text{second line} = Sf_m^{\,2}\frac{N}{f_e}\left(\left(1/m-1\right)+\left(2-1/m\right)\frac{t}{t+1}-\frac{t}{t+2}+\frac{1}{t+1}-\frac{1}{t+2}\right)$$

$$= SNf_m\left((1-m)+(2m-1)\frac{t}{t+1}+\frac{m}{t+1}-\frac{m(t+1)}{t+2}\right)$$

$$= SNf_m\left((1-m)+(m-1)\frac{t}{t+1}+\frac{mt}{t+1}+\frac{m}{t+1}-\frac{m(t+2-1)}{t+2}\right)$$

$$= SNf_m\left((1-m)\left(1-\frac{t}{t+1}\right)+m-m+\frac{m}{t+2}\right)$$

$$= SNf_m\left((1-m)\left(\frac{1}{t+1}\right)+\frac{m}{t+2}\right)$$

$$= SNf_m\left(\frac{1}{t+1}-m\left(\frac{1}{t+1}-\frac{1}{t+2}\right)\right)$$

$$= SNf_m\left(\frac{1}{t+1}-\frac{m}{(t+1)(t+2)}\right)$$

$$= SN\left(1-\frac{m}{t+2}\right)\bar{f}_S$$

where the last step follows from (8.8), i.e. $\bar{f}_S = \frac{f_m}{t+1}$. The result is equation (8.13).

## Derivation of equation (9.4)

The derivation uses the substitution $x = 1 - f/f_m$ so that $f = f_m(1-x)$ and $df/dx = -f_m$

$$\bar{f} = \frac{\int_{f_b}^{f_m} f \cdot \frac{t}{f_m}\left(1 - f/f_m\right)^{t-1} df}{\int_{f_b}^{f_m} \frac{t}{f_m}\left(1 - f/f_m\right)^{t-1} df}$$

$$= \frac{-\int_{1-b}^{0} f_m(1-x)tx^{t-1}dx}{-\int_{1-b}^{0} tx^{t-1}dx}$$

$$= \frac{\int_{0}^{1-b} f_m(1-x)tx^{t-1}dx}{\int_{0}^{1-b} tx^{t-1}dx}$$

$$= \frac{f_m\left[x^t - \frac{t}{t+1}x^{t+1}\right]_0^{1-b}}{(1-b)^t}$$

$$= f_m \frac{\left((1-b)^t - \frac{t}{t+1}(1-b)^{t+1}\right)}{(1-b)^t}$$

$$= f_m\left(1 - \left(\frac{t}{t+1}\right)(1-b)\right)$$

$$= f_m\left(\frac{1}{t+1} + \frac{tb}{t+1}\right)$$

which is (9.4)

## Derivation of equation (9.6)

The derivation uses the substitution $x = 1 - f/f_m$ so that $f = f_m(1-x)$ and $df/dx = -f_m$, and the substitution $y = 1 - u/f_m$ so that $du/dy = -f_m$

$$\hat{f} = \frac{2\int_{f_b}^{f_m} f \cdot p(f)\left[\int_f^{f_m} p(u)\,du\right]df}{\left(\int_{f_b}^{f_m} p(f)\,df\right)^2}$$

$$= \frac{2\int_{f_b}^{f_m} f \cdot \frac{t}{f_m}\left(1 - f/f_m\right)^{t-1}\left[\int_f^{f_m} \frac{t}{f_m}\left(1 - u/f_m\right)^{t-1} du\right]df}{\left(\int_{f_b}^{f_m} \frac{t}{f_m}\left(1 - f/f_m\right)^{t-1} df\right)^2}$$

$$= \frac{-2\int_{1-b}^{0} f_m(1-x)\cdot t\,x^{t-1}\left[-\int_x^0 t\,y^{t-1}\,dy\right]dx}{\left(-\int_{1-b}^{0} t\,x^{t-1}\,dx\right)^2}$$

$$= \frac{2\int_0^{1-b} f_m(1-x)\cdot t\,x^{t-1}\left[\int_0^x t\,y^{t-1}\,dy\right]dx}{\left(\int_0^{1-b} t\,x^{t-1}\,dx\right)^2}$$

$$= \frac{2f_m\int_0^{1-b}(1-x)\,t\,x^{t-1}\left[y^t\right]_0^x dx}{\left(\left[x^t\right]_0^{1-b}\right)^2}$$

$$= \frac{2f_m\int_0^{1-b}(1-x)\,t\,x^{2t-1}\,dx}{(1-b)^{2t}}$$

continuing ...

... and restating the last result

$$\hat{f} = \frac{2f_m \int_0^{1-b} (1-x)t\,x^{2t-1}\,dx}{(1-b)^{2t}}$$

$$= \frac{2f_m \left[ \frac{x^{2t}}{2} - \frac{tx^{2t+1}}{2t+1} \right]_0^{1-b}}{(1-b)^{2t}}$$

$$= \frac{2f_m \left( \frac{(1-b)^{2t}}{2} - \frac{t(1-b)^{2t+1}}{2t+1} \right)}{(1-b)^{2t}}$$

$$= f_m \left( 1 - \frac{2t(1-b)}{2t+1} \right)$$

$$= f_m \left( \frac{1}{2t+1} + \frac{2tb}{2t+1} \right)$$

which is (9.6)

## Derivation of equation (10.8)

The derivation of the expected value of the term $\alpha_1 \beta_2$ is a little more involved than the derivations for the other cross product terms in (10.6), and is set forth here.

$$
\begin{aligned}
E[\alpha_1 \beta_2] &= E\left[ 2\sum_{i=0}^{M-1} e_i \cdot \sum_{i=0}^{M-1} i\tilde{p}_i \left( 2\sum_{j=i+1}^{M-1} e_j + e_i \right) \right] \\
&= E\left[ 4\sum_{i=0}^{M-1} e_i \cdot \sum_{i=0}^{M-1} i\tilde{p}_i \sum_{j=i+1}^{M-1} e_j \right] + E\left[ 2\sum_{i=0}^{M-1} e_i \cdot \sum_{i=0}^{M-1} i\tilde{p}_i e_i \right] \\
&= E[Y] + E[Z]
\end{aligned}
$$

where the terms have been renamed for simplicity. Taking these terms individually

$$
\begin{aligned}
E[Y] &= E\left[ 4\sum_{i=0}^{M-1} e_i \cdot \sum_{i=0}^{M-1} i\tilde{p}_i \sum_{j=i+1}^{M-1} e_j \right] \\
&= \frac{4}{M} E\left[ \sum_{i=0}^{M-1} e_i \left( \sum_{i=0}^{M-1} i \sum_{j=i+1}^{M-1} e_j \right) \right] \\
&= \frac{4}{M} E\left[ \sum_{i=0}^{M-1} e_i \left( \sum_{i=0}^{M-1} i\left( e_{i+1} + e_{i+2} + \ldots e_{M-1} \right) \right) \right] \\
&= \frac{4}{M} E\left[ \sum_{i=0}^{M-1} e_i \begin{pmatrix} 0(e_1 + e_2 + e_3 + \ldots e_{M-1}) \\ +1(\quad e_2 + e_3 + \ldots e_{M-1}) \\ \vdots \\ +(M-2)(\qquad e_{M-1}) \end{pmatrix} \right] \\
&= \frac{4}{M} \sum_{i=1}^{M-1} \frac{i(i-1)}{2} E\left[ e_i^{\,2} \right] \\
&= \frac{2}{M^3} \left( \sum_{i=1}^{M-1} i^2 - \sum_{i=1}^{M-1} i \right) \\
&= \frac{2}{M^3} \left( \frac{(M-1)M(2M-1)}{6} - \frac{(M-1)M}{2} \right) \\
&= \frac{(M-1)(2M-1)}{3M^2} - \frac{(M-1)}{M^2}
\end{aligned}
$$

and

$$E[Z] = E\left[2\sum_{i=0}^{M-1} e_i \cdot \sum_{i=0}^{M-1} i\tilde{p}_i e_i\right]$$
$$= 2\sum_{i=0}^{M-1} i\tilde{p}_i E\left[e_i^{\,2}\right]$$
$$= \frac{2}{M^3} \cdot \frac{(M-1)M}{2}$$
$$= \frac{(M-1)}{M^2}$$

So

$$E[\alpha_1 \beta_2] = E[Y] + E[Z] = \frac{(M-1)(2M-1)}{3M^2}$$

which is equation (10.8).

## Derivation of equation (10.13)

Equation (10.13) is

$$\hat{B} = \frac{\sum_{i=0}^{M-1} i\,\tilde{p}_i \left(2\sum_{j=i+1}^{M-1} \tilde{p}_j + \tilde{p}_i\right) + 2e_k \sum_{i=0}^{k-1} i\,\tilde{p}_i + ke_k \left(2\sum_{j=k}^{M-1} \tilde{p}_j + e_k\right)}{(1+e_k)^2}$$

Equation (10.3), where the uniform spectrum is scaled to have a total mean power of 1, is

$$\hat{B}_D = \frac{\sum_{i=0}^{IMAX-1} i\,\tilde{p}_i \left(\sum_{j=i+1}^{IMAX-1} 2\tilde{p}_j + \tilde{p}_i\right)}{1^2}$$

The derivation of the denominator of (10.13) from the denominator of this latter equation as a result of the variation of $+e_k$ introduced in the $k$'th bin is trivial, but the derivation of

the numerator is more complicated. The main summation in the numerator is made up of contributions from bins below the $k$'th bin, from the $k$'th bin and from bins above the $k$'th bin. The contributions from bins below the $k$'th bin are affected by the extra $+2e_k$ in the bracket term. The contribution from these bins is therefore

$$\sum_{i=0}^{k-1} i\,\tilde{p}_i\left(2\sum_{j=i+1}^{M-1}\tilde{p}_j+\tilde{p}_i+2e_k\right)=\sum_{i=0}^{k-1} i\,\tilde{p}_i\left(2\sum_{j=i+1}^{M-1}\tilde{p}_j+\tilde{p}_i\right)+2e_k\sum_{i=0}^{k-1} i\,\tilde{p}_i \qquad \text{(i)}$$

The contribution to the numerator from the $k$'th bin becomes

$$\begin{aligned} k(\tilde{p}_k+e_k)\left(2\sum_{j=k+1}^{M-1}\tilde{p}_j+(\tilde{p}_k+e_k)\right) &= k\tilde{p}_k\left(2\sum_{j=k+1}^{M-1}\tilde{p}_j+\tilde{p}_k\right)+k\tilde{p}_k e_k \\ &\quad +ke_k\left(2\sum_{j=k+1}^{M-1}\tilde{p}_j+\tilde{p}_k\right)+ke_k^2 \end{aligned} \qquad \text{(ii)}$$

The contributions to the numerator from bins above the $k$'th bin are unaffected, and sum to

$$\sum_{i=k+1}^{M-1} i\,\tilde{p}_i\left(2\sum_{j=i+1}^{M-1}\tilde{p}_j+\tilde{p}_i\right) \qquad \text{(iii)}$$

The first term of the right-hand side of (i), the first term of the right-hand side of (ii) and the right-hand side of (iii) add to give the first term in the numerator of the equation (10.13) (which is the deterministic value $\hat{B}$). The second term of (i) is the second term of the numerator of (10.13), and the remaining terms of (ii) add to give

$$k\tilde{p}_k e_k+ke_k\left(2\sum_{j=k+1}^{M-1}\tilde{p}_j+\tilde{p}_k\right)+ke_k^2=ke_k\left(2\sum_{j=k}^{M-1}\tilde{p}_j+e_k\right)$$

which is the third term of the numerator of (10.13). This completes the derivation.

## REFERENCES


Aldis G.K. and Thompson R.S. (1992), "Calculation of Doppler spectral power density functions," *IEEE Trans. Biomed. Eng.*, vol. 39, pp. 1022-1031.

Angelsen B.A.J. (1980), "A theoretical study of the scattering of ultrasound from blood," *IEEE Trans. Biomed. Eng.*, vol. BME-27, pp. 61-67.

Angelsen B.A.J. (1981), "Instantaneous frequency, mean frequency, and variance of mean frequency estimators for ultrasonic blood velocity Doppler signals," *IEEE Trans. Biomed. Eng.*, vol. BME-28, pp. 733-741.

Arts M.G.J. and Roevros J.M.J.G. (1972), "On the instantaneous measurement of bloodflow by ultrasonic means," *Med. & Biol. Engng.*, vol. 10, pp. 23-34.

Brody W.R. (1972), "Theoretical analysis of the ultrasonic blood flowmeter," Ph.D. dissertation, Dep. Elec. Eng., Stanford Univ., Stanford, CA.

Bush G., Smith M.J. and Evans D.H., "Frame grabber for sequential real time video image digitisation and transfer to microcomputer system," *Med. & Biol. Eng. & Comput.*, (in press).

Caro C.G., Pedley T.J., Schroter R.C. and Seed W.A. (1978), *The mechanics of the circulation*, Oxford University Press.

Censor D., Newhouse V.L., Vontz T. and Ortega H.V. (1988), "Theory of ultrasound Doppler-spectra velocimetry for arbitrary beam and flow configurations," *IEEE Trans. Biomed. Eng.*, vol. 35, pp. 740-751.

Cobbold R.S.C., Veltink P.H. and Johnston K.W. (1983), "Influence of beam profile and degree of insonation on the C.W. Doppler ultrasound spectrum and mean velocity," *IEEE Trans. Sonics Ultrason.*, vol. SU-30, pp. 364-370.

Eriksen M. (1992), "Effect of pulsatile arterial diameter variations on blood flow estimated by Doppler ultrasound," *Med. & Biol. Eng. & Comput.*, vol. 30, pp. 46-50.

Evans D.H. (1982a), "Some aspects of the relationship between instantaneous volumetric blood flow and continuous wave Doppler ultrasound recordings - I. The effect of ultrasonic beam width on the output of maximum, mean and r.m.s. frequency processors," *Ultrasound in Med. and Biol.*, vol. 8, pp. 605-609.

Evans D.H. (1982b), "Some aspects of the relationship between instantaneous volumetric blood flow and continuous wave Doppler ultrasound recordings - III. The calculation of Doppler power spectra from mean velocity waveforms, and the results of processing these spectra with maximum, mean and RMS frequency processors," *Ultrasound in Med. and Biol.*, vol. 8, pp. 617-623.

Evans D.H. (1985), "On the measurement of the mean velocity of blood flow over the cardiac cycle using Doppler ultrasound," *Ultrasound in Med. and Biol.*, vol. 11, pp. 735-741.

Evans D.H., McDicken W.N., Skidmore R. and Woodcock J.P. (1989), *Doppler Ultrasound.* Chichester. Wiley.

Gerzberg L. and Meindl J.D. (1977), "Mean frequency estimator with applications in ultrasonic Doppler flowmeters," in *Ultrasound in Medicine*, vol.3b, Eds: D.White and R.E. Brown, New York & London, Plenum Press, pp. 1173-1180.

Gerzberg L. and Meindl J.D. (1980), "Power-spectrum centroid detection for Doppler systems applications," *Ultrasonic Imaging*, vol. 2, pp. 232-261.

Gill R.W. (1979), "Performance of the mean frequency Doppler modulator," *Ultrasound in Med. and Biol.*, vol. 5, pp. 237-247.

Gill R.W. (1982), "Accuracy calculations for ultrasonic pulsed Doppler blood flow measurements," *Australasian Physical and Engineering Sciences in Medicine*, vol. 5, pp. 51-57.

Harris F.J. (1978), "On the use of windows for harmonic analysis with the discrete Fourier transform," *Proceedings of the IEEE*, vol. 66, pp. 51-83.

Hoeks A.P.G., Ruissen C.J., Hick P. and Reneman R.S. (1985), "Transcutaneous detection of relative changes in artery diameter," *Ultrasound in Med. & Biol.*, vol. 11, pp. 51-59.

Hoeks A.P.G., Brands P.J., Smeets F.A.M. and Reneman R.S. (1990), "Assessment of the distensibility of superficial arteries," *Ultrasound in Med. & Biol.*, vol. 16, pp. 121-128.

Hokanson D.E., Strandness D.E. Jr. and Miller C.W. (1970), "An echo-tracking system for recording arterial-wall motion," *IEEE Trans. Sonics & Ultrasonics*, vol. SU-17, pp. 130-132.

Hokanson D.E., Mozersky D.J., Sumner D.S. and Strandness D.E. Jr. (1972), "A phase-locked echo tracking system for recording arterial diameter changes in vivo," *J. Appl. Physiol.*, vol. 32, pp. 728-733.

Li S., McDicken W.N. and Hoskins P.R. (1993), "Blood vessel diameter measurement by ultrasound," *Physiol. Meas.*, vol. 14, pp. 291-297.

McDonald D.A. (1974), *Blood flow in arteries*. 2nd ed. London. Edward Arnold.

Mo L.Y.L. and Cobbold R.S.C. (1986a), "A stochastic model of the backscattered Doppler ultrasound from blood," *IEEE Trans. Biomed. Eng.*, vol. BME-33, pp. 20-27.

Mo L.Y.L. and Cobbold R.S.C. (1986b), " "Speckle" in continuous wave Doppler ultrasound spectra: A simulation study," *IEEE Trans. Ultrason. Ferroelec. Freq. Contr.*, vol. UFFC-33, pp. 747-752.

Mo L.Y.L. and Cobbold R.S.C. (1992), "A unified approach to modeling the backscattered Doppler ultrasound from blood," *IEEE Trans. Biomed. Eng.*, vol. 39, pp. 450-461.

Newhouse V.L., Furgason E.S., Johnson G.F. and Wolf D.A. (1980), "The dependence of ultrasound Doppler bandwidth on beam geometry," *IEEE Trans. Sonics & Ultrasonics*, vol. SU-27, pp. 50-59.

Newhouse V.L., Censor D., Vontz T., Cisneros J.A. and Goldberg B. B. (1987), "Ultrasound Doppler probing of flows transverse with respect to beam axis," *IEEE Trans. Biomed. Eng.*, vol. BME-34, pp. 779-789.

Oppenheim A.V. and Schafer R.W. (1975), *Digital signal processing*, Prentice-Hall, New Jersey. (pp. 542-548.)

Pignoli P., Tremoli E., Poli A., Oreste P. and Paoletti R. (1986), "Intimal plus medial thickness of the arterial wall: a direct measurement with ultrasound imaging," *Circulation*, vol. 74, pp. 1399-1406.

Priestley M.B. (1981), *Spectral analysis and time series*, Academic Press. (Sixth printing 1989, p. 398.)

Roevros J.M.J.G. (1974), "Analogue processing of C.W. Doppler flowmeter signals to determine average frequency shift momentaneously without the use of a wave analyser," in *Cardiovascular applications of ultrasound.* Ed.:R.S.Reneman, Amsterdam-London: North-Holland Publ. Co., ch. 4, pp. 43-54.

Schlindwein F.S., Smith M.J. and Evans D.H. (1988), "Spectral analysis of Doppler signals and computation of the normalised first moment in real time using a digital signal processor," *Med. & Biol. Eng. & Comput.*, vol. 26, pp. 228-232.

Shung K.K., Cloutier G. and Lim C.C. (1992), "The effects of hematocrit, shear rate, and turbulence on ultrasonic Doppler spectrum from blood," *IEEE Trans. Biomed. Eng.*, vol. 39, pp. 462-469.

Walpole R.E. and Myers R.H. (1978), *Probability and statistics for engineers and scientists*. 2nd ed. London. Collier Macmillan.

Wilson L.S., Dadd M.J. and Gill R.W. (1990), "Automatic vessel tracking and measurement for Doppler studies," *Ultrasound in Med. & Biol.*, vol. 16, pp. 645-652.

Womersley J.R. (1955), "Oscillatory flow in arteries: effect of radial variation in viscosity on rate of flow," *J.Physiol.*, **127**, 38-39P.

Womersley J.R. (1957), "The mathematical analysis of the arterial circulation in a state of oscillatory motion," Wright Air Development Center, Technical Report WADC-TR56-614